

Draft Technical Report

GROUND WATER MODELING STUDIES AT IN
SITU LEACHING FACILITIES AND
EVALUATION OF DOSES AND RISKS TO OFF-
SITE RECEPTORS FROM CONTAMINATED
GROUND WATER

REVISION 2

U.S. Environmental Protection Agency
Office of Radiation and Indoor Air
Radiation Protection Division
1200 Pennsylvania Avenue
Washington, DC 20460

EPA-402-D-14-002

Draft Technical Report

GROUND WATER MODELING STUDIES AT IN SITU LEACHING
FACILITIES AND EVALUATION OF DOSES AND RISKS TO OFF-SITE
RECEPTORS FROM CONTAMINATED GROUND WATER
REVISION 2

Contract Number EP-D-10-042
Work Assignment 2-06, Task 2

Prepared by:
S. Cohen & Associates
1608 Spring Hill Road, Suite 400
Vienna, VA 22182-2241

Prepared for:
U.S. Environmental Protection Agency
Office of Radiation and Indoor Air
1200 Pennsylvania Avenue, N.W.
Washington, DC 20460

Kenneth Czyscinski
Work Assignment Manager

December 2012

Contents

List of Acronyms and Abbreviations.....	x
Executive Summary.....	1
1.0 Introduction.....	1-1
2.0 Ground Water Modeling of In-Situ Leaching Failure Scenarios.....	2-1
2.1 In-Situ Leaching Process.....	2-1
2.2 Failures during Operations.....	2-3
2.3 Failures after Shutdown.....	2-5
2.4 Ground Water Model Development.....	2-6
2.4.1 Basic Aspects of Computer (Numerical) Modeling.....	2-7
2.4.2 Conceptual Model Development.....	2-8
2.4.3 Computer Code Selection.....	2-9
2.5 Representative ISL Facility Development and General Modeling Approach ...	2-10
2.6 Development of Scenarios.....	2-13
2.6.1 Spills and Leaks.....	2-14
2.6.2 Excursion Scenarios.....	2-30
3.0 Pathway Dose and Risk Conversion Factors.....	3-1
3.1 Pathway Dose and Risk Models.....	3-3
3.1.1 Ingestion of Drinking Water.....	3-3
3.1.2 Inadvertent Ingestion of Soil.....	3-3
3.1.3 Ingestion of Vegetables.....	3-4
3.1.4 Ingestion of Milk.....	3-5
3.1.5 Ingestion of Meat.....	3-6
3.1.6 Pathway Dose and Risk Factors.....	3-6
3.1.7 Implementation.....	3-7
3.2 Input Parameters.....	3-7
3.2.1 Age Groups.....	3-7
3.2.2 Dose and Risk Conversion Coefficients.....	3-9
3.2.3 Ingestion of Drinking Water.....	3-15
3.2.4 Inadvertent Ingestion of Soil.....	3-18
3.2.5 Ingestion of Vegetables.....	3-20
3.2.6 Ingestion of Milk.....	3-23
3.2.7 Ingestion of Meat.....	3-27
3.3 Pathway Dose and Risk Conversion Factors.....	3-29
3.4 Native American Exposures.....	3-35
3.4.1 Ingestion of Drinking Water.....	3-35
3.4.2 Ingestion of Vegetables.....	3-36
3.4.3 Ingestion of Meat.....	3-37
3.4.4 Exposure in Sweat Lodge.....	3-38
3.4.5 Native American Pathway Dose and Risk Conversion Factors.....	3-45
3.5 Exposure Pathways Not Analyzed in Detail.....	3-47
3.5.1 External Exposure to Contaminated Ground.....	3-48
3.5.2 Exposure to Indoor Radon.....	3-48

3.5.3	Swimming Pool/Hot Tub Exposures	3-50
3.5.4	Exposures Due to Hydroponics and/or Aquaculture	3-50
3.5.5	Embryo and Fetus Exposure	3-51
3.5.6	Infant Consumption of Formula/Milk.....	3-52
4.0	Dose and Risk Assessment	4-1
4.1	Introduction.....	4-1
4.2	Selection of Lixiviant Concentrations and K_{ds}	4-1
4.2.1	Lixiviant Concentration	4-1
4.2.2	Selection of K_d Values	4-3
4.2.3	Recommendations for K_d and Radionuclide Source Term.....	4-6
4.3	Dose and Risk Calculations	4-7
4.3.1	Limiting Doses and Risks	4-7
4.3.2	Doses and Risks from Excursion Scenarios.....	4-7
4.3.3	Doses and Risks from Surface Leak Scenarios.....	4-13
4.4	Risks to Non-standard Receptors.....	4-15
4.5	Non-Radiological Risks	4-17
5.0	Summary and Conclusions	5-1
5.1	Ground Water Modeling Studies	5-1
5.2	Pathway Dose and Risk Conversion Factors	5-2
5.3	Dose/Risk Assessment for Modeled Scenarios.....	5-3
6.0	References.....	6-1

List of Tables

Table ES-1:	Calculated Total Pathway Dose Conversion Factors.....	4
Table ES-2:	Calculated Total Pathway Risk Conversion Factors.....	4
Table ES-3:	Typical Pathway Contributions to the Adult PDCF and PRCF	5
Table ES-4:	Calculated Pathway Dose Conversion	6
Table ES-5:	Excursion Scenario Maximum Doses and Risks – Mean Adult.....	6
Table ES-6:	Excursion Scenario Doses and Risks to Various Receptors	7
Table ES-7:	Surface Leak Scenario Doses and Risks.....	7
Table 2-1:	Representative ISL Parameter Ranges.....	2-13
Table 2-2:	Catastrophic Leak Failure Scenarios	2-19
Table 2-3:	Long-Term/Low Volume Leak Scenarios	2-22
Table 2-4:	Short-Term/High-Volume Leak Scenarios	2-28
Table 2-5:	Series 1 – 5-Spot Injection at a Spacing of 250 feet – Receptor Well at 528 feet.....	2-37
Table 2-6:	Series 2 – 5-Spot Injection at a Spacing of 50 feet – Receptor Well at 528 feet.....	2-38
Table 2-7:	Series 3 – 7-Spot Injection at a Spacing of 250 feet – Receptor Well at 528 feet.....	2-41
Table 2-8:	Series 4 – 7-Spot Injection at a Spacing of 50 feet – Receptor Well at 528 feet.....	2-44
Table 2-9:	Series 5 – 5-Spot Injection\Pumping Rates Dependent Upon Hydraulic Conductivity.....	2-46
Table 2-10:	Series 6 – 5-Spot 20-Foot Thick Mined Interval	2-49
Table 2-11:	Series 7 – Twenty-five 5-Spot Pumping/Injection Cells	2-52
Table 2-12:	Abandoned Borehole Simulations	2-54
Table 2-13:	Confining Bed Discontinuity Simulations	2-58
Table 3-1:	Age Groups Used in the Analysis.....	3-9
Table 3-2:	Radionuclide-Specific Ingestion Dose and Risk Coefficients	3-11
Table 3-3:	FGR 13 Drinking Water Cancer Morbidity / Mortality Risk Ratio.....	3-13
Table 3-4:	Risk Coefficient Uncertainty	3-14
Table 3-5:	Age-Dependent Weight Normalized Water Consumption Rates	3-15
Table 3-6:	Body Weight Distributions	3-16
Table 3-7:	Soil + Dust Ingestion	3-19
Table 3-8:	Element-Specific Input Parameters for Lognormal Distribution.....	3-20
Table 3-9:	Age-Dependent Weight Normalized Vegetable Consumption Rates.....	3-22
Table 3-10:	Age-Dependent Weight Normalized Milk Consumption Rates	3-26
Table 3-11:	Age-Dependent Weight Normalized Meat Consumption Rates.....	3-28
Table 3-12:	Calculated Total Pathway Dose Conversion Factors.....	3-29

Table 3-13:	Calculated Total Pathway Risk Conversion Factors.....	3-30
Table 3-14:	Typical Pathway Contributions to the Adult PDCF and PRCF	3-31
Table 3-15:	U-238+P Pathway Contributions to the Adult PDCF and PRCF	3-32
Table 3-16:	Typical Pathway Contributions to the Teen PDCF and PRCF	3-33
Table 3-17:	Typical Pathway Contributions to the Child PDCF and PRCF	3-34
Table 3-18:	Typical Pathway Contributions to the Infant PDCF and PRCF	3-34
Table 3-19:	Radionuclide-Specific Inhalation Dose and Risk Coefficients.....	3-39
Table 3-20:	Radionuclide-Specific Submersion Dose and Risk Coefficients.....	3-40
Table 3-21:	Other Parameters Used to Evaluate the Sweat Lodge Pathway.....	3-41
Table 3-22:	Air Moisture Content with Heat Indices of 130° F and 180° F	3-44
Table 3-23:	Calculated Native American Total Pathway Dose and Risk Conversion Factors.....	3-46
Table 3-24:	Native American Pathway Contributions to the PDCF	3-46
Table 3-25:	Native American Pathway Contributions to the PRCF.....	3-47
Table 3-26:	External Exposure to Contaminated Ground Screening Study Results	3-48
Table 3-27:	Data Used to Evaluate the PDCF for Home Radon Exposure.....	3-49
Table 3-28:	PDCF for Home Radon Exposure.....	3-50
Table 3-29:	Water Immersion Screening Calculation	3-50
Table 3-30:	Dose Coefficients to the Offspring from Chronic Intake by the Mother	3-51
Table 3-31:	PDCF to the Offspring from Chronic Intake by the Mother.....	3-52
Table 3-32:	Dose and Risk Coefficients from Breast Milk Consumption	3-53
Table 3-33:	PDCF/PRCF for Infant Milk Consumption	3-54
Table 4-1:	Representative Concentrations in Uranium Alkaline ISR Lixiviants	4-1
Table 4-2:	Highest Observed Concentrations in Pregnant Lixiviants based on a Survey of Licensing Documents.....	4-2
Table 4-3:	Estimated Range of K_d Values for Lead as a Function of Soil pH, and Equilibrium Lead Concentrations	4-4
Table 4-4:	Estimated Range of K_d Values for Uranium based on pH.....	4-5
Table 4-5:	Radium K_d Values by Soil Type.....	4-5
Table 4-6:	Summary of K_d Values and Lixiviant Concentrations Used in Dose and Risk Calculations	4-6
Table 4-7:	Radionuclide Well Limiting Concentrations	4-7
Table 4-8:	ISL Site Hydraulic Data.....	4-8
Table 4-9:	Excursion Scenario Maximum Doses and Risks – Mean Adult	4-11
Table 4-10:	Surface Leak Scenario Doses and Risks – Mean Adult.....	4-14
Table 4-11:	Excursion Scenario Non-standard Receptor Doses and Risks ^a	4-16
Table 4-12:	Leak Scenario Non-standard Receptor Doses and Risks ^a	4-16
Table 4-13:	Highest Contaminant Levels in Pregnant Lixiviant (mg/L)	4-18
Table 4-14:	Scenario Maximum Contaminant Levels Versus Limit.....	4-18

Table 5-1:	Typical Pathway Contributions to the Adult PDCF and PRCF	5-2
Table 5-2:	Typical Pathway Contributions to the PDCF and PRCF for U-234 or U-238.....	5-2
Table 5-3:	Radionuclide Source Term Limiting Concentrations – Receptor Well at 528 ft	5-3
Table 5-4:	Summary of Excursion Runs	5-4
Table 5-5:	Number of Simulations Resulting in Various Dose Levels as Function of Conductivity × Gradient Product.....	5-5
Table 5-6:	Excursion Scenario Maximum Doses and Risks	5-6
Table 5-7:	Summary of Dose Rate for Leak Scenarios – Adult Male Exposed to U nat at Receptor Well 328 ft Down-gradient.....	5-6
Table 5-8:	Comparison of Excursion Scenario Non-standard Receptor Doses and Risks Relative to 90 th Percentile Adult.....	5-7

List of Figures

Figure 1-1:	In-situ Uranium Recovery – Process Flow Diagram	1-2
Figure 2-1:	Idealized Schematic Cross Section to Illustrate Ore-Zone Geology and Lixiviant Migration from an Injection Well to a Production Well (NRC 2009b)	2-1
Figure 2-2:	Schematic Diagram of a Wellfield Showing Typical Injection/Production Well Patterns, Monitoring Wells, Manifold Buildings, and Pipelines (NRC 2009b)	2-2
Figure 2-3:	Plan View of the Model Grid for Leak Scenarios.....	2-15
Figure 2-4:	Cross Sectional View of the Model Grid for Leak Scenarios.....	2-16
Figure 2-5:	Relative Concentrations for L10 at 140 Days.....	2-23
Figure 2-6:	Relative Concentrations for L11 at 140 Days.....	2-24
Figure 2-7:	Relative Concentrations for L13 at 877 Days.....	2-25
Figure 2-8:	Relative Concentrations for L15 at 877 Days.....	2-26
Figure 2-9:	Maximum Relative Concentrations versus Time for All Leak Simulations.....	2-29
Figure 2-10:	Plan View of the Model Grid for Excursion Scenarios (Series 1 through 7)	2-31
Figure 2-11:	Cross Section View of the Model Grid for Excursion Scenarios (Series 1 through 7).....	2-32
Figure 2-12:	Plan View of Pumping\Injection Well Configurations and Receptor Locations for Excursion Scenarios (Series 1, 2, 5 and 6)	2-33
Figure 2-13:	Plan View of Pumping\Injection Well Configurations and Receptor Locations for Excursion Scenarios (Series 3 and 4)	2-34
Figure 2-14:	Example of Breakthrough Curves at Receptor Locations.....	2-35
Figure 2-15:	Plan View of the Twenty-five 5-spot Pumping/Injection Well Configurations and Receptor Locations for Excursion Scenario (Series 7)	2-51
Figure 2-16:	Plan View of the Model Grid for the Abandoned Borehole and Discontinuous Confining Bed Excursion Simulations	2-55
Figure 2-17:	Cross-Sectional View of the Model Grid for the Abandoned Borehole and Discontinuous Confining Bed Excursion Simulations	2-56
Figure 2-18:	Maximum Relative Concentrations versus Time for All Excursion Simulations	2-60
Figure 2-19:	Effect of Well Spacing at Constant Hydraulic Conductivity of 100 ft/day and Constant Hydraulic Gradient of 0.001.	2-61
Figure 2-20:	Effect of Well Spacing at Constant Hydraulic Conductivity of 100 ft/day and Hydraulic Gradients of 0.1(Runs 1a, 2a) or 0.001 (Runs 1c, 2c).....	2-61
Figure 2-21:	Effect of Well Spacing at Constant Hydraulic Conductivity of 100 ft/day and Hydraulic Gradients of 0.01(Runs 1b, 2b) and 0.001(Runs 1c, 2c).....	2-62
Figure 2-22:	Effect of Well Spacing on Concentration as a Function of Hydraulic Conductivity at a Constant Hydraulic Gradient of 0.1.	2-62

Figure 2-23:	Effect of Well Spacing on Concentration as a Function of Hydraulic Conductivity at a Constant Hydraulic Gradient of 0.01.	2-63
Figure 2-24:	Relative Concentrations as a Function of Hydraulic Conductivities and Gradients	2-63
Figure 2-25:	Relative Concentrations as a Function of Hydraulic Gradient (Run 1d - 0.1, Run 1g - 0.01) and Hydraulic Conductivity of 1 ft/day.....	2-64
Figure 2-26:	Relative Concentrations as a Function of Hydraulic Gradient (Run 1f - 0.1, Run 1i - 0.01) and Hydraulic Conductivity of 100 ft/day	2-64
Figure 2-27:	Correlation of Relative Concentration to Pumping Rate	2-65
Figure 2-28:	Correlation of Relative Concentration to Hydraulic Gradient.....	2-66
Figure 2-29:	Correlation of Relative Concentration to Hydraulic Conductivity (ft/day)	2-67
Figure 2-30:	Correlation of Relative Concentration to Hydraulic Gradient times Hydraulic Conductivity.....	2-68
Figure 2-31:	Correlation of Relative Concentration to Well Spacing	2-69
Figure 2-32:	Correlation of Relative Concentration to Pumping Array	2-70
Figure 2-33:	Correlation of Relative Concentration to Model Layer	2-71
Figure 3-1:	Exposure Pathways Analyzed.....	3-2
Figure 3-2:	Uranium Decay Series	3-10
Figure 3-3:	Distribution of Age-Dependent Weight Normalized Water Consumption Rates.....	3-16
Figure 3-4:	Distribution of Age-Dependent Water Consumption Rates Compared to Regulatory Guide 1.109 Recommended Maximum Rates	3-17
Figure 3-5:	Distribution of Age-Dependent Water Consumption Rates Compared to the RESRAD Distribution	3-18
Figure 3-6:	Distribution of Irrigation Water Application Rate.....	3-19
Figure 3-7:	Distribution of Vegetable Yields	3-22
Figure 3-8:	Distribution of Age-Dependent Weight Normalized Vegetable Consumption Rates.....	3-23
Figure 3-9:	Distribution of Fodder (Dry) Yield.....	3-25
Figure 3-10:	Distribution of Age-Dependent Weight Normalized Milk Consumption Rates.....	3-26
Figure 3-11:	Distribution of Age-Dependent Weight Normalized Meat Consumption Rates.....	3-29
Figure 3-12:	Cumulative Distributions of Pathway Contribution to the Total Adult U-238+P PCDF/PRCF	3-33
Figure 3-13:	Native American Drinking Water Rate Within the <i>Exposure Factors Handbook</i> Distribution	3-36
Figure 3-14:	Native American Vegetable Consumption Within the <i>Exposure Factors Handbook</i> Distribution	3-37
Figure 3-15:	Native American Meat Consumption Within the <i>Exposure Factors Handbook</i> Distribution	3-38

Figure 4-1:	Cumulative Distribution of ISL Site Hydraulic Data	4-9
Figure 4-2:	Excursion Scenario 6E Peak Dose Arrival Time, $K_d = 0.4$ ml/g	4-10
Figure 4-3:	Excursion Scenario Dose Results versus Time.....	4-10
Figure 4-4:	Excursion Scenario Dose Results versus Hydraulic Data.....	4-11
Figure 4-5:	Excursion Scenario Risk Results versus Time.....	4-12
Figure 4-6:	Excursion Scenario 6E Peak Dose Arrival Time, $K_d = 4.0$ ml/g	4-13
Figure 4-7:	Surface Leak Scenario Risk Results versus Time.....	4-14
Figure 4-8:	Surface Leak Scenario Risk Results versus Time.....	4-14
Figure 4-9:	28 Day Surface Leak Scenario Doses from Uranium.....	4-15

Appendices

Appendix A: Verification of Codes

Appendix B: Concentration Breakthrough Curves for Leak Scenarios Runs L-1 through L-24

Appendix C: Concentration Breakthrough Curves for Excursion Runs 1a through 7g

Appendix D: Concentration Breakthrough Curves for Abandoned Boreholes and Discontinuous Confining Unit Runs AB-R1, AB-R2, AB-R3, CBD-R1, and CBD-R2

LIST OF ACRONYMS AND ABBREVIATIONS

AMG	algebraic multi-grid
ATSDR	Agency for Toxic Substances and Disease Registry
Bq/kg	Becquerel per kilogram
CC	Change Control
CCA	Compliance Certification Application
CFR	<i>Code of Federal Regulations</i>
cm ³ /g	cubic centimeter per gram
CNWRA	Center for Nuclear Waste Regulatory Analyses
COPC	contaminant of potential concern
CRA	Compliance Recertification Application
CTUIR	Confederated Tribes of the Umatilla Indian Reservation
CVS	Concurrent Versions System
DD	Design Document
DDREF	dose and dose-rate effectiveness factor
DF	Decontamination Factor
DF _{SL}	Sweat Lodge Evaporation Decontamination Factor
DOE	U.S. Department of Energy
DW	drinking water
EFH	Exposure Factors Handbook
EPA	U.S. Environmental Protection Agency
FGR 13	Federal Guidance Report No. 13
ft/day	foot per day
g/cm ³	gram per cubic centimeter
g/day	gram per day
GCGCD	Goliad County Groundwater Conservation District
GM	geometric mean
gpm	gallons per minute
GSD	geometric standard deviation
I&C	Installation & Checkout
ICRP	International Commission on Radiological Protection
ID	Implementation Document
ISCORS	Interagency Steering Committee on Radiation Standards
ISL	in-situ leaching

ISR	in-situ recovery
K_d	distribution coefficient
kg/m^2	kilogram per square meter
kg/yr	kilogram per year
L	liter
LCF	latent cancer fatality
LET	linear energy transfer
LMG	Linked algebraic Multi-Grid solver
m	meter
m^3	cubic meter
M_{SL}	Sweat Lodge Air Moisture Content
mg/L	milligram per liter
ml/g	milliliter per gram
mrem	millirem
NAS	National Academy of Sciences
NCRP	National Council on Radiation Protection and Measurements
NRC	U.S. Nuclear Regulatory Commission
NWS	National Weather Service
PABC	Performance Assessment Baseline Calculation
PCG	Preconditioned Conjugate Gradient
pCi	picocurie
PDCF	pathway dose conversion factor
pH	measure of the acidity or alkalinity of a solution
PHA	public health assessment
PRCF	pathway risk conversion factor
psig	pounds per square inch, gauge
QA	Quality Assurance
RBE	relative biological effectiveness
RCRA	Resource Conservation and Recovery Act
RD	Requirements Document
Rf	retardation factor
SAB	Science Advisory Board (EPA)
SC&A	S. Cohen and Associates
SCMS	Software Configuration Management Plan

SIP	Strongly Implicit Procedure
SPR	Software Problem Report
Sv	sievert
UCL	upper control limits
UIC	underground injection control
UM	User's Manual
UMTRCA	Uranium Mill Tailings Radiation Control Act
U nat	natural uranium
USCB	U.S. Census Bureau
USDA	U.S. Department of Agriculture
USGS	U.S. Geological Survey
VD	Validation Document
VMS	Versions Management System
VVP	Verification and Validation Plan
WA	work assignment
WDEQ	Wyoming Department of Environmental Quality
WIPP	Waste Isolation Pilot Plant
WSDOH	Washington State Department of Health
μCi/ml	microcurie per milliliter

EXECUTIVE SUMMARY

EPA is proposing revisions to 40 CFR 192 to create a new subsection dealing specifically with in-situ mining of uranium. Since 40 CFR 192 was promulgated in 1983, there has been a shift in uranium recovery from conventional milling to in-situ leaching (ISL). In the ISL process,¹ chemical solutions are pumped underground through an array of wells into the ore body, where the uranium is dissolved in place. The uranium-rich solutions are pumped to the surface, where the uranium is extracted. The solutions are then chemically reformed and pumped back into the ore body to recover additional uranium. Several mechanisms can be postulated by which contaminants can leak from the ISL site and migrate to off-site wells. This report describes the ground water modeling studies and the calculated doses and risks to receptors residing down-gradient from a hypothetical ISL site who obtain water for drinking and agricultural purposes from a contaminated well on their property.

The steps involved in modeling doses and risks to receptors from contaminated ground water contaminated with radionuclides are as follows:

- (1) Based on an assumed initial unit source concentration C_i for the i^{th} radionuclide (1 mg/L), calculate the relative concentration in the ground water at a down-gradient receptor well (C_R). Convert to units of pCi/m³ based on specific activities.
- (2) Develop pathway dose and risk conversion factors for all components of the ingestion pathway, such as drinking water. For example, based on an annual drinking water consumption Ing_{wat} , (m³/yr) and a dose conversion factor DC_{Ing} (mrem per pCi) from EPA's Federal Guidance Report 13, the pathway dose conversion factor $PDCF_{wat}$ (mrem/yr per pCi/m³) is:

$$PDCF_{wat} = Ing_{wat} \times DC_{Ing}$$

- (3) Multiply the relative down-gradient receptor well concentration (C_R) by the ratio of the actual source concentration, C_S , to the unit source concentration (C_S/C_i) to obtain the actual down-gradient concentration, C_W . Then multiply C_W by the pathway dose conversion factor to obtain the annual dose, E_{wat} (mrem/yr) to an individual from drinking contaminated water from the receptor well:

$$E_{wat} = C_W \times PDCF_{wat}$$

The ground water modeling studies used the computer codes MODFLOW-2000 and MT3D. For all ground water simulations, an arbitrary source term concentration of 1 mg/L was assumed and concentrations at down-gradient receptor wells were calculated relative to this source term. The simulations were based on a hypothetical ISL site rather than a specific site and input parameters were selected according

¹ In-situ leaching (ISL) is also referred to as in-situ recovery (ISR).

Scenarios evaluated included excursions from wellfields which remain contained in the ore-bearing aquifer, catastrophic surface leaks such as that which might occur from a break in process piping, and slow surface leaks. For the surface leak scenarios, the leakage was assumed to reach an aquifer overlying the ore-bearing aquifer. Excursions from the ore zone to an overlying aquifer through an abandoned borehole and or through a natural pathway (e.g., a discontinuity in the intervening aquitard) between the ore-bearing aquifer and an overlying aquifer were also modeled.

A total of 63 excursion simulations involving transport of contaminants within the ore-bearing aquifer were run, of which 49 were unique simulations and the remaining 14 duplicated other model runs. Receptor wells for the leak scenarios were assumed to be located 328 ft, 656 ft, 1,640 ft and 3,280 ft down-gradient, while the excursion scenarios set the receptor well distances at down-gradient distances of 528 ft, 856 ft, 1,840 ft and 3,480 ft. The excursion scenarios involved operating an injection/extraction pattern(s) for 3 years and then shutting down the injection wells, but continuing to remove fluids from the extraction wells. The simulations were designed to evaluate the sensitivity of various physical and hydrogeologic properties to the relative down-gradient concentrations at receptor wells. Variables examined in the excursion simulations included:

- Well spacings (50, 150, and 250 ft)
- Hydraulic conductivity (1, 10, and 100 ft/day)
- Hydraulic gradient (0.001, 0.01, and 0.1 ft/ft)
- Pumping pattern (5-spot, multiple 5-spot, and 7-spot)
- Injection rates (7, 50, 150, and 500 gpm)
- Ore zone thickness (20 and 70 ft)

In all scenarios, the extraction rate was 2% greater than the injection rate during operation.

It is difficult to develop general conclusions from these excursion simulations because results of comparisons designed into the modeling runs are at times counter-intuitive. In spite of this difficulty, some conclusions are provided below, but the reader is cautioned to read the full text for complete understanding as to the limitations of these conclusions:

- As expected, steeper hydraulic gradients result in shorter travel times. Furthermore, since the pumping/injection wells are altering the regional hydraulic gradients, the arrival times are not linearly scaled.
- An increase in hydraulic conductivity causes the contaminant plume to become more elongated and leads to lower relative peak concentrations.
- At higher regional gradients, wider well spacings provide better capture of the lixiviant. At lower regional hydraulic gradients, however, better capture can be maintained at smaller well spacings.
- The 7-spot well pattern results in lower relative peak concentrations for all of the runs as compared to a 5-spot pattern.
- The effect of pumping/injection on hydraulic gradients is strongly affected by the transmissivity (i.e., hydraulic conductivity multiplied by thickness) of the geologic units.

The lower transmissivity results in shorter times to peak arrivals at the low and high gradients and a longer time at the medium gradient. These relationships are all related to how the regional and localized gradients created by the pumping/injection interact to form a capture zone. It also illustrates the complexity and need to understand the site-specific geology and flow system, since the effects of the interactions are not always intuitive.

- Comparison of a single 5-spot pattern with a multiple (25) 5-spot pattern shows that relative concentrations at down-gradient receptor wells are lower with the multiple 5-spot pattern. These results are explained by the larger capture zone that is created by the array of pumping/extraction wells.

Transport from the mined aquifer to an overlying aquifer through an abandoned borehole that was not properly cemented was also evaluated. This excursion scenario can result in significant down-gradient leakage. This emphasizes the need to carefully cement, test and inspect abandoned boreholes to insure their integrity.

As the first step in the dose/risk assessment, probabilistic pathway dose and risk conversion factors (PDCFs and PRCFs) were developed for the ingestion exposure pathway. For most of the scenarios considered here, ingestion is the only significant pathway. PDCFs/PRCFs relate the dose/risk received by an individual who utilizes the contaminated well water to the radionuclide concentration in the well water (e.g., millirem/year per picocurie/m³). Radionuclide specific pathway dose/risk conversion factors were calculated for U-234, U-238, Th-230 Ra-226, and Pb-210 based on conversion factors from FGR-13 and its supporting documents. Pathways evaluated included ingestion of milk, meat, water, contaminated soil, and vegetables. The basic mathematical models used to calculate the dose and risk from the ingestion pathways for this analysis were obtained from the Nuclear Regulatory Commission's (NRC's) Regulatory Guide 1.109. Although the numerical values for many of the parameters given in Regulatory Guide 1.109 have been updated since its publication more than 30 years ago, the basic mathematical models remain valid and form the basis for many of today's computer programs used to calculate radiological impacts. While the Regulatory Guide 1.109 models form the basis for many of today's computer programs, those computer programs often used more refined models to better reflect reality. When appropriate, these refined models have been used in this analysis.

Probabilistic PDCFs and PRCFs were generated for four age groups (Infant, Child, Teen and Adult) using Excel spreadsheets and Crystal Ball to execute Monte Carlo calculations. Table ES-1 and Table ES-2 summarize these factors. Mean pathway dose conversion factors were lowest for adults and increased for younger people.

Table ES-1: Calculated Total Pathway Dose Conversion Factors

	Adult	Teen	Child	Infant
Nuclide	Mean PDCF (mrem/yr / pCi/m³)			
Pb-210+P	6.28E-03	7.33E-03	1.10E-02	3.89E-02
Ra-226+P	1.30E-02	1.98E-02	2.62E-02	7.06E-02
Th-230	6.02E-04	3.62E-04	2.89E-04	4.27E-03
U-234	1.61E-04	1.53E-04	1.33E-04	4.19E-04
U-238+P	1.55E-04	1.47E-04	1.40E-04	4.24E-04
Nuclide	Median PDCF (mrem/yr / pCi/m³)			
Pb-210+P	5.16E-03	5.17E-03	6.91E-03	3.77E-02
Ra-226+P	1.01E-02	1.39E-02	1.65E-02	5.76E-02
Th-230	5.30E-04	2.76E-04	2.54E-04	4.37E-03
U-234	1.40E-04	1.15E-04	1.01E-04	4.11E-04
U-238+P	1.35E-04	1.10E-04	1.06E-04	4.16E-04
Nuclide	90th Percentile PDCF (mrem/yr / pCi/m³)			
Pb-210+P	1.06E-02	1.31E-02	1.40E-02	6.31E-02
Ra-226+P	2.23E-02	3.55E-02	4.28E-02	1.14E-01
Th-230	1.09E-03	7.43E-04	5.09E-04	7.28E-03
U-234	2.77E-04	2.75E-04	1.93E-04	6.97E-04
U-238+P	2.68E-04	2.64E-04	2.02E-04	7.06E-04

Table ES-2: Calculated Total Pathway Risk Conversion Factors

	Adult	Teen	Child	Infant
Nuclide	Mean PRCF (LCF/yr / pCi/m³)			
Pb-210+P	1.12E-09	1.62E-09	2.90E-09	4.33E-09
Ra-226+P	2.25E-09	3.83E-09	7.25E-09	7.60E-09
Th-230	3.07E-11	4.52E-11	4.69E-11	1.31E-10
U-234	2.21E-11	4.22E-11	6.92E-11	1.13E-10
U-238+P	2.28E-11	4.91E-11	9.00E-11	1.54E-10
Nuclide	Median PRCF (LCF/yr / pCi/m³)			
Pb-210+P	9.24E-10	1.14E-09	1.82E-09	4.20E-09
Ra-226+P	1.73E-09	2.69E-09	4.56E-09	6.23E-09
Th-230	2.69E-11	3.44E-11	4.13E-11	1.34E-10
U-234	1.91E-11	3.16E-11	5.23E-11	1.11E-10
U-238+P	1.98E-11	3.67E-11	6.80E-11	1.51E-10

Table ES-2: Calculated Total Pathway Risk Conversion Factors

	Adult	Teen	Child	Infant
Nuclide	90th Percentile PRCF (LCF/yr / pCi/m³)			
Pb-210+P	1.89E-09	2.88E-09	3.69E-09	7.00E-09
Ra-226+P	3.86E-09	6.88E-09	1.19E-08	1.23E-08
Th-230	5.60E-11	9.27E-11	8.27E-11	2.22E-10
U-234	3.79E-11	7.58E-11	1.00E-10	1.89E-10
U-238+P	3.92E-11	8.80E-11	1.30E-10	2.56E-10

LCF = latent cancer fatality

Comparing Table ES-1 to Table ES-2 shows that the dose-to-risk relationship varies by a little over an order of magnitude, from about 3×10^{-8} to 6×10^{-7} latent cancer fatality per millirem, depending on the radionuclide and age group.

The relative contributions for the modeled ingestion pathways for an adult are summarized in Table ES-3.

Table ES-3: Typical Pathway Contributions to the Adult PDCF and PRCF

Pathway – Adult		Pb-210+P	Ra-226+P	Th-230	U-234	U-238+P
Ingestion of Drinking Water		78.3%	51.2%	82.8%	76.2%	76.2%
Inadvertent Ingestion of Soil		0.1%	0.2%	0.3%	0.3%	0.3%
Ingestion of Vegetables	Leaf Deposition	13.5%	8.8%	14.3%	13.1%	13.1%
	Root Uptake	2.3%	26.5%	2.1%	2.9%	2.9%
Ingestion of Meat	Cattle Drinking	0.3%	0.2%	0.0%	0.3%	0.3%
	Leaf Deposition	1.6%	1.3%	0.2%	1.5%	1.5%
	Root Uptake	0.3%	1.1%	0.0%	0.3%	0.3%
	Soil Ingestion	0.1%	0.3%	0.0%	0.3%	0.3%
Ingestion of Milk	Cow Drinking	0.3%	0.7%	0.0%	0.4%	0.4%
	Leaf Deposition	2.2%	4.8%	0.0%	2.8%	2.8%
	Root Uptake	0.5%	4.1%	0.0%	0.6%	0.6%
	Soil Ingestion	0.5%	1.0%	0.2%	1.2%	1.2%

The water ingestion pathway dominates for all of the radionuclides.

Deterministic PDCFs and PRCFs were also developed for Native Americans whose lifestyle was significantly different from the standard adult receptor. Insufficient data on intake parameters were available to do these analyses probabilistically. In addition to the ingestion pathways evaluated for the standard receptors, exposures from sweat lodge rituals were included. Added pathways involved submersion in a steam vapor cloud and inhalation of contaminated steam. Results for PDCFs for mean adults and Native Americans are compared in Table ES-4. The PDCFs for Native Americans are about 2 to 3 times higher than the mean for standard adult receptors for Ra-226+P, Th-230, U-234, and U-238+P. For Pb-210+P, the PDCF for the mean adult is higher than for the Native American.

Table ES-4: Calculated Pathway Dose Conversion Factors for Native Americans and Adults (mean)

Nuclide	Native American PDCF (mrem/yr / pCi/m ³)	Adult (mean) PDCF (mrem/yr / pCi/m ³)
Pb-210+P	5.10E-03	6.28E-03
Ra-226+P	2.68E-02	1.30E-02
Th-230	1.94E-03	6.02E-04
U-234	4.14E-04	1.61E-04
U-238+P	3.70E-04	1.55E-04

Doses and risks were calculated for many of the excursion simulations within the ore-bearing aquifer using expected concentrations in the leaking lixiviant. In some cases, the excursion simulations used combinations of hydraulic parameters that were outside the ranges for operating ISL sites. This was done to evaluate the sensitivity of various ground water modeling parameters to variations in model output. However, dose and risk assessments were limited to parameter ranges expected at operating facilities. Based on available site information, a cumulative distribution function of hydraulic gradient \times hydraulic conductivity (as a surrogate for ground water velocity) was developed. From this distribution function, it was determined that all values of the conductivity/gradient product were <0.13 ft/day. Of the 29 unique excursion simulations that met the conductivity \times gradient cutoff of 0.13 ft/day, the dose from uranium was >15 mrem/yr in 17 simulations. The highest estimated dose from uranium at a receptor well 528 ft down-gradient was 10,072 mrem/yr, while the lowest estimated dose was $1.69\text{E}-12$ mrem/yr. The annual uranium dose at 528 ft down-gradient was less than 15 mrem for all of the scenarios with a hydraulic conductivity of 1 ft/day and a hydraulic gradient of 0.001.

Table ES-5 shows the maximum calculated dose for various radionuclides from all 37 excursion scenarios that were analyzed for the mean adult. Clearly, uranium and Ra-226 (+ progeny) are the significant contributors to dose and risk. The contribution from Th-230 is one to two orders of magnitude lower.

Table ES-5: Excursion Scenario Maximum Doses and Risks – Mean Adult

Nuclide	Dose (mrem/yr)	Risk (LCF/yr)
U nat	1.0E+04	1.4E-03
Th-230	2.4E+02	1.2E-05
Ra-226+P	2.8E+04	4.8E-03

Table ES-6 summarizes doses and risks to various receptors from excursion scenarios. From this table, it is apparent that the Mean Infant is the recipient of the largest calculated doses and risks. The Mean Infant doses and risks are about a factor of three to eight times larger than the standard receptor doses and risks. The dose and risk ratios of the other non-standard receptors to the standard receptor are less than for the Mean Infant. For example, the Native American has a calculated uranium risk that is 3.1 times greater than the standard receptor's mean uranium risk. The maximum doses and risks in Table ES-6 are for particular combinations of wellfield design parameters and hydrogeologic parameters. However, as described above, various combinations

of wellfield design and hydrogeologic parameters based on actual ISL facilities can result in annual doses of less than 15 mrem.

Table ES-6: Excursion Scenario Doses and Risks to Various Receptors

Receptor	Nuclide	Maximum	
		Dose (mrem/yr)	Risk (LCF/yr)
90 th Percentile Adult	U nat	1.7E+04	2.5E-03
	Th-230	4.4E+02	2.2E-05
	Ra-226+P	4.7E+04	8.2E-03
Mean Teenager	U nat	9.6E+03	2.9E-03
	Th-230	1.5E+02	1.8E-05
	Ra-226+P	4.2E+04	8.2E-03
Mean Child	U nat	8.7E+03	5.1E-03
	Th-230	1.2E+02	1.9E-05
	Ra-226+P	5.6E+04	1.5E-02
Mean Infant	U nat	2.7E+04	8.5E-03
	Th-230	1.7E+03	5.3E-05
	Ra-226+P	1.5E+05	1.6E-02
Native American	U nat	2.5E+04	4.3E-03
	Th-230	7.8E+02	4.0E-05
	Ra-226+P	5.7E+04	1.0E-02

a – Doses for Ra-226 include progeny

Three surface leakage scenarios were evaluated: (1) catastrophic spills ranging from 100,000 to 200,000 gallons, (2) a slow leak of 1 to 2 gpm for a period of 3 years, and (3) leaks varying from 1 to 40 gpm over a 28-day period. The highest doses were incurred for scenarios involving a slow leak over a 3-year period, while the lowest doses resulted from a 1 gpm surface leak over a 28-day period. For all scenarios, the annual doses to a mean adult from U nat were greater than 15 mrem. Results are summarized in Table ES-7.

Table ES-7: Surface Leak Scenario Doses and Risks

	Dose (mrem/yr)		Risk (LCF/yr)	
	Minimum	Maximum	Minimum	Maximum
U nat	3.2E+01	1.7E+03	4.5E-06	2.4E-04
Th-230	7.6E-01	4.0E+01	3.9E-08	2.0E-06
Ra-226 + P	8.7E+01	4.6E+03	1.5E-05	7.9E-04

The scenarios examined focus on failures of the ISR operations that are possible but unlikely if the operations are carefully monitored by the operators and the regulatory authorities. These failure scenarios contain some conservative assumptions that are typical of risk assessments and may not apply in any specific situation because of population distribution differences and the magnitude and duration of the exposure scenarios examined versus an actual occurrence. Results of these calculations point to the need for a rigorous regulatory regime applied to ISR operations.

Rigorous monitoring of the ISR operations would minimize the potential for these failure scenarios and minimize exposures if they were to happen.

1.0 INTRODUCTION

In 1983, the U.S. Environmental Protection Agency (EPA) promulgated regulations at *40 CFR Part 192 – Health and Environmental Protection Standards for Uranium and Thorium Mill Tailings* in response to the statutory requirements of the Uranium Mill Tailings Radiation Control Act (UMTRCA) of 1978 and the Atomic Energy Act of 1954 as amended. At the time 40 CFR 192 was promulgated, uranium recovery from ore was based almost exclusively on the conventional milling process, where a few pounds of uranium were recovered for each ton of ore mined and processed (milled). The residues from the milling process (the tailings) were accumulated in large piles on the surface at the mill site. Concern that these tailings piles would be a continuing source of radiation exposure unless properly reclaimed was the driving force behind the passage of UMTRCA. Virtually no attention was directed to other uranium recovery operations, such as heap leaching and in-situ leaching, since at that time, the major environmental risk was perceived to come from the conventional uranium mill tailings piles.

EPA's Office of Air and Radiation (ORIA) is currently reviewing 40 CFR Part 192 to determine what, if any, revisions are needed to the regulations to bring them up to date. In support of EPA's effort, ORIA requested SC&A, Inc. (SC&A) to perform a series of studies and analyses that evaluate the potential impacts to individuals living near an operating ISL uranium recovery facility,

The regulations under review by EPA establish standards for protection of the public health, safety, and environment from radiological and non-radiological hazards associated with uranium and thorium ore processing and their associated wastes. The cross-media standards apply to pollution emissions and site restoration. The existing 40 CFR Part 192 is utilized by the U.S. Nuclear Regulatory Commission (NRC) and its Agreement States,² and the U.S. Department of Energy (DOE) in their oversight of uranium extraction facility licensing, operations, sites, and wastes. UMTRCA requires EPA to develop health and environmental standards for both Title I inactive mill sites administered by the DOE and Title II and future NRC-licensed sites. For future NRC-licensed sites, the standards shall be "... consistent with the standards required under subtitle C of the Solid Waste Disposal Act,³ as amended, which are applicable to such hazards."⁴

Since 40 CFR 192 was promulgated, there has been a shift in uranium recovery from conventional milling to in-situ leaching (ISL) where, in a sense, a portion of the milling process is conducted underground within the ore body. In the ISL process,⁵ chemical solutions are pumped underground through an array of wells into the ore body, where the uranium is dissolved in place. A process flow diagram for a ISL facility is shown in Figure 1-1. The uranium-rich solutions are pumped to the surface, where the uranium is extracted. The solutions are then chemically reformed and pumped back into the ore body to recover additional uranium.

² There are currently 37 Agreement States that are responsible through the state radiation control directors and staff, under authority of Section 274 of the Atomic Energy Act of 1954, as amended, to regulate certain uses of radioactive materials within the state.

³ Now known as the Resource Conservation and Recovery Act (RCRA).

⁴ U.S.C. Title 42, Chapter 23, Section 2022.

⁵ In-situ leaching (ISL) is also referred to as in-situ recovery (ISR).

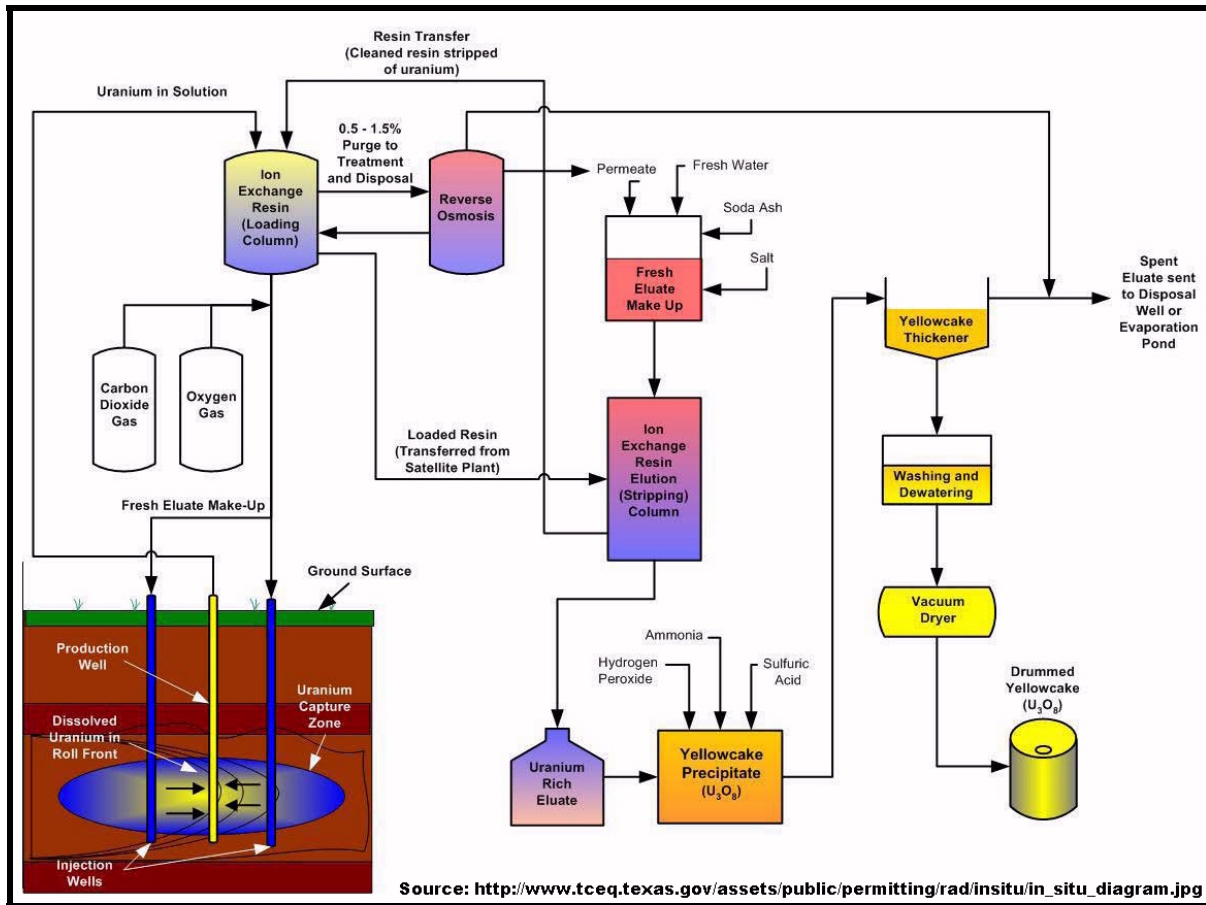


Figure 1-1: In-situ Uranium Recovery – Process Flow Diagram

ORIA requested advice from the EPA Science Advisory Board (SAB) related to the Agency’s review of 40 CFR Part 192 with regard to ISL facilities. SC&A provided a separate report summarizing relevant background information and statistical modeling approaches to assist EPA in defining the technical issues to be considered by the SAB (SC&A 2011a). Additionally, SC&A performed several other technical ISL studies in support of ORIA’s review of Part 192. For example, under Task 4 of Work Assignment (WA) 1-11 (Contract EP-D-10-042), SC&A was required to collect information pertinent to site characteristics of existing heap and in-situ leaching operations, including ground water quality and chemistry before and after leaching. This information was summarized in a report entitled *Modeling of Heap Leach and In-Situ Leaching Operations* (SC&A 2011b). This report was revised under Task 2 of WA 2-06 (SC&A 2011c) (Contract EP-D-10-042). In addition, under WA 4-17, Task 6 (Contract No. EP-D-05-002), SC&A prepared a database of ground water information as described in *Database Summary Analysis Report: Uranium Mills and In-Situ Leach Facilities* (SC&A 2008). These reports provided background information used to develop the current report.

This report presents the results of ground water modeling studies on possible releases from hypothetical ISL facilities based on a range of release scenarios. The studies were designed to demonstrate whether or under what conditions leakage of various types from an ISL site to a down-gradient receptor well can result in hazardous situations. The studies do not address

specific sites. The modeling studies considered the effects of a range of site and hydrologic variables on releases to a down-gradient receptor well. The intent was to systematically examine how changing these parameters alters the concentrations of various potentially hazardous constituents (mainly radionuclides) at down-gradient well relative to the concentration in the ore zone. As such, the ground water modeling studies did not consider retardation effects, such as radiological decay or other removal mechanisms. The relative concentrations at the receptor wells were subsequently converted to specific concentrations by taking into account the concentrations of specific elements at the point of release (based on reported values from actual ISL sites). Retardation was considered only to the extent that it staggered the arrival times of the different radionuclides at the receptor well. These specific down-gradient concentrations were then used to calculate doses and risks using a stochastic, ingestion-based biosphere model. Unlike the ground water modeling, the dose and risk modeling was limited to those combinations of hydraulic parameters that are representative of actual ISL sites. Ingestion of well water and products contaminated by well water are typically the dominant exposure pathways.

This report is not intended to provide a template as to how ground water modeling studies should be conducted at specific sites to support specific regulatory requirements, but rather its purpose is to scope the magnitude of potential problems that may be caused by mining solutions escaping from ISL wellfields. As such, in some instances assumptions were made that might result in lower radionuclide concentrations at the receptor well and/or lower doses/risks. This approach was acceptable here, since higher concentrations and/or doses/risks would only serve to make the potential problem worse. This is the converse to a typical site specific ground water modeling study, which would tend to make assumptions that result in maximizing the receptor well concentrations and/or doses/risks.

This report is divided into six chapters. Following this introductory chapter, Chapter 2 describes the ground water modeling studies, which employed the computer codes MODFLOW-2000 and MT3D. Scenarios evaluated included excursions from wellfields, which remain in the ore-bearing aquifer; catastrophic surface leaks, such as those which might occur from a break in process liquor piping; and slow surface leaks. For the surface leak scenarios, the leakage was assumed to reach an aquifer overlying the ore-bearing aquifer. Leaks from the ore zone to an overlying aquifer through an abandoned borehole and or through a natural pathway between the ore-bearing aquifer and an overlying aquifer were also modeled. One of the key objectives of the ground water modeling studies was to evaluate the range of possible releases that might occur under various hydrologic regimes. For example, the impact of hydraulic conductivity and hydraulic gradient were each examined over a range covering two orders of magnitude. While this approach was useful in delineating the sensitivity of each variable, unrealistic combinations of parameters could result. For example, in studying the effect of hydraulic conductivity, the procedure is to select a reasonable value of hydraulic gradient (based on reported data) and vary the conductivity over the range selected for evaluation. In this way one obtains a clear picture of the effect of releases as a function of hydraulic conductivity at a fixed gradient. While the generic effects are clearly delineated, the combinations of conductivity and gradient in some simulations may exceed actual site values. This possibility is addressed in the risk assessments by limiting the combinations of hydraulic gradient and hydraulic conductivity to those reported for actual ISL sites. The ground water modeling assumed a constant source term of 1 mg/L and did not consider radionuclide-specific retardation.

In Chapter 3 of this report, we describe the development of probabilistic pathway dose and risk conversion factors (PDCFs and PRCFs). Radionuclide-specific dose and risk conversion factors were based on Federal Guidance Report 13 (Eckerman et al. 1999) and information supporting that document. The PDCFs and PRCFs were developed for standard receptors and for non-standard receptors (specifically Native Americans and young children). As noted above, the ingestion pathways are the primary exposure pathways considered, except for Native Americans, where exposure during sweat lodge rituals is also included as an exposure pathway. Discussion of other exposure pathways is provided to indicate that their contribution to total radiation exposure is minimal.

In Chapter 4, doses and risks for various scenarios are developed, based on: (1) source terms for ISL sites reported in the literature, (2) documented values of distribution coefficients (K_{ds}), (3) ground water dispersion, as documented in Chapter 2, and (4) the PDCFs and PRCFs developed in Chapter 3. Since the radionuclides of interest have long half-lives (i.e., U-234, U-238, Th-230, and Ra-226), ground water retardation delays the time to peak dose, but not its magnitude. Doses and risks are calculated for both standard and non-standard receptors. The standard receptor was assumed to be an adult individual who represents the 50th percentile dose/risk. Non-standard receptors include adult individuals at the 90th percentile, teenagers, children, infants, and Native Americans.

Summary and conclusions are presented in Chapter 5, followed by the last chapter which provides a list of references used to develop this report.

2.0 GROUND WATER MODELING OF IN-SITU LEACHING FAILURE SCENARIOS

2.1 In-Situ Leaching Process

During ISL operations, chemicals such as sodium carbonate/bicarbonate, ammonia, sulfuric acid, gaseous oxygen, and hydrogen peroxide are added to the ground water to produce a concentrated oxygen-rich leaching solution called the lixiviant. The lixiviant is injected into the production zone to mobilize (dissolve) uranium from the underground formation, and this mobilized uranium is pumped back to the surface for extraction at a processing plant (Figure 2-1).

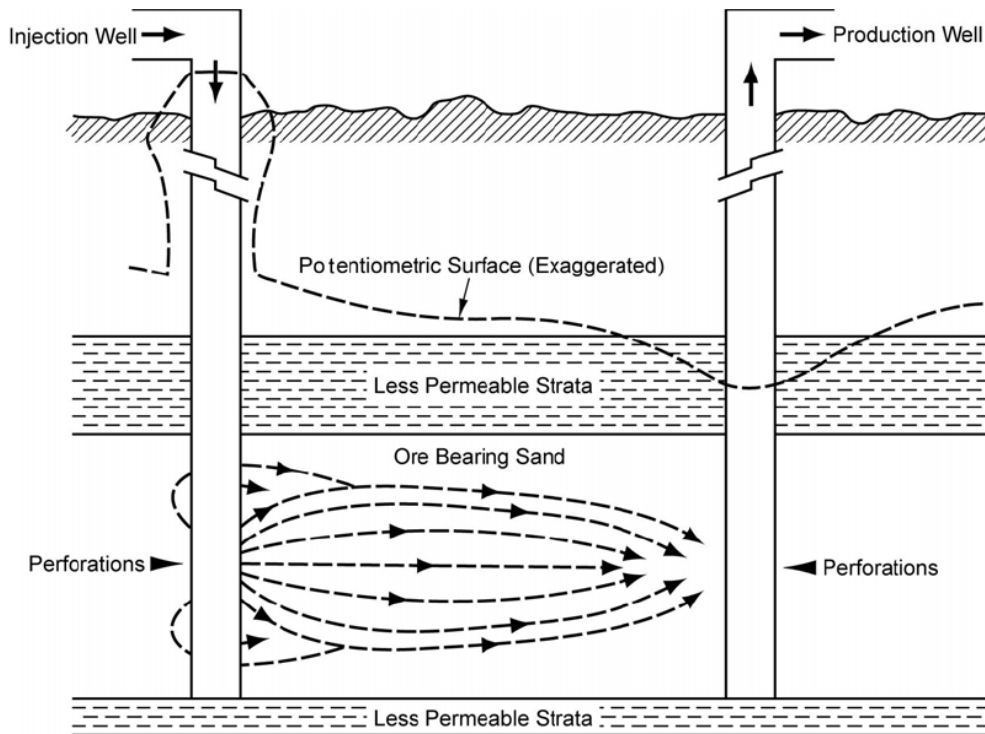


Figure 2-1: Idealized Schematic Cross Section to Illustrate Ore-Zone Geology and Lixiviant Migration from an Injection Well to a Production Well (NRC 2009b)

The most common injection/pumping patterns are 5- and 7-spot (NRC 2003). The shape of the mineralized ore body and surface topography, however, may give rise to other patterns (NRC 1997). A typical 5-spot pattern contains 4 injection wells and 1 recovery well. The dimensions of the pattern vary depending on the mineralized zone, but the injection wells are generally between 40 to 150 ft apart. In order to effectively recover the uranium and also to complete the ground water restoration, the wells are often completed so that they can be used as either injection or recovery wells. During mining operations, a slightly greater volume of water will be recovered from the mineralized zone aquifer than injected in order to create a cone of depression or a flow gradient towards the recovery wells. A typical well arrangement using 5- and 7-spot patterns is shown in Figure 2-2.

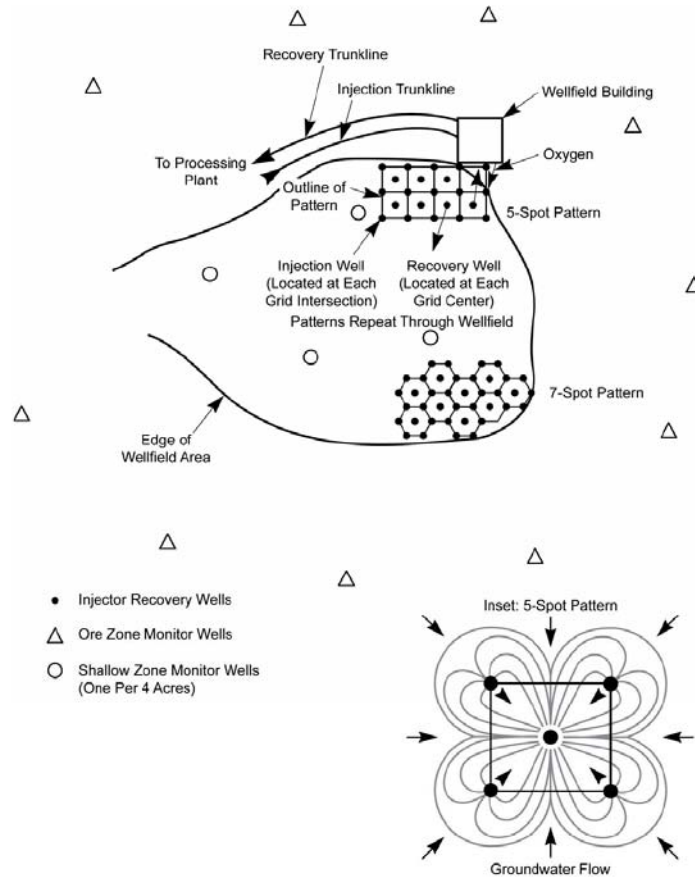


Figure 2-2: Schematic Diagram of a Wellfield Showing Typical Injection/Production Well Patterns, Monitoring Wells, Manifold Buildings, and Pipelines (NRC 2009b)

Ore body size and geometry will also influence the number of wells in a wellfield. For example, at the Crow Butte ISL facilities in Dawes County, Nebraska, the number of injection and production wells varied from about 190 in the first wellfield (MU-1) to about 900 in later wellfields (MU-5 and MU-6) (NRC 1998). Three types of wells are predominant at uranium ISL facilities:

- (1) Injection wells for introducing solutions into the uranium mineralization
- (2) Production wells for extracting uranium-enriched solutions
- (3) Monitoring wells for assessing ongoing operations

Deep injection wells permitted by the EPA or state and approved by NRC may also be drilled for liquid waste disposal. Injection and production wells are connected to manifolds in a nearby header house.

Commercial-scale uranium ISL facilities usually have more than one wellfield. For example, the Crow Butte facility in Dawes County, Nebraska, has constructed 10 wellfields since 1991 (CBR 2007). The locations and boundaries for each wellfield are adjusted as more detailed data on the

subsurface stratigraphy and uranium mineralization distribution are collected during wellfield construction.

General information on ISL facilities is included in NRC 2009b.

2.2 Failures during Operations

Potential releases that may occur during operations involve the following scenarios: (1) spills and leaks on the surface and subsequent transport to the ground water, and (2) excursions beyond the injection/production wells or into other non-mined geologic units above and/or below the mined unit.

During operations, ISL operations may affect the ground water quality near the wellfields when lixiviant moves from the production zone to beyond the boundaries of the wellfield. This unintended spread, either horizontally or vertically, of recovery solutions beyond the production zone is known as an excursion. An excursion can be caused by:

- Improper water balance between injection and recovery rates
- Undetected high permeability strata or geologic faults
- Improperly abandoned exploration drill holes
- Discontinuity within the confining layers
- Poor well integrity, such as a cracked well casing or leaking joints between casing sections
- Hydrofracturing of the ore zone or surrounding units

NRC license and underground injection control (UIC) permit conditions⁶ require that licensees conduct periodic tests to protect against excursions. These include, but are not limited to:

- Conducting pump tests for each wellfield prior to operations within the wellfield to evaluate the confinement of the production horizon.
- Continued wellfield characterization to identify geologic features (e.g., thinning confining layers, fractures, high flow zones) that might result in excursions.
- Mechanical integrity testing of each well to check for leaks or cracks in the casing. An excursion that moves laterally from the production zone is a horizontal excursion. Vertical excursions occur where barren or pregnant lixiviant migrates into other aquifers above or below the production zone.

Operators must maintain ground water monitoring programs to detect both vertical and horizontal excursions, and must have operating procedures to analyze an excursion and determine how to remediate it. Monitoring wells are sampled at least every 2 weeks during

⁶ Lixiviant injection wells are classified as Type III injection wells and must meet the requirements set forth in 40 CFR 144.

wellfield operations to verify that ISL solutions are contained within the operating wellfield (NRC 2003). Geochemical excursion indicators are identified based on wellfield pre-operational baseline water quality.

The spacing of horizontal excursion monitoring wells is based on site-specific conditions, but typically they are spaced about 90–150 m [300–500 ft] apart and screened in the production zone (NRC 1997 and 2003; Mackin et al. 2001; EIA 1995). The distance between monitoring wells and the distance of monitoring wells from the wellfield are typically similar (NRC 1997 and 2006). The specific location and spacing of the monitoring wells is established on a site-by-site basis by license condition. These are often modified according to site-specific hydrogeologic characteristics, such as the extent of the confining layer, hydraulic gradient, and aquifer transmissivity. Well placement may also be modified as the licensee gains experience detecting, recovering, and remediating these excursions. NRC licenses also include requirements to establish monitoring wells in overlying and, as appropriate, in underlying aquifers to detect vertical excursions. Although uranium deposits are typically located in hydrogeologic units bounded above and below by adequately confining units, the possibility of vertical contaminant transport must be considered. Historically, these monitoring wells are more widely spaced than those within the host aquifer, although underlying aquifer monitoring wells may not be required under some circumstances (Mackin et al. 2001). Frequency of vertical monitoring wells at licensed ISL facilities has been (1) 1 monitoring well per 4 acres of wellfield in the first overlying aquifer, (2) 1 monitoring well per 8 acres in each higher aquifer, and (3) 1 monitoring well per 4 to 8 acres in the underlying aquifer (Mackin et al. 2001). These monitoring wells are typically sampled every 2 weeks during operations.

An excursion is defined to occur when two or more excursion indicators in a monitoring well exceed their upper control limits (UCLs) (NRC 2003).⁷ Alternatively, since the advent of performance-based licensing, procedures to identify excursions can be imposed through site-specific license conditions. For example, an excursion may be defined to occur when one excursion indicator is exceeded in a monitoring well by a certain percentage. If an excursion is detected, the licensee takes several steps including notifying NRC and confirming the excursion through additional and more frequent sampling (NRC 2003, Chapter 8). As described in NRC guidance (NRC 2003, Section 5.7.8.3), licensees typically recover from horizontal excursions by adjusting the flow rates of the nearby injection and production wells to increase process bleed in the area of the excursion. To address vertical excursions, licensees may adjust injection and production flow rates in the area of the excursion and pump directly from the affected monitoring wells or from other wells drilled for that purpose. Vertical excursions are more difficult to recover from, persisting for years in some cases. If an excursion cannot be recovered,

⁷ “Upper control limits are concentrations for excursion indicator constituents [e.g., *chloride, total dissolved solids or bicarbonate*] that provide early warning that leaching solutions are moving away from the well fields and that groundwater outside the monitor well ring may be threatened. Excursion indicator constituents should be parameters that are strong indicators of the *in situ* leach process and that are not significantly attenuated by geochemical reactions in the aquifers. If possible, the chosen parameters should be easily analyzed to allow timely data reporting. The upper control limit concentrations of the chosen excursion indicators should be set high enough that false positives (false alarms from natural fluctuations in water chemistry) are not a frequent problem, but not so high that significant ground-water quality degradation could occur by the time an excursion is identified. A minimum of three excursion indicators should be proposed” (NRC 2003).

the licensee may be required to stop injection of lixiviant into a wellfield (NRC 2003, Section 5.7.8.3).

2.3 Failures after Shutdown

Prior to implementing post-closure monitoring, aquifer restoration activities are conducted. The purpose of aquifer restoration is to return wellfield water quality parameters to the standards in 10 CFR 40, Appendix A, Criterion 5(B)(5) or another standard approved by NRC. Ground water adjacent to the exempted portion of the aquifer, however, must still be protected. Prior to wellfield operations, applicants and licensees must determine baseline ground water quality for the production zone (NRC 2003). In their applications, applicants or licensees identify the NRC-accepted list of constituents to be sampled. Operators may identify other constituents, or remove constituents, as long as a basis for the constituent(s) is provided and approved by NRC. State and other federal agencies with jurisdiction over ground water could also specify constituents, which may or may not be included in the NRC-accepted list. In this case, the applicant would be accountable to the subject state or federal agency for characterizing and restoring these constituents. To determine baseline water quality conditions prior to wellfield operations, applicants or licensees collect at least four sets of samples, spaced sufficiently in time to establish seasonal variability, and analyze the samples for the identified constituent (NRC 2003). An NRC-acceptable set of samples should include all wellfield perimeter monitoring wells and all upper and lower monitoring wells. Additionally, the applicant or licensee should sample at least one production/injection well per acre in the wellfield, or enough production/injection wells to provide an adequate statistical population if less than one well per acre is used. NRC verifies the accuracy of baseline water quality data by ensuring that the applicant's or licensee's procedures include (1) acceptable sample collection methods, (2) a set of sampled parameters that is appropriate for the site and ISL extraction method, and (3) collection of sample sets that are sufficient to represent natural spatial and temporal variations in water quality.

After uranium recovery has ended, the ground water in the wellfield contains constituents that were mobilized by the lixiviant. Licensees usually begin aquifer restoration in each wellfield soon after the uranium recovery operations end (NRC 2008). Aquifer restoration criteria for the site-specific baseline constituents are determined either on a well-by-well or wellfield-by-wellfield basis. NRC licensees are required to return water quality parameters to the standards in 10 CFR Part 40, Appendix A, Criterion 5B(5) or to another standard approved in their NRC license (NRC 2009a). Aquifer restoration programs typically use a combination of methods, including (1) ground water transfer, (2) ground water sweep, (3) reverse osmosis with permeate injection, (4) ground water recirculation, and (5) stabilization monitoring (EIA 1995; Mackin et al. 2001; Davis and Curtis 2007). NRC allows licensees the flexibility to select the restoration methods to be used for each wellfield (NRC 2003). The EPA or state authorized to implement the EPA underground injection control program reviews any aquifer restoration plans for compliance with the applicable terms and conditions of the UIC permit requirements. NRC staff review any aquifer restoration plans for compliance with the NRC license to protect human health, safety, and the environment.

2.4 Ground Water Model Development

To investigate potential impacts caused by ISL facilities on ground water, the following activities were performed as described in this report: (1) development of a representative ISL facility, (2) implementation of a deterministic modeling methodology, (3) definition of release scenarios, (4) performance of a sensitivity analysis, and (5) calculation of risks based upon potential doses to receptors for selected simulations.

Ground water flow and contaminant transport modeling are frequently conducted at ISL facilities to evaluate possible effects of proposed and ongoing mining. For instance, a three-dimensional ground water flow and contaminant transport model was constructed to evaluate the ISL facility in Goliad County, Texas (DBS&A 2007). This modeling was performed for the Goliad County Groundwater Conservation District (GCGCD) and the major objectives of the modeling study were to (1) evaluate the practicality of controlling injection fluid excursions from escaping downdip, (2) evaluate the practicality of controlling injection fluid excursions from escaping vertically into non-mined aquifer zones, and (3) determine the amount of bleed water required to control or eliminate such excursions. **ADD NRDC 2012**

The modeling at the Goliad site is particularly relevant to this current task for the following reasons: (1) several of the modeling objectives are very similar, (2) the modeling approach that was taken is analogous to the approach undertaken here, and (3) the computer codes that were used are identical to those used for the modeling in this report. Furthermore, as presented below, the modeling conclusions have implications with respect to the occurrence of potential for excursions during active mining, the placement and depths of monitoring wells, sampling frequencies, and post-closure monitoring timeframes. As described in DBS&A 2007:

Simulation results indicate that capture of injected fluids within the mined zone with 1 percent bleed water is feasible, although the simulation results are very sensitive to well placement, selected injection and pumping rates, and hydraulic conductivity of the aquifer. In some cases, an increase of even 20 feet in the well spacing caused the simulated bleed water to increase by about 6 percent.

In addition, the nature of the hydraulic groundwater flow field that may develop due to mining leads to the formation of long, low-velocity travel paths in certain areas of the injection-capture system; impacted groundwater within or near these travel paths may not be extracted during the life of the mining operation if a specific approach is not designed and implemented to account for these aquifer regions. Most of the injected fluid is extracted at capture wells within a time frame of about 3 years or less for the scenarios evaluated. At the cessation of ISL mining, monitoring locations should be selected carefully in order to identify potential groundwater impacts in the vicinity of these longer, low-velocity pathways. In addition, groundwater monitoring should be continued for an extended period of time.

The simulation results also indicate that ISL fluids can, and likely would, migrate vertically between aquifer layers. The ISL scenario evaluated assumes that

injection and pumping would occur in the uppermost layer of the Evangeline aquifer (Goliad Sand), which has a saturated thickness of approximately 105 feet in the model. ISL fluids migrate vertically downward in the vicinity of the injection well. Once these fluids enter the model layer below the mined layer, they are not recaptured by the pumping wells, but rather migrate with the ambient groundwater flow velocity of the deeper aquifer layer.

2.4.1 Basic Aspects of Computer (Numerical) Modeling

The flow and transport modeling performed for this analysis uses finite-difference techniques, which require that the ground water system be divided ('discretized') into finite-sized blocks or 'cells.' Each cell is assigned unique hydraulic properties depending on the available field data and the goals for the analysis. In this way, complex features of the ground water system can be accommodated in the model. The time represented by the modeling effort must also be divided into discrete periods or 'time steps.' These steps must be short enough to provide an accurate solution, but not so short that they require an excessive number of calculations to run a simulation. The finite-difference method also requires that values for head be assigned at flow boundaries (referred to as 'boundary conditions'), as well as for the initial time period of the simulation (referred to as 'initial conditions'). This is a requirement for producing a unique solution with any numerical method that depends on iteration, as does the finite-difference method. Models were applied that simulate ground water flow and chemical transport.

The three-dimensional computer model for analyzing ground water flow generates a flow field (array of head values) representing average conditions in the model area. The flow model is used as the basis for the transport model.

The chemical transport model evaluates how the average flow field, along with other transport parameters, affects chemical movement in ground water and plume development from lixiviant sources. The chemical transport model simulates the expansion of the plume, both during the active leaching activities time as well as the post-closure stage.

After assigning material properties and initial and boundary conditions, the finite-difference equations for flow are solved to produce a mathematically 'approximate,' but scientifically reliable, value of the average ground water head (potentiometric surface elevation) within each cell. Models that use the finite-difference numerical techniques allow rapid analysis of complex, time-dependent ground water systems.

Numerical models are operated by a computer code or program. The code is a generalized set of steps, to which specific field conditions, such as initial and boundary conditions, are imposed. Because computer codes are generic in nature and must be adapted to actual field conditions, a clear understanding of the existing physical system (a conceptual model) is required.

It is important to establish why the model is being created, and to properly design the model simulations to sufficiently address the objectives. The model development for each of the failure scenarios followed the steps detailed below:

- (1) Developing a conceptual model to guide creation of model attributes
- (2) Selecting an appropriate computer code(s) for the analysis
- (3) Establishing the time period represented by the model and the duration of subdivisions of this period (time steps) required for modeling
- (4) Selecting a suitable model domain and determining the dimensional (horizontal and vertical) limits of the analysis
- (5) Establishing the model structure by determining the number of model layers and the grid spacing requirements for the flow analysis
- (6) Incorporating hydraulic boundaries and features, including the shape and characteristics of constant-head boundaries, precipitation/recharge, and pumping/injection
- (7) Assigning hydraulic conductivity values
- (8) Specifying initial head values (ground water surface elevation)
- (9) Evaluating and assigning appropriate model computational characteristics; for example, solution method, iteration limits, and convergence criteria, to enhance model stability, computational efficiency, and solution accuracy
- (10) Evaluating the sensitivity of model results to changes in model parameters
- (11) Establishing the model structure, including determining the number of model layers and the grid spacing requirements for the transport analysis
- (12) Assigning the characteristics of chemical sources (e.g., leaks, spills) consisting of dimensions, locations, concentrations, and time dependency
- (13) Assigning transport parameters, including the dispersivities and porosities
- (14) Conducting chemical transport simulations and exporting the observed concentrations at pre-specified locations
- (15) Processing the data within Excel spreadsheets

2.4.2 Conceptual Model Development

The general components of the conceptual model that serve as the basis for the construction of the ground water flow and contaminant transport models are described below. This conceptual model summarizes the theoretical understanding of the primary conditions that affect ground water flow and chemical transport and fate. More detailed descriptions (e.g., pumping/extraction well configurations) are presented within discussions of the respective failure scenarios.

As contaminant plumes move down-gradient from the source area, they tend to spread laterally and vertically, thereby lowering the average contaminant concentration as the plume expands. The shape taken by an individual plume varies depending primarily on the nature of the geologic materials making up the aquifer, but also secondarily on the rate of ground water flow.

In fine-grained unconsolidated sediments, such as sands and silts, plumes tend to spread out laterally in a fan shape as they move down-gradient. This process is called dispersion. Vertical

flow also occurs and is controlled by the uniformity of the sediments, as well as the vertical hydraulic gradient. When all the aquifer materials are of essentially the same size and are well-rounded, vertical flow can easily take place, assuming a vertical hydraulic gradient exists. Fine-grained layers of sediments such as clays and silts in an otherwise coarse-grained aquifer prevent or retard downward (or upward) vertical flow. Ground water flowing at a moderate to fast rate tends to minimize both horizontal and vertical dispersion, while slower flow (normally in fine-grained materials) allows greater dispersion. All of these processes, however, will be complicated by the effects caused by the injection and withdrawal of ground water.

Contaminant plumes extend down-gradient from the source area over time until a steady state condition is reached, based on the rate of contaminant flux to the ground water and the degree of chemical degradation/sorption taking place in the aquifer. Contaminant concentrations decline as down-gradient flow occurs, because processes such as dispersion, adsorption, and chemical transformation are constantly taking place in the aquifer. The length of a plume will depend on (1) how rapidly these processes work, (2) the rate of ground water flow, (3) the rate of chemical releases to the aquifer, (4) chemical interactions between the ground water and aquifer matrix, and (5) other environmental factors, such as temperature and the basic chemistry of the ground water. Ultimately, even with a constant source of contamination to the aquifer, any plume will reach a point beyond which it can no longer expand and will more or less stabilize. This stabilization, or steady state condition, occurs when degradation and/or sorption processes in the aquifer remove as much contaminant mass as is being released to the aquifer in the source area.

If the source of contamination is cut off, for example by pump and treat extraction wells, a reduction in chemical concentrations will occur down-gradient of the source area and will be especially noticeable along the axis of the plume. Over time, the reduction in plume concentrations will be propagated farther down-gradient consistent with the hydraulic conductivity of the aquifer. Subsequently, the plume will begin to contract in areal extent.

In the case of ISL facilities, the contaminants are mobilized by the lixiviant, which is often injected into units that are straddled above and below by aquifers that are used as drinking sources. In fact, at least one ISL facility injects lixiviant into the same aquifer as that used as a nearby drinking water source (Rice 2006).

2.4.3 Computer Code Selection

The computer codes that were used for this analysis are MODFLOW-2000 and MT3D-MS. MODFLOW-2000, the U.S. Geological Survey (USGS) finite-difference ground water flow model, is a popular and widely used computer code (Harbaugh et al. 2000). Ground water flow within the aquifer is simulated using a block-centered finite-difference approach. Layers can be simulated as confined, unconfined, or a combination of confined and unconfined. Flow associated with external stresses, such as wells, areal recharge, evapotranspiration, drains, and streams, can also be simulated.

The modular three-dimensional (3-D) transport model referred to as MT3D-MS was originally developed by Zheng and Wang (1999) at S.S. Papadopoulos & Associates, Inc., and subsequently documented for the Robert S. Kerr Environmental Research Laboratory of the EPA. In the past

several years, various versions of the MT3D code have been commonly used in contaminant transport modeling and remediation assessment studies. MT3D-MS does not explicitly simulate geochemical reactions, but can be used to simulate changes in concentrations of miscible contaminants in ground water considering advection, dispersion, diffusion and some aggregate chemical reactions (i.e., distribution coefficient), with various types of boundary conditions and external sources and/or sinks. The basic chemical reactions included in the model are equilibrium-controlled or rate-limited linear or non-linear sorption, and first-order irreversible or reversible kinetic reactions. Somewhat more sophisticated, multispecies chemical reactions can be simulated by add-on reaction packages.

MODFLOW2000 and MT3D-MS are commonly applied at ISL facilities to evaluate how the average flow field, together with other transport parameters, affects chemical movement in ground water and plume development from lixiviant sources. The chemical transport model is often used to simulate the expansion of the plume, both during the active leaching activities time as well as the post-closure stage.

The pre- and post-processing of data input/output for these codes was performed with Groundwater Vistas (Rumbaugh and Rumbaugh 1998).

2.5 Representative ISL Facility Development and General Modeling Approach

Prior to discussing the model input and parameter ranges, it is important that the overall goal of the modeling be reiterated. The central question to be addressed by the modeling is whether health-based standards may be exceeded under representative injection/extraction configurations and realistic parameter combinations. To meet this objective, the model does not need to simulate flow processes at the interstitial pore level (e.g., heterogeneity, dispersivity) or geochemical processes at the molecular level (e.g., kinetics and thermodynamics). Instead simplifying assumptions are made in the modeling to adequately capture the overall effects of very complex processes affecting ground water flow and contaminant transport.

An important aspect in constructing the model was to ensure that the assumptions were not so conservative as to render the results unproductive by routinely exceeding the health-based standards. In some instances, assumptions are made that may underestimate the predicted downgradient plume concentrations. This approach is justified because even under the nonconservative assumptions, the health-based standards are still exceeded in some cases. It is important to keep in mind that this modeling does not replace the need for site-specific modeling, nor is it intended to provide a framework upon which to perform site-specific modeling.

In deciding whether to perform deterministic or stochastic modeling, several factors were considered, including (1) the ability to meet the overall objectives, (2) difficulty in setting up and explaining the model (e.g., treatment of correlation, defining parameter distributions), (3) complexities of running the model (e.g., demonstrating statistical convergence); and (4) effort required to interpret the results. After evaluating these considerations, a deterministic approach was selected, since it could meet the objectives, is simpler to set-up and explain, and the interpretation of the results is more straightforward.

A thorough review of readily available ISL facility information indicates that there are several important factors that need to be considered in evaluating their potential impacts on ground water and must be conceptualized in the numerical model. These common elements provide a framework from which the sensitivity analyses for each of the scenarios was conducted. Those attributes that are specific to each scenario (e.g., model domain and grid spacings) will be presented under each of the respective sections.

As part of the deterministic approach, the sensitivity of the results to the most uncertain parameter values was assessed. These parameters include hydraulic gradients and conductivities, leak, pumping and injection rates, and durations. All of the concentrations are calculated as relative concentrations assuming a 1-mg/L source term and are adjusted to actual concentrations during the dose assessment (Section 4). Ranges for the representative model input parameters are presented in Table 2-1 and discussed below.

The regional hydraulic gradient is an estimated parameter based upon a literature review of natural gradients under nonstressed conditions. For a set value of hydraulic conductivity and effective porosity, a higher hydraulic gradient results in a faster ground water velocity, less dispersion and higher doses. There may be cases where pumping at the ISL facility creates hydraulic gradients that are greater than those estimated for the modeling. Therefore, as part of the sensitivity analysis, the range of hydraulic gradients was increased to 0.1 ft/ft.

One of the common strategies at all of the ISL facilities is to better understand the most probable fate and transport of uranium and other constituents during and after ISL operations. To achieve this goal, mathematical modeling of chemical reaction kinetic equations or equilibrium thermodynamic equations are often used to describe chemical interactions among dissolved chemical species, the dissolution of immobile solid phases, or the formation and precipitation of new, immobile solid phases. EPA recognizes the importance of understanding the geochemical processes and has entered into a corporative agreement with the U.S. Geological Survey under a Regional Applied Research Effort (RARE). The main objective of this work is to provide a predictive model that describes the ground water flow and geochemical changes along with longer-term transport of dissolved constituents during and after the uranium ISL mining process.

To accomplish this goal, analysis of the lithology, ore and ground water chemistry is being characterized at the Dewey Burdock uranium project site. This site is located approximately 65 miles southeast of Rapid City, South Dakota, which is one of the areas being considered for in-situ leaching (ISL) of uranium. The available ground water flow and transport data will be input into MODFLOW and MT3D-MS. More quantitative reactive transport modeling will also be conducted using PHT3D, which couples MODFLOW to PHREEQC (an advanced thermodynamically based geochemical code).

To meet the objectives of the current ISL modeling, however, a more simplistic approach is taken to simulate the geochemical behavior. In this method, the net effect from all of the geochemical processes are expressed as a distribution coefficient (K_d). The distribution coefficient is subsequently used to estimate the amount of retardation that each of the contaminants would experience along the travel path. Since all of the key radionuclides have long half lives, the amount of retardation does not significantly affect the peak doses. Therefore,

retardation and radioactive decay are not explicitly simulated in the modeling. Arrival times (i.e., breakthrough curves) are corrected for retardation as part of the risk assessment presented in Section 4.

Areal recharge impacts ground water flow and contaminant transport in several ways, including (1) altering the horizontal and vertical hydraulic gradients, (2) affecting the geochemistry, and (3) depressing the plume deeper into the aquifer as a function of distance. Since the analyses were performed over a range of hydraulic gradients, the effects of recharge on the gradients are implicitly considered. Any recharge water infiltrating to the depths being mined by the ISL facilities will take sufficiently long that the system will approach equilibrium conditions. Furthermore, any transient effects of recharge on geochemistry and contaminant mobility are expected to be minimal compared to the geochemical mobilization properties of the lixiviant. The prevailing geochemical conditions within the mined unit and aquifers are assumed to result in low sorption properties for the contaminants (Section 4.2.2).

Although areal recharge may depress the plume, these effects would not significantly affect the peak dose and are therefore ignored. For these reasons, no areal recharge was explicitly assigned in the modeling.

With respect to hydrostratigraphy, the major sandstone roll-front uranium deposits found in Wyoming, South Dakota, Nebraska, New Mexico, and Texas have similar depositional histories, which have resulted in similar rock compositions. Typically, the roll-front deposits consist of sandstones of fluvial origin that are generally interbedded between siltstones and mudstones (NRC 2009a). Sandstones generally have moderate hydraulic conductivities, and the modeling assumes a range from 1 to 100 ft/day (Nicot et al. 2010). To simplify the analysis, the hydraulic conductivities in each of the simulations is assumed to be homogeneous and isotropic. Heterogeneity and preferential pathways from the simulations are addressed in several ways. First, the hydraulic conductivities are sampled over several orders of magnitude and should adequately bracket the potential impacts of heterogeneities on contaminant arrival times. Second, as discussed in greater detail below, the dispersivities have been set to the high end of the expected range. This assumption spreads out the plume to better simulate the effects of potential heterogeneities. Finally, although discrete features and lower dispersivities could lead to releases greater than those predicted, the dose limits were already exceeded (see Section 4.3) without their consideration, thereby removing the need to further evaluate their potential impacts.

Dispersivity is a geometric property of a porous medium which determines the dispersion characteristics of the medium by relating the components of pore velocity to the dispersion coefficient. The amount of dispersion is scale dependent and describes the degree to which the plume spreads out and elongates along the travel path. Longitudinal dispersivity is often assigned a value of about 10% of the travel distance. The transverse dispersivity is about 10% of the longitudinal and the vertical dispersivity is about 10% of the transverse. The nearest receptor for the dose assessment is assumed to be about 328 feet downgradient from the ISL facility. The dispersivities assigned in the modeling are held constant for all simulations and are 65 ft, 6.5 ft and 0.65 ft, for the longitudinal, transverse and vertical, respectively. Although these values are somewhat higher than would be expected, they are reflective of potential heterogeneities that are not captured in the homogeneous and isotropic assumptions.

The effective porosity describes the amount of interconnected pore space. A constant value of 20% was used for all of the simulations. Although it is likely that the porosity and permeability/connectivity of the aquifer will change as the uranium is extracted from the production areas, these impacts will be greatest within the mined areas, rather than those areas where downgradient excursions are occurring. The possibility that changes in porosity and permeability could cause greater excursions is captured by the simulations where the high range of hydraulic conductivities is selected.

Pumping of wells in the vicinity of the ISL facility may affect hydraulic gradients as well as the amount of dilution. As discussed above, higher gradients have been investigated to capture potential pumping effects. To compensate for dilution effects, the dispersivity is set to a relatively high value and the plume is assumed to be completely mixed within the entire thickness of the aquifer. Although this assumption may underestimate peak doses, health-based standards are still exceeded in a number of scenarios.

Since long-term average injection/extraction rates are assumed, all of the flow simulations are performed to steady-state solutions controlled by constant head values. Head values can change for many reasons and over various time scales as a result of severe, short-term weather disturbances, seasonal variations, or longer-term variations most likely due to human activities. Long-term variations (year to decade time scales) could occur in the arid, western portion of the United States where there could be increased competition for water resources from aquifers. It is recognized that changes in the boundary conditions could increase or decrease the probability and severity of excursions away from an ISL site. It is unlikely, however, that the releases would fall outside of the range of those predicted. Furthermore, the transport analysis is conducted for a time period that is sufficiently long to allow for contaminant concentrations to peak at the nearest receptor well.

Table 2-1: Representative ISL Parameter Ranges

Model Input Parameter	Potential Range of Values	References	
Regional Hydraulic Gradient (ft/ft)	0.001–0.01	Estimated parameter	
Recharge	0.09-0.15	Chowdhury and Mace 2007	
Effective Porosity (%)	5–30	Freeze and Cherry 1979	
Dispersivity (ft)		$\alpha_L = 0.1(\text{plume length})$ $\alpha_T = 0.1(\alpha_L)$ $\alpha_V = 0.1(\alpha_T)$	Gelhar et al. 1992
Longitudinal	10–1000		
Transverse	1–100		
Vertical	0.1–10		
Injection Fluid Conc. (milligram per L)	1	Normalized concentration	
Hydraulic Conductivities (ft/day)		Nicot et al. 2010	
Over- and underlying aquifers	10-100		
Sandstone (mined interval)	1–10		
Injection/Extraction Well Spacing (ft)	40–150	NRC 2009b	
Range of Injection Rates (gpm)	20–200	NRC 2009b	
Operating Life of ISL Well Pattern (yrs)	1–3	NRC 2009b	

2.6 Development of Scenarios

Two scenarios are investigated that are associated with the active phase of the mining activities; (1) spills and leaks on the surface and subsequent transport to the ground water, and (2) excursions beyond the injection/production wells or into other non-mined geologic units above the mined unit. The general question that the flow and transport modeling will assist in addressing is: What concentrations of contaminants could reach nearby domestic wells and over what timeframes? The modeling does not make any assumptions with respect to whether best management practices are being followed, and simply relies on published data for parameter ranges and distributions. In many cases, it is likely that a leak would be detected and remedied before any contamination reaches nearby receptors.

2.6.1 Spills and Leaks

During ISL operations and aquifer restoration, barren and pregnant uranium-bearing process solutions are moved through pipelines to and from the wellfield and among different surface facilities (e.g., processing circuit, evaporation ponds). To investigate the potential effects of a pipeline rupture or failure, the Spills and Leaks scenario investigated three general types of spills and leaks, including (1) catastrophic failure (e.g., break of a pipe or breach of an evaporation pond), (2) long-term/low-volume leak of an underground pipe or well transferring or withdrawing lixiviant, and (3) short-term/high-volume leak of an underground pipe or well transferring or withdrawing lixiviant.

The model grid is identical for all of the spills and leaks simulations and consists of a domain that has an area of 1 square mile (Figure 2-3). It is assumed that ground water is flowing due south and the model grid is oriented perpendicular to ground water flow. Constant head boundaries are assigned along the northern and southern boundaries in order to simulate the regional gradient. Boundaries on the east and west of the model domain are oriented perpendicular to ground water flow (i.e., hydraulic divide) and, therefore, ground water does not enter or exit the model along these boundaries (i.e., no-flow boundary conditions). This boundary configuration makes the solutions to the flow problem more unique than would be obtained if constant head boundaries surrounded the entire domain. The base of the model is also represented by a no-flow boundary condition.

The aquifer is assigned a thickness of 130 ft that is discretized into 10 layers (Figure 2-4).

Horizontal grid spacing is on 10-ft centers in the vicinity of the spill, and is gradually increased to a spacing of 250 ft at the model boundaries. The vertical grid spacing ranges from 2 ft at the top of the model to 50 ft at the base. The smaller grid spacing in the area of the contaminant source reduces numerical dispersion, provides better mass balance and allows for more rapid numerical convergence of the solver.

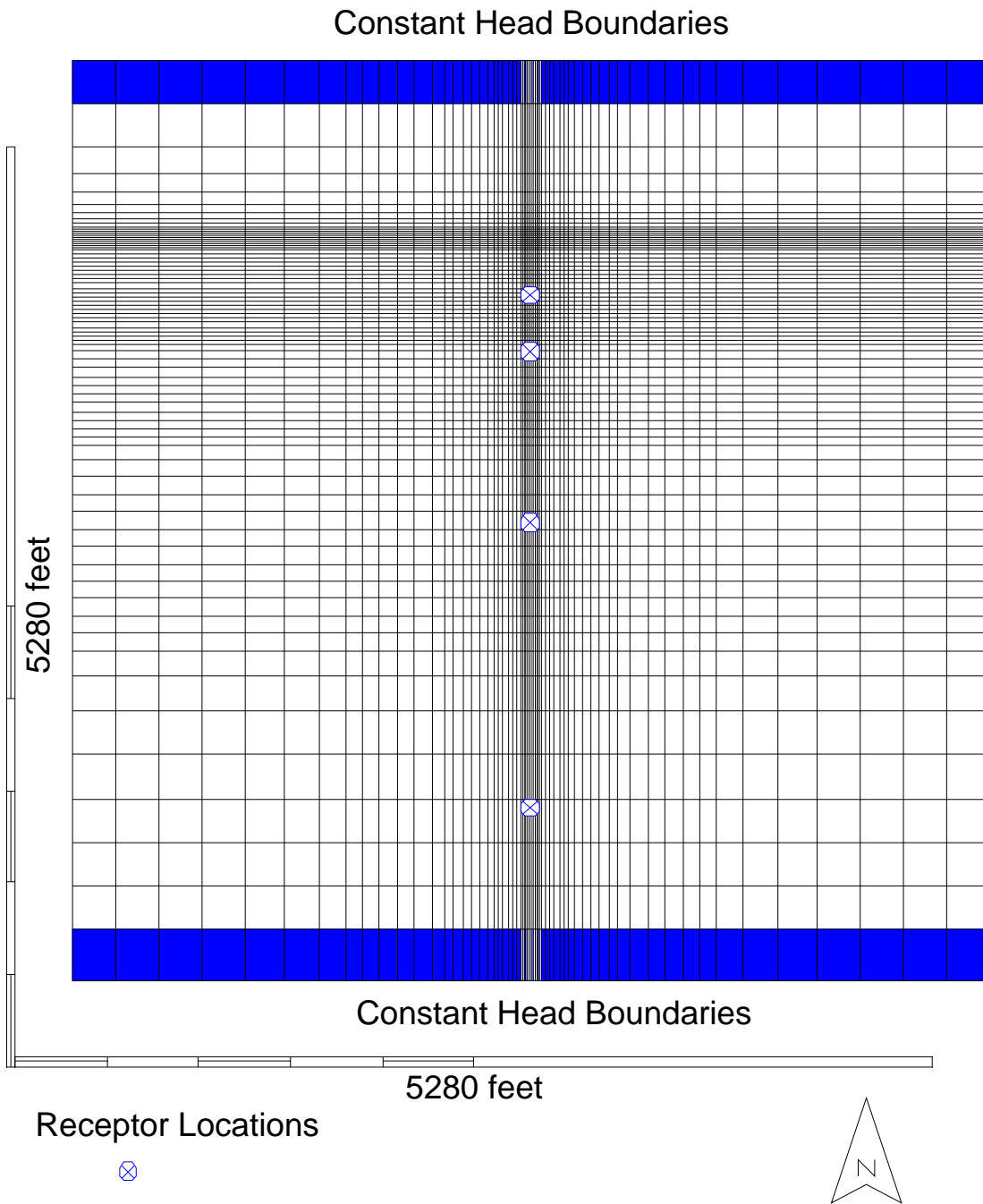


Figure 2-3: Plan View of the Model Grid for Leak Scenarios.

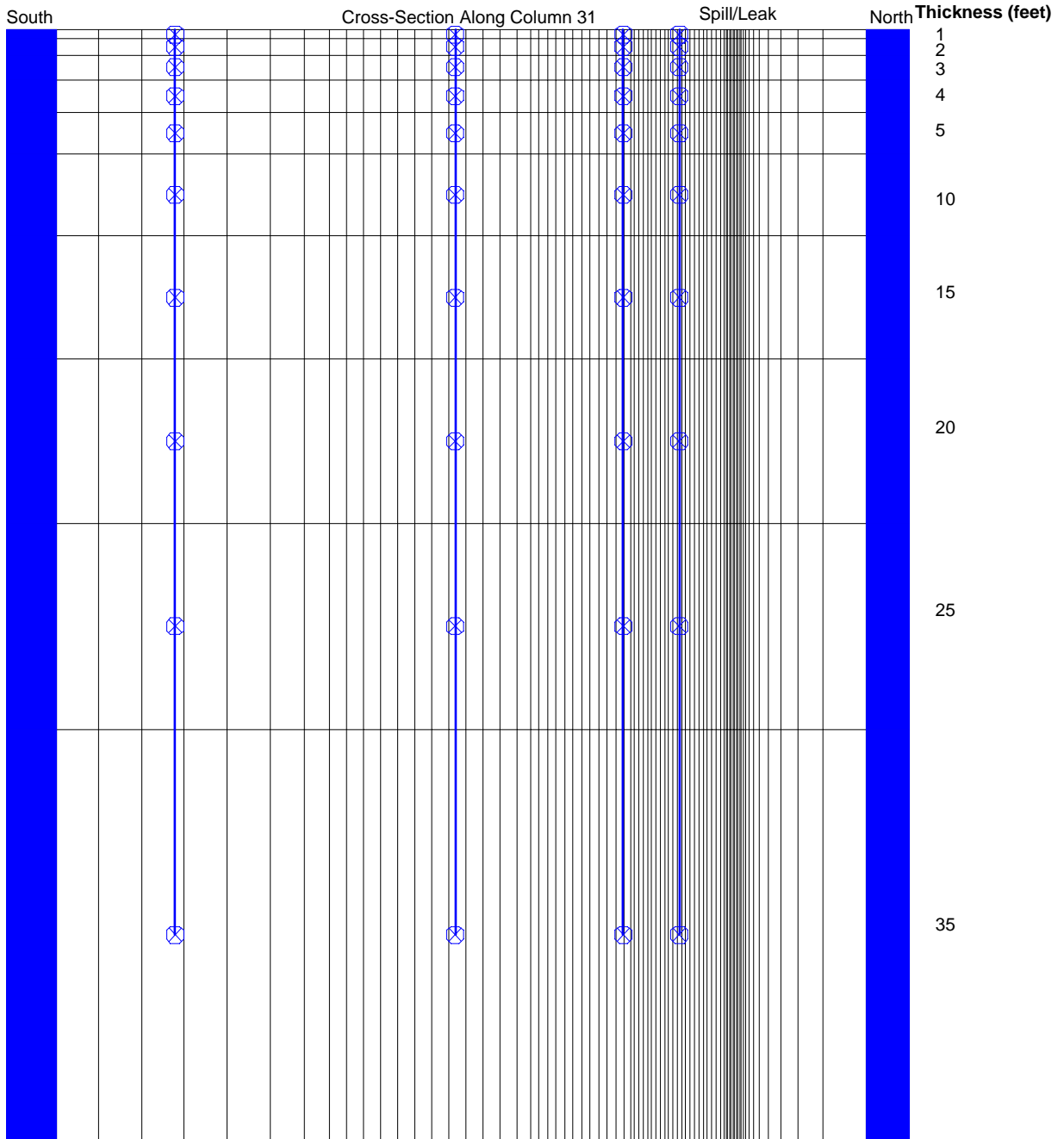


Figure 2-4: Cross Sectional View of the Model Grid for Leak Scenarios.

All fluid entering the model does so as recharge through a 100-ft² area. The rationale for this assumption is that leaks from even small releases are likely to spread out at least 10 ft as the fluid migrates through the unsaturated zone.

The minerals within the vadose zone may have significantly different chemical properties than those of the aquifer leading to different solute retardation behavior than assumed for the underlying aquifer. In the case where there is greater sorption in the vadose zone than in the

underlying aquifer, receptor dose could be significantly decreased. In some cases, the contaminants may diffuse into the finer grained matrix, precipitate and/or be adsorbed. This could result in the vadose zone being a potential long-term source of contaminants that could leach into the ground water. None of these processes are explicitly simulated in the model and flow through the unsaturated zone is assumed to be instantaneous. This assumption is made because the focus of the modeling is on cases where the unsaturated zone does not inhibit the migration of contaminants or act as a long-term contaminant sink.

Hydraulic conductivities are assigned homogeneous and isotropic properties. Since contaminant concentrations at receptor locations are averaged across the entire aquifer to simulate pumping effects, this assumption will not bias the results. Hydraulic conductivities are assigned values of 1, 10 and 100 ft/day to represent the transmissive properties of the aquifer. These values are within those ranges presented for overlying aquifers in the south Texas uranium province (Nicot et al. 2010), and are at the high end of the range for lithologic units within the United States where ISL mining is practical.

Potential receptors are assumed to be located at 328 ft (100 m), 656 ft (200 m), 1,640 ft (500 m) and 3,280 ft (1,000 m). In the discussion that follows, all of the relative peak arrival times and concentrations cited are for the potential receptor located at 328 ft down-gradient of the release. Breakthrough curves (i.e., concentrations as a function of time and distance) for all of the potential receptors are provided in Appendix B.

All source fluid concentrations are assigned a relative concentration of 1 mg/L. As part of the dose assessment (Section 4), the relative concentrations arriving at the receptor well(s) are corrected to actual concentrations of the source fluid, and dose calculations are conducted. For example, if the injection fluid concentration of uranium is 3 mg/L and a relative concentration of 0.01 mg/L reaches a receptor, this would result in a concentration of 0.03 mg/L for the dose calculation. The breakthrough curves for all of the leak simulations are included in Appendix B.

It should be noted that for all the modeling runs discussed in Chapter 2, no retardation is considered. Retardation effects are considered in Chapter 4. In the absence of significant radioactive decay, Retardation only affects the time of the peak dose and not its magnitude.

Catastrophic Leak Failures

As described in NRC 2009b, the Wyoming Department of Environmental Quality (WDEQ) identified more than 80 spills at the Smith-Ranch Highland site during commercial operations from 1988 to 2007. This is the largest NRC-licensed ISL uranium recovery facility. The size of the spills at Smith Ranch-Highland has ranged from a 50- to 100-gallon spill in February 2004 to a 198,500-gal spill of injection fluid in June 2007. The spills most commonly involved injection fluids containing 0.5 to 3.0 mg/L uranium, although spills of production fluids containing 10.0 to 152 mg/L uranium also have occurred. These spills have been caused predominantly by the failure of joints, flanges, and unions of pipelines and at wellheads. The large June 2007 spill at Smith Ranch-Highland was the apparent result of a failed fitting.

Nine simulations were conducted (L1 through L9) to simulate the potential effects of a catastrophic failure (Table 2-2). Leak rates for this scenario range from 100,000 to 200,000 and introduction to the ground water takes place over a 7-day period. Although the largest reported leak is 200,000 gallons and most of that water was discharged to surface water, it is still conceivable that it could take 7 days to detect and remedy a similar release. Since the fluid is released over 7 days, the rate is about 19 gallons per minute (gpm). Other release rates (i.e., 9.5 and 14 gpm) are also investigated. The catastrophic failure simulations also investigate the effects of hydraulic gradient and conductivities.

Table 2-2: Catastrophic Leak Failure Scenarios

CATASTROPHIC LEAK FAILURES											
General Assumptions – All Runs		Run	L1	L2	L3	L4	L5	L6	L7	L8	L9
Receptor Locations (ft)	328, 656, 1,640, 3,280	Regional Hydraulic Gradient	0.1	0.01	0.001	0.01	0.01	0.01	0.01	0.01	0.01
Simulation Time (yr)	53	Effective Porosity (%)	20	20	20	20	20	20	20	20	20
Leak Time (day)	7	Dispersivity (ft)									
		Longitudinal	65	65	65	65	65	65	65	65	65
		Transverse	6.5	6.5	6.5	6.5	6.5	6.5	6.5	6.5	6.5
		Vertical	0.65	0.65	0.65	0.65	0.65	0.65	0.65	0.65	0.65
Model Area (ft ²)	5,280 (ft) × 5,280 (ft) = 1 mi ²	Leaking Fluid Conc. (milligram per L)	1	1	1	1	1	1	1	1	1
Leak Area (ft ²)	100	Hydraulic Conductivities (ft/day)	10	10	10	1	10	100	1	10	100
Model Layers	10	Distribution coefficients (ml/g)	Rf ¹ Specified in Spreadsheet	Rf Specified in Spreadsheet							
Minimum/Maximum Grid Spacing (ft)	10/250	Leakage (gallons)	150,000	150,000	150,000	100,000	100,000	100,000	200,000	200,000	200,000
All Layers	Homogenous	Time until Peak Arrival (days)	3.96×10 ¹	3.61×10 ²	4.52×10 ³	3.60×10 ³	3.61×10 ²	3.96×10 ¹	3.60×10 ³	3.61×10 ²	3.96×10 ¹
		Relative Peak Concentration	8.75×10 ⁻³	6.17×10 ⁻³	7.18×10 ⁻³	4.15×10 ⁻³	4.25×10 ⁻³	4.89×10 ⁻³	7.94×10 ⁻³	8.01×10 ⁻³	9.48×10 ⁻³

¹ Rf = retardation factor calculated in Section 4

Simulations L1 through L3 were focused on evaluating the effects of hydraulic gradients on the release concentrations and arrival times. The leak rate is 14 gpm (150,000 gallons) and the hydraulic gradients for L1, L2 and L3 are 0.1, 0.01 and 0.001, respectively. Hydraulic conductivities for these three runs are all set to the median value investigated (i.e., 10 ft/day). As shown in Appendix B and presented in Table 2-2, the peak arrival times for simulations L1 through L3 are 40, 361 and 452 days, respectively. Since all parameters are constant except for hydraulic gradients, the model predictions are as expected and the steeper hydraulic gradients result in shorter travel times. Furthermore, since the leak volume is creating a recharge mound and affecting the hydraulic gradients, the arrival times are not linearly scaled (i.e., a factor of 10 increase in gradient does not result in a factor of 10 reduction in travel time). Relative peak concentrations are 8.75×10^{-3} , 6.17×10^{-3} and 7.18×10^{-3} . The shape and longevity of the recharge mound also affect the contaminant concentrations and lead to an apparent discrepancy in the arrival concentrations in which the maximum relative concentrations observed for a hydraulic gradient of 0.01 are less than those observed under a gradient of 0.001.

Simulations L4 through L6 were designed to investigate the sensitivity of the results to hydraulic conductivities (Table 2-2). The assigned values for hydraulic conductivities are 1, 10 and 100 ft/day, respectively. A hydraulic gradient of 0.01 ft/ft and a leak rate of 9.5 gpm are common to all three simulations. The arrival times for simulations L4 through L6 are 3,600, 361 and 39.6 days, respectively (Table 2-2). Since ground water velocities are linearly related to hydraulic conductivities, there is almost a factor of 10 difference in the peak arrival times. As was previously observed in simulations L1 through L3, the relationship is not exactly linear, because the recharge causes some mounding and subsequently alters the hydraulic gradients as a function of the hydraulic conductivities.

Relative peak concentrations for simulations L4 through L6 are 4.15×10^{-3} , 4.25×10^{-3} and 4.89×10^{-3} . As indicated by the results, the peak concentrations are slightly higher for the higher hydraulic conductivities and are related to the greater dispersive effects at the lower hydraulic conductivities, as observed by the wider breakthrough curves presented in Appendix B.

Simulations L7 through L9 are identical to L4 through L6 except that the leak volume has been increased to 200,000 gallons (Table 2-2). The arrival times for simulations L7 through L9 are 3,600, 361 and 39.6 days, respectively. The arrival times are identical to those observed for simulations L4 through L6 and indicate that the additional 100,000 gallons added as recharge do not appreciably alter the hydraulic gradients. The relative peak concentrations, however, are about a factor of 2 higher, which is consistent with the increase of twice the mass of contaminant introduced to the system.

Long-Term/Low-Volume Leak(s)

To evaluate the potential effects of a longer-term leak (3 years) at a lower volume release rate (i.e., 1 to 2 gpm), nine simulations were conducted (L10 through L18). All of the parameters are identical to the previous leak simulations except the leak volume and timeframes (Table 2-3). The 3-year timeframe was selected, because this is the upper range of the times that individual cells (e.g., in a 5-spot pattern) are mined. It is postulated that underground piping would be either moved or inspected within this timeframe. A 1- to 2-gallon leak is assumed because this volume

is sufficiently small to where a long-term leak would possibly go either undetected or uncorrected.

Simulations L10 through L12 are designed to evaluate the effects of hydraulic gradients on the release concentrations and arrival times. The leak rate is 1.5 gpm for 3 years, and the hydraulic gradients for L10, L11 and L12 are 0.1, 0.01 and 0.001, respectively. Hydraulic conductivities for these three runs are all set to the median value investigated (i.e., 10 ft/day). The peak arrival times for simulations L10 through L12 are 353, 1,180 and 4,950 days, respectively (Table 2-3). As has been previously observed, the steeper hydraulic gradients accelerate the peak arrivals, but do not behave linearly. As the hydraulic gradients flatten, the leak has a more pronounced impact on the arrival times. For example, the peak arrival for a gradient of 0.01 ft/ft is approximately 3 times longer than for a peak arrival at a gradient of 0.1 ft/ft, and is about 4 times slower than the peak arrival at a gradient of 0.001 ft/ft.

Relative peak concentrations for simulations L10 through L12 are 1.11×10^{-2} , 6.87×10^{-2} and 9.19×10^{-2} , respectively (Table 2-3). As shown in the Appendix B charts, the leading edge of the breakthrough curve for peak arrivals under a gradient of 0.1 ft/ft is very steep, with the maximum concentration maintained for about 800 days. The breakthrough curves for runs L11 and L12 exhibit more traditional behavior and are depicted by a more gradual arrival, a defined peak, and gradual tapering off. The difference in this behavior can be explained, because the very steep hydraulic gradient leads to a compact plume with very small concentration gradients. Furthermore, the plume that forms under the higher gradients (Figure 2-5) becomes far less elongated than at lower gradients (Figure 2-6), and the mass is distributed over a larger area, which results in lower relative peak concentrations.

In runs L13 through L15, the hydraulic gradient is set to 0.01 ft/ft and the leak rate is 1 gpm (Table 2-3). The hydraulic conductivity, however, is assigned a value of either 1 ft/day (L13), 10 ft/day (L14) or 100 ft/day (L15). The peak arrival times are 4,160, 1,180 and 451 days, respectively. As expected, the lower hydraulic conductivities lead to longer travel times.

The relative peak concentrations for simulations L13 through L15 are 6.02×10^{-2} , 4.77×10^{-2} and 5.92×10^{-3} , respectively (Table 2-3). The peak concentrations are higher at lower hydraulic conductivities, because although the same amount of mass has entered the system, the plume created by the lower hydraulic conductivity remains more compact and is less elongated, as shown in Figure 2-7 and Figure 2-8.

Table 2-3: Long-Term/Low Volume Leak Scenarios

LONG-TERM/LOW VOLUME LEAK FAILURES											
General Assumptions – All Runs		Run	L10	L11	L12	L13	L14	L15	L16	L17	L18
Receptor Locations (ft)	328, 656, 1,640, 3,280	Regional Hydraulic Gradient	0.1	0.01	0.001	0.01	0.01	0.01	0.01	0.01	0.01
Simulation Time (yr)	53	Effective Porosity (%)	20	20	20	20	20	20	20	20	20
Leak Time (yr)	3	Dispersivity (ft)									
		Longitudinal	65	65	65	65	65	65	65	65	65
		Transverse	6.5	6.5	6.5	6.5	6.5	6.5	6.5	6.5	6.5
		Vertical	0.65	0.65	0.65	0.65	0.65	0.65	0.65	0.65	0.65
Model Area (ft ²)	5,280 (ft) × 5,280 (ft) = 1 mi ²	Leaking Fluid Conc. (milligram per L)	1	1	1	1	1	1	1	1	1
Leak Area (pipe - in ²)	28	Hydraulic Conductivities (ft/day)	10	10	10	1	10	100	1	10	100
Model Layers	10	Distribution coefficients (ml/g)	Rf ¹ Specified in Spreadsheet	Rf Specified in Spreadsheet							
Minimum/Maximum Grid Spacing (ft)	10/250	Leak Rates (gallons/min)	1.5	1.5	1.5	1	1	1	2	2	2
All Layers	Homogenous	Time until Peak Arrival (days)	3.53×10 ²	1.18×10 ³	4.95×10 ³	4.16×10 ³	1.18×10 ³	4.51×10 ²	4.27×10 ³	1.18×10 ³	2.95×10 ²
		Relative Peak Concentration	1.11×10 ⁻²	6.87×10 ⁻²	9.19×10 ⁻²	6.12×10 ⁻²	4.77×10 ⁻²	5.92×10 ⁻³	1.04×10 ⁻¹	8.80×10 ⁻²	1.18×10 ⁻²

¹ Rf = retardation factor calculated in Section 4

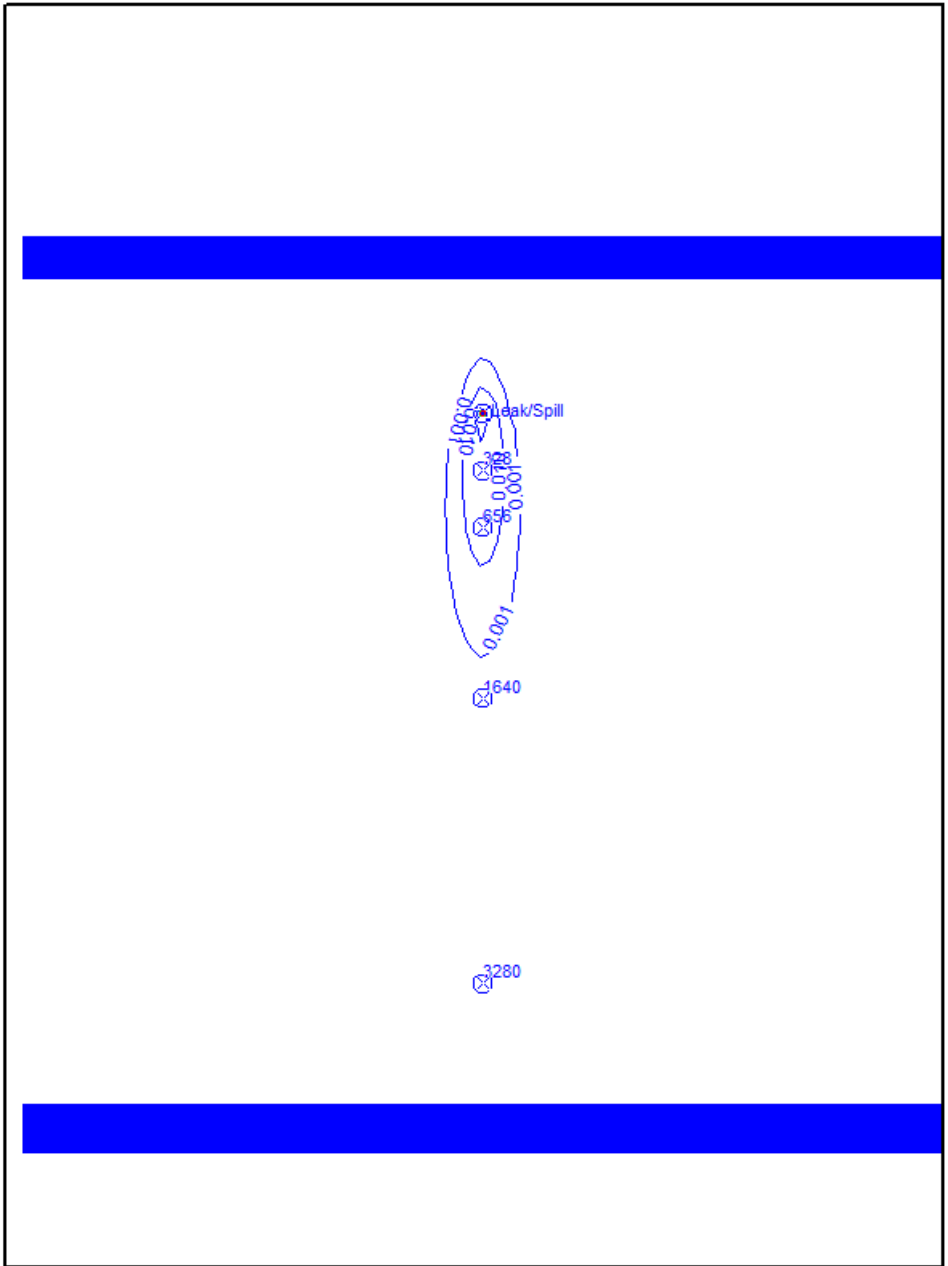


Figure 2-5: Relative Concentrations for L10 at 140 Days

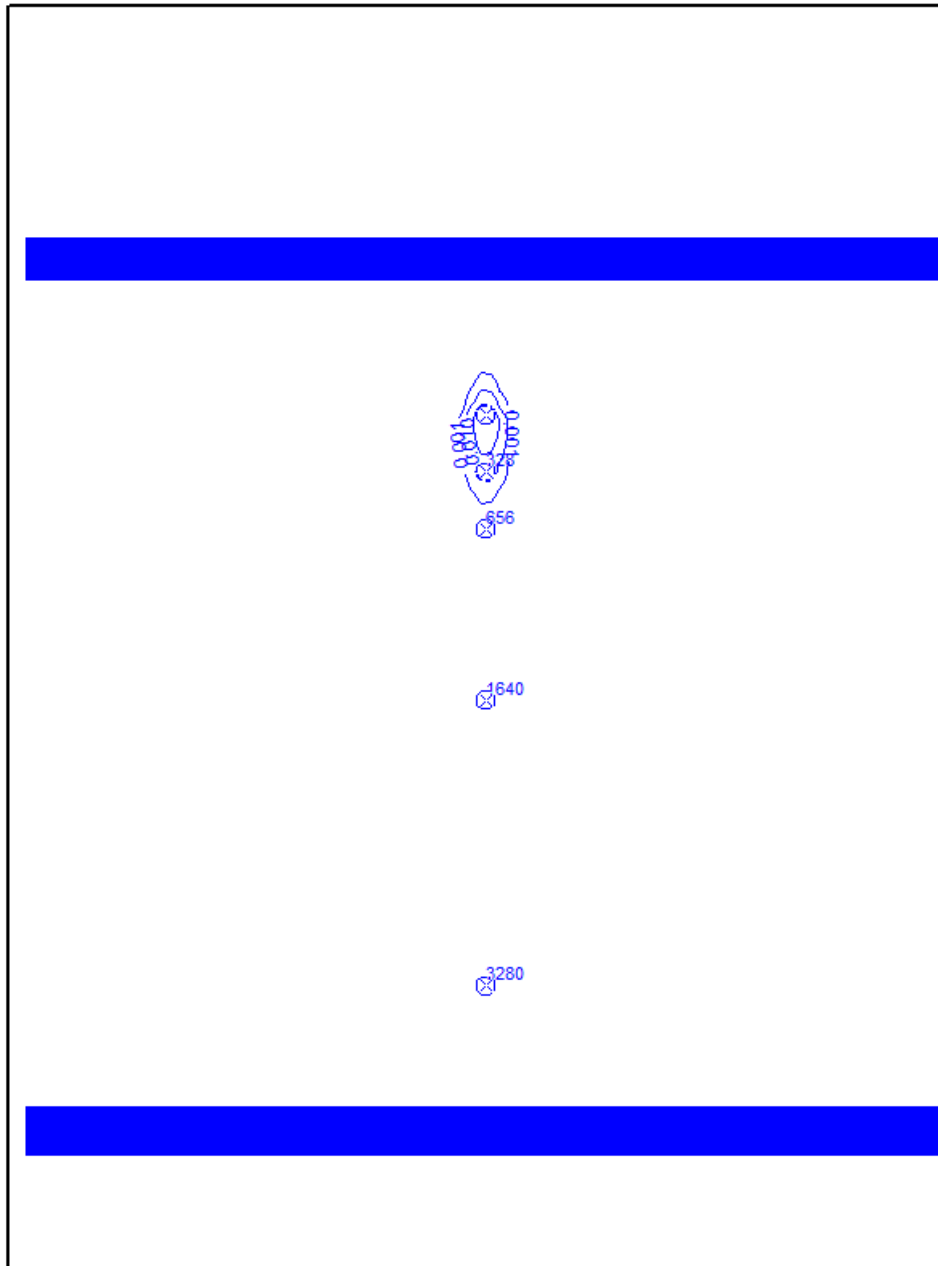


Figure 2-6: Relative Concentrations for L11 at 140 Days

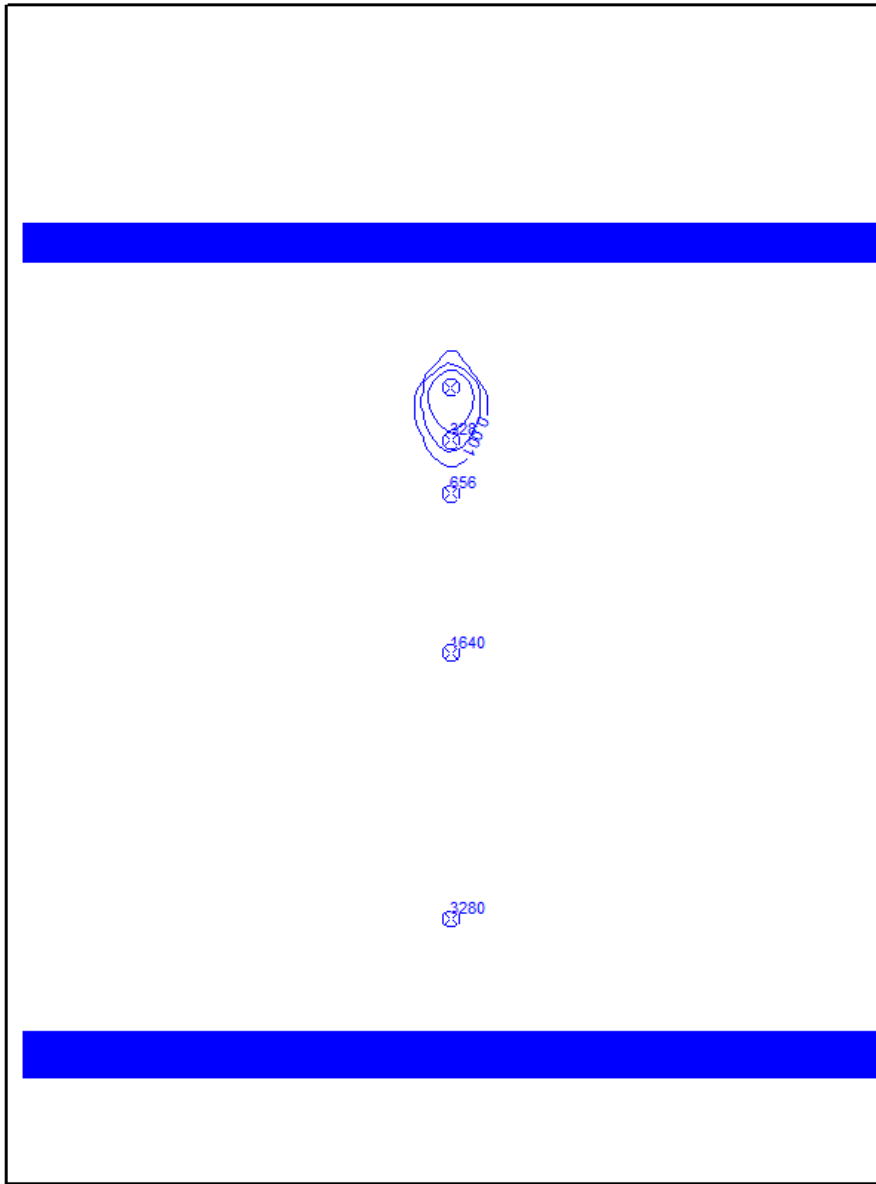


Figure 2-7: Relative Concentrations for L13 at 877 Days

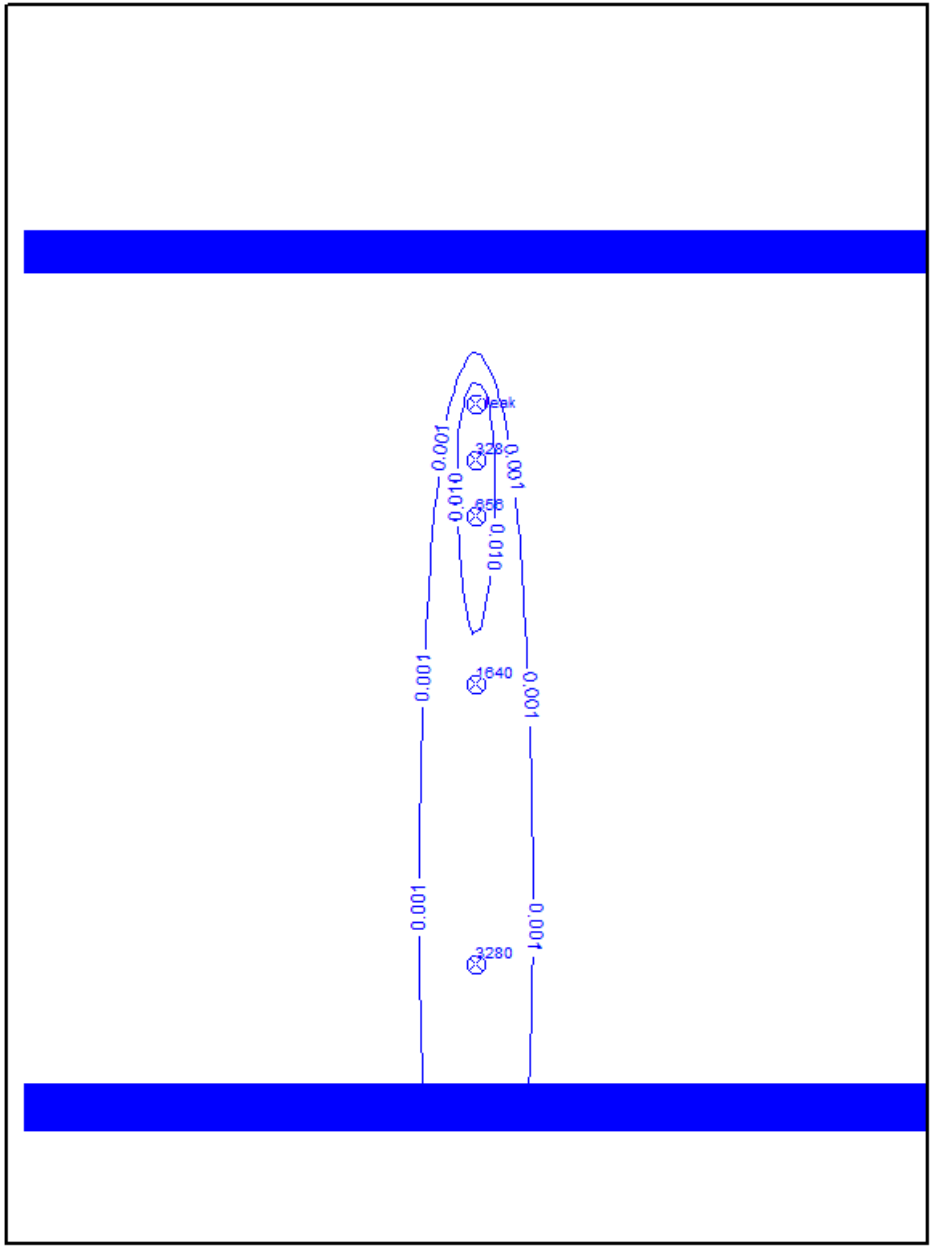


Figure 2-8: Relative Concentrations for L15 at 877 Days

Simulations L16 through L18 were conducted to investigate the sensitivity of the results to leak rates (Table 2-3). These runs are paired with simulations L13 through L15 and, with the exception of leak rate, all of the input parameters for these runs are identical for each pair (i.e., L16 and L13, L17 and L14, and L15 and L18). The relative peak arrival time for L16 (4,270 days) is longer than L13 (4,160 days), which may seem counterintuitive since L16 should have steeper gradients and faster velocities. An inspection of the output files, however, reveals that the additional volume of water (2 vs. 1 gpm) does increase the velocity, but the increase in mass redistributes the center of mass leading to a longer time before the peak concentration is reached. At a hydraulic conductivity of 10 ft/day (L14 and L17), the relative peak arrival times (1,180 days) are virtually the same. The relative peak concentrations, however, vary by a factor of a little less than 2, with the peak concentration of L14 being 4.77×10^{-2} , and 8.80×10^{-2} for L18. These relationships indicate that the changes caused to the flow field by the higher injection rates are balanced by the additional mass. The differences observed between runs L18 and L15 are more pronounced, with the peak arrival time for L18 being 295 days versus the 451 days for L15; and the relative peak concentrations are 1.18×10^{-2} and 5.92×10^{-3} for runs L18 and L15, respectively. These results indicate that, since the plume at higher hydraulic conductivities is more elongated and there is less movement of the plume in the transverse direction relative to the longitudinal, the concentration gradients within the plume are less pronounced and lead to a greater differentiation in travel times and relative concentrations.

Short-Term/High-Volume Leak(s)

The final leak scenario pertains to shorter-term, higher-volume leaks and involves six simulations (L19 through L24) (Table 2-4). In these simulations, the release time has been decreased to 28 days. All of the parameters are identical with the exception of the leak rates, which vary from 1 gpm to 40 gpm. Although it is very unlikely that 20 and 40 gpm leaks would continue undetected for 28 days, these leak rates are included to provide an upper bound on the sensitivity analysis. The hydraulic conductivity is set to 10 ft/day and the hydraulic gradient is 0.01 ft/ft.

The peak arrival times for all six simulations are identical at 382 days, thus indicating that any changes to the hydraulic gradients are balanced by the increased introduction of mass. The leak rates for runs L19 and L20 are 1 and 2 gpm, respectively. The relative peak concentration for L19 is 2.00×10^{-3} , which is approximately one-half of the peak relative concentration for L20 of 3.90×10^{-3} . This nearly linear relationship between the amount of mass released and the relative peak concentrations is maintained for runs L21 (3 gpm) and L22 (4 gpm) in which the relative peak concentrations are 5.70×10^{-3} and 7.40×10^{-3} , respectively. For the higher concentrations, however, the linear relationship is not as apparent and relative peak concentrations for L23 (20 gpm) and L24 (40 gpm) are 3.07×10^{-2} and 5.38×10^{-2} , respectively. All the peak arrival breakthrough curves are presented in Appendix B.

Table 2-4: Short-Term/High-Volume Leak Scenarios

SHORT-TERM/ HIGH VOLUME LEAK SCENARIOS								
General Assumptions – All Runs		Run	L19	L20	L21	L22	L23	L24
Receptor Locations (ft)	328, 656, 1,640, 3,280	Regional Hydraulic Gradient	0.01	0.01	0.01	0.01	0.01	0.01
Simulation Time (yr)	53	Effective Porosity (%)	20	20	20	20	20	20
Leak Time (days)	28	Dispersivity (ft)						
		Longitudinal	65	65	65	65	65	65
		Transverse	6.5	6.5	6.5	6.5	6.5	6.5
		Vertical	0.65	0.65	0.65	0.65	0.65	0.65
Model Area (ft ²)	5,280 (ft) × 5,280 (ft) = 1 mi ²	Leaking Fluid Conc. (milligram per L)	1	1	1	1	1	1
Leak Area (pipe - in ²)	28	Hydraulic Conductivities (ft/day)	10	10	10	10	10	10
Model Layers	10	Distribution coefficients (ml/g)	Rf ¹ Specified in Spreadsheet	Rf Specified in Spreadsheet				
Minimum/Maximum Grid Spacing (ft)	10/250	Leak Rates (gallons/min)	1	2	3	4	20	40
All Layers	Homogenous	Time until Peak Arrival (days)	3.82×10 ²	3.82×10 ²	3.82×10 ²	3.82×10 ²	3.82×10 ²	3.82×10 ²
		Relative Peak Concentration	2×10 ⁻³	3.9×10 ⁻³	5.7×10 ⁻³	7.4×10 ⁻³	3.07×10 ⁻²	5.38×10 ⁻²

¹ Rf = retardation factor calculated in Section 4

Summary and Conclusions of Leak Scenarios

A total of three leak and/or spill scenarios were conducted to investigate the potential impacts to nearby receptors. Nine simulations were performed to evaluate catastrophic leaks. Long-term/low-volume releases were also simulated with nine simulations, and short-term/high-volume releases were simulated with six simulations. The sensitivity analysis was focused on those parameters that are most uncertain. These parameters include hydraulic gradients and conductivities, leak rates, and durations. All of the concentrations are calculated as relative concentrations assuming a 1-mg/L source term and will be adjusted to actual concentrations during the dose assessment (Section 4).

All of the relative peak concentrations versus peak arrival times are shown in Figure 2-9. The highest relative concentrations are associated with L12, L16 and L17. All three of these simulations are associated with the long-term/low-volume leaks. Runs L12 and L16 both have low ground water velocities. In the case of run L12, this is due to the low gradient (0.001 ft/ft), whereas the slow ground water velocity for run L16 is because of the low hydraulic conductivity (1 ft/day). The input for simulation L17 is identical to L16 except that the hydraulic conductivity in L17 is set to 10 ft/day. This explains the shorter peak arrival time.

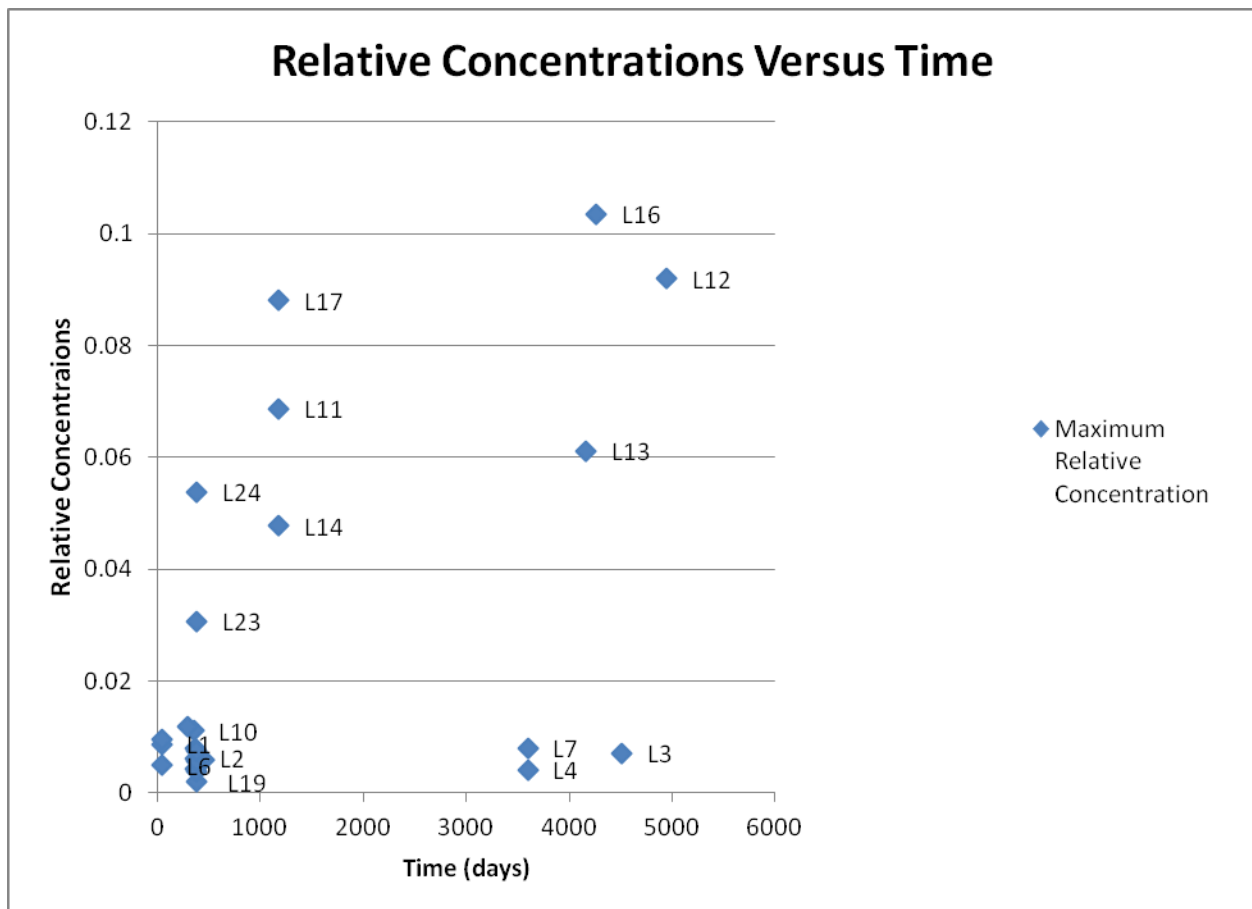


Figure 2-9: Maximum Relative Concentrations versus Time for All Leak Simulations

In all cases where the hydraulic conductivity was set to 100 ft/day and/or the hydraulic gradient was specified as 0.1 ft/ft, the relative concentrations did not exceed 0.012 and the peak arrival times were less than 452 days. These results are explained by the fact that under more rapid velocities, the plume becomes more elongated and distributes the mass over a larger volume.

2.6.2 Excursion Scenarios

To investigate the potential effects of excursions beyond the active injection/production wells or into other non-mined geologic units above and/or below the mined unit, three excursion scenarios were developed: (1) injection fluid excursions downgradient within the same lithologic unit, (2) fluid excursions into overlying units through abandoned boreholes, and (3) fluid excursions into overlying units through discontinuous aquitard(s). The model runs performed for Scenario 1 are divided into 7 series with each series consisting of 9 simulations for a total of 63 simulations. Three simulations were conducted to investigate Scenario 2, and two abandoned borehole simulations were performed (Scenario 3). Summaries of all of the simulations are provided in Tables 2-5 through 2-11.

Of the 63 simulations, 54 involve either 5- or 7-spot injection\pumping well configurations (Figure 2-2). The remaining 9 simulate multiple 5-spot well configurations. As discussed in Section 2.6.2.7, these multiple 5-spot simulations results in longer transport times and lower peak concentrations.

The results from the single 5- and 7-spot scenarios, however, are more representative of the mining practices for extracting uranium from isolated outliers and uranium-rich stringers.

The areal extent of the model grid is identical for all of the excursion simulations and consists of an area that covers 6.25 mi² (Figure 2-10). Horizontal grid spacing is on 10-ft centers in the vicinity of the spill, and is gradually increased to a spacing of 1,000 ft at the model boundaries.

The model grid for all of the scenarios is divided into nine layers (Figure 2-11). The vertical grid spacing, however, is different for Series 1 through 6 of Scenario 1 than it is for Series 7 of Scenario 1 and for Scenarios 2 and 3. For Series 1 through 6, all the layers are a uniform 75 ft thick (Figure 2-11). For the 7th series of Scenario 1 and Scenarios 2 and 3, variable layer thicknesses are assigned and the mined interval thickness is reduced from 75 to 20 ft thick (Figure 2-11).

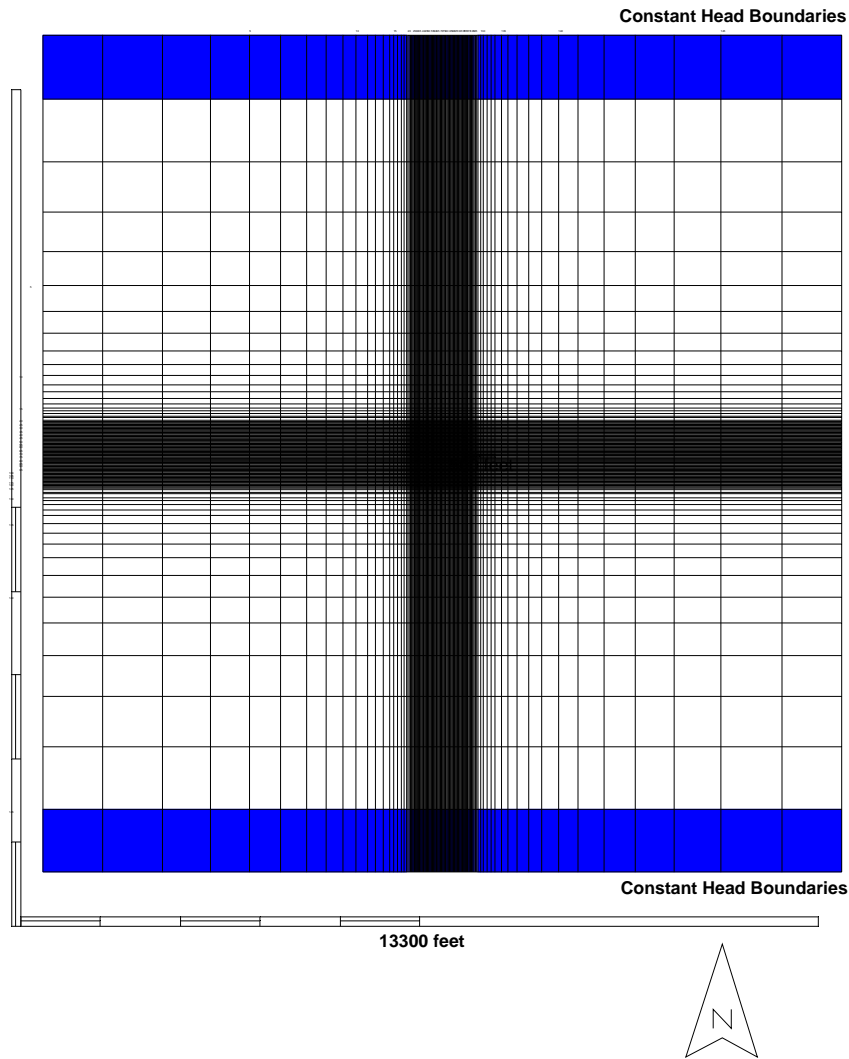


Figure 2-10: Plan View of the Model Grid for Excursion Scenarios (Series 1 through 7)

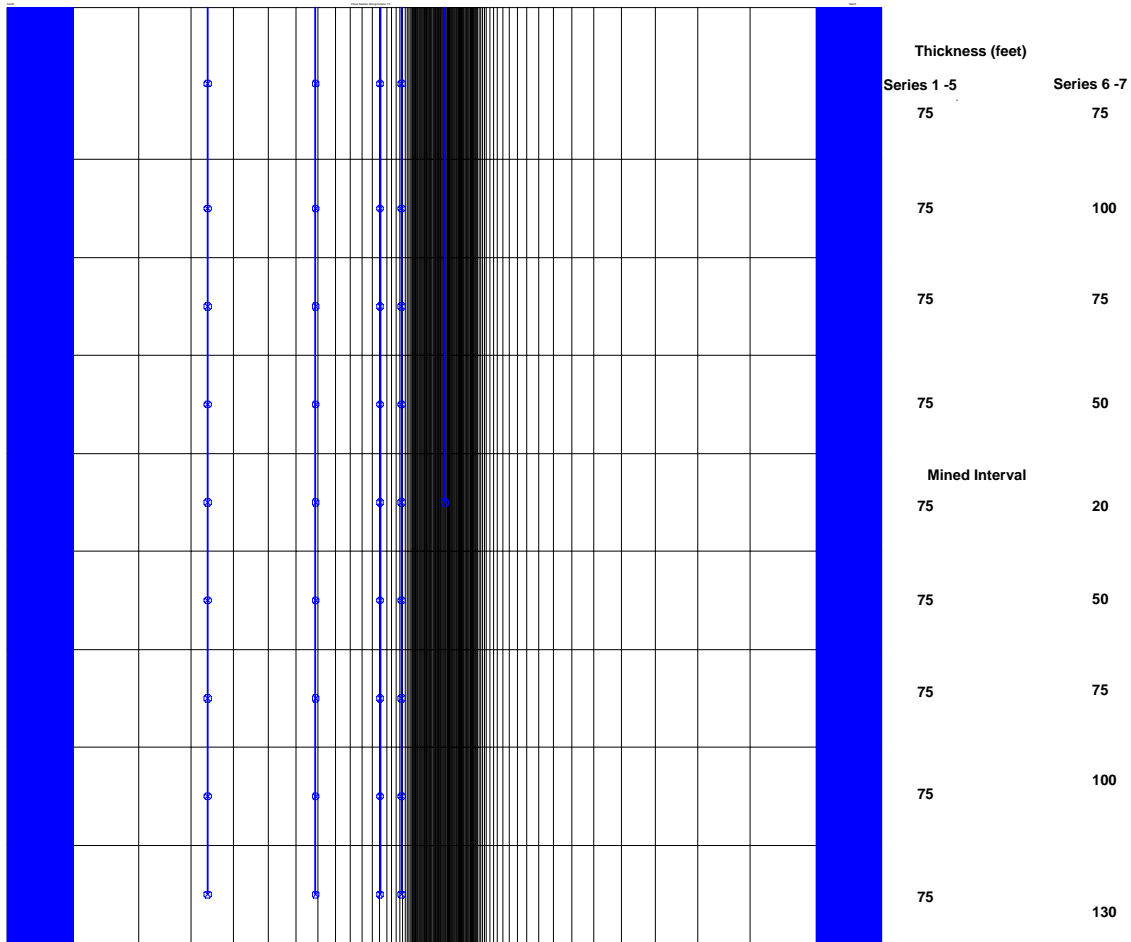


Figure 2-11: Cross Section View of the Model Grid for Excursion Scenarios (Series 1 through 7)

It is assumed that ground water is flowing due south and the model grid is oriented perpendicular to ground water flow. Constant head boundaries are assigned along the northern and southern boundaries in order to simulate the regional gradient (Figure 2-10). Boundaries on the east and west of the model domain are oriented perpendicular to ground water flow (i.e., hydraulic divide) and, therefore, ground water does not enter or exit the model along these boundaries (i.e., no-flow boundary conditions). This boundary configuration makes the solutions to the flow problem more unique than would be obtained if constant head boundaries surrounded the entire domain. The base of the model is also represented by a no-flow boundary condition.

Since the most common injection/pumping patterns are 5- and 7-spot configurations, both types of arrangements have been simulated (Figure 2-12 and Figure 2-13, respectively). The extraction well is always assumed to be in the center with the injection wells along the periphery of the pattern. Although the injection is only assumed to occur for 3 years, the extraction wells remain on for the entire simulation and remove between 1% to 3% more than the volume of water being injected. If the specified pumping rate is 153 gpm, then each of the four injection wells (5-spot pattern) will be injecting at a rate of 37.5 gpm.

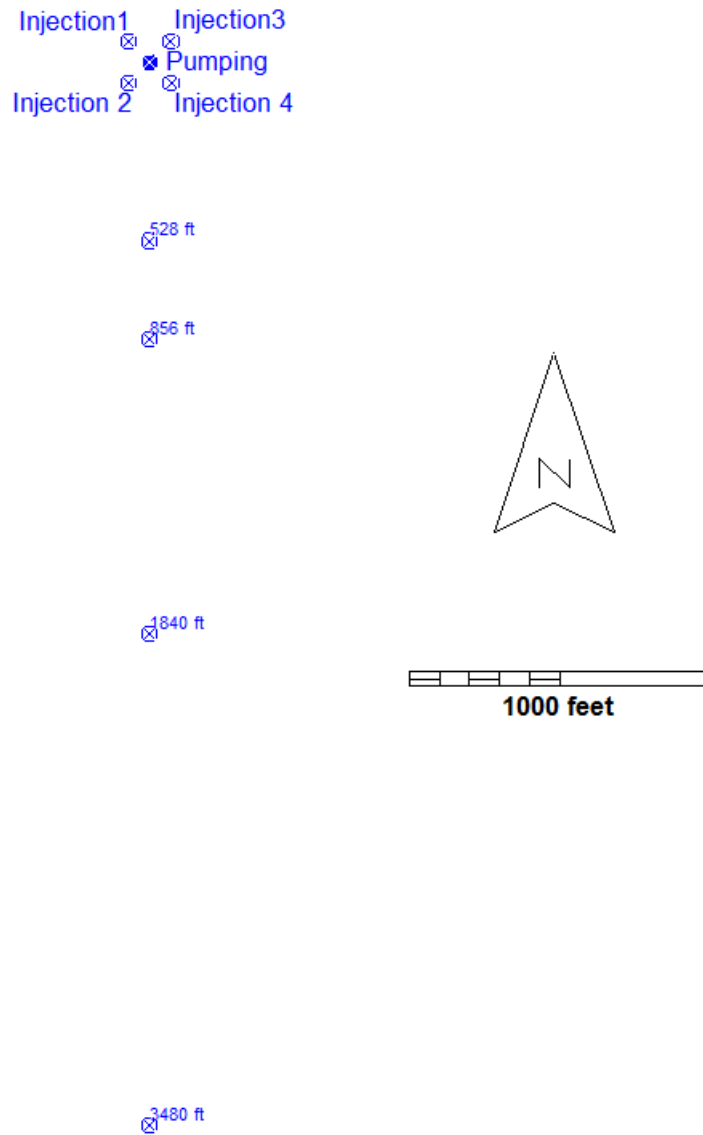


Figure 2-12: Plan View of Pumping/Injection Well Configurations and Receptor Locations for Excursion Scenarios (Series 1, 2, 5 and 6)

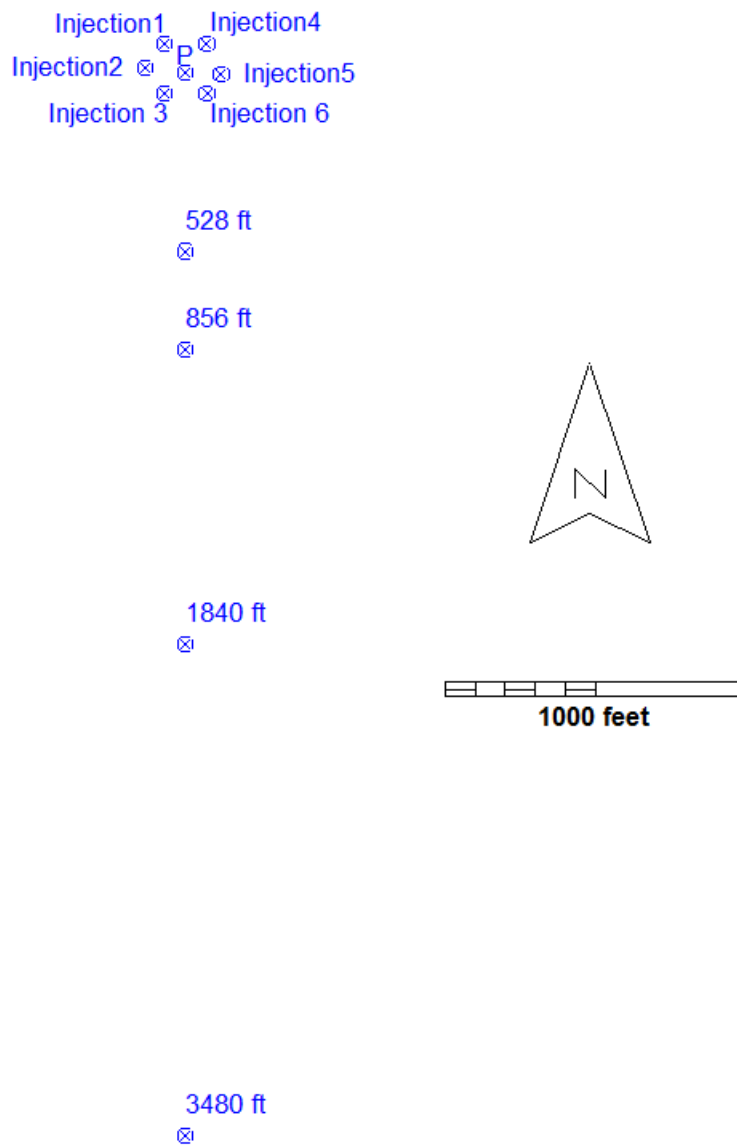


Figure 2-13: Plan View of Pumping/Injection Well Configurations and Receptor Locations for Excursion Scenarios (Series 3 and 4)

Potential receptors are assumed to be located at 528 ft, 856 ft, 1,840 ft and 3,480 ft down-gradient. In the discussion that follows, all of the relative peak arrival times and concentrations cited are for the potential receptor located at 528 ft down-gradient of the release (Figure 2-14). Breakthrough curves (i.e., concentrations as a function of time and distance) for all of the potential receptors are provided in Appendix C. These curves are based on a retardation factor of 1. Radionuclide-specific retardation effects are considered in Chapter 4.

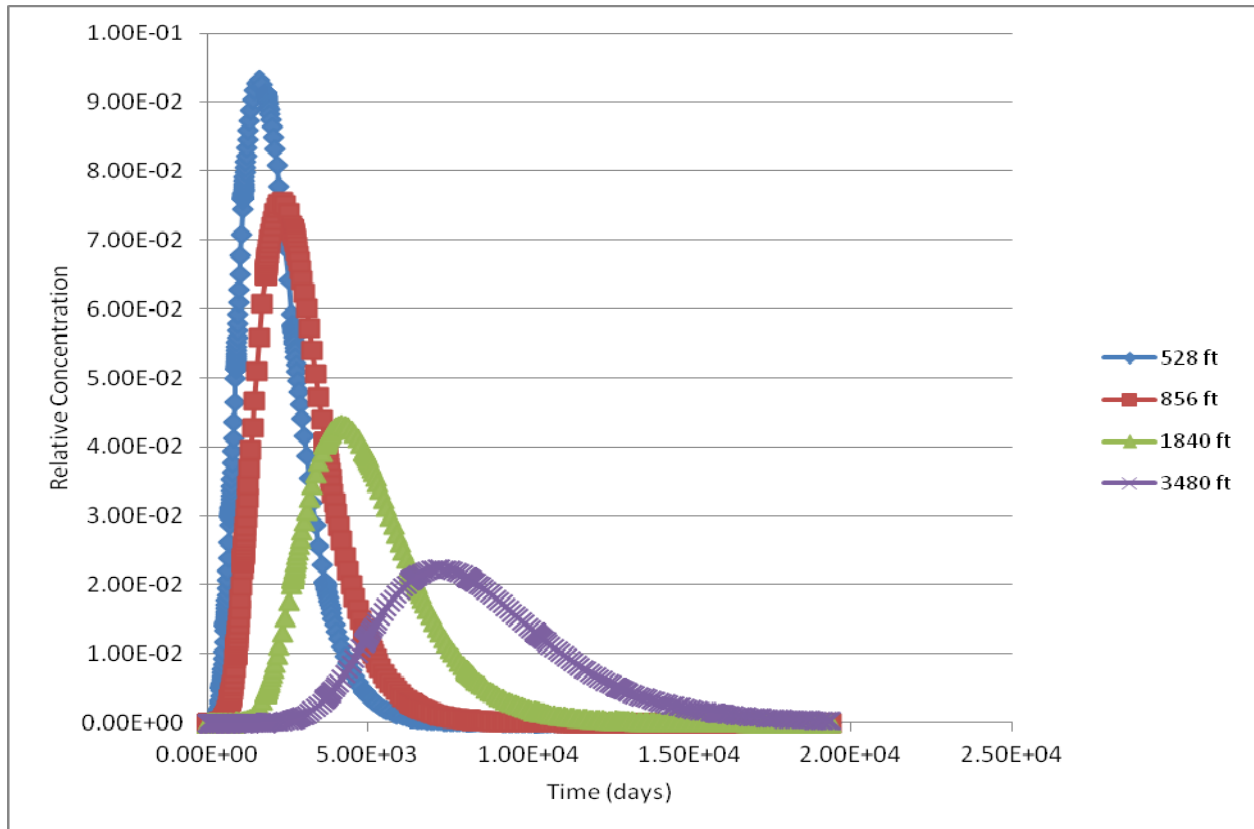


Figure 2-14: Example of Breakthrough Curves at Receptor Locations

All source fluid concentrations are assigned a relative concentration of 1 mg/L. As part of the dose assessment (Section 4), the relative concentrations arriving at the receptor well(s) are corrected to hypothesized concentrations of the source fluid and dose calculations are conducted.

2.6.2.1 Series 1 – 5-Spot 250-ft Spacing

The first series of simulations for Scenario 1 not only investigated the sensitivity of the results to hydraulic conductivities, gradients and extraction/injection rates, but also allowed an evaluation of the sensitivity to injection well spacing when compared to Series 2 (Section 2.6.2.2) counterpart simulations (Table 2-5 and Table 2-6). Since an injection/extraction well spacing of 250 ft is on the upper bound of well spacings typically used, this value was assigned in order to accentuate the differences in the results when compared against smaller spacings. Of the nine series of simulations, two series (1 and 3) assumed this upper bound on the well spacing. For the

remaining series, the wells were spaced at more commonly used intervals between 50 and 150 ft apart.

The only difference among model runs 1a, 1b and 1c is that the hydraulic gradients are specified as either 0.1, 0.01, or 0.001, respectively.

As shown in Appendix C and presented in Table 2-5, the peak arrival times for simulations 1a through 1c are 193, 1,080 and 1,600 days, respectively. Since all parameters are constant except for hydraulic gradients, the model predictions are as expected, and the steeper hydraulic gradients result in shorter travel times. Furthermore, since the pumping/injection wells are altering the regional hydraulic gradients, the arrival times are not linearly scaled (i.e., a factor of 10 increase in gradient does not result in a factor of 10 reduction in travel time).

Relative peak concentrations for runs 1a, 1b and 1c are 6.94×10^{-3} , 6.54×10^{-2} and 9.32×10^{-2} mg/L at a receptor well at a distance of 528 ft. The difference in these results can be explained by the fact that a steeper hydraulic gradient leads to a more elongated plume in which the mass is distributed over a larger down-gradient area, resulting in lower relative peak concentrations. Thus, the peak arrival concentration of run 1a is lower than run 1b, and relative concentrations of 1b are less than run 1c.

Simulations 1d, 1e and 1f are designed to investigate the impact that hydraulic conductivity has on the peak arrival times and relative peak concentrations. Hydraulic conductivities are 1, 10 and 100 ft/day, which coincide with the peak arrival times of 1,700, 1,100 and 193 days, respectively. As expected, the longer arrival times are associated with the lower hydraulic conductivities. Also of interest is that the peak arrival times of runs 1b and 1e are very close (1,080 and 1,100, respectively) and runs 1c and 1d are also similar (1,600 and 1,700, respectively). These similarities are related to the fact that velocities will be controlled by the product of hydraulic conductivity multiplied by the hydraulic gradient. For runs 1b and 1e, this product is 1.0, and for runs 1c and 1d the product is 0.1.

Relative peak concentrations for runs 1d, 1e and 1f are 2.14×10^{-1} , 6.55×10^{-2} and 6.94×10^{-3} mg/L. As has been observed for other simulations, an increase in hydraulic conductivity causes the plume to become more dispersed and leads to lower relative peak concentrations (Table 2-5).

Table 2-5: Series 1 – 5-Spot Injection at a Spacing of 250 feet – Receptor Well at 528 feet

SERIES 1 – 5-SPOT INJECTION AT 250 FOOT SPACING											
General Assumptions – All Runs		Run	1a	1b	1c	1d	1e	1f	1g	1h	1i
Receptor Locations (ft)	528, 856, 1,840, 3,480	Regional Hydraulic Gradient	0.1	0.01	0.001	0.1	0.1	0.1	0.01	0.01	0.01
Simulation Time (yr)	53	Effective Porosity (%)	20	20	20	20	20	20	20	20	20
Well Configuration	5-Spot (pumping from center well)	Dispersivity (ft)									
		Longitudinal	65	65	65	65	65	65	65	65	65
		Transverse	6.5	6.5	6.5	6.5	6.5	6.5	6.5	6.5	6.5
		Vertical	0.65	0.65	0.65	0.65	0.65	0.65	0.65	0.65	0.65
Well Spacing (ft)	250	Injection Fluid Conc. (milligram per L)	1	1	1	1	1	1	1	1	1
Injection Time (yr)	3	Hydraulic Conductivities (ft/day)	100	100	100	1	10	100	1	10	100
Model Area (ft ²)	13,300 (ft) × 13,300 (ft) = 6.25 mi ²	Distribution coefficients (ml/g)	Rf ¹ Specified in Spreadsheet	Rf Specified in Spreadsheet							
Model Layers	9	Injection/Extraction Well Spacing (ft)	5-spot – 250	5-spot - 250	5-spot - 250	5-spot - 250	5-spot - 250	5-spot - 250	5-spot - 250	5-spot - 250	5-spot - 250
Minimum/Maximum Grid Spacing (ft)	10/1000	Injection Rate (gpm)	150	150	150	150	150	150	150	150	150
All Layers	Homogenous	Pumping Rate (gpm)	153	153	153	153	153	153	153	153	153
		Operating Life of ISL Well Pattern (yrs)	3	3	3	3	3	3	3	3	3
		Time until Peak Arrival (days)	1.93×10 ²	1.08×10 ³	1.60×10 ³	1.70×10 ³	1.1×10 ³	1.93×10 ²	2.6×10 ⁴	1.60×10 ³	1.08×10 ³
		Relative Peak Concentration	6.94×10 ⁻³	6.54×10 ⁻²	9.32×10 ⁻²	2.14×10 ⁻¹	6.55×10 ⁻²	6.94×10 ⁻³	1.90×10 ⁻⁴	9.27×10 ⁻²	6.54×10 ⁻²

¹ Rf = retardation factor calculated in Section 4

Table 2-6: Series 2 – 5-Spot Injection at a Spacing of 50 feet – Receptor Well at 528 feet

SERIES 2 – 5-SPOT INJECTION AT 50 FOOT SPACING											
General Assumptions – All Runs		Run	2a	2b	2c	2d	2e	2f	2g	2h	2i
Receptor Locations (ft)	528, 856, 1,840, 3,480	Regional Hydraulic Gradient	0.1	0.01	0.001	0.1	0.1	0.1	0.01	0.01	0.01
Simulation Time (yr)	53	Effective Porosity (%)	20	20	20	20	20	20	20	20	20
Well Configuration	5-Spot (pumping from center well)	Dispersivity (ft)									
		Longitudinal	65	65	65	65	65	65	65	65	65
		Transverse	6.5	6.5	6.5	6.5	6.5	6.5	6.5	6.5	6.5
		Vertical	0.65	0.65	0.65	0.65	0.65	0.65	0.65	0.65	0.65
Well Spacing (ft)	50	Injection Fluid Conc. (milligram per L)	1	1	1	1	1	1	1	1	1
Injection Time (yr)	3	Hydraulic Conductivities (ft/day)	100	100	100	1	10	100	1	10	100
Model Area (ft ²)	13,300 (ft) × 13,300 (ft) = 6.25 mi ²	Distribution coefficients (ml/g)	Rf ¹ Specified in Spreadsheet	Rf Specified in Spreadsheet							
Model Layers	9	Injection/Extraction Well Spacing (ft)	5-spot - 50	5-spot - 50	5-spot - 50	5-spot - 50	5-spot - 50	5-spot - 50	5-spot - 50	5-spot - 50	5-spot - 50
Minimum/Maximum Grid Spacing (ft)	10/1000	Injection Rate (gpm)	150	150	150	150	150	150	150	150	150
All Layers	Homogenous	Pumping Rate (gpm)	153	153	153	153	153	153	153	153	153
		Operating Life of ISL Well Pattern (yrs)	3	3	3	3	3	3	3	3	3
		Time until Peak Arrival (days)	1.32×10 ²	1.05×10 ³	1.60×10 ³	1.52×10 ³	1.05×10 ³	1.32×10 ²	8.22×10 ³	1.60×10 ³	1.05×10 ³
		Relative Peak Concentration	9.62×10 ⁻³	2.35×10 ⁻²	8.75×10 ⁻³	1.18×10 ⁻²	2.35×10 ⁻²	9.62×10 ⁻³	3.39×10 ⁻⁶	8.22×10 ⁻³	2.35×10 ⁻²

¹ Rf = retardation factor calculated in Section 4

The hydraulic gradient assigned to simulations 1g, 1h and 1i is 0.01 ft/ft. The effect that the regional hydraulic gradient will have on the results is evaluated by comparing simulation output from these runs to results obtained from runs 1d, 1e and 1f, which are assigned a regional gradient of 0.1 ft/ft.

The peak arrival times for simulations 1g, 1h and 1i are 26,000, 1,600 and 1,080 days, respectively. The arrival time for run 1g is about 11 times that of run 1d (1,700 days), which is close to what would be expected, since the hydraulic gradient is 10 times lower in run 1g than in run 1d. This same relationship for the peak arrival times for 1h and 1i, however, are not maintained when compared to runs 1e and 1f, respectively. This is primarily due to the fact that the injection rates are held constant across all the simulations and the relative effects on hydraulic gradients will be much greater at lower hydraulic conductivities.

Relative peak concentrations for runs 1g, 1h and 1i are 1.80×10^{-4} , 9.27×10^{-2} and 6.54×10^{-2} mg/L. These results indicate that with flatter gradients (i.e., 0.01), the capture zone for the pumping wells becomes more pronounced laterally and more of the injectant is captured by the extraction wells. The inter-relationship between the hydraulic conductivities, regional gradient and pumping rates is complex, but in general, there is an internal consistency to the results. For instance, the relative concentrations for runs 1b and 1e are very similar and, upon inspection of the data files, it is evident that the product of hydraulic conductivity and gradient is 1.0 for both simulations. This same relationship is observed for runs 1c and 1h where the product is equal to 0.1.

2.6.2.2 Series 2 – 5-Spot 50-ft Spacing

The input parameters to all of the Series 2 simulations are identical to those performed in Series 1 with the exception that the spacing between the injection wells is decreased from 250 ft to 50 ft (Table 2-6).

Relative peak arrival times for runs 2a, 2b and 2c are 132, 1,050 and 1,600 days, respectively. These values are similar to the peak arrival times for simulations 1a through 1c, which are 193, 1,080 and 1,600 days. The fact that run pairs 2b:1b and 2c:1c are so close indicates that the hydraulic gradients beyond the capture zone are very similar and any excursions will migrate at very similar rates. The peak arrival times for runs 2a and 1a, however, show a greater divergence in which the smaller well spacing and higher hydraulic gradient (0.1) results in a shorter travel time (i.e., 132 versus 193 days). This is because the larger well spacing affects (flattens) the hydraulic gradient over a larger area and achieves a better degree of capture, as is confirmed by comparing the relative peak concentrations.

Relative peak concentrations for runs 2a, 2b and 2c are 9.62×10^{-3} , 2.35×10^{-2} and 8.75×10^{-3} mg/L. The peak concentration for run 2a is somewhat higher than that observed for run 1a (i.e., 6.94×10^{-3}), indicating that at higher regional gradients, the wider well spacing provides better capture of the lixiviant. At lower regional hydraulic gradients, however, better capture can be maintained at smaller well spacings, as evidenced by the lower peak concentrations observed in runs 2b and 2c when compared to their counterparts.

Simulations 2d, 2e and 2f are designed to investigate the sensitivity of hydraulic conductivity (i.e., 1, 10 and 100). Relative peak arrival times for these runs are 1,520, 1,050 and 132 days, respectively. These results indicate somewhat shorter times than those predicted with the larger well spacings. Peak arrival times of simulations 1d, 1e and 1f are 1,700, 1,100 and 193 days, respectively. These results indicate that the larger well spacing tends to level out the hydraulic gradients to a greater degree, thus resulting in longer travel times.

Relative peak concentrations for runs 2d, 2e and 2f are 1.18×10^{-2} , 2.35×10^{-2} and 9.62×10^{-3} mg/L, and the relative peak concentrations for runs 1d, 1e and 1f are 2.14×10^{-1} , 6.55×10^{-2} and 6.94×10^{-3} mg/L. The lower concentrations of 2d and 2e than 1d and 1e indicate that the closer well spacing leads to better capture and lower excursion concentrations at lower hydraulic conductivities.

The hydraulic gradient assigned to simulations 2g, 2h and 2i is 0.01 ft/ft and the hydraulic conductivities are 1, 10 and 100, respectively. Peak arrival times for these simulations are 8,220, 1,600 and 1,050 days. The peak arrival times for counterpart simulations 1g, 1h and 1i are 26,000, 1,600 and 1,080 days, respectively. Based upon these results, the hydraulic gradients are most impacted by well spacing at the lower hydraulic conductivities. This is because at higher hydraulic conductivities, the impacts of injection/withdrawal are in closer proximity to the pumping/injection well(s). Therefore, a wider well spacing will tend to spread out the effects of pumping over a larger area, although this does not necessarily mean that the capture of the lixiviant is greater at a larger well spacing, as is evidenced by the relative peak concentrations.

Relative peak concentrations for runs 2g, 2h and 2i are 3.39×10^{-6} , 8.22×10^{-3} and 2.35×10^{-2} mg/L, and relative peak concentrations for runs 1g, 1h and 1i are 1.80×10^{-4} , 9.27×10^{-2} and 6.54×10^{-2} mg/L. These results indicate that under moderate hydraulic gradients and at lower hydraulic conductivities, concentrations of the excursions will be lower. At the higher hydraulic conductivity (i.e., 100 ft/day), however, and smaller well spacing (run 2i), the excursion reaches the receptor at higher concentrations as compared to the larger well spacing (run 1i). Although the larger well spacing flattens out the gradient and slows the migration more relative to the smaller well spacing, the capture zone for the smaller well spacing does not extend as far in the lateral directions (perpendicular to flow) as the larger well spacing. Furthermore, there tends to be more lixiviant that escapes between the wells at the larger spacing.

2.6.2.3 Series 3 – 7-Spot 250-ft Spacing

The input parameters to all of the Series 3 simulations are identical to those performed in Series 1 with the exception that the extraction and injection wells are in a 7-spot well configuration (Figure 2-13).

Relative peak arrival times for runs 3a, 3b and 3c are 235, 1,100 and 1,900 days, respectively (Table 2-7). These values are very similar to the peak arrival times for simulations 1a through 1c, which are 193, 1,080 and 1,600 days. These results indicate that the 7-spot well configuration does not significantly alter the travel times as compared to the 5-spot well configuration over a range of hydraulic gradients (i.e., 0.1, 0.01 and 0.001) and at a hydraulic conductivity of 100 ft/day.

Table 2-7: Series 3 – 7-Spot Injection at a Spacing of 250 feet – Receptor Well at 528 feet

SERIES 3 – 7-SPOT INJECTION AT 250 FOOT SPACING											
General Assumptions – All Runs		Run	3a	3b	3c	3d	3e	3f	3g	3h	3i
Receptor Locations (ft)	528, 856, 1840, 3480	Regional Hydraulic Gradient	0.1	0.01	0.001	0.1	0.1	0.1	0.01	0.01	0.01
Simulation Time (yr)	53	Effective Porosity (%)	20	20	20	20	20	20	20	20	20
Well Configuration	7-spot (pumping from center well)	Dispersivity (ft)									
		Longitudinal	65	65	65	65	65	65	65	65	65
		Transverse	6.5	6.5	6.5	6.5	6.5	6.5	6.5	6.5	6.5
		Vertical	0.65	0.65	0.65	0.65	0.65	0.65	0.65	0.65	0.65
Well Spacing (ft)	250	Injection Fluid Conc. (milligram per L)	1	1	1	1	1	1	1	1	1
Injection Time (yr)	3	Hydraulic Conductivities (ft/day)	100	100	100	1	10	100	1	10	100
Model Area (ft ²)	13,300 (ft) × 13,300 (ft) = 6.25 mi ²	Distribution coefficients (ml/g)	Rf ¹ Specified in Spreadsheet	Rf Specified in Spreadsheet							
Model Layers	9	Injection/Extraction Well Spacing (ft)	7-spot - 250	7-spot - 250	7-spot - 250	7-spot - 250	7-spot - 250	7-spot - 250	7-spot - 250	7-spot - 250	7-spot - 250
Minimum/Maximum Grid Spacing (ft)	10/1000	Injection Rate (gpm)	150	150	150	150	150	150	150	150	150
All Layers	Homogenous	Pumping Rate (gpm)	153	153	153	153	153	153	153	153	153
		Operating Life of ISL Well Pattern (yrs)	3	3	3	3	3	3	3	3	3
		Time until Peak Arrival (days)	2.35×10 ²	1.1×10 ³	1.90×10 ³	1.97×10 ³	1.1×10 ³	2.35×10 ²	4.00×10 ⁴	1.90×10 ³	1.10×10 ³
		Relative Peak Concentration	2.78×10 ⁻³	3.53×10 ⁻²	6.79×10 ⁻²	1.41×10 ⁻¹	3.53×10 ⁻²	2.78×10 ⁻³	1.06×10 ⁻⁴	6.75×10 ⁻²	3.53×10 ⁻²

¹ Rf = retardation factor calculated in Section 4

Relative peak concentrations for runs 3a, 3b and 3c are 2.78×10^{-3} , 3.53×10^{-2} and 6.79×10^{-2} mg/L, and relative peak concentrations for runs 1a, 1b and 1c are 6.94×10^{-3} , 6.54×10^{-2} and 9.32×10^{-2} mg/L. Within each series, the flatter regional hydraulic gradients result in higher concentrations due to the plumes being less elongated and the mass more confined. The 7-spot well configuration, however, results in lower relative peak concentrations for all of the runs. This is because the additional pumping/extraction wells allow more overlap of the capture zone(s). In a 7-spot pattern, the distance from an injection to an extraction well is 250 ft, while for a 5-spot pattern it is 176 ft.

Hydraulic conductivities for runs 3d, 3e and 3f are 1, 10 and 100 ft/day, which coincide with relative peak arrival times of 1,970, 1,100 and 235 days, respectively. Relative peak arrivals for simulations 1d, 1e and 1f are 1,700, 1,100 and 193 days. Therefore, the peak arrival times for both sets of simulations are relatively similar over a range of hydraulic conductivities.

Relative peak concentrations for runs 3d, 3e and 3f are 1.41×10^{-1} , 3.53×10^{-2} and 2.78×10^{-3} mg/L, and relative peak concentrations for runs 1d, 1e and 1f are 2.14×10^{-1} , 6.55×10^{-2} and 6.94×10^{-3} mg/L. Lower concentrations are correlated to the higher hydraulic conductivities. As was previously observed for runs 3a-c and 1a-c, the 7-spot configuration results in lower relative peak concentrations for all of the simulations.

The hydraulic gradient assigned to simulations 3g, 3h and 3i is 0.01 ft/ft and the hydraulic conductivities are 1, 10 and 100, respectively. Peak arrival times for these simulations are 40,000, 1,900 and 1,100 days. The peak arrival times for counterpart simulations 1g, 1h and 1i are 26,000, 1,600 and 1,080 days, respectively. Based upon these results, the travel times at the higher hydraulic conductivities are very similar for the hydraulic conductivity of 1 ft/day (run 3g and 1g), however, the time until peak arrival for the 7-spot well configuration is considerably longer. This observation is primarily due to the effect that the additional wells have on flattening out the hydraulic gradient.

Relative peak concentrations for runs 3g, 3h and 3i are 1.06×10^{-4} , 6.75×10^{-2} and 3.53×10^{-2} mg/L, and relative peak concentrations for runs 1g, 1h and 1i are 1.80×10^{-4} , 9.27×10^{-2} and 6.54×10^{-2} mg/L. These results indicate that under moderate hydraulic gradients and at lower hydraulic conductivities, concentrations of the excursions will be lower. Furthermore, the relative peak concentrations for all of the 7-spot well configurations are lower than those for the analogous 5-spot well simulations.

2.6.2.4 Series 4 – 7-Spot 50-ft Spacing

The input parameters to all of the Series 4 simulations are identical to those performed in Series 3 with the exception that the extraction and injection wells are spaced at 50 ft instead of at 250 ft.

Relative peak arrival times for runs 4a, 4b and 4c are 186, 1,100 and 1,450 days, respectively (Table 2-8). For comparable simulations in Series 3, the relative peak arrival times for runs 3a, 3b and 3c are 235, 1,100 and 1,900 days, respectively (Table 2-7). These results indicate that at the high (4c:3c) and low (4a:3a) hydraulic gradients, the relative peak arrival times are shorter

for the more narrowly spaced wells. This relationship was also observed when the output for Series 1 and 2 was compared (Section 2.6.2.2) and is caused by greater flattening of the hydraulic gradient over a larger area with the wider well spacing. At the moderate gradient (0.01 ft/ft), however, the peak arrival times for runs 3b and 4b are essentially the same. This is because at the moderate gradient, there is a balance between the regional gradient and the gradients caused by the pumping/injection in which the net gradients that result are not as sensitive to the well spacing.

Relative peak concentrations for runs 4a, 4b and 4c are 1.25×10^{-2} , 4.03×10^{-3} and 9.01×10^{-3} mg/L, and relative peak concentrations for runs 3a, 3b and 3c are 2.78×10^{-3} , 3.53×10^{-2} and 6.79×10^{-2} mg/L. The peak concentration for run 4a is somewhat higher than that observed for run 3a, indicating that at higher regional gradients, the wider well spacing provides better capture of the lixiviant. At lower regional hydraulic gradients, however, better capture can be maintained at smaller well spacings, as evidenced by the lower peak concentrations observed in runs 4b and 4c when compared to their counterparts. This same relationship was observed when Series 1a, b, and c was compared to Series 2a, b, and c (Section 2.6.2.2).

Hydraulic conductivities for runs 4d, 4e and 4f are 1, 10 and 100 ft/day, which coincide with relative peak arrival times for runs of 1,390, 1,020 and 186 days, respectively. Relative peak arrival times for runs 3d, 3e and 3f are 1,970, 1,100 and 235 days. As is expected, the longer arrival times are associated with the lower hydraulic conductivities. The peak arrival times of 4e and 3e are very close (1,020 and 1,100, respectively). For the remaining simulations, however, the results are similar, but do not compare as well. Due to the hydraulic gradients not being affected over as large an area, the smaller well spacing results in shorter peak arrival times.

Relative peak concentrations for runs 4d, 4e and 4f are 3.07×10^{-2} , 4.03×10^{-2} and 1.25×10^{-2} mg/L, and relative peak concentrations for runs 3d, 3e and 3f are 1.41×10^{-1} , 3.53×10^{-2} and 2.78×10^{-3} mg/L. With exception of the 4e:3e run comparison, the closer well spacing leads to lower relative peak concentrations. The closer well spacing also leads to better capture, in general, as evidenced by the similar release concentrations among runs 4d, 4e and 4f.

The hydraulic gradient for runs 4g, 4h, and 4i is 0.01 ft/ft and the hydraulic conductivities are 1, 10 and 100 ft/day, respectively. Relative peak arrival times for runs 4g, 4h and 4i are 7,840, 1,450 and 1,100 days, respectively (Table 2-8). For comparable simulations in Series 3, the relative peak arrival times for runs 3g, 3h and 3i are 40,000, 1,900 and 1,100 days. At the lower hydraulic conductivities (4g and 4h), the closer well spacing results in shorter arrival times. For a hydraulic conductivity of 100 ft/day, the arrival times (4i:3i) are identical.

Table 2-8: Series 4 – 7-Spot Injection at a Spacing of 50 feet – Receptor Well at 528 feet

SERIES 4 – 7-SPOT INJECTION AT 50 FOOT SPACING											
General Assumptions – All Runs		Run	4a	4b	4c	4d	4e	4f	4g	4h	4i
Receptor Locations (ft)	528, 856, 1,840, 3,480	Regional Hydraulic Gradient	0.1	0.01	0.001	0.1	0.1	0.1	0.01	0.01	0.01
Simulation Time (yr)	53	Effective Porosity (%)	20	20	20	20	20	20	20	20	20
Well Configuration	7-Spot (pumping from center well)	Dispersivity (ft)									
		Longitudinal	65	65	65	65	65	65	65	65	65
		Transverse	6.5	6.5	6.5	6.5	6.5	6.5	6.5	6.5	6.5
		Vertical	0.65	0.65	0.65	0.65	0.65	0.65	0.65	0.65	0.65
Well Spacing (ft)	50	Injection Fluid Conc. (milligram per L)	1	1	1	1	1	1	1	1	1
Injection Time (yr)	3	Hydraulic Conductivities (ft/day)	100	100	100	1	10	100	1	10	100
Model Area (ft ²)	13,300 (ft) × 13,300 (ft) = 6.25 mi ²	Distribution coefficients (ml/g)	Rf ¹ Specified in Spreadsheet	Rf Specified in Spreadsheet							
Model Layers	9	Injection/Extraction Well Spacing (ft)	7-spot - 50	7-spot - 50	7-spot - 50	7-spot - 50	7-spot - 50	7-spot - 50	7-spot - 50	7-spot - 50	7-spot - 50
Minimum/Maximum Grid Spacing (ft)	10/1000	Injection Rate (gpm)	150	150	150	150	150	150	150	150	150
All Layers	Homogenous	Pumping Rate (gpm)	153	153	153	153	153	153	153	153	153
		Operating Life of ISL Well Pattern (yrs)	3	3	3	3	3	3	3	3	3
		Time until Peak Arrival (days)	1.86×10 ²	1.10×10 ³	1.45×10 ³	1.39×10 ³	1.02×10 ³	1.86×10 ²	7.84×10 ³	1.45×10 ³	1.10×10 ³
		Relative Peak Concentration	1.25×10 ⁻²	4.03×10 ⁻³	9.01×10 ⁻³	3.07×10 ⁻²	4.03×10 ⁻²	1.25×10 ⁻²	2.14×10 ⁻⁶	8.94×10 ⁻³	4.03×10 ⁻²

¹ Rf = retardation factor calculated in Section 4

Relative peak concentrations for runs 4g, 4h and 4i are 2.14×10^{-6} , 8.94×10^{-3} and 4.03×10^{-2} mg/L. These outcomes indicate that capture of the injectant is more effective at the lower hydraulic conductivities and results in lower relative peak concentrations. A comparison against simulations 4d, 4e and 4f indicates that the steeper hydraulic gradient results in larger releases because the lateral capture is not as effective.

Relative peak concentrations for runs 4g, 4h and 4i are lower than those observed for runs 3g, 3h and 3i, which are 1.06×10^{-4} , 6.75×10^{-2} and 3.53×10^{-2} mg/L. These results support earlier findings indicating that the closer well spacing captures more of the injectant.

2.6.2.5 Series 5 – 5-Spot Injection/Pumping Rates Dependent Upon Hydraulic Conductivity

The injection/pumping rates specified in all of the simulations performed in Series 1 through 4 are 150 gpm (injection) and 153 gpm (pumping). Although these rates are the same, in actuality, the hydraulic conductivities would be considered in determining the amount of water that is pumped and injected. This correlation was not factored into the Series 1 through 4 simulations because it would make it very difficult to isolate the effects of the other parameters (e.g., hydraulic gradients, well configuration and spacing). For Series 5, however, the injection/pumping rates have been adjusted to more realistically reflect the hydraulic conductivity of the system.

To estimate pumping/injection rates at hydraulic conductivities of 1, 10 and 100 ft/day, a constant head boundary was set to an elevation representative of the approximate pumping level in each of the wells. MODFLOW output files provide the amount of water removed by the constant head boundary, and this value was subsequently used as input for the pumping/injection rates. The specified rates for hydraulic conductivities of 1, 10 and 100 ft/day are 7.15/7, 51/50 and 510/500 gpm, respectively (Table 2-9).

In addition to the change in the pumping/extraction rates, the well spacing for the Series 5 simulations is set to 150 ft, as opposed to the 50 or 250 spacings assigned in the earlier simulations.

Table 2-9: Series 5 – 5-Spot Injection\Pumping Rates Dependent Upon Hydraulic Conductivity

SERIES 5 – 5-SPOT INJECTION/PUMPING RATES DEPENDENT UPON HYDRAULIC CONDUCTIVITY											
General Assumptions - All Runs		Run	5a	5b	5c	5d	5e	5f	5g	5h	5i
Receptor Locations (ft)	528, 856, 1840, 3480	Regional Hydraulic Gradient	0.1	0.01	0.001	0.01	0.01	0.01	0.001	0.001	0.001
Simulation Time (yr)	53	Effective Porosity (%)	20	20	20	20	20	20	20	20	20
Well Configuration	5-Spot (pumping from center well)	Dispersivity (ft)									
		Longitudinal	65	65	65	65	65	65	65	65	65
		Transverse	6.5	6.5	6.5	6.5	6.5	6.5	6.5	6.5	6.5
		Vertical	0.65	0.65	0.65	0.65	0.65	0.65	0.65	0.65	0.65
Well Spacing (ft)	150	Injection Fluid Conc. (milligram per L)	1	1	1	1	1	1	1	1	1
Injection Time (yr)	3	Hydraulic Conductivities (ft/day)	10	10	10	1	10	100	1	10	100
Model Area (ft ²)	13,300 (ft) × 13,300 (ft) = 6.25 mi ²	Distribution coefficients (ml/g)	Rf ¹ Specified in Spreadsheet	Rf Specified in Spreadsheet							
Model Layers	9	Injection/Extraction Well Spacing (ft)	5-spot - 150	5-spot - 150	5-spot - 150	5-spot - 150	5-spot - 150	5-spot - 150	5-spot - 150	5-spot - 150	5-spot - 150
Minimum/Maximum Grid Spacing (ft)	10/1000	Injection Rate (gpm)	50	50	50	7	50	500	7	50	500
All Layers	Homogenous	Pumping Rate (gpm)	51	51	51	7.15	51	510	7.15	51	510
		Operating Life of ISL Well Pattern (yrs)	3	3	3	3	3	3	3	3	3
		Time until Peak Arrival (days)	1.10×10 ³	1.52×10 ³	1.8×10 ⁴	1.01×10 ⁴	1.52×10 ³	1.05×10 ³	1.28×10 ⁴	1.8×10 ⁴	1.10×10 ³
		Relative Peak Concentration	3.76×10 ⁻²	6.79×10 ⁻²	8.24×10 ⁻⁴	1.53×10 ⁻²	6.79×10 ⁻²	1.01×10 ⁻¹	1.05×10 ⁻¹⁶	8.24×10 ⁻⁴	1.08×10 ⁻¹

¹ Rf = retardation factor calculated in Section 4

The hydraulic gradients for runs 5a, 5b and 5c are 0.1, 0.01 and 0.001 ft/ft. All of the hydraulic conductivities are set to 10 ft/day with an accompanying pumping/injection rate of 51/50 gpm. Relative peak arrival times for runs 5a, 5b and 5c are 1,100, 1,520 and 18,000 days, respectively (Table 2-9). Since so many parameters have been changed from those assigned to simulations in the previous series, it is difficult to draw inter-series comparisons. The arrival time of 18,000 days, however, is one of the longest times observed.

Relative peak concentrations for runs 5a, 5b and 5c are 3.76×10^{-2} , 6.79×10^{-2} and 8.24×10^{-4} mg/L and indicate that the capture zone is most effective at the lowest hydraulic gradient of 0.001 ft/ft (run 5c). Results for runs 5a and 5b indicate that although the capture is more effective at a gradient of 0.01 than 0.1 ft/ft, the injectant becomes more widely dispersed in the down-gradient direction under the 0.1 ft/ft gradient due to the higher velocities.

Runs 5d, 5e and 5f are all performed with a hydraulic gradient of 0.01 ft/ft; hydraulic conductivities of 1, 10 and 100 ft/day; and with the pumping/injection rates varying as a function of the hydraulic conductivity. Relative peak arrival times for runs 5d, 5e and 5f are 10,100, 1,520 and 1,050 days. The arrival time for 5d is almost 10 times that of 5a, which is expected since the hydraulic gradient is decreased by a factor of 10. This result also reflects the fact that the pumping rate for 5d of 7.15 gpm was similarly scaled to a hydraulic conductivity of 1, as was the pumping rate of 50 gpm to a hydraulic conductivity of 10 ft/day.

Relative peak concentrations for runs 5d, 5e and 5f are 1.53×10^{-2} , 6.79×10^{-2} and 1.01×10^{-1} mg/L. The concentrations increase as a function of increasing pumping/injection rates and hydraulic conductivities and indicate that capture is more complete at the lower hydraulic conductivities. These results also suggest that the bleed rate (i.e., difference between pumping and injection rates) should be increased as a function of hydraulic conductivity in order to increase the capture zone at hydraulic conductivities.

The input for runs 5g, 5h and 5i are identical to that for runs 5d, 5e and 5f, except that the hydraulic gradient is set to 0.001 ft/ft instead of 0.01 ft/ft. The peak arrival times for runs 5g, 5h and 5i are 12,800, 18,000 and 1,100 days. With the exception of runs 5h and 5e, the arrival times for the 5g-e and 5i-f pairs are very similar. This suggests that the hydraulic gradients created by the pumping/injection wells are large enough to overwhelm the differences in the regional hydraulic gradients. With respect to run 5h, it appears that the long peak arrival time observed is due to the very low relative peak concentration (i.e., 1.05×10^{-16}) in which numerical dispersion may be a significant contributor.

Relative peak concentrations for runs 5g, 5h and 5i are 1.05×10^{-16} , 8.24×10^{-4} and 1.08×10^{-1} mg/L. These results, when compared against those obtained for runs 5d, 5e and 5f, indicate that the flatter gradients allow better capture and that at the conductivity of 100 ft/day, the injection/pumping is large enough to overwhelm the differences in regional gradients.

2.6.2.6 Series 6 – 5-Spot 20-ft Thick Mined Interval

All of the simulations performed in Series 6 are identical to those conducted for Series 5 except that the model layers vary in thickness and the mined interval was reduced from a thickness of 70 ft to 20 ft (Figure 2-11).

The relative peak arrival times for run 6a, 6b and 6c are 1,700, 1,100 and 20,600 days, respectively (Table 2-10). As described in Section 2.6.2.5, the relative peak arrival times for runs 5a, 5b and 5c are 1,100, 1,520 and 18,000 days. The effect of pumping/injection on hydraulic gradients is strongly affected by the transmissivity (i.e., hydraulic conductivity multiplied by thickness) of the geologic units. The lower transmissivity results in shorter times to peak arrivals at the low and high gradients (runs 6a and 6c) and a longer time at the medium gradient (run 6b). These relationships are all related to how the regional and localized gradients created by the pumping/injection interact to form a capture zone. It also illustrates the complexity and need to understand the geology and flow system, since the effects of the interactions are not always intuitive.

Relative peak concentrations for runs 6a, 6b and 6c are 3.31×10^{-1} , 4.75×10^{-1} and 1.30×10^{-3} mg/L and, as was observed with runs 5a, 5b and 5c, indicate that the capture zone is most effective at the lowest hydraulic gradient (0.001 ft/ft). All of the relative concentrations are approximately an order of magnitude higher than the relative peak concentrations for runs 5a, 5b and 5c (i.e., 3.76×10^{-2} , 6.79×10^{-2} and 8.24×10^{-4} mg/L). The higher concentration at the lower transmissivity is due to the injectant being concentrated within a smaller volume.

Runs 6d, 6e and 6f are all performed with a hydraulic gradient of 0.01 ft/ft; hydraulic conductivities of 1, 10 and 100 ft/day; and with the pumping/injection rates varying as a function of the hydraulic conductivity. Relative peak arrival times for runs 6d, 6e and 6f are 9,930, 1,520 and 1,050 days. The times are very similar for runs 6d-5d and essentially identical for runs 6e-5e and 6f-5f. Therefore, for the same regional gradient, the peak arrival times are insensitive to the transmissivity.

Relative peak concentrations for runs 6d, 6e and 6f are 1.06×10^{-1} , 4.75×10^{-1} and 6.45×10^{-1} mg/L, and, as was observed with the 6a, b, and c versus 5a, b, and c series, are all considerably higher than their counterparts where the relative peak concentrations for runs 5d, 5e and 5f are 1.53×10^{-2} , 6.79×10^{-2} and 1.01×10^{-1} mg/L. These results demonstrate that the lower transmissivities will result in higher relative concentrations.

The peak arrival times for runs 6g, 6h and 6i are 288,000, 20,700 and 1,210 days. The very long peak arrival time for run 6g and low peak concentration (i.e., 7.40×10^{-5}) indicate that capture at the lowest hydraulic conductivity is essentially complete. The relative peak arrival times for 5h and 5i (i.e., 18,000 and 1,100 days) are very close to those observed for runs 6h and 6i, which indicate that similar hydraulic gradients are being created for both sets of simulations.

Table 2-10: Series 6 – 5-Spot 20-Foot Thick Mined Interval

SERIES 6 – 5-SPOT – 20-FOOT THICK MINED INTERVAL											
General Assumptions - All Runs		Run	6a	6b	6c	6d	6e	6f	6g	6h	6i
Receptor Locations (ft)	528, 856, 1,840, 3,480	Regional Hydraulic Gradient	0.1	0.01	0.001	0.01	0.01	0.01	0.001	0.001	0.001
Simulation Time (yr)	53	Effective Porosity (%)	20	20	20	20	20	20	20	20	20
Well Configuration	5-Spot (pumping from center well)	Dispersivity (ft)									
		Longitudinal	65	65	65	65	65	65	65	65	65
		Transverse	6.5	6.5	6.5	6.5	6.5	6.5	6.5	6.5	6.5
		Vertical	0.65	0.65	0.65	0.65	0.65	0.65	0.65	0.65	0.65
Well Spacing (ft)	150	Injection Fluid Conc. (milligram per L)	1	1	1	1	1	1	1	1	1
Injection Time (yr)	3	Hydraulic Conductivities (ft/day)	10	10	10	1	10	100	1	10	100
Model Area (ft ²)	13,300 (ft) × 13,300 (ft) = 6.25 mi ²	Distribution coefficients (ml/g)	Rf ¹ Specified in Spreadsheet	Rf Specified in Spreadsheet							
Model Layers	9 The thickness of layer 5 is decreased to 20 ft thick and has the monitoring/injection/pumping wells.	Injection/Extraction Well Spacing (ft)	5-spot - 150	5-spot - 150	5-spot - 150	5-spot - 150	5-spot - 150	5-spot - 150	5-spot - 150	5-spot - 150	5-spot - 150
Minimum/Maximum Grid Spacing (ft)	10/1000	Injection Rate (gpm)	50	50	50	7	50	500	7	50	500
All Layers	Homogenous	Pumping Rate (gpm)	51	51	51	7.15	51	510	7.15	51	510
		Operating Life of ISL Well Pattern (yrs)	3	3	3	3	3	3	3	3	3
		Time until Peak Arrival (days)	1.70×10 ³	1.10×10 ³	2.06×10 ⁴	9.93×10 ³	1.52×10 ³	1.05×10 ³	2.88×10 ⁵	2.07×10 ⁴	1.21×10 ³
		Relative Peak Concentration	3.31×10 ⁻¹	4.75×10 ⁻¹	1.30×10 ⁻³	1.06×10 ⁻¹	4.75×10 ⁻¹	6.45×10 ⁻¹	7.40×10 ⁻⁵	1.30×10 ⁻³	6.26×10 ⁻¹

¹ Rf = retardation factor calculated in Section 4

Relative peak concentrations for runs 6g, 6h and 6i are 7.40×10^{-5} , 1.30×10^{-3} and 6.26×10^{-1} mg/L. These results, when compared against those obtained for runs 5g, 5h and 5i (i.e., 1.05×10^{-16} , 8.24×10^{-4} and 1.08×10^{-1}), are all higher and, as was observed between the 6d, e, and f and 5d, e, and f comparisons, the lower transmissivities result in higher relative concentrations.

2.6.2.7 Series 7 – Twenty-Five 5-Spot Pumping/Injection Cells

To evaluate the potential cumulative effects of multiple pumping/injection cells, the simulations in Series 7 consist of twenty-five 5-spot injection cells (Figure 2-15). With the exception of the multiple cells, all of the other input parameters for Series 7 are identical to those for Series 6, where only one 5-spot pattern was modeled (Table 2-11).

The only difference among model runs 7a, 7b and 7c is that the hydraulic gradients are specified as 0.1, 0.01 or 0.001, respectively. The relative peak arrival times for runs 7a, 7b, and 7c are 1,090, 4,830 and 1,280 days, while the relative peak arrival times for runs 6a, 6b and 6c are 1,700, 1,100 and 20,600 days. The observed differences are associated with the degree to which the multiple cells affect the hydraulic gradients as compared to the single pumping/injection cell. At the highest gradient (runs 7a and 6a), both simulations impact the hydraulic gradients to a relatively similar degree. At the moderate gradient, however, the multiple cells are more effective at flattening the hydraulic gradients, which is reflected in the longer peak arrival times in run 7b as compared to run 6b. For the runs with the relatively flat regional gradients (7c and 6c), the impact of the pumping/injection for the multiple cells in run 7c overwhelms the effects of the regional gradient, as expressed by the very long travel time in run 6c.

Relative peak concentrations for runs 7a, 7b and 7c are 3.12×10^{-1} , 6.61×10^{-4} and 2.70×10^{-4} mg/L, and the relative peak concentrations for runs 6a, 6b and 6c are 3.31×10^{-1} , 4.75×10^{-1} and 1.30×10^{-3} mg/L. Except for the simulations with the steep regional gradient (7a and 6a), the peak relative concentrations with the multiple cells are orders of magnitude lower than the single cell simulations. These results indicate that at lower hydraulic gradients, the majority of the injectant that is not recaptured is lost from the injection wells that are located to the furthest east and west and not very much is lost from the line of injection wells located in between. Under the steeper hydraulic gradient, however, the capture is not complete along the entire line of wells running east-west and, therefore, the relative peak concentrations for runs 7a and 6a are at similarly elevated levels.

Runs 7d, 7e and 7f are all performed with a hydraulic gradient of 0.01 ft/ft, and hydraulic conductivities of 1, 10 and 100 ft/day. Relative peak arrival times for runs 7d, 7e and 7f are 48,700, 4,800 and 1,100 days. At the lower hydraulic conductivities, these results indicate slower velocities than the comparable runs in Series 6 (6d and 6e), which are 9,930, and 1,520 days and indicate the formation of flatter gradients formed by the array of pumping/injection wells. At the hydraulic conductivity of 100 ft/day, however, the arrival time for run 7f is nearly the same as that for run 6f (1,050 days), indicating that the gradients are less affected by the pumping/injection at higher hydraulic conductivities.

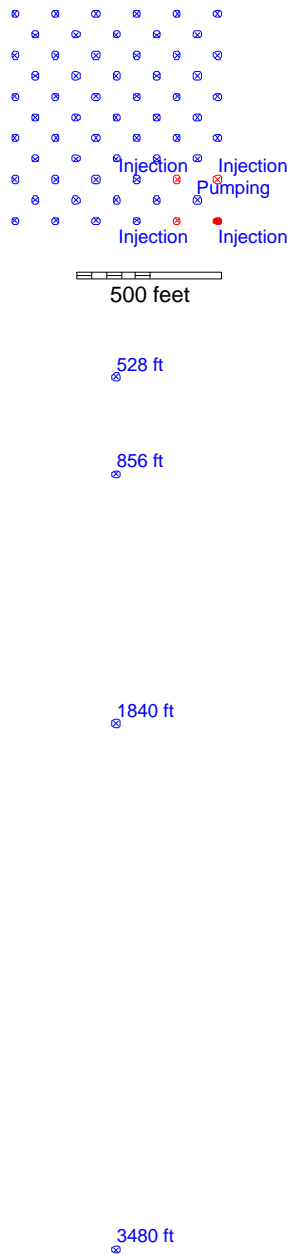


Figure 2-15: Plan View of the Twenty-five 5-spot Pumping/Injection Well Configurations and Receptor Locations for Excursion Scenario (Series 7)

Table 2-11: Series 7 – Twenty-five 5-Spot Pumping/Injection Cells

SERIES 7 – TWENTY-FIVE (25) 5-SPOT PUMPING/INJECTION CELLS											
General Assumptions - All Runs		Run	7a	7b	7c	7d	7e	7f	7g	7h	7i
Receptor Locations (ft)	528, 856, 1,840, 3,480	Regional Hydraulic Gradient	0.1	0.01	0.001	0.01	0.01	0.01	0.001	0.001	0.001
Simulation Time (yr)	53	Effective Porosity (%)	20	20	20	20	20	20	20	20	20
Well Configuration	5-Spot (pumping from center well)	Dispersivity (ft)									
		Longitudinal	65	65	65	65	65	65	65	65	65
		Transverse	6.5	6.5	6.5	6.5	6.5	6.5	6.5	6.5	6.5
		Vertical	0.65	0.65	0.65	0.65	0.65	0.65	0.65	0.65	0.65
Well Spacing (ft)	150	Injection Fluid Conc. (milligram per L)	1	1	1	1	1	1	1	1	1
Injection Time (yr)	3	Hydraulic Conductivities (ft/day)	10	10	10	1	10	100	1	10	100
Model Area (ft ²)	13,300 (ft) × 13,300 (ft) = 6.25 mi ²	Distribution coefficients (ml/g)	Rf ¹ Specified in Spreadsheet	Rf Specified in Spreadsheet							
Model Layers	9 The thickness of layer 5 is decreased to 20 ft thick and has the monitoring/injection/pumping wells.	Injection/Extraction Well Spacing (ft)	5-spot - 150	5-spot - 150	5-spot - 150	5-spot - 150	5-spot - 150	5-spot - 150	5-spot - 150	5-spot - 150	5-spot - 150
Minimum/Maximum Grid Spacing (ft)	10/1000	Injection Rate (gpm)	50	50	50	7	50	500	7	50	500
All Layers	Homogenous	Pumping Rate (gpm)	51	51	51	7.15	51	510	7.15	51	510
		Operating Life of ISL Well Pattern (yrs)	3	3	3	3	3	3	3	3	3
		Time until Peak Arrival (days)	1.09×10 ³	4.83×10 ³	1.28×10 ³	4.87×10 ⁴	4.80×10 ³	1.10×10 ³	6.63×10 ³	1.28×10 ³	1.10×10 ³
		Relative Peak Concentration	3.12×10 ⁻¹	6.61×10 ⁻⁴	2.70×10 ⁻⁴	2.35×10 ⁻⁵	6.61×10 ⁻⁴	1.10×10 ⁻²	5.25×10 ⁻⁵	2.70×10 ⁻⁴	4.50×10 ⁻⁴

¹ Rf = retardation factor calculated in Section 4

Relative peak concentrations for runs 7d, 7e and 7f are 2.35×10^{-5} , 6.61×10^{-4} and 1.10×10^{-2} mg/L and are all significantly lower than for their Series 6 counterparts, where relative peak concentrations for runs 6d, 6e and 6f are 1.06×10^{-1} , 4.75×10^{-1} and 6.45×10^{-1} mg/L. These results indicate that, not only is the degree of capture a function of the hydraulic conductivity, but also that a significant amount of the injectant that is not captured is from the injection into the wells located farthest to the east and to the west. This conclusion is based on the fact that the receptor well(s) are placed on the plume centerline and, therefore, in the case with the single injection well, the concentration will be impacted by any uncaptured releases from the wells to the east, west and between the pumping and injection wells. For the multiple injection array, however, the receptor well is farther from the injection wells to the east and west, and therefore, the injectant concentrations detected at the well are not as high.

The model input parameters for runs 7g, 7h and 7i are identical to those assigned in runs 7d, 7e and 7f except that the hydraulic gradient was changed from 0.01 to 0.001 ft/ft. The peak arrival times for runs 7g, 7h and 7i are 6,630, 1,280 and 1,100 days and, except at the highest hydraulic conductivity, are much shorter than for runs 6g, 6h and 6i, which are 288,000, 20,700 and 1,210 days. These results indicate that at the low and moderate hydraulic conductivities (1 and 10 ft/day) and flat gradients (0.001), the multiple well configuration does not flatten the hydraulic gradients as much as the single pumping/injection cell configuration.

Relative peak concentrations for runs 7g, 7h and 7i are 5.25×10^{-5} , 2.70×10^{-4} and 4.50×10^{-4} mg/L. These values are all lower than the relative peak concentrations for runs 6g, 6h and 6i, which are 7.40×10^{-5} , 1.30×10^{-3} and 6.26×10^{-1} mg/L. These results are explained by the larger capture zone that is created by the array of pumping/extraction wells.

While simulations with a single 5- or 7-spot pattern are useful in understanding the interactions and sensitivity to various modeling parameters, this modeling approach produces conservative results (i.e., high relative concentration at the receptor well). In general, modeling of multiple injection/extraction patterns, which are a closer approximation to a full-scale wellfield, results in lower relative concentrations.

2.6.2.8 Abandoned Borehole Pathway

Several modeling simulations were performed to investigate the potential impacts on overlying aquifers of an exploratory borehole that penetrates into the mined unit (Table 2-12). The major conceptual components of the modeled system are a 60-ft thick low-conductivity confining unit (1×10^{-6} ft/day) that separates a 30-ft thick mined interval from an overlying aquifer with an assigned thickness of either 50 or 100 ft, depending upon the simulation. The abandoned borehole hydraulically connects the overlying aquifer to the mined unit through a 1-ft² high hydraulic conductivity damaged rock zone created as the borehole was cored.

To simulate this system, a 5-layer model was constructed that covers approximately a 1-mi² area (Figure 2-16). Grid spacing in the horizontal direction ranges from 1 to 50 ft and in the vertical direction from 20 to 100 ft (Figure 2-17). The aquifer and mined unit are represented by single layers and are separated by an aquitard that is divided into 3 layers.

Table 2-12: Abandoned Borehole Simulations

ABANDONED BOREHOLE SIMULATIONS					
General Assumptions - All Runs		Run	AB-R1	AB-R2	AB-R3
Receptor Locations (ft)	528, 856, 1,840	Regional Hydraulic Gradient	0.01	0.01	0.01
Simulation Time (yr)	53	Effective Porosity (%)	20	20	20
Well Configuration	5-Spot (pumping from center well)	Dispersivity (ft)			
		Longitudinal	65	65	65
		Transverse	6.5	6.5	6.5
		Vertical	0.65	0.65	0.65
Well Spacing (ft)	150	Injection Fluid Conc. (milligram per L)	1	1	1
Injection Time (yr)	3	Upper Aquifer 1 Hydraulic Conductivity (ft/day)	100	10	100
Model Area (ft ²)	5,280 (ft) × 5,280 (ft) = 1 mi ²	Upper Aquifer Thickness (ft)	100	100	50
Model Layers	5 The thickness of the mined interval (layer 5) is 30 ft and has the monitoring/injection/pumping wells.	Mined Interval Hydraulic Conductivity (ft/day)	10	10	10
Minimum/ Maximum Grid Spacing (ft)	1/50	Retardation Factor	1	1	1
All Layers	Confining units separate upper aquifer from production zone	Injection/Extraction Well Spacing (ft)	5-spot - 100	5-spot - 100	5-spot - 100
Disturbed Rock Zone Around Borehole (ft ²)	1	Injection Rate (gpm)	50	50	50
		Pumping Rate (gpm)	51	51	51
		Operating Life of ISL Well Pattern (yrs)	3	3	3
		Time until Peak Arrival (days)	2.98×10 ³	4.15×10 ³	2.06×10 ³
		Relative Peak Concentration	5.81×10 ⁻¹	5.12×10 ⁻¹	8.00×10 ⁻¹

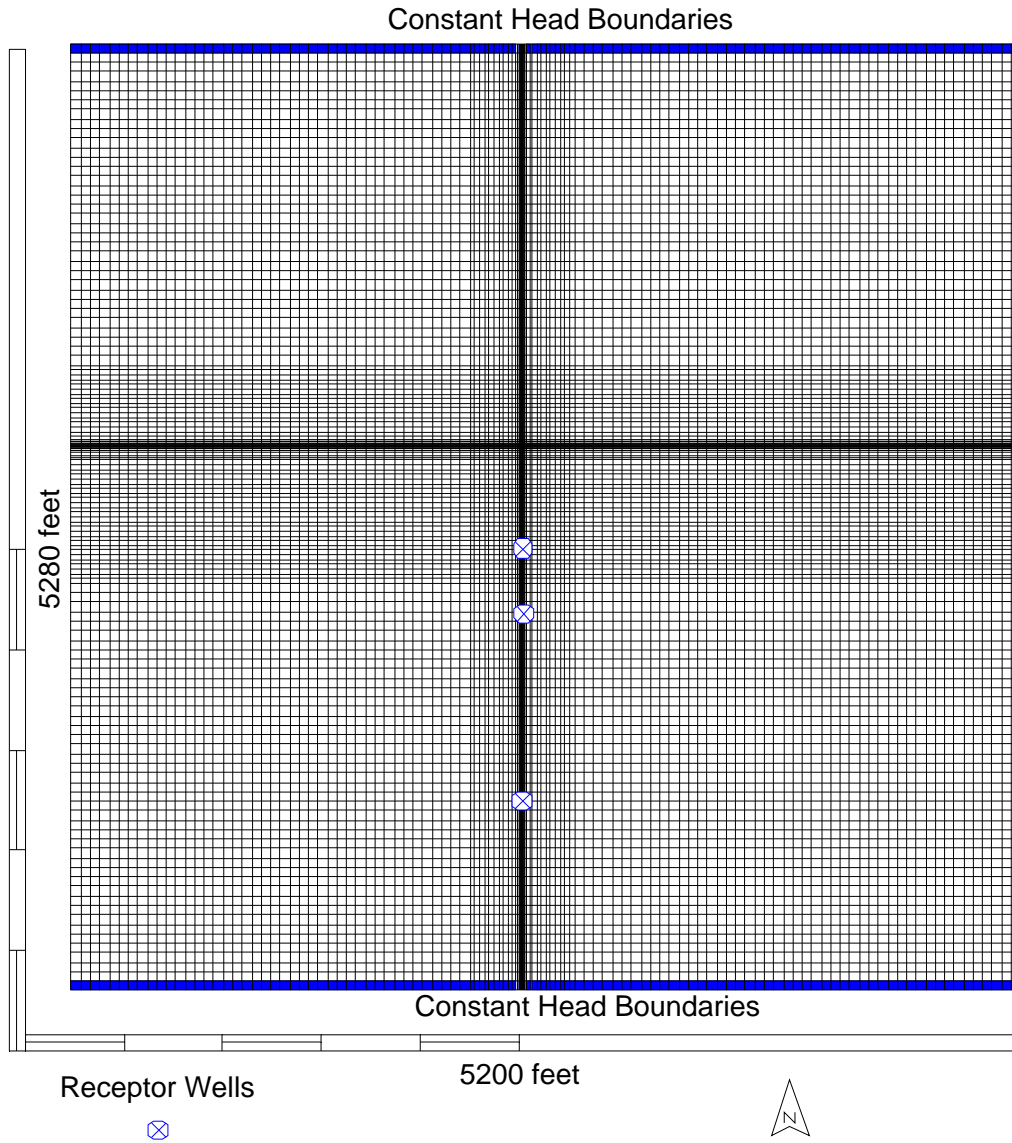


Figure 2-16: Plan View of the Model Grid for the Abandoned Borehole and Discontinuous Confining Bed Excursion Simulations

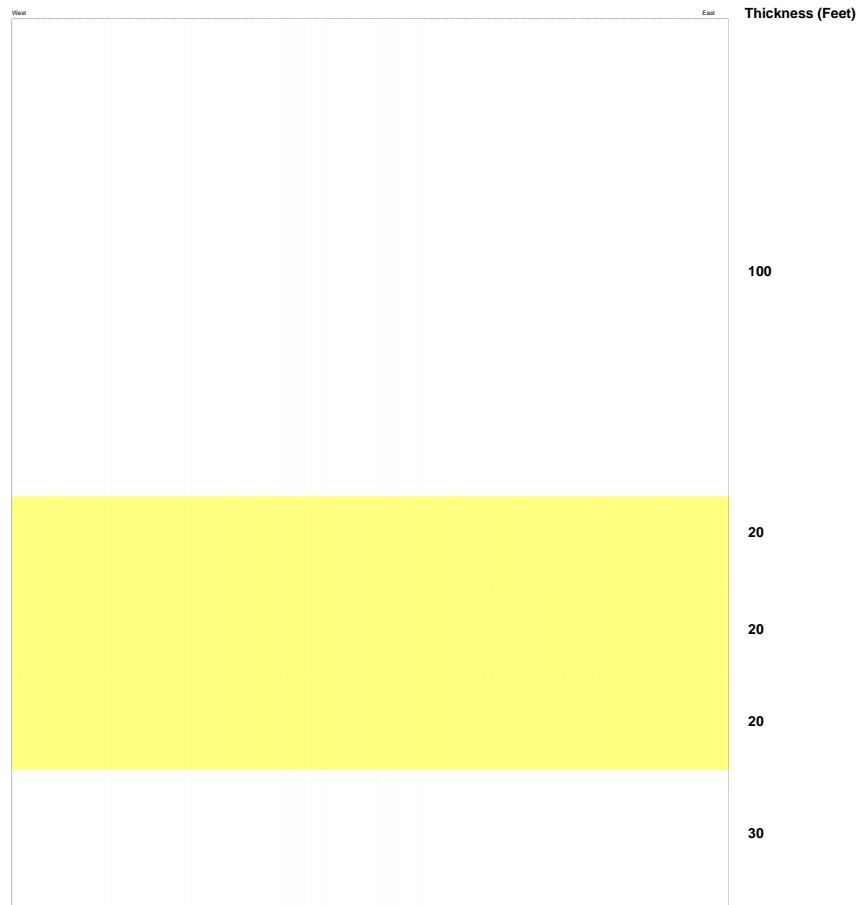


Figure 2-17: Cross-Sectional View of the Model Grid for the Abandoned Borehole and Discontinuous Confining Bed Excursion Simulations

Three model simulations were performed to investigate the effects of aquifer thickness and aquifer conductivity. It is recognized that the results would be influenced by many parameters (e.g., size and permeability of the damaged rock zone), but the primary objective was to assess whether, under a reasonable set of assumptions, vertical migration via a borehole could result in significant releases. It should be kept in mind, however, that for this type of release to occur, there has to be an upward vertical gradient and the damaged rock zone has to be of sufficient hydraulic conductivity to allow vertical movement.

The peak arrival time for the base case abandoned borehole simulation (AB-R1) is 2,980 days and the peak concentration is 5.81×10^{-1} . This is one of the most significant releases predicted across all of the potential failure scenarios (i.e., leaks and excursions).

The effect that a lower aquifer hydraulic conductivity has on the results is evaluated in run AB-R2 where the hydraulic conductivity is lowered from 100 to 10 ft/day. The peak arrival time for this simulation (AB-R2) is 4,150 days and the peak concentration is 5.12×10^{-1} . The travel time has increased from the base case because of the lower ground water velocities. The peak

concentrations, however, remain very similar. In previous excursion simulations, the higher hydraulic conductivities typically had lower peak concentrations. In this comparison, however, the higher hydraulic conductivity has a higher release. This relationship occurs because the vertical gradient is affected by the hydraulic conductivity of the overlying aquifer. At higher hydraulic conductivities, the vertical gradient allows more injectant to enter the aquifer via the borehole. The amount of water entering the upper aquifer also impacts the horizontal gradients within the aquifer.

The impact of the reduction in aquifer thickness from 100 to 50 ft is investigated in run AB-R3. The peak arrival time for this simulation is 2,060 days and the peak concentration is 8.00×10^{-1} . The shorter peak arrival time can be explained by the steeper hydraulic gradients in the aquifer, which are due to the water flowing up the borehole encountering a lower transmissivity (hydraulic conductivity multiplied by thickness). The higher relative concentration occurs because the amount of injectant entering the aquifer is distributed over a smaller vertical area (or volume). Breakthrough curves are included in Appendix D.

2.6.2.9 Confining Bed Discontinuity

To investigate the potential effects of a discontinuous confining unit between the mined aquifer and the overlying aquifer, two simulations were performed (Table). For both of these simulations, the model grid, domain and input parameters are identical to those of the abandoned borehole base case (AB-R1), except that the abandoned borehole is replaced by an area of either 10 or 100 ft², where the hydraulic conductivity is high (100 ft/day). Conceptually, this area is representative of an erosional or depositional surface that has been filled with the material from the overlying aquifer (e.g., a sand lens).

For run CBD-R1, this area of discontinuity is specified as 100 ft². The peak arrival time for this simulation is 11,900 days and the peak concentration is 5.09×10^{-1} . This longer arrival time from that observed for the abandoned borehole simulations occurs because the high transmissivity zone (i.e., damaged rock zone) does not extend through the entire aquifer. Therefore, injectant entering the aquifer must do so only at the base, and it takes longer for the injectant to mix with the water in the aquifer to reach a peak concentration. The peak concentration, however, is very similar to those observed in runs AB-R1 and AB-R2.

The area of discontinuity was decreased from 100 ft² to 25 ft² in run CBD-R2. The peak arrival time for this simulation is 45,700 days and the peak concentration is 4.73×10^{-1} . The longer peak arrival time for the smaller area is related to the smaller amount of injectant that is migrating vertically upward. The effect of the smaller area is also reflected in the lower relative peak concentration. Breakthrough curves are included in Appendix D. Since the potential releases through the discontinuous layers result in uranium concentrations that are almost the same as those observed in the wellfield, there was no need to calculate the health-based standards for these scenarios.

Furthermore, although this analysis was focused upon overlying aquifers, similar results would be obtained from potential excursions to underlying aquifers.

Table 2-13: Confining Bed Discontinuity Simulations

CONFINING BED DISCONTINUITY SIMULATIONS				
General Assumptions-All Runs		Run	CBD-R1	CBD-R2
Receptor Locations (ft)	528, 856, 1,840	Regional Hydraulic Gradient	0.01	0.01
Simulation Time (yr)	53	Effective Porosity (%)	20	20
Well Configuration	5-Spot (pumping from center well)	Dispersivity (ft)		
		Longitudinal	65	65
		Transverse	6.5	6.5
		Vertical	0.65	0.65
Well Spacing (ft)	150	Injection Fluid Conc.(milligram per L)	1	1
Injection Time (yr)	3	Upper Aquifer 1 Hydraulic Conductivity (ft/day)	100	100
Model Area (ft ²)	5,280 (ft) × 5,280 (ft) = 1 mi ²	Upper Aquifer Thickness (ft)	100	100
Model Layers	5 The thickness of the mined interval (layer 5) is 30 ft and has the monitoring/ injection/pumping wells.	Mined Interval Hydraulic Conductivity (ft/day)	10	10
Minimum/ Maximum Grid Spacing (ft)	1/50	Area of Confining Bed Discontinuity (ft ²)	100	25
All Layers	Confining units separate upper aquifer from production zone	Retardation Factor	1	1
		Injection/Extraction Well Spacing (ft)	5-spot - 100	5-spot - 100
		Injection Rate (gpm)	50	50
		Pumping Rate (gpm)	51	51
		Operating Life of ISL Well Pattern (yrs)	3	3
		Time until Peak Arrival (days)	1.19×10 ⁴	4.57×10 ⁴
		Relative Peak Concentration	5.09×10 ⁻¹	4.73×10 ⁻¹

2.6.2.10 Summary and Conclusions of Excursion Scenarios

Three excursion scenarios were developed to investigate the potential impacts to nearby receptors. Forty-nine (49) unique simulations were performed to evaluate excursions within the mined unit beyond the pumping/injection wells. Potential flow up an abandoned borehole was investigated with three simulations, and two simulations were conducted to evaluate potential migration through a discontinuous aquitard.

The sensitivity analysis was focused on those parameters that are most uncertain and for which the results are most sensitive. These parameters include hydraulic gradients and conductivities, pumping/injection well spacing, aquifer thickness and size of the discontinuity. All of the concentrations are calculated as relative concentrations and are adjusted to actual concentrations during the dose assessment (Chapter 4).

All of the relative peak concentrations versus peak arrival times are shown in Figure 2-18. The highest relative concentrations are associated with the abandoned borehole, the discontinuous

confining unit, and Series 6 simulations. The mined interval in the Series 6 simulations is reduced to a thickness of 20 ft, as compared to 70 ft in the other excursion simulations within the mined interval.

Several graphs have been constructed that show the effect of well spacing at a hydraulic conductivity of 100 ft/day and a gradient of 0.001 ft/ft (Figures 2-19 and 2-21). As depicted in the figures, the relative concentrations are always higher at the larger well spacing because of the injectant escaping between the wells. This relationship is maintained over a range of hydraulic conductivities, as shown in Figures 2-22 and 2-23.

Relative concentrations as a function of hydraulic conductivities and gradients are shown in Figures 2-24 through 2-26. As depicted in the figures, the relative concentration is generally higher for those simulations with lower hydraulic conductivities and gradients. This relationship occurs because at the higher concentrations and gradients, the injectant reaches the receptor more quickly, and at lower concentrations, the injectant mass is distributed over a larger area, which decreases the concentration within the plume.

A statistical analysis was conducted to assess whether there are correlations among any of the parameters investigated. The results of this analysis are shown in Figures 2-27 through 2-33 and demonstrate that there is very little correlation among the parameters tested. In each of these figures, the relative concentrations are plotted both on a linear and a logarithmic scale. The plots were initially prepared using a linear concentration scale and exhibited no significant correlations. However, in numerous runs, the relative concentrations were below 0.1 mg/L. To expand the delineation of data in this region, the scatter plots were redone using a logarithmic scale for the ordinate data. Again, very little correlation between concentration and the various model parameters was noted.

The higher ratios of advection to dispersion resulted in higher peak concentrations. Furthermore, an important result regarding the interplay of the local and regional gradients is that the steeper the regional gradient the narrower the capture zone and the greater the contaminant releases.

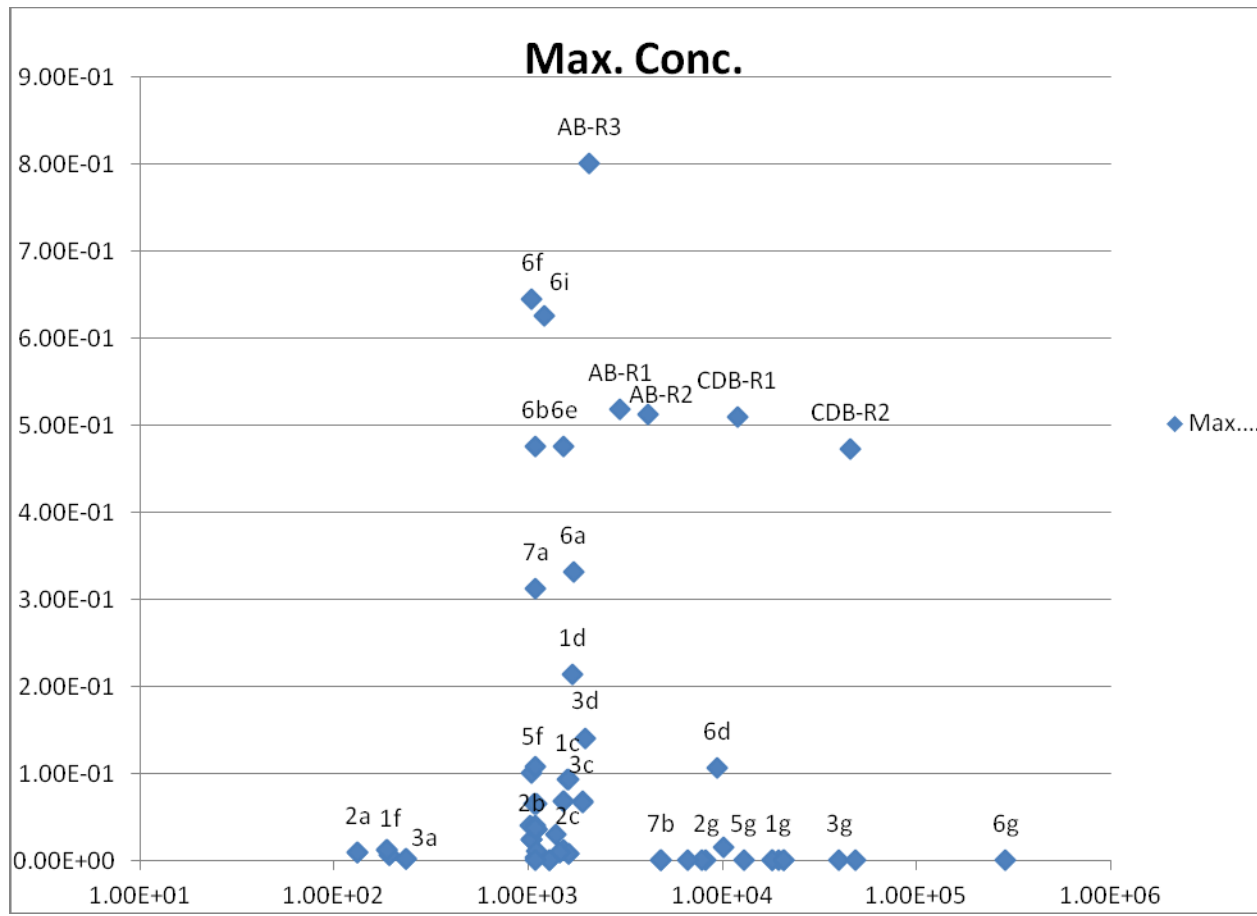


Figure 2-18: Maximum Relative Concentrations versus Time for All Excursion Simulations

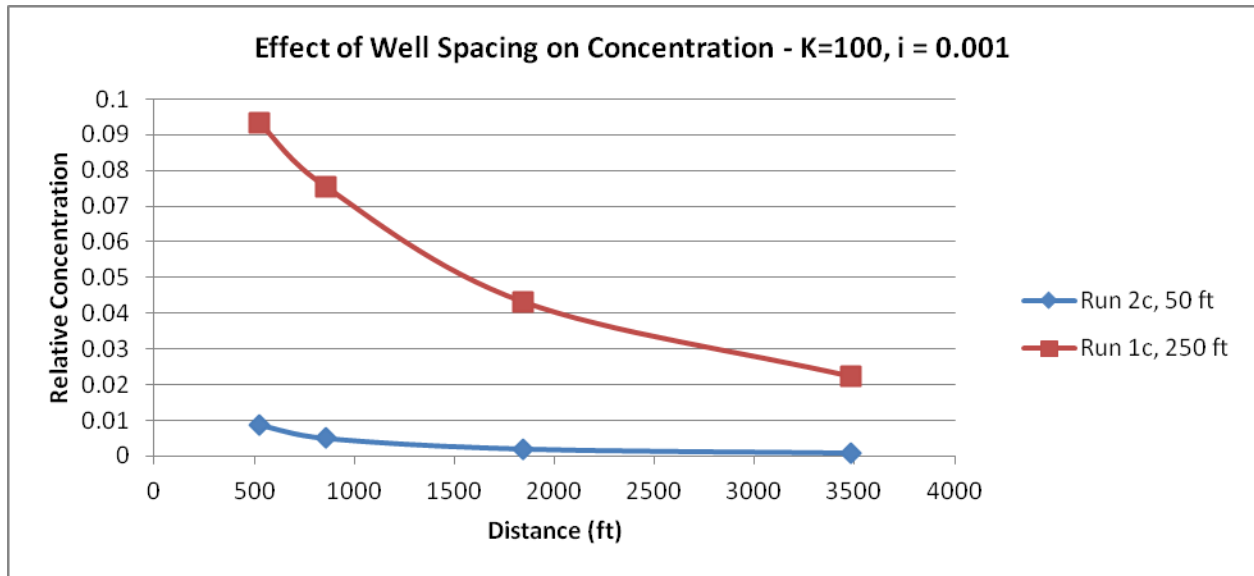


Figure 2-19: Effect of Well Spacing at Constant Hydraulic Conductivity of 100 ft/day and Constant Hydraulic Gradient of 0.001.

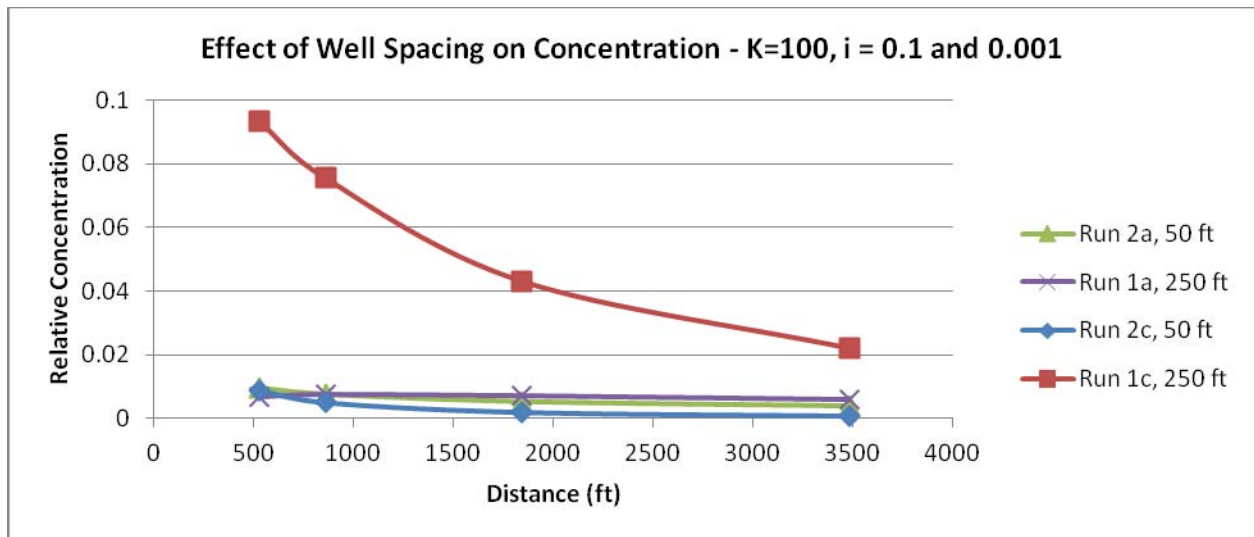


Figure 2-20: Effect of Well Spacing at Constant Hydraulic Conductivity of 100 ft/day and Hydraulic Gradients of 0.1 (Runs 1a, 2a) or 0.001 (Runs 1c, 2c).

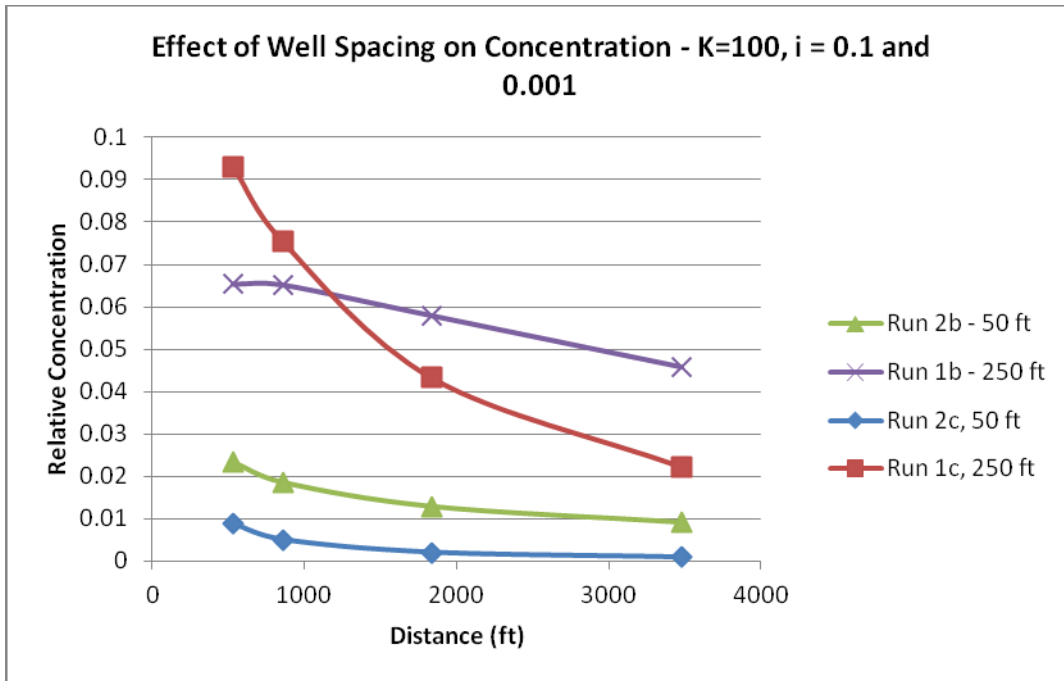


Figure 2-21: Effect of Well Spacing at Constant Hydraulic Conductivity of 100 ft/day and Hydraulic Gradients of 0.01(Runs 1b, 2b) and 0.001(Runs 1c, 2c).

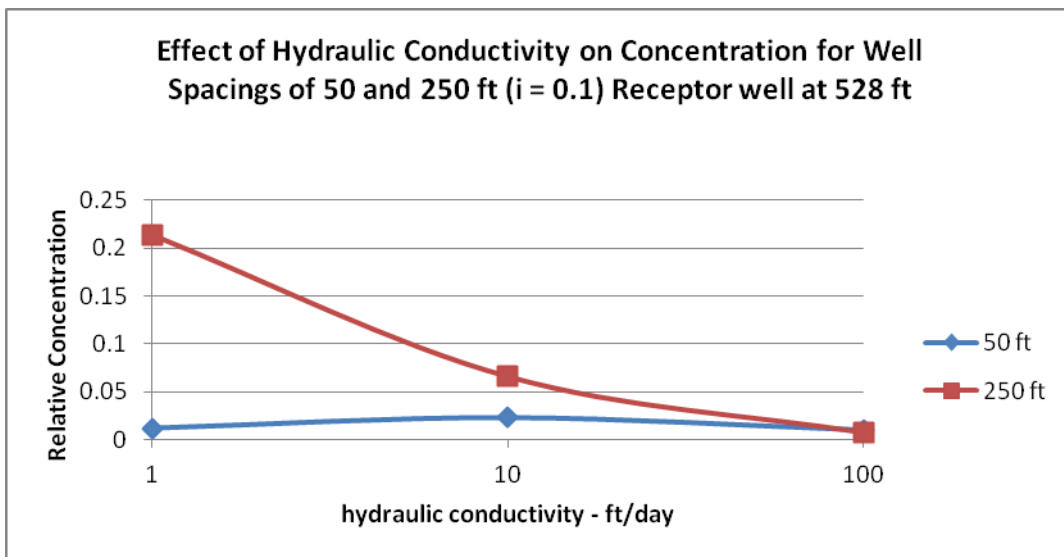


Figure 2-22: Effect of Well Spacing on Concentration as a Function of Hydraulic Conductivity at a Constant Hydraulic Gradient of 0.1.

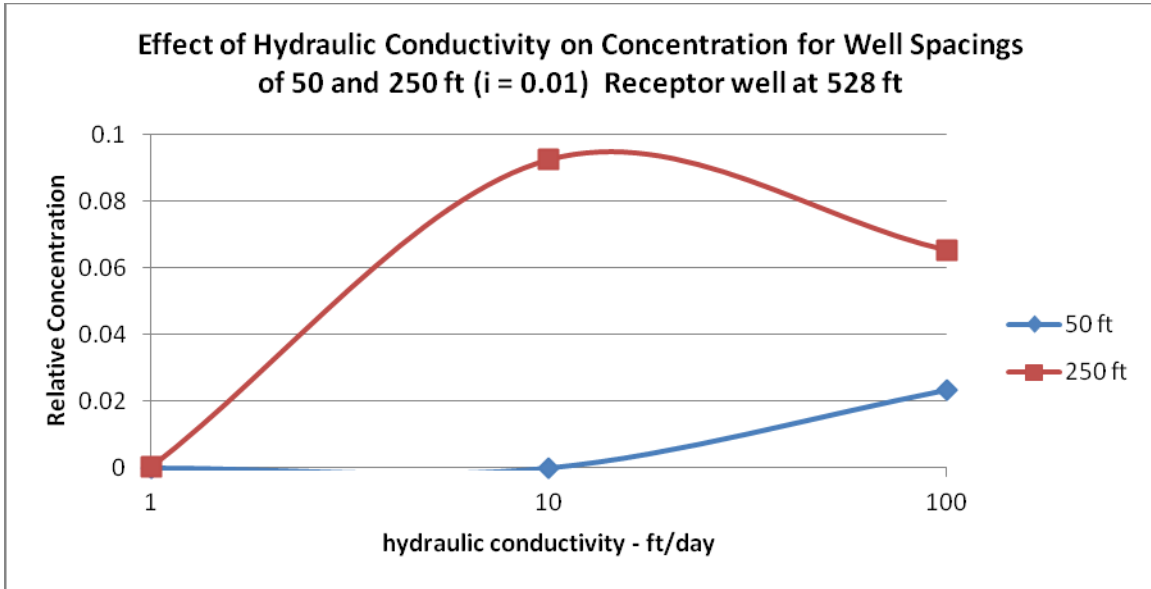


Figure 2-23: Effect of Well Spacing on Concentration as a Function of Hydraulic Conductivity at a Constant Hydraulic Gradient of 0.01.

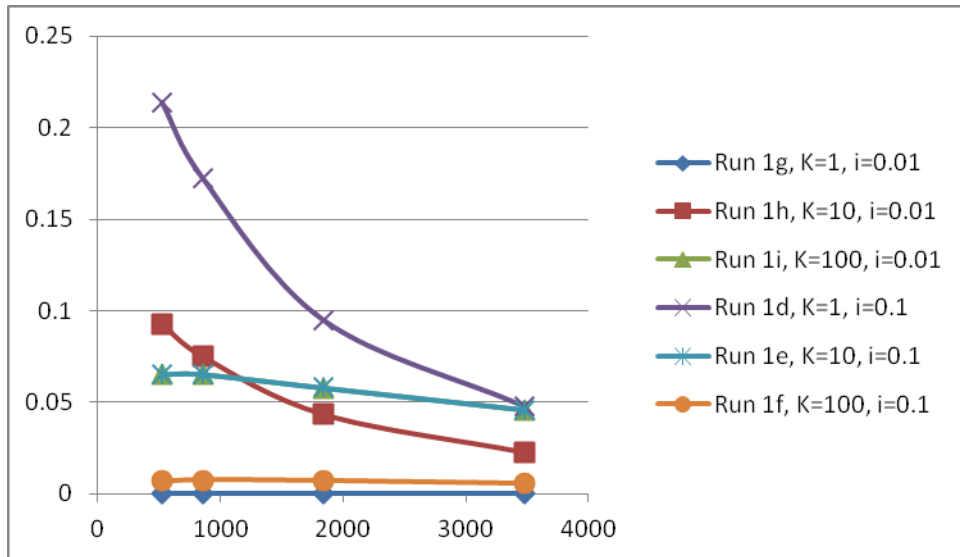


Figure 2-24: Relative Concentrations as a Function of Hydraulic Conductivities and Gradients

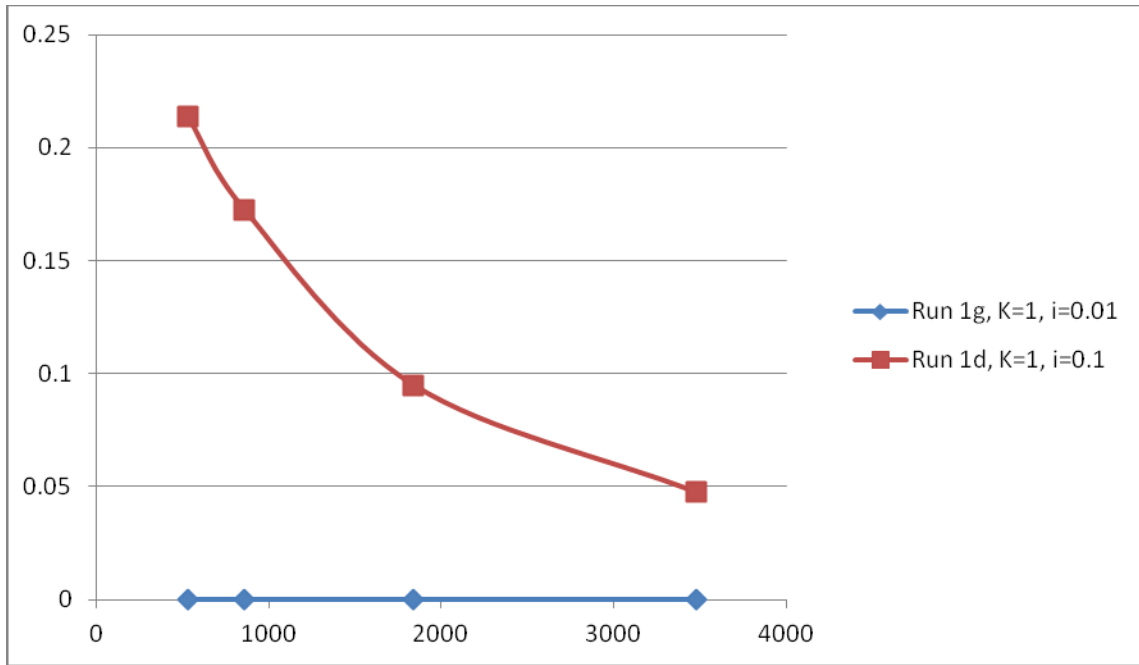


Figure 2-25: Relative Concentrations as a Function of Hydraulic Gradient (Run 1d - 0.1, Run 1g - 0.01) and Hydraulic Conductivity of 1 ft/day

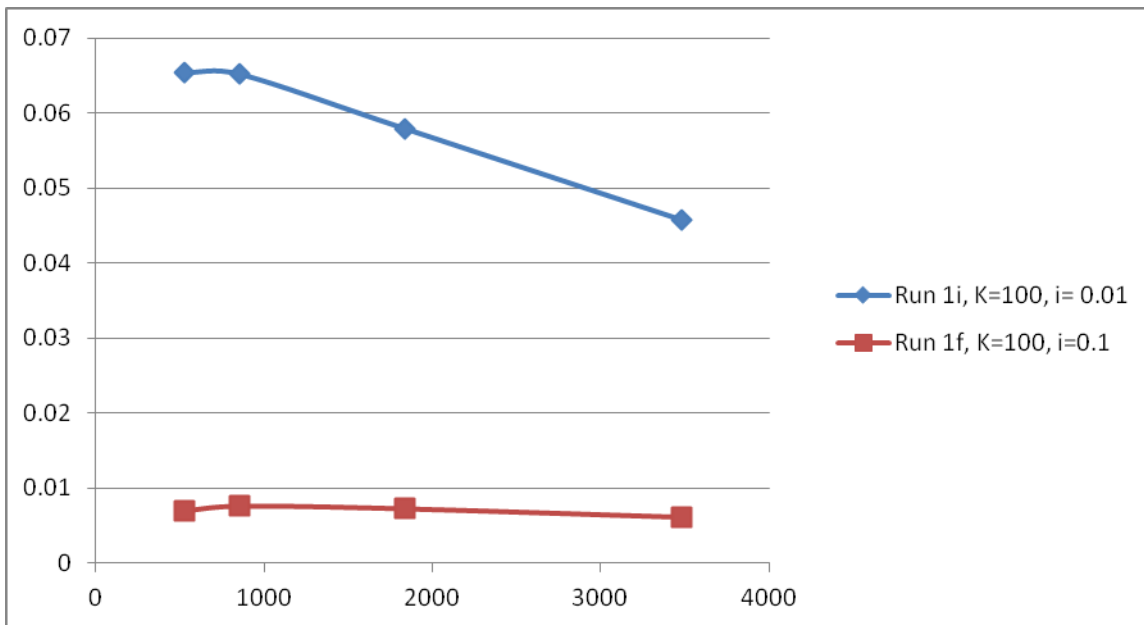


Figure 2-26: Relative Concentrations as a Function of Hydraulic Gradient (Run 1f - 0.1, Run 1i - 0.01) and Hydraulic Conductivity of 100 ft/day

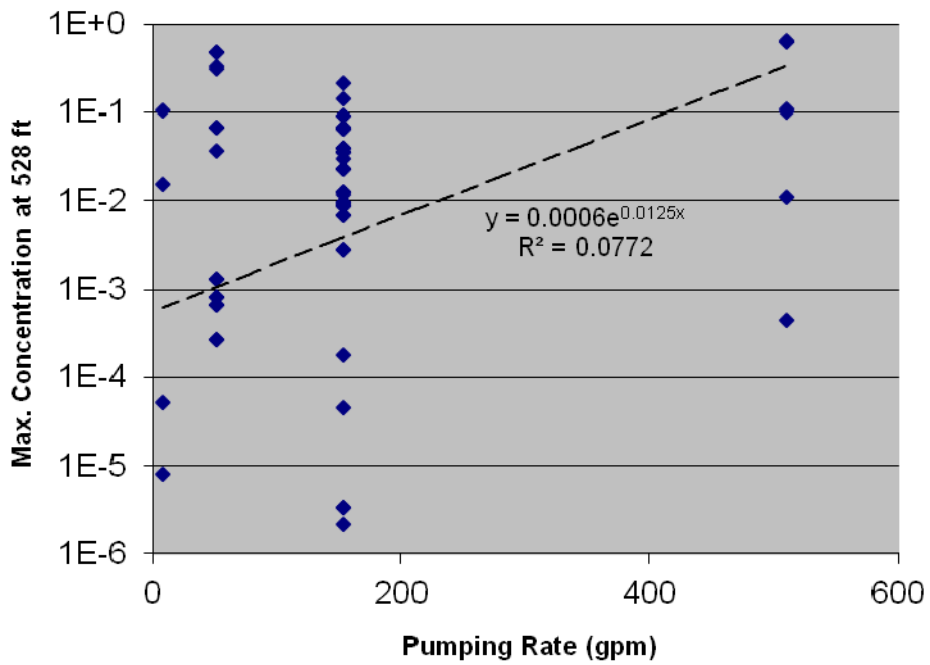
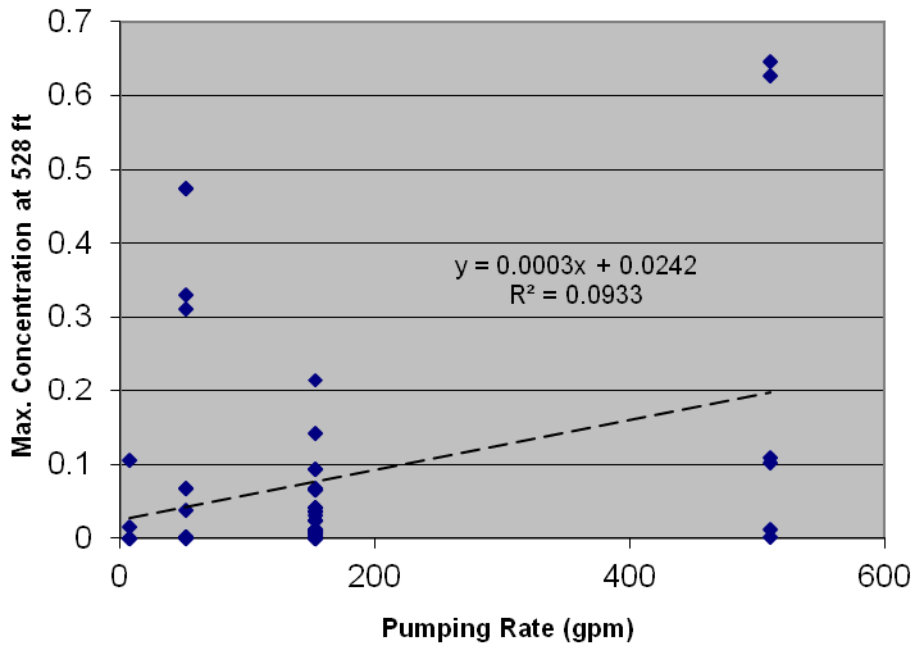


Figure 2-27: Correlation of Relative Concentration to Pumping Rate

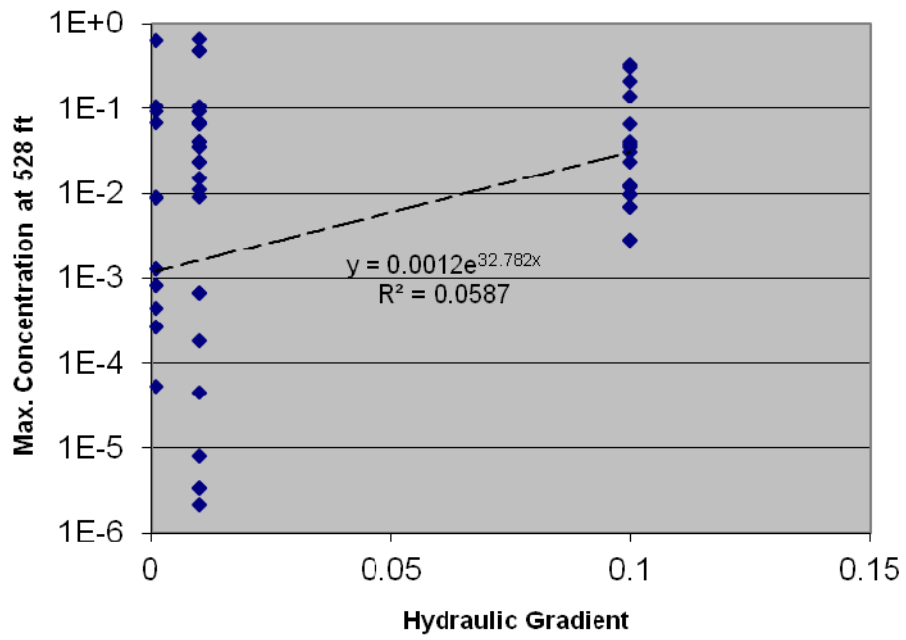
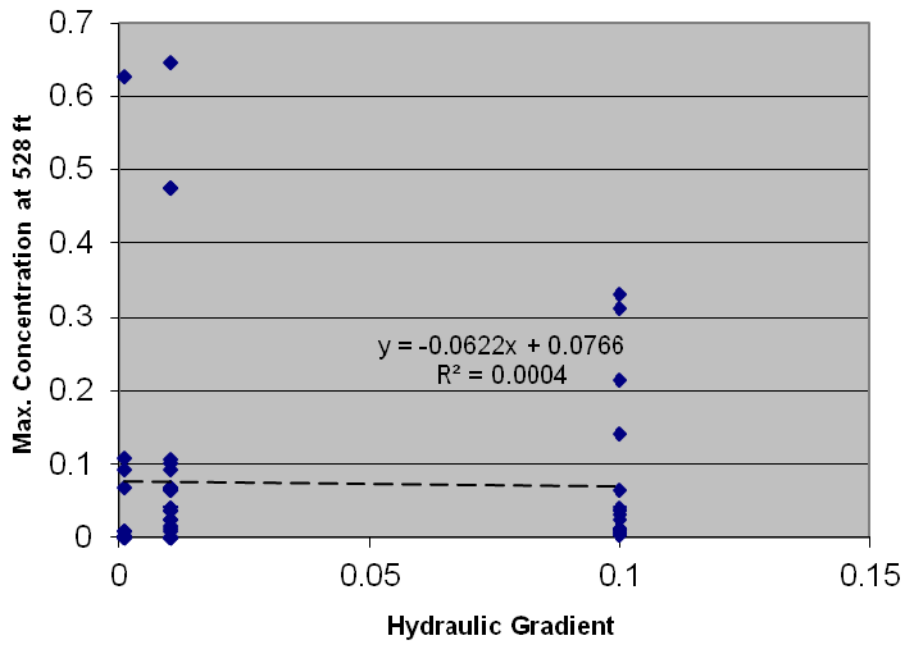


Figure 2-28: Correlation of Relative Concentration to Hydraulic Gradient

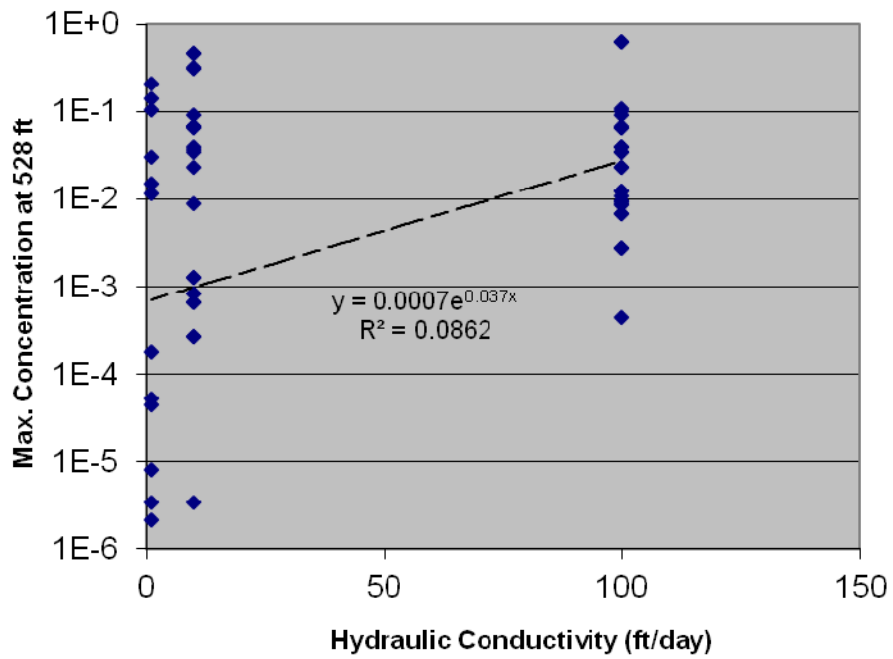
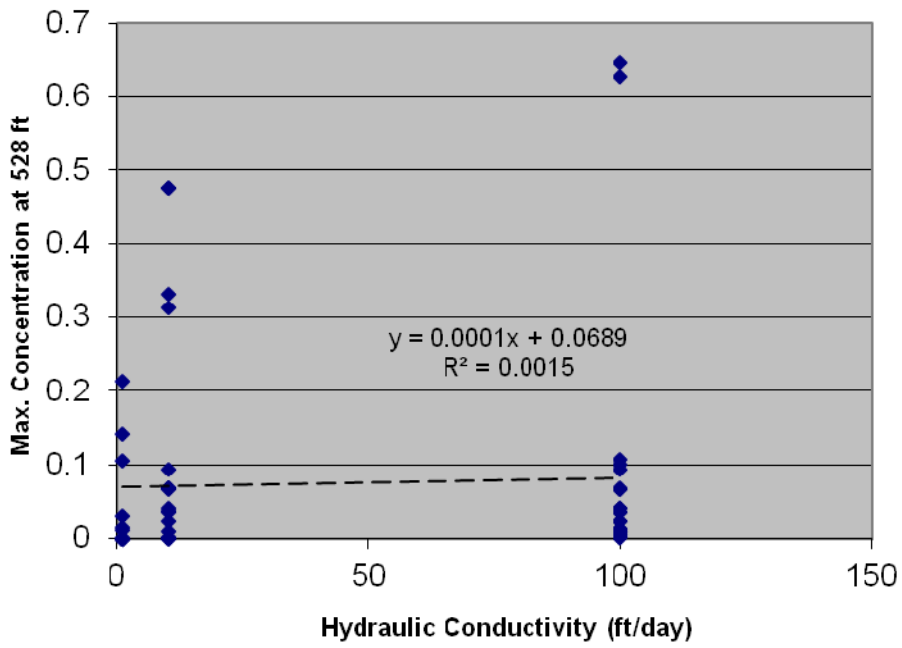


Figure 2-29: Correlation of Relative Concentration to Hydraulic Conductivity (ft/day)

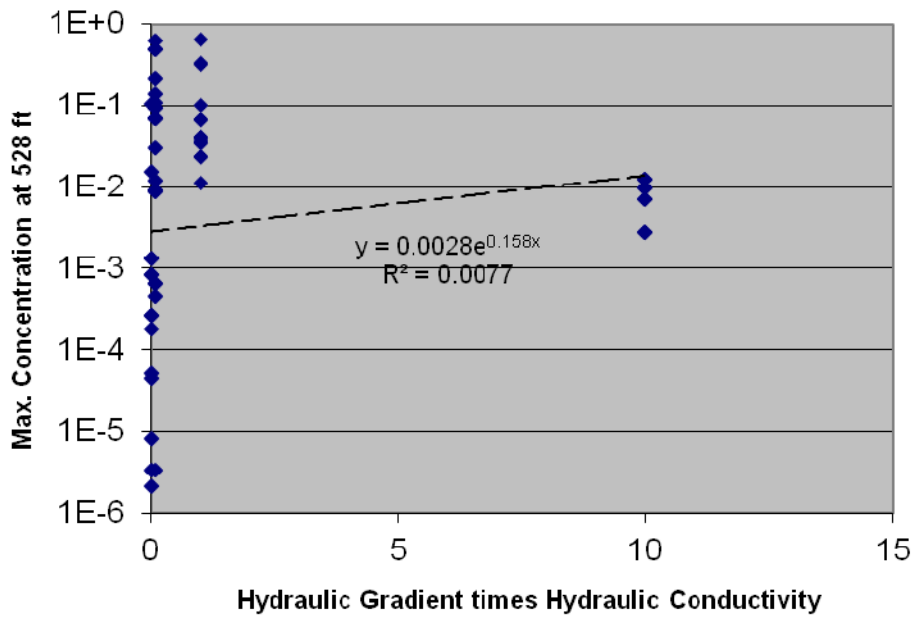
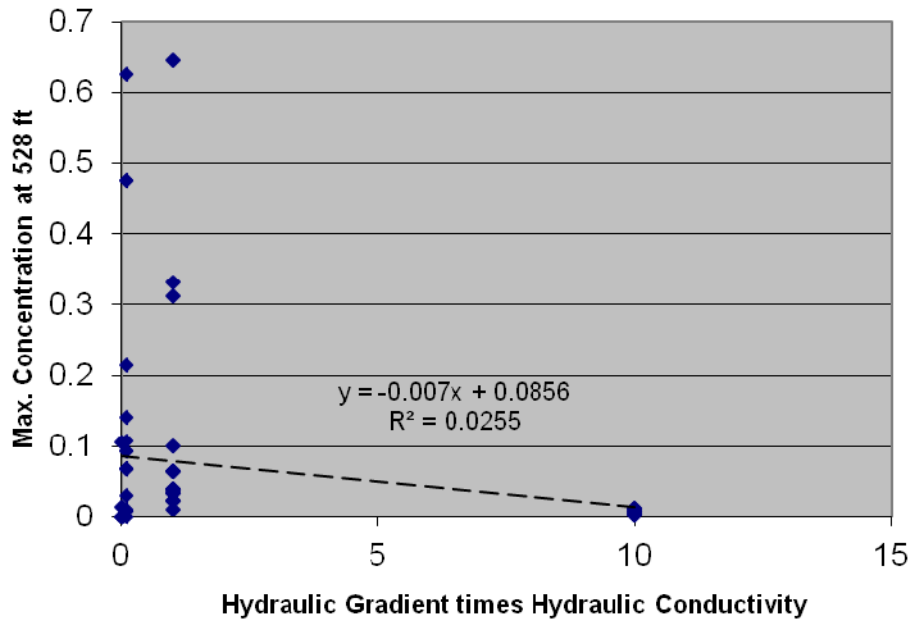
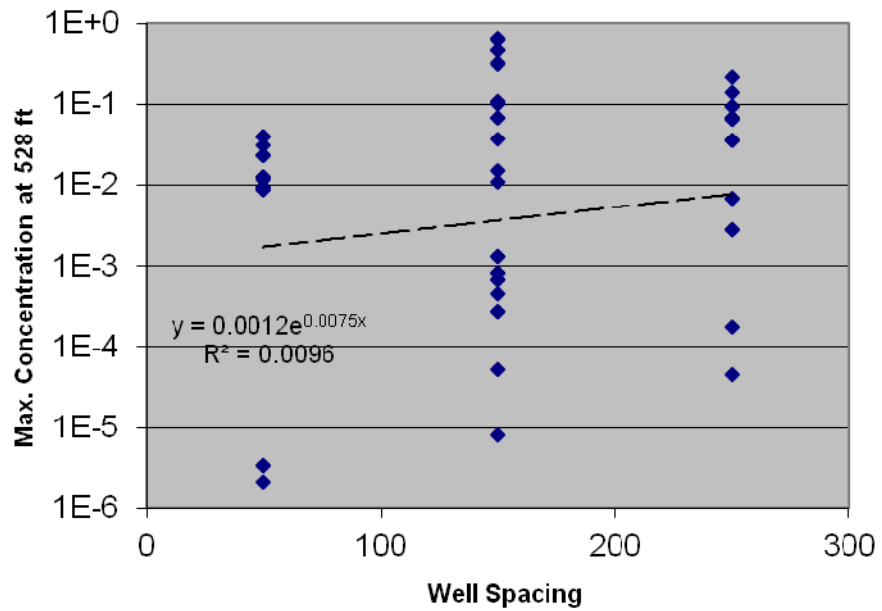
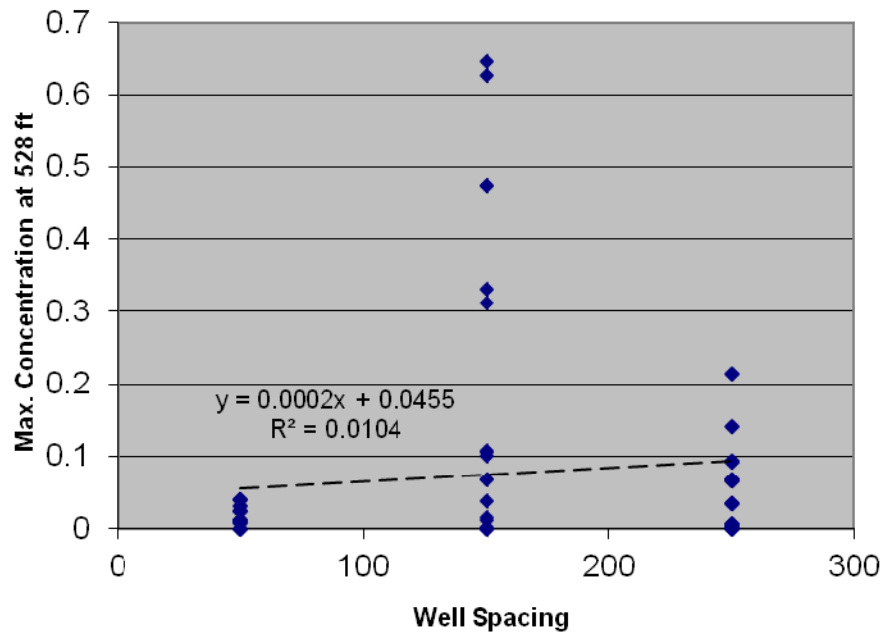


Figure 2-30: Correlation of Relative Concentration to Hydraulic Gradient times Hydraulic Conductivity



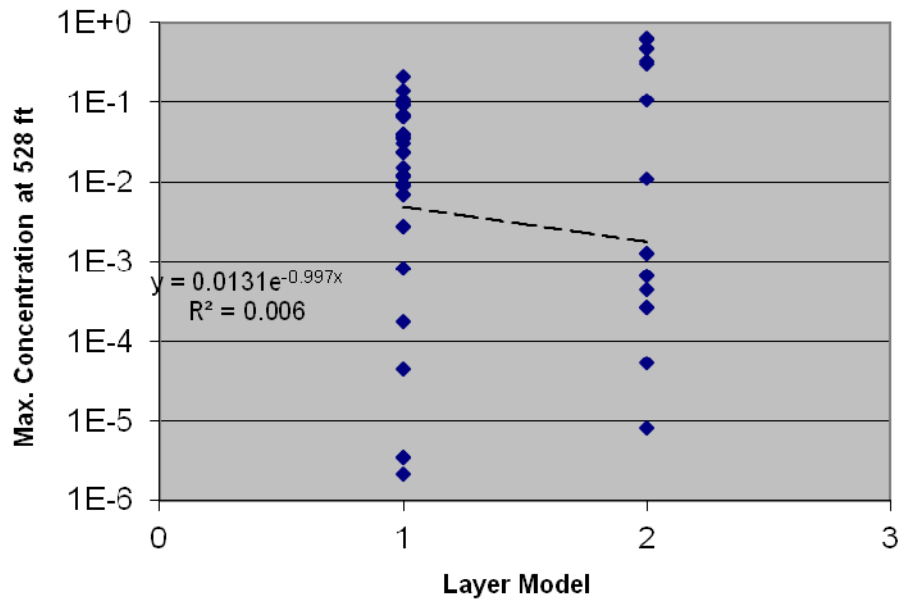
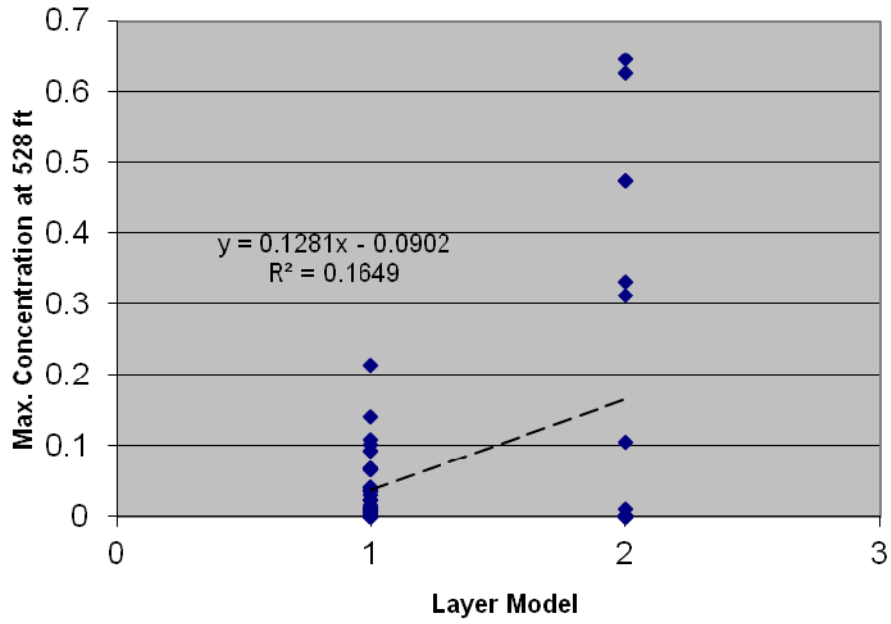


Figure 2-33: Correlation of Relative Concentration to Model Layer

3.0 PATHWAY DOSE AND RISK CONVERSION FACTORS

To calculate doses and risks to individuals who use water from a well that is contaminated with radioactivity from the ISL facility, pathway dose and risk conversion factors (PDCFs and PRCFs) were developed and used.⁸ PDCFs/PRCFs are defined as the dose/risk received by an individual (e.g., millirem/year or latent cancer fatality [LCF]/year) divided by the radionuclide concentration in the well water (e.g., pCi/m³). Because of linearity, the annual dose/risk can be calculated by multiplying the calculated radionuclide concentration in ground water by the corresponding PDCF/PRCF. PDCFs/PRCFs include dose and risk coefficients due to the intake of radionuclides into the human body. The radionuclide-specific dose and risk coefficients used in calculating the PDCFs/PRCFs were obtained from Federal Guidance Report No. 13 (FGR 13) (Eckerman et al. 1999 and EPA 2002; see Section 3.2.2 of this report). PDCFs/PRCFs also include factors that describe the movement and uptake of the radionuclide within the biosphere (e.g., irrigation rates, plant and animal bioaccumulation factors, weathering and other removal mechanisms, etc.), as well as human ingestion rates. As described in Section 3.2, for this analysis, ranges of values were selected for each of these factors and the PDCF/PRCF model was implemented in spreadsheet form to allow calculation of doses via the ingestion pathway from the use of well water for drinking and irrigation. The total PDCFs/PRCFs are composed of the following individual ingestion pathways:

- Ingestion of Drinking Water
- Inadvertent Ingestion of Soil
- Ingestion of Vegetables
- Ingestion of Milk
- Ingestion of Meat

The general equations for calculating the total PDCFs/PRCFs are shown below:

$$\begin{aligned}
 PDCF_{Total} &= \sum_P PDCF_P = \sum_P DC_{Ing} Ing_P f(b,r)_P \\
 PRCF_{Total} &= \sum_P PRCF_P = \sum_P RC_{Ing} Ing_P f(b,r)_P
 \end{aligned}
 \tag{3-1}$$

where DC_{Ing} and RC_{Ing} are the dose and risk coefficients from FGR 13, Ing_P is the exposure pathway human ingestion rate, and $f(b,r)_P$ is a pathway-specific function that describes the buildup (b) and removal (r) (if any) of the radionuclide in water, soil, vegetables, milk, or meat. For example, the direct consumption of well water, $f(b,r)_P$ is set to 1.

Figure 3-1 shows the exposure pathways that were considered in this analysis, while Section 3.1 describes the specific mathematical equations (including the form of $f(b,r)_P$) for each exposure pathway that was analyzed in detail. In addition to the pathways that were analyzed in detail, there were a number of exposure pathways that were considered, but not analyzed, these are discussed in Section 3.5 and are shown in grey in Figure 3-1.

⁸ Pathway dose/risk conversion factors are sometimes referred to as biosphere dose/risk conversion factors.

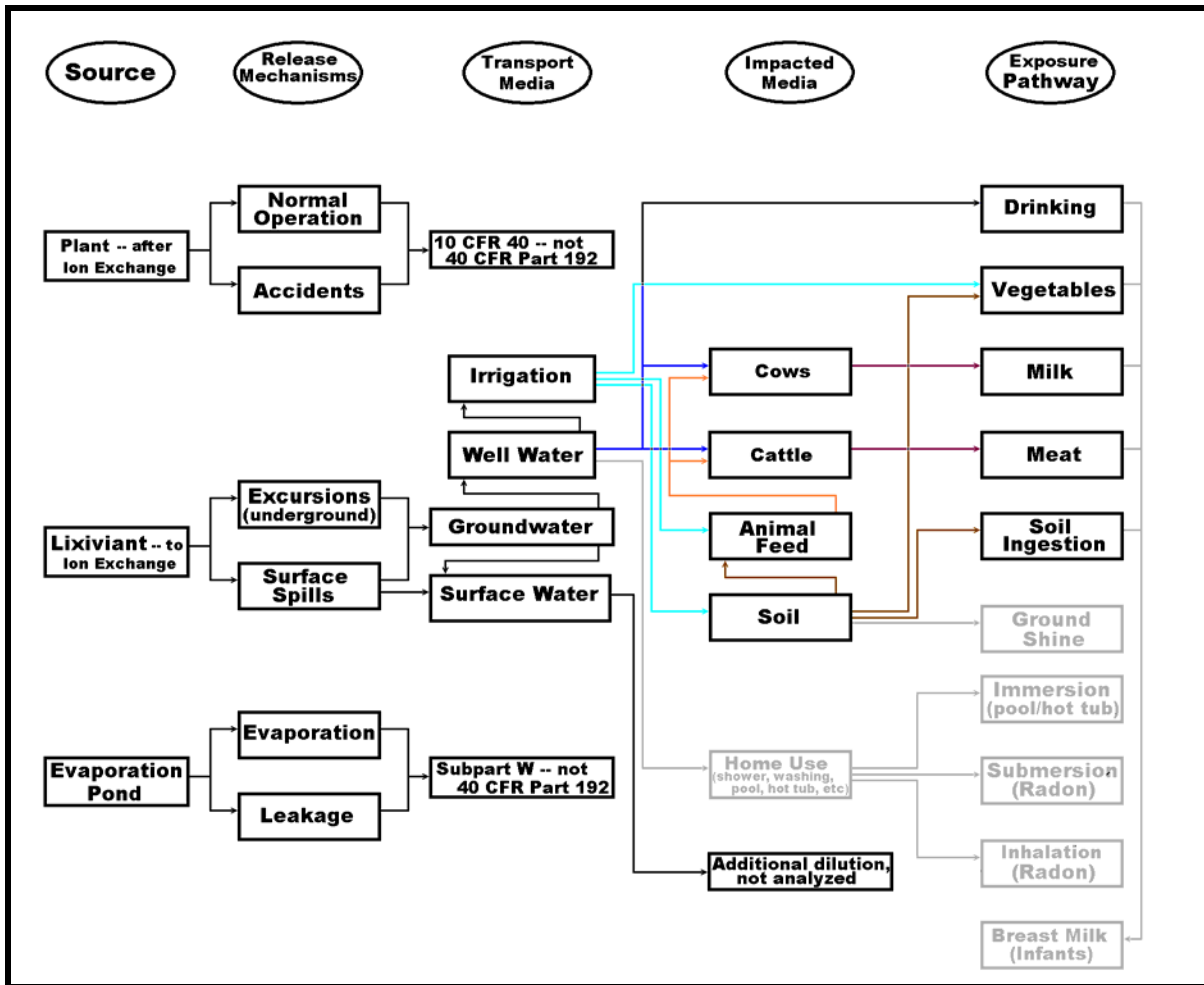


Figure 3-1: Exposure Pathways Analyzed

Figure 3-1 also shows that there are three sources of radioactivity at an ISL facility: the Plant, where uranium is removed from the lixiviant; the Lixiviant; and Evaporation (or Holding) Ponds. This analysis only considers exposures due to the Lixiviant source, because (as indicated in Figure 3-1) the Plant is regulated under 10 CFR Part 40, by the Nuclear Regulatory Commission (or an Agreement State), and Evaporation Ponds are regulated by the EPA under 40 CFR Part 61, Subpart W. Finally, Figure 3-1 shows that lixiviant surface spills and ground water containing lixiviant from an excursion could flow to a surface water body. While these pathways exist, they were not analyzed in this report because the additional dilution provided by the surface water body would result in lower exposures to an individual than exposures from the ground water to well pathway.

PDCFs and PRCFs were developed for the following longer-lived radionuclides in the U-238 decay series: U-238, U-234, Th-230, Ra-226, and Pb-210 (see Section 3.2.2).

3.1 Pathway Dose and Risk Models

The basic mathematical models used to calculate the dose and risk from the ingestion pathways for this analysis were obtained from the NRC's Regulatory Guide 1.109 (NRC 1977). Although the numerical values for many of the parameters given in Regulatory Guide 1.109 have been updated in the 30-plus years since its publication, the basic mathematical models remain valid and form the basis for many of today's computer programs used to calculate radiological impacts, including CAP88 (Trinity 2007), GENII (PNL 1988), and RESRAD (ANL 2001). While the Regulatory Guide 1.109 models form the basis for many of today's computer programs, those computer programs often have refined the models to more accurately reflect reality. When appropriate, those refined models have been used in this analysis, and are pointed out in the following discussion.

This section presents the mathematical models that were used to calculate the PDCFs/PRCFs, while Section 3.2 presents and discusses the values that were assumed for each of the parameters used in the models.

3.1.1 Ingestion of Drinking Water

The annual effective dose ($E_{Wat,A}$, mrem/yr) and risk ($R_{Wat,A}$, LCF/yr) to a human of age group A ⁹ from the consumption of unfiltered drinking water is given by:

$$\begin{aligned} E_{Wat,A} &= C_W \text{Ing}_{Wat,A} DC_{Ing,A} \\ R_{Wat,A} &= C_W \text{Ing}_{Wat,A} RC_{Ing,A,DW} \end{aligned} \quad 3-2$$

where C_W is the radionuclide concentration in the well from which the water is taken (pCi/m³), $\text{Ing}_{Wat,A}$ is the water consumption rate for an individual of age group A (m³/yr), $DC_{Ing,A}$ is the ingestion dose coefficient for age group A (mrem/pCi), and $RC_{Ing,A,DW}$ is the drinking water risk coefficient for age group A (LCF/pCi).

3.1.2 Inadvertent Ingestion of Soil

Soil can be inadvertently ingested by humans. The annual effective dose ($E_{Soil,A}$, mrem/yr) and risk ($R_{Soil,A}$, LCF/yr) to a human of age group A from the inadvertent ingestion of soil is given by:

$$\begin{aligned} E_{Soil,A} &= C_{Soil} \text{Ing}_{Soil,A} DC_{Ing,A} \\ R_{Soil,A} &= C_{Soil} \text{Ing}_{Soil,A} RC_{Ing,A,Diet} \end{aligned} \quad 3-3$$

where C_{Soil} is the radionuclide concentration in the soil (pCi/kg), $\text{Ing}_{Soil,A}$ is the inadvertent soil ingestion rate for an individual of age group A (kg/yr), $DC_{Ing,A}$ is the ingestion dose coefficient

⁹ Age Group A is a generic designator for various age groups for which PDCFs and PRCFs are calculated as described in detail in Section 3.2.1.

for age group A (mrem/pCi), and $RC_{Ing,A,Diet}$ is the dietary ingestion risk coefficient for age group A (LCF/pCi).¹⁰

The radionuclide concentration in the surface soil (C_{Soil}), which is available to an individual for inadvertent ingestion, is given by:

$$C_{Soil} = Irr \frac{[1 - e^{-(\lambda + \lambda_R)t_b}]}{P(\lambda + \lambda_R)} C_W \quad 3-4$$

where Irr is the irrigation rate (m/yr), λ is the radionuclide decay constant (yr^{-1}), λ_R is the removal rate from soil (yr^{-1}), t_b is the period of time soil is irrigated with contaminated water (yr), and P is the effective “surface density” for soil, (kg/m^2).

Although Regulatory Guide 1.109 does not calculate exposures from soil ingestion, equation 3-4 is based on the soil buildup portion of Regulatory Guide 1.109 equation A-8 (NRC 1977). In addition to radiological decay, equation 3-4 includes removal from the soil by physical processes (λ_R), which is not included in Regulatory Guide 1.109 equation A-8. This term is intended to model the leaching of radionuclide from the surface layer to soil depths where the radionuclides are no longer available for uptake by humans, plants, and/or animals. This approach is used in models such as Peterson (1983), PATHWAY (Whicker and Kirchner 1987), GENII (Napier et al. 1988), Abbott and Rood (1993), RESRAD (Yu et al. 2002), and CAP88 (Trinity 2007).

3.1.3 Ingestion of Vegetables

The annual effective dose ($E_{Veg,A}$, mrem/yr) and risk ($R_{Veg,A}$, LCF/yr) to a human of age group A from the consumption of vegetables grown with unfiltered irrigation water is given by:

$$\begin{aligned} E_{Veg,A} &= C_{Veg} DD_{Veg} Ing_{Veg,A} DC_{Ing,A} \\ R_{Veg,A} &= C_{Veg} DD_{Veg} Ing_{Veg,A} RC_{Ing,A,Diet} \end{aligned} \quad 3-5$$

where C_{Veg} is the radionuclide concentration in vegetables (pCi/kg), $Ing_{Crop,A}$ is the vegetable ingestion rate for an individual of age group A (kg/yr), DD_{Veg} is the fraction of radioactivity retained on leafy vegetables and produce after washing, $DC_{Ing,A}$ is the ingestion dose coefficient for age group A (mrem/pCi), and $RC_{Ing,A,Diet}$ is the dietary ingestion risk coefficient for age group A (LCF/pCi).

According to Regulatory Guide 1.109, the radionuclide concentration in vegetation results from deposition onto the plant foliage and from uptake from the soil of activity deposited on the ground. The equation that models the radionuclide concentration in vegetation (C_{Veg}) is:

¹⁰ FGR 13 lists a single dose conversion factor for ingestion of each radionuclide, while separate risk conversion factors are cited for drinking water (DW) and dietary (Diet) ingestion.

$$C_{veg} = Irr \left[\frac{r_v \left[1 - e^{-(\lambda + \lambda_w)t_v} \right]}{Y_v (\lambda + \lambda_w)} + \frac{(B_v + B'_v) \left[1 - e^{-(\lambda + \lambda_R)t_b} \right]}{P(\lambda + \lambda_R)} \right] C_W \quad 3-6$$

where r_v is the fraction of deposited activity retained on vegetables (dimensionless), λ_w is the removal rate constant for physical removal by weathering (yr^{-1}), t_v is the length of the vegetable growing season (yrs), Y_v is the vegetable crop productivity or yield (kg/m^2), B_v is the element-specific vegetable uptake factor from soil (pCi/kg vegetables per pCi/kg soil), and B'_v represents the net effect of all resuspension processes (NCRP 1999).

In equation 3-6, the first term in brackets relates to the concentration derived from direct foliar deposition during the growing season, while the second term relates to root uptake of radionuclide contamination from soil and reflects the long-term deposition during operation of the uranium recovery facility.

Equation 3-6 is based on Regulatory Guide 1.109, equation A-8 (NRC 1977), except that two additional features have been included in the root uptake term. First, in addition to radiological decay, equation 3-6 includes removal due to removal from the soil (λ_R), which was described in Section 3.1.2. Second, as stated by the National Council on Radiation Protection and Measurements (NCRP) in Report No. 129 (NCRP 1999, page 92):

In the case of contamination by resuspended soil, the mechanisms can be quite complex. Not only can airborne resuspension and subsequent redeposit contaminate the vegetation, but also phenomena such as rain splash, saltation and mechanical disturbances during harvest. Thus, B'_v must also be determined empirically for the particular site or type of site and the type of vegetation.

To include this effect, Regulatory Guide 1.109, equation A-8 has been modified to include a transfer factor representing the net effect of all resuspension processes (B'_v), as recommended by the NCRP Report No. 129, equation 5.2 (NCRP 1999).

3.1.4 Ingestion of Milk

The annual effective dose ($E_{Mk,A}$, mrem/yr) and risk ($R_{Mk,A}$, LCF/yr) to a human of age group A from the consumption of milk from a cow that ingests contaminated well water, fodder grown with unfiltered irrigation water, and contaminated soil is given by:

$$\begin{aligned} E_{Mk,A} &= C_{Mk} \text{Ing}_{Mk,A} DC_{\text{Ing},A} \\ R_{Mk,A} &= C_{Mk} \text{Ing}_{Mk,A} RC_{\text{Ing},A,\text{Diet}} \end{aligned} \quad 3-7$$

where C_{Mk} is the radionuclide concentration in milk (pCi/L) and $\text{Ing}_{Mk,A}$ is the individual milk consumption rate (L/yr). The C_{Mk} term is calculated using the following equation:

$$C_{Mk} = CF_{Mk} \left(\text{Ing}_{Mk,W} C_W + \text{Ing}_{Mk,F} C_{Fod} + \text{Ing}_{Mk,Soil} C_{Soil} \right) \quad 3-8$$

where CF_{Mk} is the element-specific cow's intake to milk transfer coefficient (pCi/L milk per pCi/day intake), C_{Fod} is the radionuclide concentration in the animal's fodder (pCi/kg) (see equation 3-9), $Ing_{Mk,Fod}$ is the consumption rate of fodder by the cow (kg fresh weight of fodder/day), $Ing_{Mk,W}$ is the consumption rate of water by the cow (m³/day), C_{Soil} is the radionuclide concentration in the soil (Bq/kg) (see equation 3-4), and $Ing_{Mk,Soil}$ is the consumption rate of soil by the cow (kg/day). The radionuclide concentration in animal fodder is given by:

$$C_{Fod} = Irr \left[\frac{r_f \left[1 - e^{-(\lambda + \lambda_w) t_f} \right]}{Y_f (\lambda + \lambda_w)} + \frac{(B_f + B'_f) \left[1 - e^{-(\lambda + \lambda_R) t_b} \right]}{P (\lambda + \lambda_R)} \right] C_W \quad 3-9$$

where r_f is the fraction of deposited activity retained on fodder (dimensionless), λ_w is the removal rate constant for physical removal by weathering (yr⁻¹), t_f is the length of the fodder growing season (yrs), Y_f is the fodder productivity or yield (kg/m²), B_f is the element-specific concentration fodder uptake factor from soil (pCi/kg fodder / pCi/kg soil), and B'_f represents the net effect of all resuspension processes (NCRP 1999).

3.1.5 Ingestion of Meat

The annual effective dose ($E_{Mt,A}$, mrem/yr) and risk ($R_{Mt,A}$, LCF/yr) to a human of age group A from the consumption of meat from cattle that ingests contaminated well water, fodder grown with unfiltered irrigation water, and contaminated soil is given by:

$$\begin{aligned} E_{Mt,A} &= C_{Mt} Ing_{Mt,A} DC_{Ing,A} \\ R_{Mt,A} &= C_{Mt} Ing_{Mt,A} RC_{Ing,A,Diet} \end{aligned} \quad 3-10$$

where C_{Mt} is the radionuclide concentration in meat (pCi/kg) and $Ing_{Mt,A}$ is the individual consumption rate of the animal product (kg/yr). The C_{Mt} term is calculated using the following equation:

$$C_{Mt} = CF_{Mt} (Ing_{Mt,W} C_W + Ing_{Mt,F} C_{Fod} + Ing_{Mt,Soil} C_{Soil}) \quad 3-11$$

where CF_{Mt} is the element-specific cattle intake to meat transfer coefficient (pCi/kg meat per pCi/day intake), C_{Fod} is the radionuclide concentration in the animal's fodder (pCi/kg fresh weight of fodder) (see equation 3-9), $Ing_{Mt,Fod}$ is the consumption rate of fodder by cattle (kg fresh weight of fodder/day), $Ing_{Mt,W}$ is the consumption rate of water by cattle (m³/day), C_{Soil} is the radionuclide concentration in the soil (pCi/kg) (see equation 3-4), and $Ing_{Mt,Soil}$ is the consumption rate of soil by cattle (kg/day).

3.1.6 Pathway Dose and Risk Factors

The pathway dose and risk factors are calculated by dividing the above derived exposure equations by the radionuclide concentration in the well from which the water is taken and then summing over all of the exposure pathways, as shown below:

$$PDCF_{Total,A} = \sum_P PDCF_{P,A} = \sum_P \frac{E_{P,A}}{C_W}$$

$$PRCF_{Total,A} = \sum_P PRCF_{P,A} = \sum_P \frac{R_{P,A}}{C_W}$$
3-12

where P identifies the exposure pathway (i.e., drinking water, soil ingestion, vegetable ingestion, ingestion of milk, and ingestion of meat), and A identifies the age group (i.e., infant, child, teen, and adult).

3.1.7 Implementation

In order to calculate the PDCFs and PRCFs, the above equations were programmed into an Excel® spreadsheet. To propagate the uncertainty in the value for many of the parameters used in the above equations, the Excel add-in Crystal Ball was used to solve for the PDCFs and PRCFs using a Monte Carlo simulation. Parameter uncertainty is due to both natural variation between individuals (e.g., drinking water, vegetable, milk, and meat consumption rates [$Ing_{DW,A}$, $Ing_{Veg,A}$, $Ing_{Mk,A}$, and $Ing_{Mt,A}$], etc.) and uncertainty as to the “true” value for the parameter (e.g., vegetable, fodder, milk, and meat transfer coefficients [B_v , B_f , CF_{milk} , and CF_{meat}], etc.). Instead of selecting a single value to represent each parameter, the Crystal Ball Monte Carlo simulation will randomly sample from a range of values for each parameter and solve for the PDCFs and PRCFs, and then it will repeat the entire process until it has calculated a range of PDCFs and PRCFs. From this range of values, mean, median, 90th percentile, and other measures can be selected. For this analysis, the Monte Carlo simulation repeated the calculations 1,000 times.

3.2 Input Parameters

This section describes how the values for the various input parameters were selected and identifies those parameters for which parameter distributions were specified.

3.2.1 Age Groups

As shown above in Section 3.1 and in keeping with Regulatory Guide 1.109, the PDCFs and PRCFs have been calculated for four age groups—infant, child, teen, and adult. In order to calculate the age-specific PDCFs and PRCFs, it was necessary to use age-specific dose and risk conversion factors and exposure factors (e.g., water and food consumption rates). Fortunately, the source documents for these parameters present age-dependent data. Unfortunately, the manner in which the data are grouped by age is not uniform across each source document, or even for different parameters within a single source document.

The age-dependent parameters used in this analysis were obtained from two primary sources: Federal Guidance Report No. 13 CD Supplement (EPA 2002) for dose and risk coefficients, and the *Exposure Factors Handbook* (EFH) (EPA 2011b) for usage factors.

The dose and risk coefficients used in this report were developed based on the recommendations of the International Commission on Radiological Protection (ICRP). Starting in the mid 1980s, the ICRP began developing age-dependent dose coefficients for members of the public (ICRP 2006). For example, in Publication 72 (ICRP 1995), the ICRP has indicated that the following six age-specific dose coefficients are appropriate for calculating doses for the indicated age ranges:

ICRP Age Group	Applicable Age Range
3 months	from 0 to 1 year
1 year	from 1 year to 2 years
5 year	more than 2 years to 7 years
10 year	more than 7 years to 12 years
15 year	more than 12 years to 17 years
Adult	more than 17 years

However, in Publication 101 (ICRP 2006), the ICRP recommended:

... that the annual dose for the representative person should be defined by three age categories. These categories are 0–5 years (infant), 6–15 years (child), and 16–70 years (adult). The shorter time period is selected for the infant age category, when dosimetric characteristics are changing most rapidly, to avoid any unwarranted reduction in the importance attached to doses to younger age groups. Use of these three age categories is sufficient to characterize the radiological impact of a source and to ensure consideration of younger, more sensitive populations. For practical implementation of this recommendation, dose coefficients and habit data for a 1-year-old (infant), a 10-year-old (child), and an adult should be used to represent the three age categories. (ICRP 2006)

The age grouping recommendations from ICRP Publication 101 are summarized in the following table.

Age category (years)	Name of age category	Dose coefficient and habit data to be used
0–5	Infant	1 year old
6–15	Child	10 year old
16–70	Adult	Adult

Unlike the dose and risk coefficients, the exposure factors used in this study were taken from the EPA's *EFH* (EPA 2011b). Many of the exposure factors presented in the Handbook are broken down by age, and the age grouping (at least for children) is that recommended by the EPA (EPA 2005). EPA 2005, Table 4, recommends the following 10 age groups for children under the age of 21 years:

Children <1 Year	Children >1 Year
Birth to <1 month	1 to <2 years
1 to <3 months	2 to <3 years
3 to <6 months	3 to <6 years
6 to <12 months	6 to <11 years
	11 to <16 years
	16 to <21 years

Table 3-1 presents the age groups for the various parameters from each source document mapped into the four age groups used in this analysis. The four age groups used in this analysis assume that the population is made up of infants, children, teenagers, and adults (NRC 1977). In Table 3-1, the parameter (or distribution) values used in this analysis are shown in bold.

Table 3-1: Age Groups Used in the Analysis

Age Group	FGR 13*		Exposure Factors Handbook*			
	Risk Coefficients	Dose Coefficients	Water Consumption	Soil and Dust	Vegetables, Milk and Meat	Body Weight
Infant	0 to 5 yr**	100 days 1 yr	Birth to <1 mo 1 to <3 mos 3 to <6 mos 6 to <12 mos	6 wks to <1 yr	Birth to 1 yr	Birth to <1 mo 1 to <3 mos 3 to <6 mos 6 to <12 mos
Child	5 to 15	5 10	1 to <2 2 to <3 3 to <6 6 to <11	1 to <6 3 to <6	1 to 2 3 to 5 6 to 12	1 to <2 2 to <3 3 to <6 6 to <11
Teen	15 to 25	15	11 to <16 16 to <18	6 to 21	13 to 19	11 to <16 16 to <21
Adult	25 to 70	20	18 to <21 ≥21 ≥65	6 to 21	20 to 49 ≥50	21 to <30 30 to <40 40 to <50 50 to <60 60 to <70 70 to <80 ≥80

* Items in bold were selected for use in this analysis.

** For Child, Teen, and Adult, all ages are given in years.

Although different groupings could be made, based on the analysis performed by the ICRP (ICRP 2006), it is not anticipated that any alternative age grouping would have a significant effect on the calculated doses and risks.

3.2.2 Dose and Risk Conversion Coefficients

Naturally occurring uranium found in the ground contains (by weight) 99.3% U-238, 0.7% U-235, and a trace amount of U-234. In terms of the amount of radioactivity, natural uranium contains approximately 48.6 % U-238, and 49.2 % U-234, and 2.2 % U-235. Because U-235 composes such a small portion of the radioactivity in natural uranium and because the U-235 ingestion dose and risk conversion coefficients are very similar to the U-234 and U-238 coefficients, U-235 has not been included in this analysis. In addition to being radioactive, uranium is hazardous from the standpoint of chemical toxicity. The main chemical effect associated with exposure to uranium is irreversible kidney damage. Although this section focuses on uranium's radioactive toxicity, its chemical toxicity risk is discussed in Section 4.5, along with the chemical toxicity risk of various other metals found in the ore.

As shown in Figure 3-2, the uranium radioactive decay series contains five radionuclides with half-lives of over a year. They are U-238 (4.5×10^9 years), U-234 (2.4×10^5 years), Th-230 (7.7×10^4 years), Ra-226 (1,600 years), and Pb-210 (22.3 years). This analysis focuses on these

five radionuclides. If other shorter-lived radionuclides are initially present in the lixiviant, they will decay before they reach the receptor well. However, the longer-lived radionuclides will decay as they travel to the receptor well, so the shorter-lived radionuclides will be present at the well. This analysis addresses the in-growth of the shorter-lived radionuclides by including the dose and risk coefficients of the short-lived progeny with the parent's coefficients. For example, the Ra-226 ingestion dose and risk coefficients used in this analysis include the contributions from Po-210, Bi-210, Pb-210, Bi-214, and Pb-214 [the FGR 13 CD Supplement (EPA 2002) does not provide ingestion dose or risk factors for Pa-234m, Rn-222, Po-218, or Po-214, likely because Rn-222 is a noble gas, and the two polonium isotopes and protactinium half-lives are too short for them to enter the food chain, as shown in Figure 3-2].

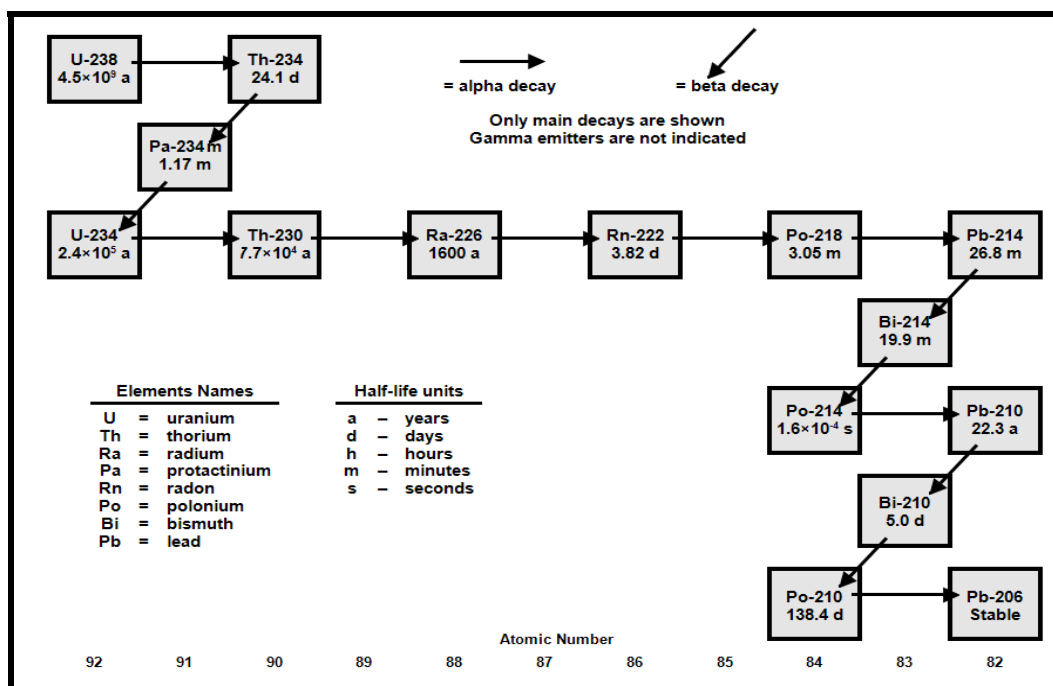


Figure 3-2: Uranium Decay Series

The dose and risk coefficients used in this analysis were obtained from FGR 13 (Eckerman et al. 1999). FGR 13 does not actually present age-specific risk coefficients or any dose coefficients. Instead, it presents risk coefficients that are representative of the U.S. population. However, in order to calculate the FGR 13 risk coefficients, it was necessary to calculate age-specific dose and risk coefficients. Those age-specific dose and risk coefficients are included in data files supplied with the FGR 13 CD Supplement (EPA 2002):¹¹ FGR13ING.GBD contains the dose coefficients due to ingestion of radioactive material and FRG13ING.RBS contains both the drinking water and dietary ingestion risk coefficients. The dose conversion factors use the latest methods and models from the ICRP and are analogous to the dose factors contained in ICRP Publication 72 (ICRP 1995). The dose and risk coefficients from FGR 13 that were used in this

¹¹ FGR13ING.GBD and FGR13ING.RBS, containing age-dependent ingestion dose and risk factors, are also supplied with the CAP88 and GENII computer programs.

analysis are shown in Table 3-2. In Table 3-2, the Ra-226 ingestion dose and risk factors that include the contribution from the short-lived progeny are shown as Ra-226+P.

Table 3-2: Radionuclide-Specific Ingestion Dose and Risk Coefficients

Nuclide	Mortality Coefficient – Drinking (LC/Sv)			
	Infant	Child	Teen	Adult
	0- 5	5- 15	15- 25	25- 70
Po-210	2.56E-07	1.02E-07	4.58E-08	2.47E-08
Bi-210	1.71E-09	6.93E-10	1.92E-10	3.30E-11
Pb-210	1.25E-07	6.92E-08	3.08E-08	8.78E-09
Pb-210+P	3.83E-07	1.72E-07	7.68E-08	3.35E-08
Bi-214	3.55E-11	1.62E-11	9.51E-12	1.86E-12
Pb-214	6.51E-11	2.80E-11	1.34E-11	2.61E-12
Ra-226	3.92E-08	2.59E-08	1.97E-08	3.07E-09
Ra-226+P	4.22E-07	1.98E-07	9.65E-08	3.66E-08
Th-230	1.27E-08	5.02E-09	2.73E-09	1.07E-09
U-234	9.99E-09	4.59E-09	2.05E-09	6.60E-10
Th-234	4.48E-09	1.81E-09	5.19E-10	7.78E-11
U-238	9.06E-09	4.16E-09	1.86E-09	6.05E-10
U-238+P	1.35E-08	5.97E-09	2.38E-09	6.83E-10
Nuclide	Mortality Coefficient – Dietary (LCF/Sv)			
	Infant	Child	Teen	Adult
	0- 5	5- 15	15- 25	25- 70
Po-210	2.52E-07	1.03E-07	4.6E-08	2.61E-08
Bi-210	1.71E-09	6.95E-10	1.95E-10	3.74E-11
Pb-210	1.24E-07	6.93E-08	3.10E-08	9.38E-09
Pb-210+P	3.78E-07	1.73E-07	7.72E-08	3.55E-08
Bi-214	3.54E-11	1.62E-11	9.5E-12	2.18E-12
Pb-214	6.48E-11	2.80E-11	1.34E-11	3.00E-12
Ra-226	3.86E-08	2.59E-08	1.99E-08	3.31E-09
Ra-226+P	4.16E-07	1.99E-07	9.71E-08	3.88E-08
Th-230	1.20E-08	5.03E-09	2.73E-09	1.18E-09
U-234	9.94E-09	4.60E-09	2.06E-09	7.30E-10
Th-234	4.49E-09	1.81E-09	5.25E-10	8.90E-11
U-238	9.01E-09	4.17E-09	1.87E-09	6.68E-10
U-238+P	1.35E-08	5.98E-09	2.40E-09	7.57E-10

Table 3-2: Radionuclide-Specific Ingestion Dose and Risk Coefficients

Nuclide	Effective Dose Coefficient (Sv/Bq)			
	Infant	Child	Teen	Adult
	100 days	5 yrs	15 yrs	20 yrs
Po-210	2.60E-05	4.37E-06	1.57E-06	1.21E-06
Bi-210	1.50E-08	4.84E-09	1.63E-09	1.31E-09
Pb-210	8.31E-06	2.18E-06	1.92E-06	6.96E-07
Pb-210+P	3.43E-05	6.55E-06	3.49E-06	1.91E-06
Bi-214	1.37E-09	3.66E-10	1.42E-10	1.12E-10
Pb-214	2.17E-09	5.21E-10	2.03E-10	1.39E-10
Ra-226	4.65E-06	6.16E-07	1.52E-06	2.80E-07
Ra-226+P	3.90E-05	7.18E-06	5.01E-06	2.19E-06
Th-230	4.13E-06	3.09E-07	2.19E-07	2.14E-07
U-234	3.69E-07	8.84E-08	7.45E-08	4.95E-08
Th-234	3.99E-08	1.26E-08	4.23E-09	3.40E-09
U-238	3.34E-07	8.01E-08	6.71E-08	4.45E-08
U-238+P	3.74E-07	9.27E-08	7.13E-08	4.79E-08

Source: FGR 13 CD Supplement (EPA 2002)

The dose factors from Table 3-2 were converted to the dose coefficients for ingestion ($DC_{Ing,A}$, mrem/pCi) by multiplying by 0.037×10^5 (Bq/pCi)(mrem/Sv), while the risk factors from Table 3-2 were converted to the risk coefficients for ingestion ($RC_{Ing,A,DW}$ and $RC_{Ing,A,Diet}$, LCF/pCi) by multiplying by 0.037 (Bq/pCi).

Mortality Versus Morbidity Risk Coefficients

For risks due to non-radiological sources, the EPA typically bases its rulemaking on cancer morbidity risk, e.g., the National Contingency Plan (55 *Federal Register* 8665-8865, March 8, 1990). However, for risks due to radiological sources, the EPA has traditionally used cancer mortality as the basis for their rulemaking, e.g., the Radiation Protection Standards for Yucca Mountain (73 *Federal Register* 61256- 61289, October 15, 2008). A brief comparison of cancer morbidity to mortality risks is presented here.

Based on analysis by the EPA (EPA 1999a), the Interagency Steering Committee on Radiation Standards (ISCORS 2002) recommended a cancer morbidity risk coefficient of 8×10^{-4} per rem (8×10^{-6} per sievert) and a cancer mortality risk coefficient of 6×10^{-4} per rem (6×10^{-6} per sievert). Thus, the morbidity to mortality risk ratio is 1.33. Alternatively, the National Academy of Sciences uses a ratio of 1.5 for total cancer incidence to fatal cancer incidence. *Depending upon exposure pathways, radionuclide, total inventory and site characteristics, the ratio of 1.5 could be off by a factor of 2.* (NAS 1995, page 51)

Finally, Table 3-3 shows the morbidity to mortality risk ratio based on the FGR 13 drinking water risk coefficients. As Table 3-3 shows, the ratio ranges from 1.30 for the adult Ra-226+P risk coefficients to 1.70 for the infant U-238+P risk coefficients.

Table 3-3: FGR 13 Drinking Water Cancer Morbidity / Mortality Risk Ratio				
Nuclide	Morbidity / Mortality Risk Ratio			
	Infant	Child	Teen	Adult
	0- 5	5- 15	15- 25	25- 70
Po-210	1.43	1.42	1.38	1.30
Bi-210	1.81	1.80	1.80	1.77
Pb-210	1.42	1.41	1.36	1.30
Pb-210+P	1.43	1.42	1.37	1.30
Bi-214	1.23	1.23	1.17	1.17
Pb-214	1.44	1.42	1.30	1.29
Ra-226	1.55	1.49	1.42	1.38
Ra-226+P	1.44	1.43	1.38	1.31
Th-230	1.56	1.56	1.46	1.39
U-234	1.64	1.61	1.53	1.44
Th-234	1.81	1.81	1.80	1.80
U-238	1.64	1.61	1.52	1.43
U-238+P	1.70	1.67	1.58	1.47

Dose/Risk Coefficient Uncertainty

In FGR 13, the dose and risk coefficients are presented as single values, rather than as a distribution or range of values. However, in order to calculate the FGR 13 dose and risk coefficients, numerous assumptions had to be made regarding biokinetic, dosimetric, and radiogenic cancer risk models. Different values could have been assumed regarding these models and/or parameter values, which would have resulted in different values for the dose and risk coefficients. FGR 13, Table 2.4 and Appendix D, briefly describe the uncertainty in the dose and risk coefficients that result from these assumptions. Pawel et al. (2007) provide additional insight into the uncertainty associated with the FGR 13 risk coefficients. As Pawel et al. (2007) explains:

Assigned levels of uncertainty were based on sensitivity analyses in which various combinations of plausible biokinetic and dosimetric models and radiogenic cancer risk models were used to generate alternative risk coefficients. Uncertainties relating to the validity of the linear-no-threshold hypothesis were not addressed in the analysis because this is not feasible.

The uncertainty in a risk coefficient was viewed as the net result of uncertainties in the following main components of the derivation: biokinetic models describing the biological behavior of ingested or inhaled radionuclides; specific energies that relate emissions from source organs to energy deposition in target organs; risk model coefficients representing the risk of cancer per unit absorbed dose to sensitive tissues from low-LET radiation at high dose and high dose rate; tissue-

specific dose and dose rate effectiveness factor (DDREF); and tissue-specific high-dose relative biological effectiveness (RBE).

Although this analysis will use the FGR 13 dose and risk coefficients as single values, the following discussion is given to provide some understanding of the implication of this assumption.

The results of the Pawel et al. (2007) uncertainty analysis were assigned to one of five “uncertainty categories” (A through E), depending on the ratio of the 5th to the 95th percentiles of the calculated risk coefficients. For the five radionuclides of interest in this analysis, Table 3-4 presents the results of the Pawel et al. (2007) uncertainty analysis.

Table 3-4: Risk Coefficient Uncertainty

Nuclide	Uncertainty Category	Category Range*
Pb-210	C	$35 < Q_{95}/Q_5 < 50$
Ra-226	C	$35 < Q_{95}/Q_5 < 50$
Th-230	D	$50 < Q_{95}/Q_5 < 150$
U-234	C	$35 < Q_{95}/Q_5 < 50$
U-238	B	$15 < Q_{95}/Q_5 < 35$

* Q_5 and Q_{95} are the 5% and 95% sample quantiles of the risk coefficients generated by combining plausible variations of the biokinetic, dosimetric, and risk models.

Table 3-4 shows that for the five radionuclides of interest, U-238 has the least uncertainty (at between a factor of 15 to 35), while Th-230 has the most (at between a factor of 50 to 150). For several radionuclides, Pawel et al. (2007) provides a brief discussion of the basis of the uncertainty. As it happens, these brief discussions were provided for two of the five radionuclides of interest for this analysis, and they have been reproduced below.

Regarding the uncertainty of the Ra-226 ingestion risk factors, Pawel et al. (2007) states:

Risk and dose models contribute ~90% and 10% of uncertainty, respectively. GI uptake and systemic biokinetics reasonably well established. Important cancer sites include bone, for which the risk model is highly uncertain, and colon, for which risk model is moderately uncertain.

Regarding the uncertainty of the U-234 ingestion risk factors, Pawel et al. (2007) states:

Risk and dose models contribute ~90% and 10% of uncertainty, respectively. GI uptake and most of the important aspects of systemic biokinetics reasonably well known. Important cancer sites include colon, for which risk model is moderately well established, and bone, for which risk model is poorly established.

Although it is not possible to incorporate this risk coefficient uncertainty into the present analysis, the following two examples demonstrate the potential impact of this uncertainty.

If it is assumed that the FGR 13 U-238 dietary risk coefficient of $1.51 \times 10^{-9} \text{ Sv}^{-1}$ is halfway between the 5th to the 95th percentiles, and that Q_{95}/Q_5 is equal to 15, then the average U-238 risk coefficient has a range from 3.90×10^{-10} to $5.85 \times 10^{-9} \text{ Sv}^{-1}$, rather than the FGR 13 value.

Likewise, if it is assumed that the FGR 13 Th-230 dietary risk coefficient of $2.16 \times 10^{-9} \text{ Sv}^{-1}$ is halfway between the 5th to the 95th percentiles, and that Q_{95}/Q_5 is equal to 150, then the average Th-230 risk coefficient has a range from 1.76×10^{-10} to $2.65 \times 10^{-8} \text{ Sv}^{-1}$, rather than the FGR 13 value.

3.2.3 Ingestion of Drinking Water

As shown by equation 3-2, the only parameters necessary to calculate the $PDCF_{Wat,A}$ and $PRCF_{Wat,A}$ are the age-dependent drinking water consumption rates. The age-dependent drinking water consumption rates were obtained by multiplying the weight normalized water consumption rate provided in EFH, Table 3-41 (EPA 2011b), and shown in Table 3-5, by the age-specific body weight, as shown in Table 3-6.

Table 3-5: Age-Dependent Weight Normalized Water Consumption Rates

Percentile	Water Intake – mL/kg-day			
	Infant	Child	Teen	Adult
	3 to <6 mos	3 to 6 yrs	11 to 16 yrs	≥21 yrs
10%	8	7	4	6
25%	50	14	7	12
50%	95	24	13	19
75%	132	37	20	29
90%	163	52	33	41
95%	186	63	44	50
99%	238	96	66	70

Source: EPA 2011b, Table 3-41

In order to demonstrate that the water consumption rate data from the EFH was entered into and used correctly by Crystal Ball, Figure 3-3 shows the distributions of the four age-dependent water consumption rates calculated by the Crystal Ball Monte Carlo simulation for this analysis and compares them to the Table 3-5 EFH distributions. As shown, there is very good agreement between the EFH distributions and the distributions used in this analysis.

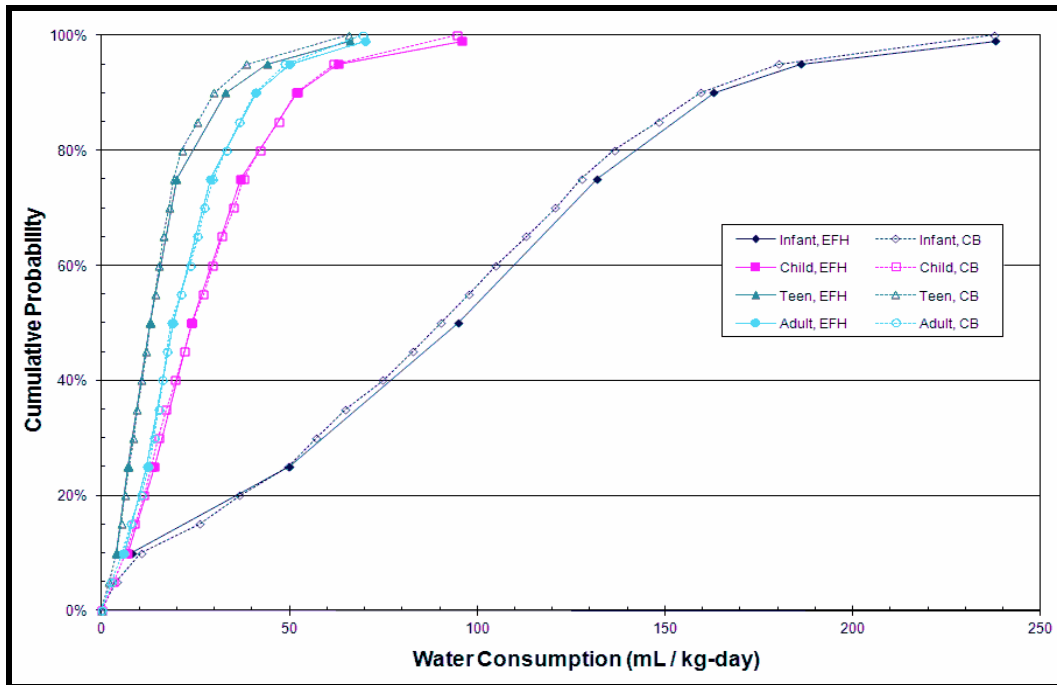


Figure 3-3: Distribution of Age-Dependent Weight Normalized Water Consumption Rates

As indicated above, the daily weight normalized water consumption rates from Table 3-5 were converted to the individual water ingestion rate (Ing_{wat} , m^3/yr) by multiplying by 365.25×10^{-6} (day/yr)(m^3/mL), and then multiplying by the individual's body weight. Table 3-6 presents the age-dependent body weight distributions that were obtained from the EFH, Table 8-3 (EPA 2011b).

Table 3-6: Body Weight Distributions

Percentile	Body Weight – kg			
	Infant	Child	Teen	Adult
	3 to <6 mos	3 to <6 yrs	11 to <16 yrs	30 to <40 yrs
5%	5.7	13.5	34.0	53.5
10%	6.1	14.4	37.2	57.4
15%	6.3	14.9	40.6	60.1
25%	6.7	15.8	45.0	66.1
50%	7.3	17.8	54.2	77.9
75%	8.0	20.3	65.0	92.4
85%	8.4	22.0	73.0	101.0
90%	8.7	23.6	79.3	107.0
95%	9.1	26.2	88.8	118.0

Source: EPA 2011b, Table 8-3

Figure 3-4 shows the Crystal Ball (CB) calculated combined body weight and drinking water consumption distributions for all four age groups, and compares them to the Regulatory Guide 1.109, Table E-5 maximum exposed recommended age dependent annual drinking water rates.

Notice that the R.G. 1.109 recommended maximum rate for adults corresponds to 2 liters per day, which is commonly used in risk assessments. Also, notice that all of the R.G. 1.109 recommended maximum rates falls within the CB calculated distributions.

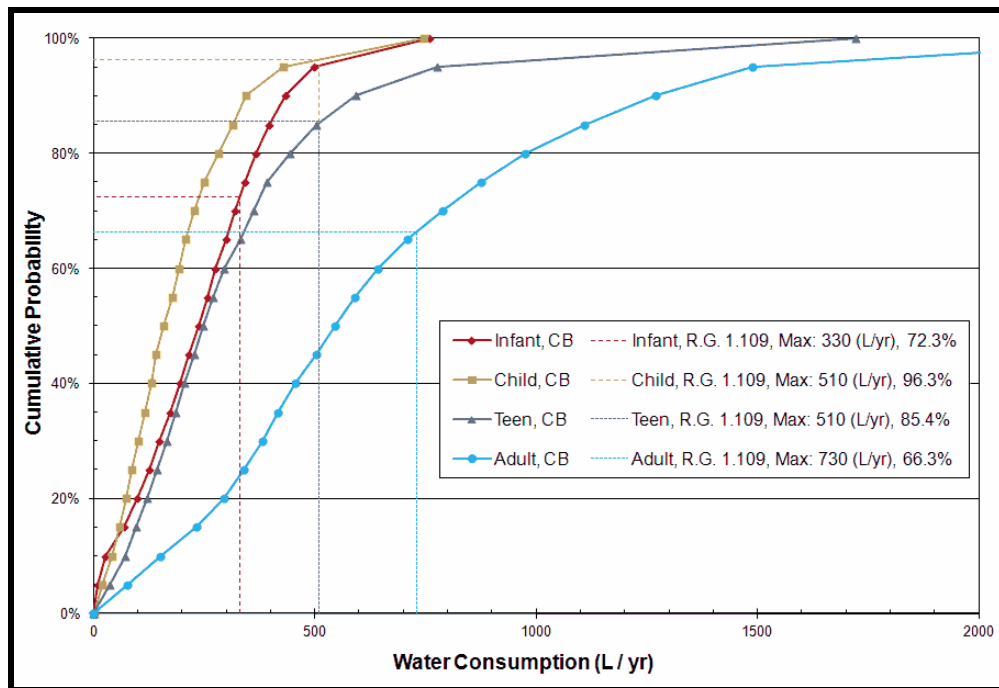


Figure 3-4: Distribution of Age-Dependent Water Consumption Rates Compared to Regulatory Guide 1.109 Recommended Maximum Rates

Figure 3-5 compares the CB calculated combined adult body weight and drinking water consumption distribution to the drinking water distribution recommended in the RESRAD documentation (NUREG/CR-6697, Attachment C, Section 5.2). For a cumulative probability of less than 20%, the RESRAD distribution is larger than the CB distribution, at 50% cumulative probability the CB value is 33% larger than the RESRAD value, while at 93.3% cumulative probability the maximum difference of 66% between the CB and RESRAD values was calculated.

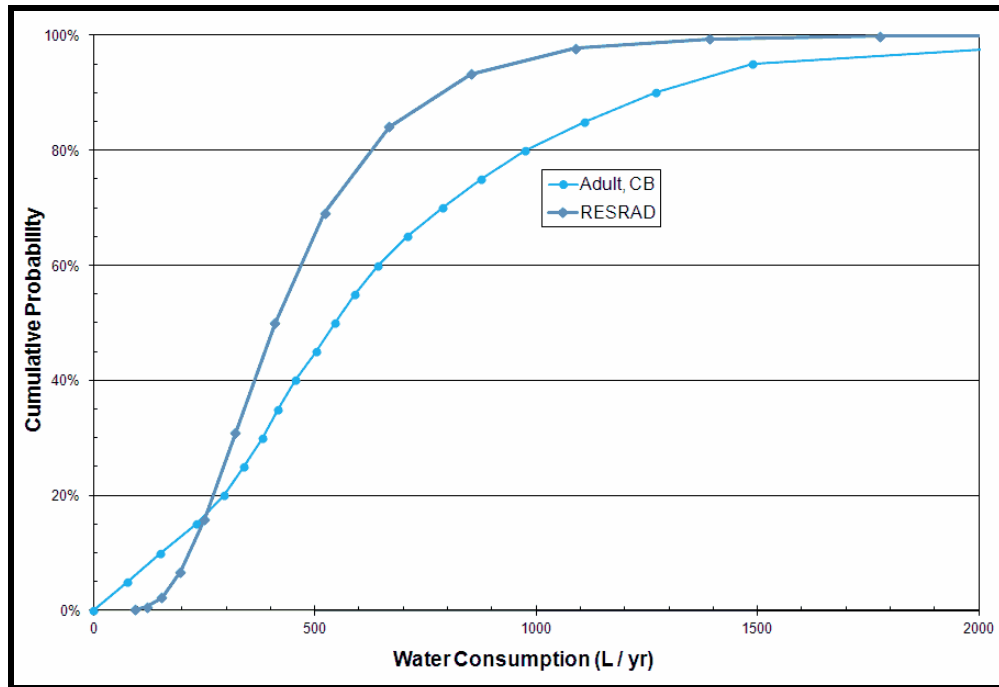


Figure 3-5: Distribution of Age-Dependent Water Consumption Rates Compared to the RESRAD Distribution

Based on Figure 3-4 and Figure 3-5 it is concluded that the Crystal Ball calculated combined EFH body weight distributions and weight-normalized water consumption rate distributions are consistent with both Regulatory Guide 1.109 and RESRAD water consumption rates. It is reasonable to assume that similar results would be obtained for other distributions that result from the coupling of variables.

3.2.4 Inadvertent Ingestion of Soil

As shown in Section 3.1.2, in order to calculate the $PDCF_{Soil,A}$ and $PRCF_{Soil,A}$, it is necessary to know:

- The irrigation rate (Irr)
- The removal rate from soil (λ_w)
- The duration period for irrigation (t_b)
- The effective “surface density” for soil (P)
- The removal rate constant for physical removal by weathering (λ_w)
- Age-dependent inadvertent soil ingestion rates ($Ing_{Soil,A}$)

The irrigation rate (Irr) was obtained from the 2002 Census of Agriculture Farm and Ranch Irrigation Survey (USDA 2004), which presented the area of farmland irrigated and the volume of irrigation water used for each state. Irrigation rates (m/yr) were calculated for each state, and the cumulative distribution shown in Figure 3-6 was developed and used in this analysis. As a check of the 2002 census data, NUREG/CR-5512 (SNL 1999) was consulted. Table 6.18 of NUREG/CR-5512, Volume 3, contains data from the 1992 Census of Agriculture for 27 states.

Figure 3-6 contains the cumulative distribution of the NUREG/CR-5512 data, which shows very good agreement with the 2002 Census of Agriculture cumulative distribution.

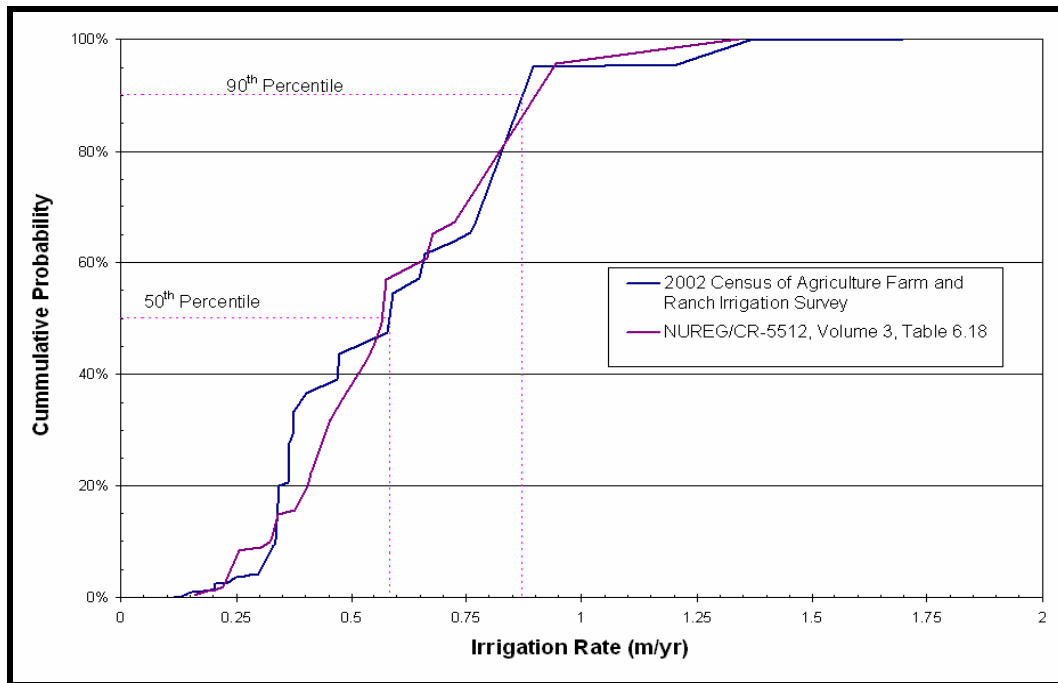


Figure 3-6: Distribution of Irrigation Water Application Rate

The removal rate from soil (λ_R) and the duration period for irrigation (t_b) were taken from the CAP88 Users Manual (Trinity 2007) as a constant $0.02 \text{ (yr}^{-1}\text{)}$ and 100 yrs, respectively. Based on NUREG/CR-6697, Appendix C, Section 3.1 (ANL 2000), the effective “surface density” for soil (P) was assumed to have a normal distribution, with a mean and standard deviation of 1.52 and 0.23 g/cm^3 , and minimum and maximum values of 0.83 and 2.21 g/cm^3 .

The inadvertent soil ingestion rates were modeled as a triangular distribution, with minimum, most likely, and maximum values for each age group, as shown in Table 3-7. The most likely soil ingestion rates in Table 3-7 were obtained from the general population central tendency values in EFH (EPA 2011b), Table 5-1 for soil plus dust ingestion. Likewise, the maximum Child soil ingestion rate was obtained from the child general population upper percentile value in EFH (EPA 2011b), Table 5-1 for soil plus dust ingestion. The minimum and the other age group maximum values were assumed.

Table 3-7: Soil + Dust Ingestion

Age Group	Soil Ingestion Rate (mg/day)		
	Minimum	Most Likely*	Maximum
Infant	0	60	200
Child	0	100	200*
Teen	0	50	200
Adult	0	50	200

* EPA 2011b, Table 5-1

3.2.5 Ingestion of Vegetables

As shown in Section 3.1.3, in order to calculate the $PDCF_{veg,A}$ and $PRCF_{veg,A}$, it is necessary to know:

- The fraction of radioactivity retained on leafy vegetables and produce after washing (DD_{veg})
- The fraction of deposited activity retained on vegetables (r_v)
- The removal rate constant for physical removal by weathering (λ_w)
- The length of the vegetable growing season (t_v)
- The vegetable productivity or yield (Y_v)
- The element-specific vegetable uptake factor from soil (B_v)
- The net effect of all resuspension processes (B'_v)
- Age-dependent vegetable ingestion rates ($Ing_{veg,A}$)

The following terms have already been defined in Section 3.2.4:

- The irrigation rate (Irr)
- The removal rate from soil (λ_w)
- The duration period for irrigation (t_b)
- The effective “surface density” for soil (P)
- The removal rate constant for physical removal by weathering (λ_w)

The geometric means and standard deviations of the lognormal distributions for the element-specific vegetable uptake factor from soil (B_v) used in this analysis were taken from NCRP 1999, and are shown in Table 3-8.

Table 3-8: Element-Specific Input Parameters for Lognormal Distribution

Element	B_v Vegetable Uptake (pCi/g vegetables per pCi/g soil)		B_f Fodder Uptake (pCi/g fodder per pCi/g soil)		CF_{Mt} Meat Transfer (pCi/kg meat per pCi/day intake)		CF_{Mk} Milk Transfer (pCi/L milk per pCi/day intake)	
	GM	GSD	GM	GSD	GM	GSD	GM	GSD
Pb	4E-03	2.5	0.09	2.5	8E-04	2.0	3E-04	2.5
Ra	0.04	2.5	0.2	2.5	1E-03	2.0	1E-03	1.6
Th	1E-03	2.5	1E-03	2.5	1E-04	2.8	5E-06	2.5
U	2E-03	2.5	0.01	2.5	8E-04	2.0	4E-04	1.8

Note: GM is the geometric mean, and GSD is the geometric standard deviation

Source: NCRP (1999)

The fraction of deposited activity retained on vegetables (r_v) was assumed to be a uniform distribution with a minimum of 0.1 and a maximum of 0.6, as recommended for leafy and other vegetables by NUREG/CR-5512, Volume 3, Table 6.76 (SNL 1999). The fraction of radioactivity retained on leafy vegetables and produce after washing (DD_{veg}) was taken as 0.5, as specified in Section 10.2 of the *CAP88 Users Manual* (Trinity 2007).

The removal rate constant for physical removal by weathering (λ_w) was assumed to be a triangular distribution with minimum, maximum, and most likely values of 5.1, 84, and 18 yr⁻¹, respectively, as recommended by NUREG/CR-6697, Appendix C, Section 6.6 (ANL 2000). It is noted that the most likely value has a weathering half-life of 14 days, which is identical to the value recommended in CAP88, Section 10 (Trinity 2007); Regulatory Guide 1.109, Table E-15 (NRC 1977); and NUREG/CR-5512, Volume 3, Table 6.30 (SNL 1999).

As described in Section 3.1.3, equation 3-6 includes a term to account for the net effect of all resuspension processes (B'_v) on the radionuclide concentration in vegetables. For this analysis, a lognormal distribution with a mean of 0.001 and a standard deviation of 2.2 was assumed for B'_v , as recommended by NCRP 1999, Table 5.7, for vegetables grown in a heavily vegetated rural area.

For this analysis, the length of the vegetable growing season (t_v) was assumed to be 60 days, as recommended in the *CAP88 Users Manual* (Trinity 2007).

The vegetable productivity or yield (Y_v) was obtained from the U.S. Department of Agriculture's (USDA's) 2010 vegetable summary (USDA 2011). In the 2010 vegetable summary, the USDA presents the area harvested and production values for 21 different vegetables grown in 2008, 2009, and 2010. The vegetables included in the USDA report were artichokes, asparagus, snap beans, broccoli, cabbage, carrots, cauliflower, celery, sweet corn, cucumbers, garlic, head lettuce, leaf lettuce, romaine lettuce, onions, bell peppers, chili peppers, pumpkins, spinach, squash, and tomatoes. The data from the USDA report were converted into a cumulative distribution of the vegetable yield, as shown in Figure 3-7. This is the vegetable yield (Y_v) distribution that was used for this analysis. For comparison, Figure 3-7 also presents the cumulative distribution of vegetable yield for non-leafy vegetables obtained from NUREG/CR-6697, Appendix C, Section 6.5 (ANL 2000), and shows that the NUREG/CR-6697 yield is substantially lower than the USDA's yield. For example, at the 50th percentile, the NUREG/CR-6697 yield is 1.75 kg/m², while the USDA's yield is 3.61 kg/m². Of course, the NUREG/CR-6697 yield is for non-leafy vegetables, which tend to have lower yields than leafy vegetables included in the USDA's yield distribution. However, since the yield is being used in equation 3-6 to calculate the vegetable radionuclide concentration due to leaf deposition, it is believed to be correct to include leafy vegetables in the yield cumulative distribution. Finally, Figure 3-7 shows that the head lettuce (as a representative of leafy vegetables) has a yield of about 4.1 kg/m².

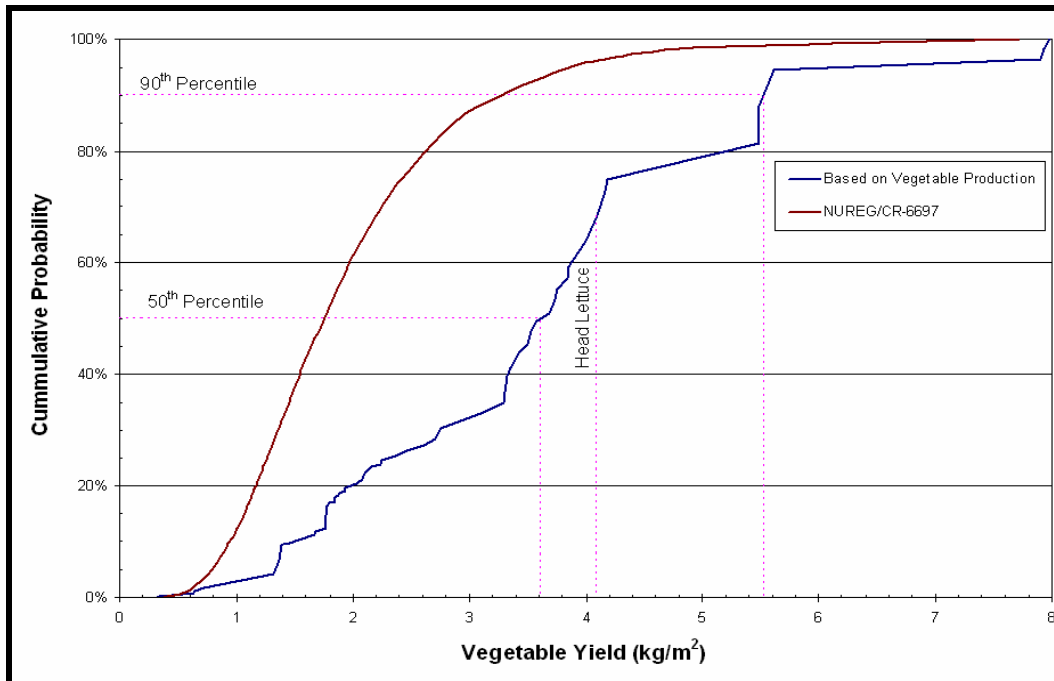


Figure 3-7: Distribution of Vegetable Yields

The age-dependent vegetable consumption rates ($Ing_{veg,A}$) were obtained by multiplying the weight normalized vegetable consumption rates provided in EFH, Table 9-4 (EPA 2011b) and shown in Table 3-9, by the age-specific body weight, as shown in Table 3-6.

Table 3-9: Age-Dependent Weight Normalized Vegetable Consumption Rates

Percentile	Consumption Rate (g/kg-day)			
	Infant	Child	Teen	Adult
	<1 yr	3-5 yrs	13-19 yrs	20-49 yrs
1%	0	0.1	0	0.1
5%	0.1	0.6	0.3	0.4
10%	0.4	1.5	0.5	0.7
25%	2.6	2.3	1.1	1.3
50%	5.5	4.2	1.8	2.2
75%	10.1	7.2	3	3.3
90%	14.5	10.6	4.3	4.9
95%	18.1	13.4	5.5	5.9
99%	22.7	21.4	8.9	8.6
100%	36.1	30.3	20	18.3

Source: EPA 2011b, Table 9-4

In order to demonstrate that the vegetable consumption rate data from the EFH was entered into and used correctly by Crystal Ball, Figure 3-8 shows the distributions of the four age-dependent vegetable consumption rates calculated by the Crystal Ball Monte Carlo simulation for this

analysis and compares them to the Table 3-9 EFH distributions. As shown, there is very good agreement between the EFH distributions and the distributions used in this analysis.

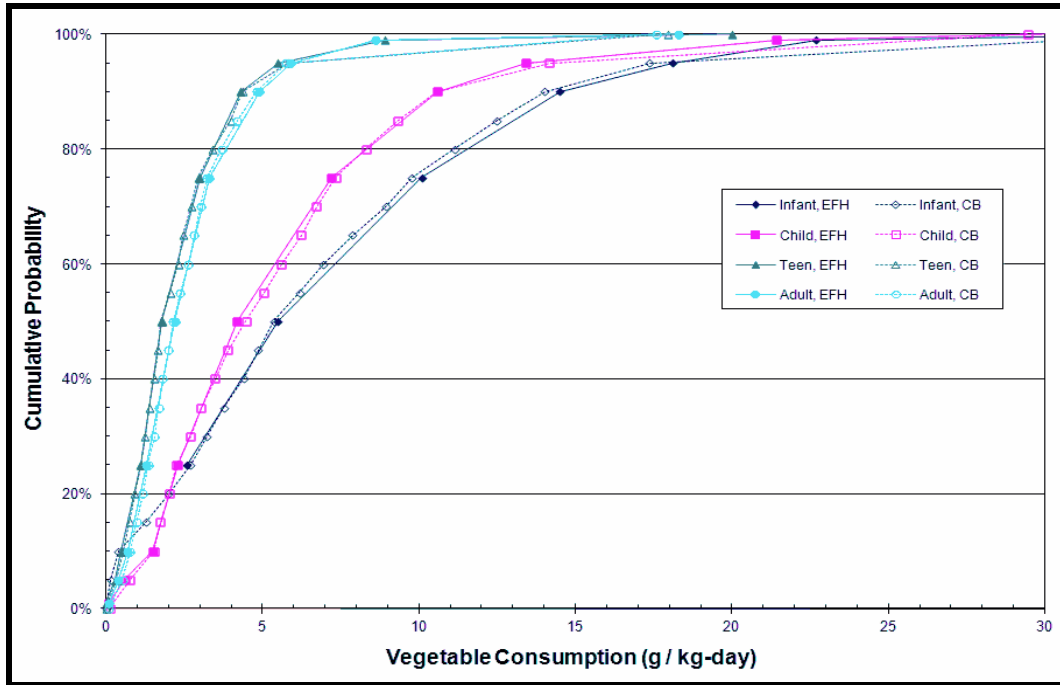


Figure 3-8: Distribution of Age-Dependent Weight Normalized Vegetable Consumption Rates

As stated above, the Table 3-6 body weight distributions and the Table 3-9 vegetable consumption distributions were used together to calculate the vegetable consumption rates ($Ing^{veg,A}$) used in this analysis.

3.2.6 Ingestion of Milk

As shown in Section 3.1.4, in order to calculate the $PDCF_{Mk,A}$ and $PRCF_{Mk,A}$, it is necessary to know:

- The element-specific cow's intake to milk transfer coefficient (CF_{Mk})
- The consumption rate of water by the cow ($Ing_{Mk,W}$)
- The consumption rate of fodder by the cow ($Ing_{Mk,Fod}$)
- The fraction of deposited activity retained on fodder (r_f)
- The length of the fodder growing season (t_f)
- The fodder productivity or yield (Y_f)
- The element-specific fodder uptake factor from soil (B_f)
- The net effect of all resuspension processes on fodder (B'_f)
- The ingestion rate of soil by the cow ($Ing_{Mk,Soil}$)
- The age-dependent milk ingestion rates ($Ing_{Mk,A}$)

The following terms used to calculate the dose and risk due to milk ingestion have already been defined in Section 3.2.4:

- The irrigation rate (Irr)
- The removal rate from soil (λ_w)
- The duration period for irrigation (t_b)
- The effective “surface density” for soil (P)
- The removal rate constant for physical removal by weathering (λ_w)

The element-specific cow’s intake-to-milk transfer coefficient (CF_{Mk}) and the element-specific fodder uptake factor from soil (B_f) are shown in Table 3-8, and were taken from NCRP 1999, Appendix D.

As discussed in Section 3.2.5, NCRP Report No. 129 (NCRP 1999) includes a term to account for the net effect of all resuspension processes on the radionuclide concentration of fodder (B'_f). For this analysis, a lognormal distribution with a mean of 0.05 and a standard deviation of 1.4 was assumed for the (B'_f), as recommended by NCRP 1999, Table 5.7, for fodder grown in a heavily vegetated rural area.

The consumption rates of water ($Ing_{Mk,W}$) and fodder ($Ing_{Mk,Fod}$) by cows were based on information provided by the National Academy of Sciences’ National Research Council (NAS 2001) and New Mexico State University (Looper and Waldner 2002). Fodder consumption rates are a function of the weight of the animal and how much milk the cow produces. Looper and Waldner (2002) present dry matter intakes for a typical sized dairy cow for various milk production rates, which range from 42 to 60 lbs/day. Thus, for this analysis, the consumption rate of fodder by dairy cows ($Ing_{Mk,Fod}$) was specified as a uniform distribution, with minimum and maximum values of 19.1 and 27.2 kg/day, respectively.

NAS 2001 also indicates that cattle water consumption rates are dependent on the dry matter (i.e., fodder) intake, temperature, milk production, and the amount of dietary sodium. Looper and Waldner (2002) indicate a range of dairy cow water consumption rates between 18.4 and 35.6 gallons/day. Thus, for this analysis, the consumption rate of water by cattle ($Ing_{Mk,W}$) was specified as a uniform distribution, with minimum and maximum values of 69.7 and 134.8 L/day.

The ingestion rate of soil by the cow ($Ing_{Mk,Soil}$) was based on NCRP 1999, Section 5.2.3, which states, “estimates in the literature indicate that on average an animal on pasture all year long will ingest an amount of soil equivalent to about six percent of its total dry matter intake.”

The fraction of deposited activity retained on fodder (r_f) was assumed to have a triangular distribution, with minimum, maximum, and most likely values of 0.06, 0.95, and 0.67, respectively, as recommended in NUREG/CR-6697, Attachment C, Section 6.7.

The length of the fodder growing season (t_f) was assumed to be 30 days, as recommended in Section 10 of the *CAP88 Users Manual* (Trinity 2007).

The fodder productivity or yield (Y_f) was obtained from the U.S. Department of Agriculture's 2007 Census of Agriculture (USDA 2009). In the census, the USDA presents area and quantity harvested in each of the 50 states for 6 types of animal feed: forage (36.0%), hay (32.0%), alfalfa-hay (15.5%), other-tame-hay (12.5%), wild-hay (2.1%), and small-grain-hay (1.8%). From these data, it was possible to calculate the yields and to construct a cumulative distribution of the yield, as shown in Figure 3-9. This is the fodder yield (Y_f) distribution that was used for this analysis. For comparison, *CAP88 Users Manual* (Trinity 2007, Section 10) and Regulatory Guide 1.109 (NRC 1977, Table E-7) recommend an agricultural productivity by unit area for the grass-cow-milk-man pathway of 0.28 and 0.7 kg/m², respectively. These are equivalent to the 1.6 and 76.4 percentiles in Figure 3-9.

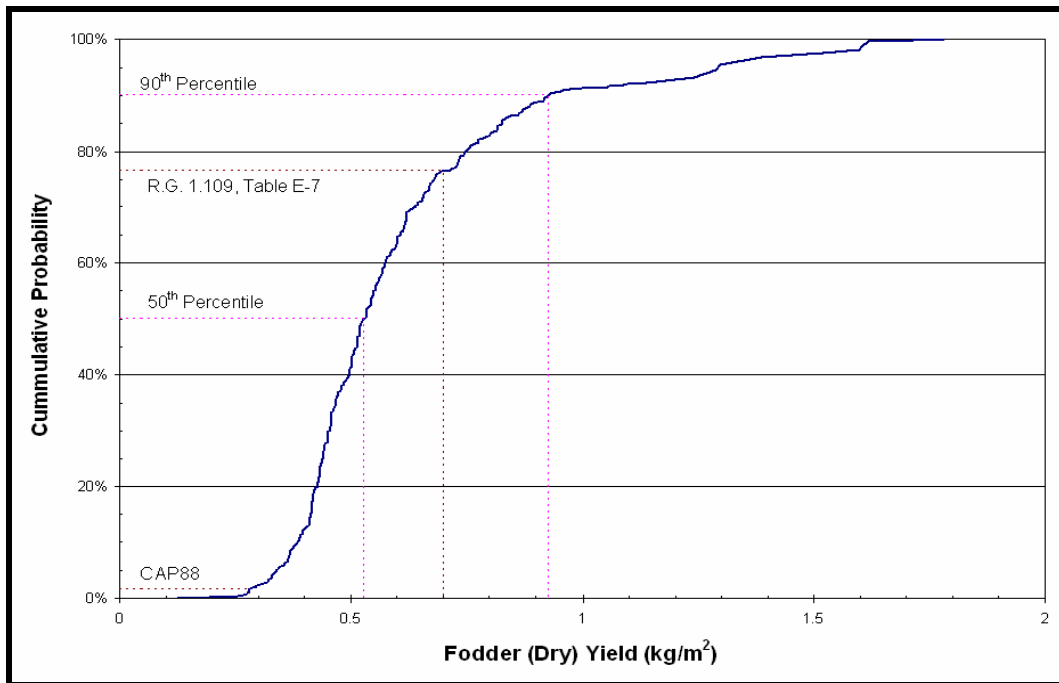


Figure 3-9: Distribution of Fodder (Dry) Yield

The age-dependent milk consumption rates ($Ing_{Mk,A}$) were obtained by multiplying the weight normalized milk consumption rates from EFH, Table 11-3 (EPA 2011b), and shown in Table 3-10, by the age-specific body weight, as shown in Table 3-6.

Table 3-10: Age-Dependent Weight Normalized Milk Consumption Rates

Percentile	Consumption Rate (g/kg-day)			
	Infant	Child	Teen	Adult
	<1 yr	3-5 yrs	13-19 yrs	20-49 yrs
1%	0	0.9	0.1	0
5%	0	4.5	0.4	0.2
10%	0	8.3	0.6	0.4
25%	1.2	13.6	1.6	1
50%	6.4	20.7	4	2.4
75%	11.5	32	7.6	4.7
90%	19.6	41.9	12.3	8.1
95%	43.2	51.1	16.4	10.3
99%	83.1	68.2	24.9	17.1
100%	163.9	154.5	45.0	52.7

Source: EPA 2011b, Table 11-3

In order to demonstrate that the milk consumption rate data from the EFH was entered into and used correctly by Crystal Ball, Figure 3-10 shows the distributions of the four age-dependent milk consumption rates calculated by the Crystal Ball Monte Carlo simulation for this analysis and compares them to the Table 3-10 EFH distributions. As shown, there is very good agreement between the EFH distributions and the distributions used here.

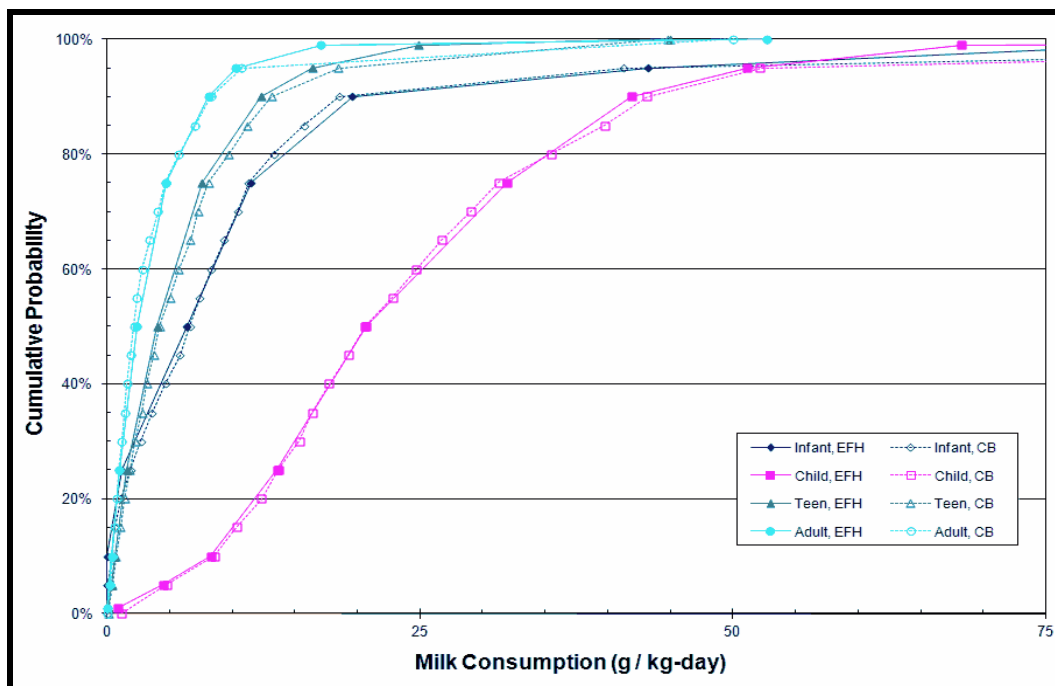


Figure 3-10: Distribution of Age-Dependent Weight Normalized Milk Consumption Rates

As stated above, the Table 3-10 and Figure 3-10 milk consumption rates are presented as a function of the body weight of the individual consuming the milk. Therefore, Table 3-6 presents the age-dependent body weight distributions that were obtained from the EFH (EPA 2011b), Table 8-3. The Table 3-6 body weight distributions and the Table 3-10 milk consumption distributions were used together to calculate the milk consumption rates used in this analysis.

3.2.7 Ingestion of Meat

As shown in Section 3.1.5, in order to calculate the $PDCF_{Mt,A}$ and $PRCF_{Mt,A}$, it is necessary to know:

- The cattle intake-to-meat transfer coefficient (CF_{Mt})
- The consumption rate of water by cattle ($Ing_{Mt,W}$)
- The consumption rate of fodder by cattle ($Ing_{Mt,Fod}$)
- The ingestion rate of soil by cattle ($Ing_{Mt,Soil}$)
- Age-dependent meat ingestion rates ($Ing_{Mt,A}$)

The following terms used to calculate the dose and risk due to meat ingestion have already been defined in Section 3.2.6:

- The fraction of deposited activity retained on fodder (r_f)
- The length of the fodder growing season (t_f)
- The fodder productivity or yield (Y_f)
- The element-specific fodder uptake factor from soil (B_f)
- The net effect of all resuspension processes on fodder (B'_f)

The following terms used to calculate the dose and risk due to meat ingestion have already been defined in Section 3.2.4:

- The irrigation rate (Irr)
- The removal rate from soil (λ_w)
- The duration period for irrigation (t_b)
- The effective “surface density” for soil (P)
- The removal rate constant for physical removal by weathering (λ_w)

The element-specific cattle intake-to-meat transfer coefficient (CF_{Mt}) is shown in Table 3-8, and was taken from NCRP 1999, Appendix D.

The consumption rates of water ($Ing_{Mt,W}$) and fodder ($Ing_{Mt,Fod}$) by cattle were based on information provided by the National Research Council (NAS 2000) and the Oklahoma State University (Lalman 2004). Fodder consumption rates are a function of the weight of the animal, the nutrition content of the feed, and how much the animal is growing. Table 5 of Lalman (2004) presents dry matter intakes for various sized animals and various growth rates, which range from 13.7 to 27.4 lbs/day. Thus, for this analysis, the consumption rate of fodder by cattle ($Ing_{Mt,Fod}$)

was specified as a uniform distribution, with minimum and maximum values of 6.2 and 12.4 kg/day, respectively.

NAS 2000 indicates that cattle water consumption rates are dependent on the dry matter (i.e., fodder) intake, temperature, precipitation, and the amount of dietary salt. Table 6-1 of NAS 2000 indicates a range of “finishing” cattle water consumption rates between 22.7 and 78.0 L/day. Thus, for this analysis, the consumption rate of water by cattle ($Ing_{Mt,W}$) was specified as a uniform distribution, with minimum and maximum values of 22.7 and 78.0 L/day.

The ingestion rate of soil by cattle ($Ing_{Mt,Soil}$) was based on NCRP 1999, Section 5.2.3, which states, “estimates in the literature indicate that on average an animal on pasture all year long will ingest an amount of soil equivalent to about six percent of its total dry matter intake.”

The age-dependent meat consumption rates ($Ing_{Mt,A}$) were obtained by multiplying the weight normalized meat consumption rates from EFH, Table 11-3 (EPA 2011b), and shown in Table 3-11, by the age-specific body weight, as shown in Table 3-6.

Table 3-11: Age-Dependent Weight Normalized Meat Consumption Rates

Percentile	Consumption Rate (g/kg-day)			
	Infant	Child	Teen	Adult
	<1 yr	3–5 yrs	13–19 yrs	20–49 yrs
1%	0	0	0	0
5%	0	0.7	0.3	0.3
10%	0	1.4	0.6	0.5
25%	0	2.1	1	1
50%	0	3.3	1.7	1.6
75%	1.7	5	2.7	2.4
90%	3.6	7.6	3.8	3.4
95%	5.4	8.5	4.7	4.1
99%	9.3	12.4	6.8	5.7
100%	18.7	19.5	13.5	12

Source: EPA 2011b, Table 11-3

In order to demonstrate that the meat consumption rate data from the EFH was entered into and used correctly by Crystal Ball, Figure 3-11 shows the distributions of the four age-dependent meat consumption rates calculated by the Crystal Ball Monte Carlo simulation for this analysis and compares them to the Table 3-11 EFH distributions. As shown, there is very good agreement between the EFH distributions and the distributions used in this analysis.

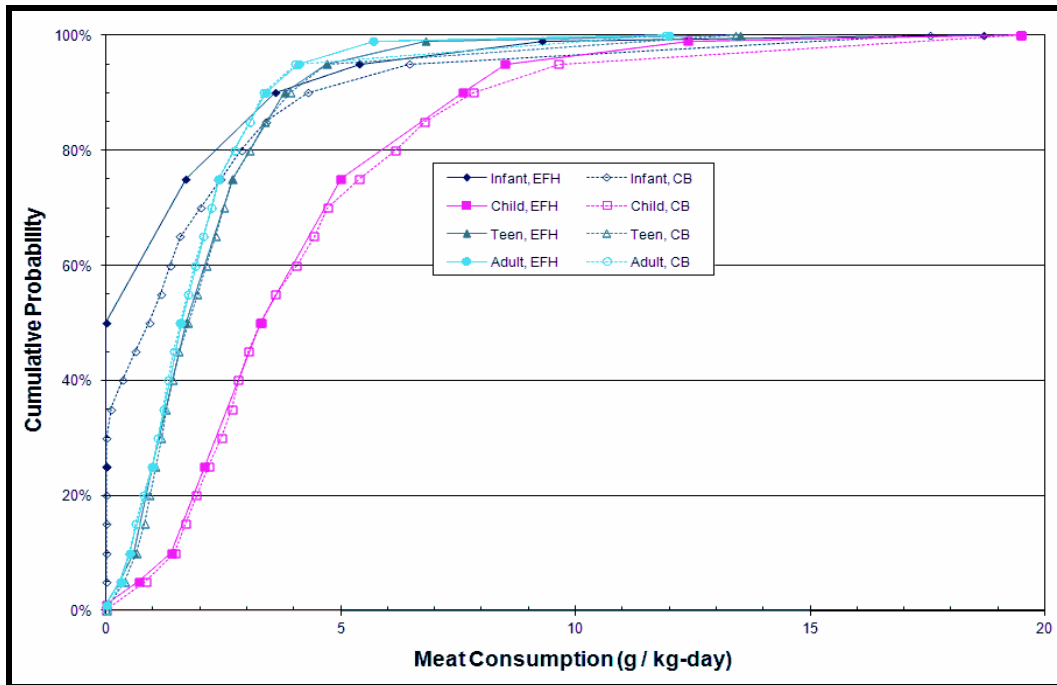


Figure 3-11: Distribution of Age-Dependent Weight Normalized Meat Consumption Rates

As stated above, the Table 3-11 and Figure 3-11 meat consumption rates are presented as a function of the body weight of the individual consuming the meat. Therefore, Table 3-6 presents the age-dependent body weight distributions that were obtained from the EFH (EPA 2011b), Table 8-3. The Table 3-6 body weight distributions and the Table 3-11 meat consumption distributions were used together to calculate the meat consumption rates used in this analysis.

3.3 Pathway Dose and Risk Conversion Factors

As described in Section 3.1.7, the Excel add-in Crystal Ball was used to solve for the PDCFs and PRCFs using Monte Carlo simulations. To solve for the PDCFs and PRCFs, the Monte Carlo simulations were performed 1,000 times, and the resultant mean, median, and 90th percentile PDCFs were calculated as shown in Table 3-12. The resultant PRCFs are shown in Table 3-13.

Table 3-12: Calculated Total Pathway Dose Conversion Factors

	Adult	Teen	Child	Infant
Nuclide	Mean PDCF (mrem/yr / pCi/m³)			
Pb-210+P	6.28E-03	7.33E-03	1.10E-02	3.89E-02
Ra-226+P	1.30E-02	1.98E-02	2.62E-02	7.06E-02
Th-230	6.02E-04	3.62E-04	2.89E-04	4.27E-03
U-234	1.61E-04	1.53E-04	1.33E-04	4.19E-04
U-238+P	1.55E-04	1.47E-04	1.40E-04	4.24E-04

Table 3-12: Calculated Total Pathway Dose Conversion Factors

	Adult	Teen	Child	Infant
Nuclide	Median PDCF (mrem/yr / pCi/m³)			
Pb-210+P	5.16E-03	5.17E-03	6.91E-03	3.77E-02
Ra-226+P	1.01E-02	1.39E-02	1.65E-02	5.76E-02
Th-230	5.30E-04	2.76E-04	2.54E-04	4.37E-03
U-234	1.40E-04	1.15E-04	1.01E-04	4.11E-04
U-238+P	1.35E-04	1.10E-04	1.06E-04	4.16E-04
Nuclide	90th Percentile PDCF (mrem/yr / pCi/m³)			
Pb-210+P	1.06E-02	1.31E-02	1.40E-02	6.31E-02
Ra-226+P	2.23E-02	3.55E-02	4.28E-02	1.14E-01
Th-230	1.09E-03	7.43E-04	5.09E-04	7.28E-03
U-234	2.77E-04	2.75E-04	1.93E-04	6.97E-04
U-238+P	2.68E-04	2.64E-04	2.02E-04	7.06E-04

Table 3-13: Calculated Total Pathway Risk Conversion Factors

	Adult	Teen	Child	Infant
Nuclide	Mean PRCF (LCF/yr / pCi/m³)			
Pb-210+P	1.12E-09	1.62E-09	2.90E-09	4.33E-09
Ra-226+P	2.25E-09	3.83E-09	7.25E-09	7.60E-09
Th-230	3.07E-11	4.52E-11	4.69E-11	1.31E-10
U-234	2.21E-11	4.22E-11	6.92E-11	1.13E-10
U-238+P	2.28E-11	4.91E-11	9.00E-11	1.54E-10
Nuclide	Median PRCF (LCF/yr / pCi/m³)			
Pb-210+P	9.24E-10	1.14E-09	1.82E-09	4.20E-09
Ra-226+P	1.73E-09	2.69E-09	4.56E-09	6.23E-09
Th-230	2.69E-11	3.44E-11	4.13E-11	1.34E-10
U-234	1.91E-11	3.16E-11	5.23E-11	1.11E-10
U-238+P	1.98E-11	3.67E-11	6.80E-11	1.51E-10
Nuclide	90th Percentile PRCF (LCF/yr / pCi/m³)			
Pb-210+P	1.89E-09	2.88E-09	3.69E-09	7.00E-09
Ra-226+P	3.86E-09	6.88E-09	1.19E-08	1.23E-08
Th-230	5.60E-11	9.27E-11	8.27E-11	2.22E-10
U-234	3.79E-11	7.58E-11	1.00E-10	1.89E-10
U-238+P	3.92E-11	8.80E-11	1.30E-10	2.56E-10

LCF = latent cancer fatality

Comparing Table 3-12 to Table 3-13 shows that the dose-to-risk relationship varies by a little over an order of magnitude, from about 3×10^{-8} to 6×10^{-7} latent cancer fatality per millirem, depending on the radionuclide and the age group. This is consistent with the dose-to-risk relationship for the FGR 13 dose and risk coefficients shown in Table 3-2. Furthermore, the Interagency Steering Committee on Radiation Standards (ISCORS 2002) recommends a nominal

cancer mortality dose-to-risk factor of 6×10^{-7} per millirem, which is at the high end of the range, based on the Table 3-12 PDCFs and the Table 3-13 PRCFs. However, ISCORS 2002 points out that the nominal conversion factor varies from radionuclide to radionuclide and may overestimate the risk by about an order of magnitude for some of bone-seeking radionuclides. Since radium and uranium are bone-seekers, the Table 3-12 PDCFs and Table 3-13 PRCFs are consistent with the findings in ISCORS 2002.

“Typical” contributions to the adult, teen, child, and infant total PDCFs and PRCFs from each exposure pathway are presented in Table 3-14, Table 3-16, Table 3-17, and Table 3-18, respectively. The contributions shown on these tables were calculated deterministically using the mean or 50th percentile parameter values, so for any 1 of the 1,000 Monte Carlo trials, any 1 of the pathways would be expected to contribute more or less to the dose/risk than is shown. Nonetheless, the following tables provide a good indication as to which pathways are the major contributors and which are only minor contributors.

Table 3-14: Typical Pathway Contributions to the Adult PDCF and PRCF

Pathway – Adult		Pb-210	Ra-226+P	Th-230	U-234	U-238
Ingestion of Drinking Water		78.3%	51.2%	82.8%	76.2%	76.2%
Inadvertent Ingestion of Soil		0.1%	0.2%	0.3%	0.3%	0.3%
Ingestion of Vegetables	Leaf Deposition	13.5%	8.8%	14.3%	13.1%	13.1%
	Root Uptake	2.3%	26.5%	2.1%	2.9%	2.9%
Ingestion of Meat	Cattle Drinking	0.3%	0.2%	0.0%	0.3%	0.3%
	Leaf Deposition	1.6%	1.3%	0.2%	1.5%	1.5%
	Root Uptake	0.3%	1.1%	0.0%	0.3%	0.3%
	Soil Ingestion	0.1%	0.3%	0.0%	0.3%	0.3%
Ingestion of Milk	Cow Drinking	0.3%	0.7%	0.0%	0.4%	0.4%
	Leaf Deposition	2.2%	4.8%	0.0%	2.8%	2.8%
	Root Uptake	0.5%	4.1%	0.0%	0.6%	0.6%
	Soil Ingestion	0.5%	1.0%	0.2%	1.2%	1.2%

For the adult PDCFs and PRCFs, Table 3-14 indicates that the drinking water pathway is the major contributor for all radionuclides. Ingestion of vegetables is the second most important contributor for all of the radionuclides. For Ra-226, the root uptake portion of the vegetable ingestion pathway is significant, due to radium’s high concentration soil uptake factor for vegetables (B_v), as indicated in Table 3-8. For the other radionuclides, the leaf deposition portion of the ingestion pathways is always the higher contributor. For all radionuclides, the milk and meat pathways are only minor contributors to the adult total PDCFs and PRCFs. Finally, the inadvertent ingestion of soil is a very minor contributor to the adult total PDCFs and PRCFs for all radionuclides.

The percentage contributions shown in Table 3-14 are only typical, and will vary for each of the 1000 realizations that was calculated. Table 3-15 shows how this variation in each pathway’s contribution to the total adult U-238 PDCF and PRCF. For each pathway, Table 3-15 shows the typical contribution to the total PDCF/PRCF from Table 3-14, as well as the contributions at the

10th, 50th, and 90th percentiles of the PDCF/PRCF, and the range of the contribution over all 1000 realizations.

Table 3-15: U-238+P Pathway Contributions to the Adult PDCF and PRCF

Pathway – Adult		Typical (Table 3-14)	Percentile			Range	
			10 th	50 th	90 th	Minimum	Maximum
Ingestion of Drinking Water		76.2%	86.0%	95.0%	60.0%	0.3%	99.1%
Inadvertent Ingestion of Soil		0.3%	0.5%	0.2%	0.4%	0.0%	5.5%
Ingestion of Vegetables	Leaf Deposition	13.1%	5.3%	1.3%	10.8%	0.1%	79.2%
	Root Uptake	2.9%	0.4%	2.1%	5.7%	0.0%	68.9%
Ingestion of Meat	Cattle Drinking	0.3%	0.1%	0.1%	0.4%	0.0%	8.8%
	Leaf Deposition	1.5%	0.4%	0.3%	0.8%	0.0%	52.8%
	Root Uptake	0.3%	0.2%	0.1%	1.8%	0.0%	14.9%
	Soil Ingestion	0.3%	0.2%	0.1%	1.4%	0.0%	7.1%
Ingestion of Milk	Cow Drinking	0.4%	0.6%	0.0%	1.6%	0.0%	10.3%
	Leaf Deposition	2.8%	3.7%	0.2%	2.2%	0.0%	67.1%
	Root Uptake	0.6%	1.9%	0.1%	5.0%	0.0%	23.8%
	Soil Ingestion	1.2%	0.6%	0.4%	9.9%	0.0%	49.6%

The range values shown in Table 3-15 may be misleading, since they may represent a single Monte Carlo realization. Alternatively, Figure 3-12 shows the cumulative distribution of each exposure pathway's contribution to the total adult U-238 PDCF/PRCF. For example, Figure 3-12 shows that for 50% of the realizations the drinking water exposure pathway contributes less than 77% and for 50% of the realizations it contributes more than 77% to the total PDCF/PRCF. Similarly, Figure 3-12 shows that for 80% of the realizations the leaf deposition component of the vegetable ingestion pathway contributes 21% or less to the total PDCF/PRCF. Finally, Figure 3-12 shows that for only 19% of the realizations did the drinking water pathway contribute less than 50% to the total PDCF/PRCF.

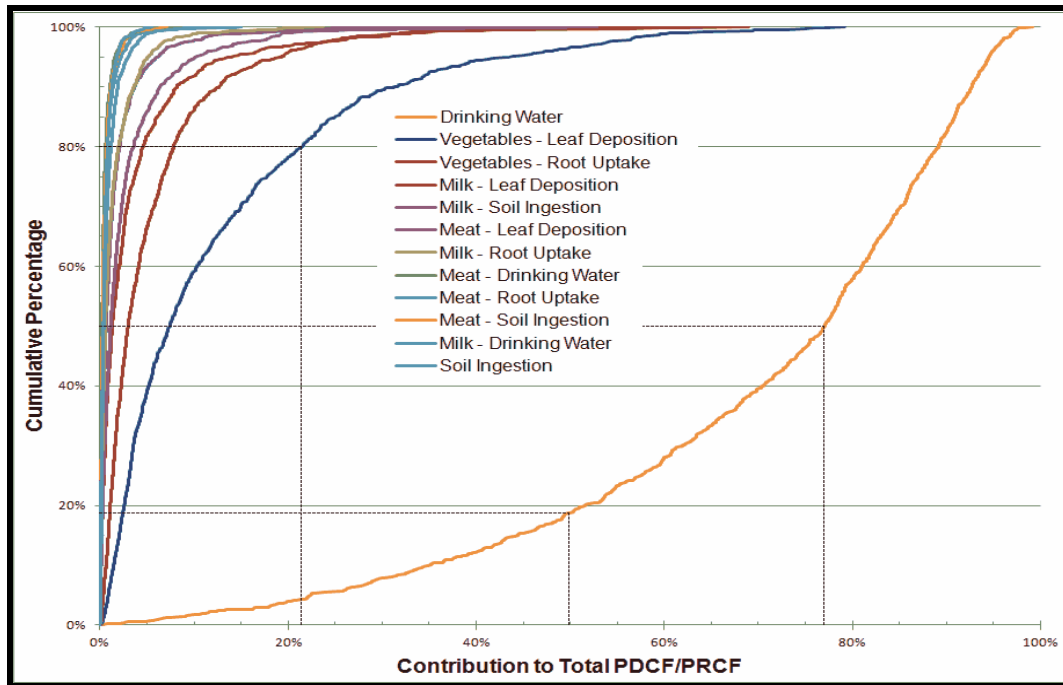


Figure 3-12: Cumulative Distributions of Pathway Contribution to the Total Adult U-238+P PCDF/PRCF

Although Table 3-15 and Figure 3-12 are specific for the U-238+P adult PCDF/PRCF it is reasonable to assume that the pathway contributions for the other radionuclides and age groups will behave similarly.

Table 3-16: Typical Pathway Contributions to the Teen PCDF and PRCF

Pathway – Teen		Pb-210	Ra-226+P	Th-230	U-234	U-238
Ingestion of Drinking Water		71.5%	41.4%	79.6%	68.1%	68.1%
Inadvertent Ingestion of Soil		0.3%	0.3%	0.6%	0.5%	0.5%
Ingestion of Vegetables	Leaf Deposition	14.7%	8.5%	16.4%	14.0%	14.0%
	Root Uptake	2.5%	25.6%	2.4%	3.1%	3.1%
Ingestion of Meat	Cattle Drinking	0.4%	0.3%	0.1%	0.4%	0.4%
	Leaf Deposition	2.2%	1.6%	0.3%	2.1%	2.1%
	Root Uptake	0.5%	1.4%	0.1%	0.4%	0.4%
	Soil Ingestion	0.2%	0.3%	0.1%	0.4%	0.4%
Ingestion of Milk	Cow Drinking	0.7%	1.3%	0.0%	0.9%	0.9%
	Leaf Deposition	4.9%	9.4%	0.1%	6.2%	6.2%
	Root Uptake	1.1%	8.0%	0.0%	1.3%	1.3%
	Soil Ingestion	1.2%	1.9%	0.4%	2.6%	2.6%

The pathway contributions to the teen total PCDFs and PRCFs are similar to the adult pathway contributions. Specifically, drinking water is the major contributor for all radionuclides. Ingestion of vegetables is the second most important contributor for all radionuclides, and

inadvertent ingestion of soil is a very minor contributor for all pathways, as are the cattle/cow drinking water and soil ingestion for the meat and milk pathways.

The milk pathway (and to a lesser extent, the meat pathway) starts to become more of a contributor to the teen PDCF/PRCFs than it was for the adult. For example, for Ra-226, the milk pathway contributes about 20% to the teen total PDCF/PRCF, but only about 11% to the adult total PDCF/PRCF. Similar relative increases are observed for the other radionuclides.

Table 3-17: Typical Pathway Contributions to the Child PDCF and PRCF

Pathway – Child		Pb-210	Ra-226+P	Th-230	U-234	U-238
Ingestion of Drinking Water		59.9%	28.1%	74.1%	54.2%	54.2%
Inadvertent Ingestion of Soil		0.7%	0.7%	1.9%	1.4%	1.4%
Ingestion of Vegetables	Leaf Deposition	15.6%	7.3%	19.3%	14.1%	14.1%
	Root Uptake	2.6%	22.0%	2.9%	3.1%	3.1%
Ingestion of Meat	Cattle Drinking	0.3%	0.2%	0.1%	0.3%	0.3%
	Leaf Deposition	2.0%	1.1%	0.3%	1.8%	1.8%
	Root Uptake	0.4%	1.0%	0.1%	0.4%	0.4%
	Soil Ingestion	0.2%	0.2%	0.1%	0.4%	0.4%
Ingestion of Milk	Cow Drinking	1.6%	2.5%	0.0%	1.9%	1.9%
	Leaf Deposition	11.4%	17.9%	0.2%	13.8%	13.8%
	Root Uptake	2.5%	15.3%	0.0%	2.9%	2.9%
	Soil Ingestion	2.9%	3.7%	1.0%	5.7%	5.7%

The contributions to the child total PDCFs and PRCFs from the milk pathway illustrate the growing importance of this pathway. For Ra-226, it is the dominant pathway, exceeding both ingestion of drinking water and vegetables. For the other radionuclides (except Th-230), the drinking water pathway remains the most significant pathway, but the milk pathway is next in importance. For Th-230, the milk pathway continues to be a minor contributor to the child total PDCF/PRCF due to its very low milk uptake (CF_{milk}) and pasture uptake (B_p) factors, as shown in Table 3-8.

Table 3-18: Typical Pathway Contributions to the Infant PDCF and PRCF

Pathway – Infant		Pb-210	Ra-226+P	Th-230	U-234	U-238
Ingestion of Drinking Water		88.6%	58.9%	87.6%	81.2%	81.2%
Inadvertent Ingestion of Soil		0.4%	1.2%	1.8%	1.6%	1.6%
Ingestion of Vegetables	Leaf Deposition	7.6%	6.1%	9.0%	8.4%	8.4%
	Root Uptake	1.3%	18.2%	1.3%	1.9%	1.9%
Ingestion of Meat	Cattle Drinking	0.0%	0.0%	0.0%	0.0%	0.0%
	Leaf Deposition	0.0%	0.0%	0.0%	0.0%	0.0%
	Root Uptake	0.0%	0.0%	0.0%	0.0%	0.0%
	Soil Ingestion	0.0%	0.0%	0.0%	0.0%	0.0%

Table 3-18: Typical Pathway Contributions to the Infant PDCF and PRCF

Pathway – Infant		Pb-210	Ra-226+P	Th-230	U-234	U-238
Ingestion of Milk	Cow Drinking	0.2%	1.0%	0.0%	0.5%	0.5%
	Leaf Deposition	1.3%	7.1%	0.1%	3.9%	3.9%
	Root Uptake	0.3%	6.1%	0.0%	0.8%	0.8%
	Soil Ingestion	0.3%	1.5%	0.2%	1.6%	1.6%

For the infant total PDCF and PRCF, Table 3-18 indicates that the ingestion of drinking water is the major contributor for all five radionuclides; the ingestion of vegetables is the second most important contributor after drinking water. The inadvertent soil ingestion and meat pathways continue to be minor contributors to total PDCF and PRCF.

3.4 Native American Exposures

For the five ingestion pathways, the equations described in Section 3.1 for the PDCF and PRCF calculations also apply to the Native American; the only difference is the parameter values for the various individual consumption rates (i.e., $Ing_{Wat,A}$, $Ing_{Soil,A}$, $Ing_{Veg,A}$, $Ing_{Mk,A}$, and $Ing_{Mt,A}$). A detailed literature search was unable to locate usage rates that were specific to Native Americans living in Texas, Colorado, and/or Wyoming (the locations most likely to support ISL facilities). Thus, the analysis used the Native American usage rates, which were obtained from a number of sources focusing on tribes in the Pacific Northwest, including DOE 1997, WSDOH 2003, Harris and Harper 2004, Rittmann 2004, PNNL 2006, Harper et al. 2007, and Harper and Ranco 2009.

3.4.1 Ingestion of Drinking Water

According to Harper and Ranco (2009, Section 8.3.1), the Native American drinking water consumption rate depends on where the individual lives within the United States. For those Native Americans that live in cool and wet climates (e.g., in Maine), the conventional water consumption rate of 2 L/day (EPA 1991) should be used. For Native Americans living in areas with a hot, arid climate (e.g., the Columbia basin), a higher water consumption rate of 3 L/day was recommended. For this analysis, the higher water consumption rate of 3 L/day was used. Figure 3-13 compares this Native American water consumption rate to the water consumption distribution given in Table 3-5 and distribution from the EFH, Table 3-11 (EPA 2011b).

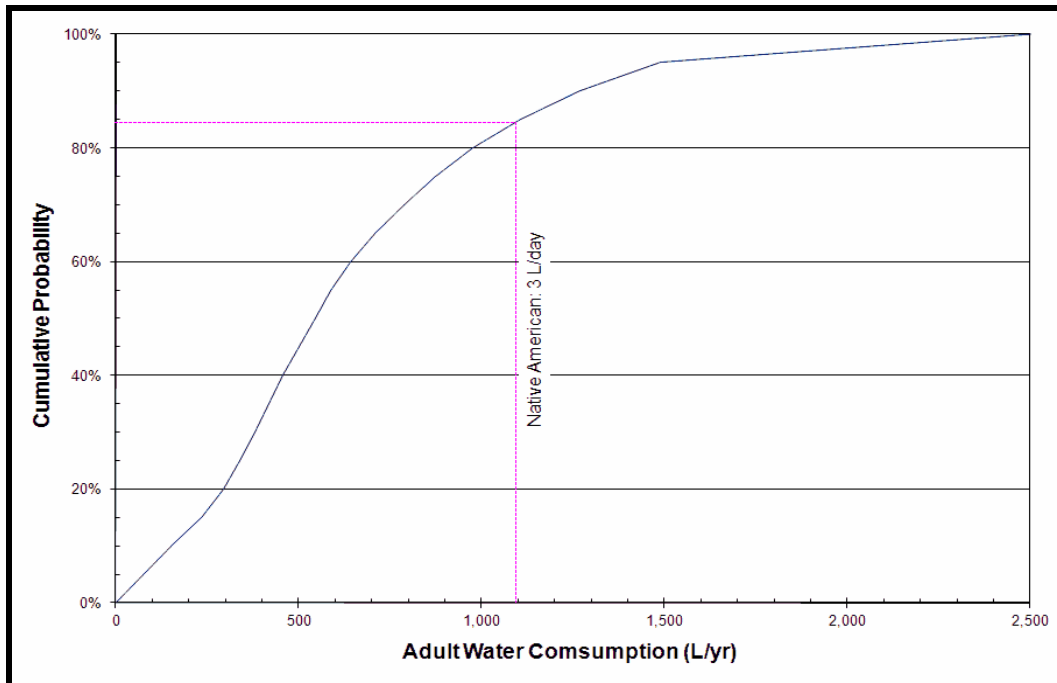


Figure 3-13: Native American Drinking Water Rate Within the Exposure Factors Handbook Distribution

As Figure 3-13 demonstrates, the annual Native American drinking water consumption assumed for this analysis is at about the 85th percentile of the EFH distribution.

3.4.2 Ingestion of Vegetables

DOE (1997, Table 5.7) gives the Native American subsistence resident consumption rate of fruits and vegetables as 660 grams per day, with a range of 200 to 800. Rittmann (2004, Table A4) indicates that the breakdown of the 660 g/day is 6.6% leafy vegetables, 30.2% grains, 31.4% fruit, and 31.8% other vegetables. For this analysis, it was assumed that the entire intake of 660 g/day was of vegetables irrigated with contaminated well water. Figure 3-14 compares this Native American vegetable consumption rate to the vegetable consumption distribution used to calculate the PDCF and PRCF, which (as explained in Section 3.2.5) is a combination of the body weight distribution (Table 3-6) and vegetable consumption distributions (Table 3-9) from the EFH (EPA 2011b).

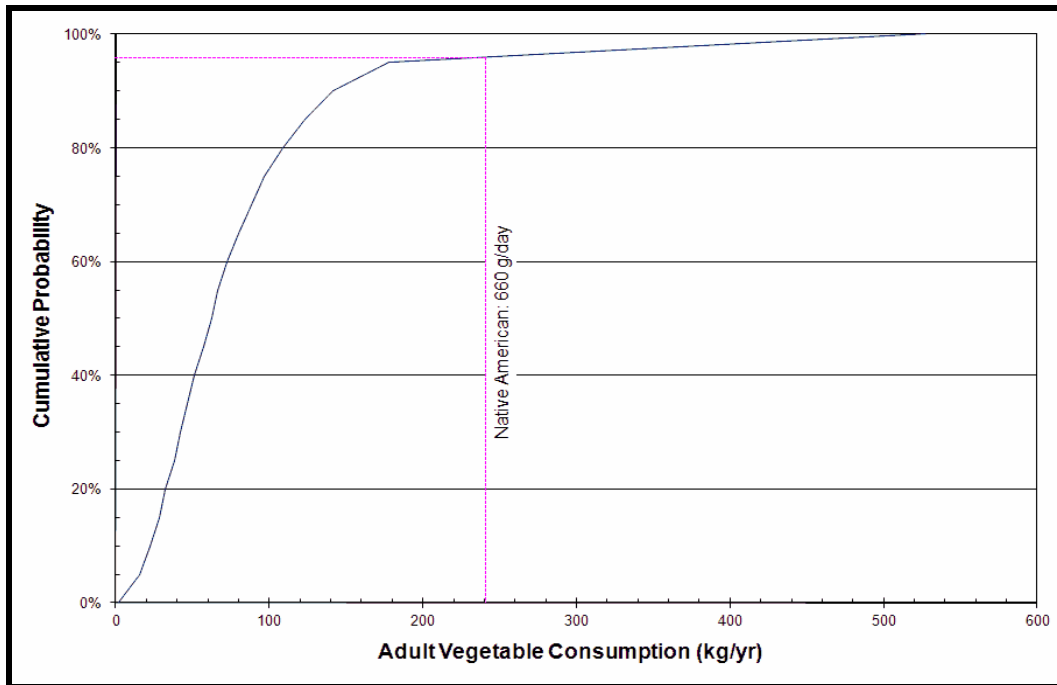


Figure 3-14: Native American Vegetable Consumption Within the *Exposure Factors Handbook* Distribution

As Figure 3-14 demonstrates, the annual Native American vegetable consumption assumed in this analysis is at about the 95th percentile of the EFH distribution.

Terry (2011) indicated that gardening and/or full-scale production of fruits and vegetables on the Navajo Reservation is virtually nonexistent. He also indicated that fruit and vegetable consumption (even from outside locales) is probably also lower among residents of the Navajo Reservation than for the U.S. population as a whole. Unfortunately, Terry (2011) did not provide any numerical estimates of the Navajo vegetable consumption that could be used in this analysis, other than to eliminate the pathway all together.

3.4.3 Ingestion of Meat

Rittmann (2004, Table A4) provides the Native American beef consumption rate as 34 kg/yr and another 70 kg/yr for game, broken down to 22 kg/y deer, 32 kg/y wild birds, and 16 kg/y wild bird eggs. These values are consistent with Table 5.7 of DOE (1997), which gives the following consumption rates: 150 g/day (55 kg/yr) animal protein, 18 g/day (7 kg/yr) upland birds, 70 g/day (26 kg/yr) waterfowl, and 45 g/day (16 kg/yr) wild bird eggs. The beef and deer consumption rates from Rittmann (2004) are equivalent to the animal protein rates from DOE (1997). Since game would not be expected to consume well water or fodder that was irrigated, the beef consumption rate of 34 kg/yr was used in this analysis. However, it is recognized that use of the meat consumption rate for northwestern Native Americans (such as those given in Rittmann 2004 and DOE 1997) may under estimate the meat consumption of southwestern Native Americans, due to the large amount of fish consumed by northwestern Native Americans.

Terry (2011) indicated that meat consumption by residents of the Navajo Reservation, particularly lamb, mutton, and their internal organs, is much higher than for the United States population as a whole. He noted that sheep on the Navajo Nation are not fed in feedlots or farmyards, but rely almost exclusively on grazing, and that ingestion of (contaminated) soil by grazing livestock is probably much higher than in other locales, owing to the semi-arid climate and overgrazing. Unfortunately, Terry (2011) did not provide any numerical estimates of the Navajo meat consumption that could be used in this analysis.

Although both Harper and Ranco (2009) and Harper et al. (2007) provide data on the Native American consumption of game, neither provides any data regarding the consumption of beef by Native Americans, so they were not used in this analysis.

Figure 3-15 compares this Native American beef consumption rate to the meat consumption distribution used to calculate the PDCFs and PRCFs, which (as explained in Section 3.2.7) is a combination of the body weight distributions and meat consumption distributions from the EFH (EPA 2011b).

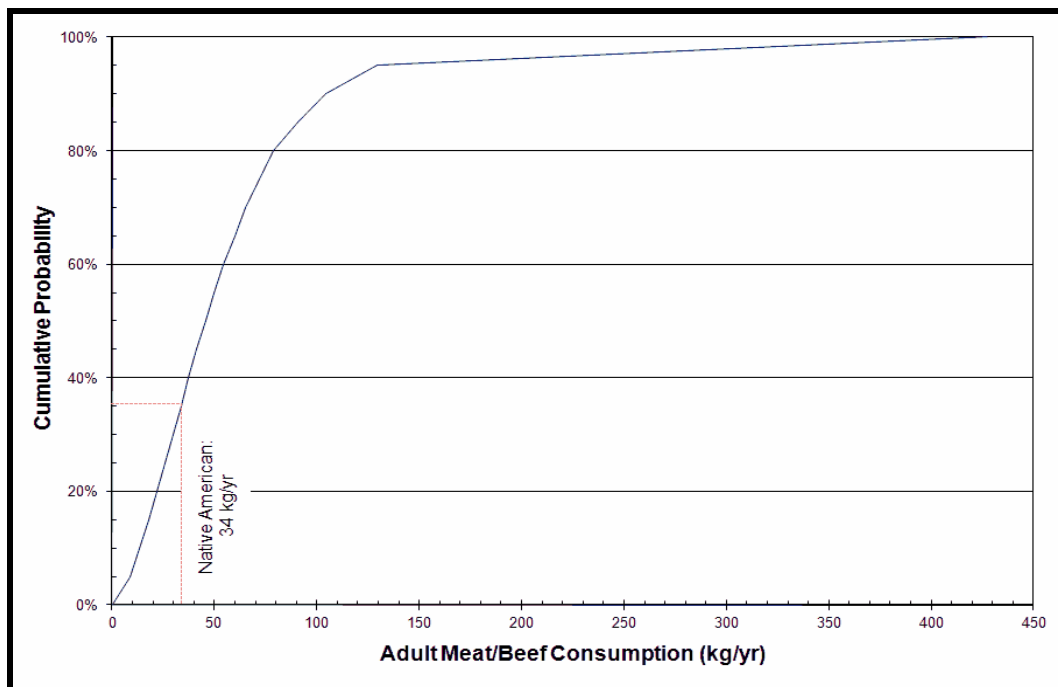


Figure 3-15: Native American Meat Consumption Within the Exposure Factors Handbook Distribution

Figure 3-15 shows that the Native American beef consumption rate is only at about the 35th percentile of the meat consumption distribution, based on EFH (EPA 2011b) data.

3.4.4 Exposure in Sweat Lodge

The Sweat Lodge Ceremony is a traditional Native American custom. Based on tribal descriptions, PNNL 2006 (page 3-56) stated that between 0.5 and 3 hours/day could be spent

sweat bathing, with the inside of the sweat lodge kept at 60°–80° Centigrade (145°–180° Fahrenheit). For sweat lodge exposure, three sub-pathways were evaluated; inhalation of airborne radionuclides, external exposure due to submersion in the airborne radionuclides, and drinking additional water to make up for water lost while in the sweat lodge. The annual individual effective dose ($E_{SL,NA}$, mrem/yr) and risk ($R_{SL,NA}$, LCF/yr) to a Native American from time spent in the sweat lodge is given by:

$$E_{SL,NA} = C_W \left[Ing_{Wat,NA,SL} DC_{Ing} + \frac{M_{SL}}{\delta DF_{SL}} (B_{NA} DC_{Inh} + DC_{Sub}) D_{SL} N_{SL} \right] \quad 3-13$$

$$R_{SL,NA} = C_W \left[Ing_{Wat,NA,SL} RC_{Ing,DW} + \frac{M_{SL}}{\delta DF_{SL}} (B_{NA} RC_{Inh} + RC_{Sub}) D_{SL} N_{SL} \right]$$

where C_W is the radionuclide concentration in the well from which the water is taken ($\text{pCi}/\text{m}^3_{\text{water}}$), $Ing_{Wat,NA,SL}$ is the water consumed to make up for water lost while inside the sweat lodge (m^3/sweat), DC_{Ing} is the dose coefficient for ingestion (mrem/pCi), M_{SL} is the moisture content of the air inside the sweat lodge ($\text{kg}/\text{m}^3_{\text{air}}$), δ is the density of water ($\text{kg}/\text{m}^3_{\text{water}}$), DF_{SL} is the evaporation decontamination factor (see below), B_{NA} is the Native American's breathing rate while inside the sweat lodge ($\text{m}^3_{\text{air}}/\text{sec}$), DC_{Inh} is the dose coefficient for inhalation (mrem/pCi), DC_{Sub} is the dose coefficient for submersion within a cloud (mrem/hr per pCi/m^3), D_{SL} is the sweat duration (hr/sweat), N_{SL} is the number of sweats (sweats/yr), $RC_{Ing,DW}$ is the risk coefficient for ingestion (LCF/pCi), RC_{Inh} is the risk coefficient for inhalation (LCF/pCi), and RC_{Sub} is the risk coefficient for submersion within a cloud (LCF/hr per pCi/m^3).

As with the ingestion dose and risk coefficients, the inhalation and submersion dose and risk coefficients were obtained from FGR 13. The inhalation dose and risk coefficients used in this analysis are shown in Table 3-19, while the submersion dose and risk coefficients are shown in Table 3-20.

Table 3-19: Radionuclide-Specific Inhalation Dose and Risk Coefficients

Nuclide	Mortality Coefficient (Bq^{-1})			
	Infant	Child	Teen	Adult
	0- 5	5- 15	15- 25	25- 70
Po-210	2.08E-06	1.13E-06	4.56E-07	2.20E-07
Bi-210	6.61E-08	3.56E-08	1.41E-08	6.83E-09
Pb-210	2.67E-06	1.23E-06	3.51E-07	2.64E-07
Bi-214	3.67E-09	2.37E-09	1.09E-09	4.85E-10
Pb-214	4.68E-09	3.00E-09	1.48E-09	6.12E-10
Ra-226	4.42E-06	2.17E-06	7.59E-07	4.53E-07
Ra-226+P	9.24E-06	4.57E-06	1.58E-06	9.45E-07
Th-230	4.36E-06	2.15E-06	1.03E-06	5.06E-07
U-234	4.37E-06	2.14E-06	7.49E-07	4.47E-07
Th-234	4.68E-09	2.26E-09	8.88E-10	3.76E-10
U-238	3.77E-06	1.82E-06	6.27E-07	3.81E-07

Table 3-19: Radionuclide-Specific Inhalation Dose and Risk Coefficients

Nuclide	Effective Dose Coefficient (Sv/Bq)			
	Infant	Child	Teen	Adult
	100 days	5 yrs	15 yrs	20 yrs
Po-210	1.78E-05	8.62E-06	5.12E-06	4.27E-06
Bi-210	5.60E-07	2.72E-07	1.59E-07	1.33E-07
Pb-210	1.83E-05	1.15E-05	5.83E-06	5.61E-06
Pb-210+P	3.67E-05	2.04E-05	1.11E-05	1.00E-05
Bi-214	9.24E-08	3.26E-08	1.84E-08	1.54E-08
Pb-214	6.92E-08	2.81E-08	1.53E-08	1.47E-08
Ra-226	3.35E-05	1.89E-05	1.04E-05	9.51E-06
Ra-226+P	7.03E-05	3.93E-05	2.15E-05	1.95E-05
Th-230	2.07E-04	1.41E-04	1.00E-04	1.02E-04
U-234	3.31E-05	1.87E-05	1.03E-05	9.40E-06
Th-234	4.08E-08	1.69E-08	9.07E-09	7.69E-09
U-238	2.85E-05	1.61E-05	8.69E-06	8.04E-06
U-238+P	2.85E-05	1.61E-05	8.70E-06	8.05E-06

Source: FGR 13 CD Supplement (EPA 2002)

Table 3-20: Radionuclide-Specific Submersion Dose and Risk Coefficients

Nuclide	Mortality Coefficient (m ³ /Bq-s)				Effective Dose Coefficient (Sv/s)/(Bq/m ³)
	Infant	Child	Teen	Adult	
	0- 5	5- 15	15- 25	25- 70	
Po-210	4.63E-20	4.55E-20	3.48E-20	1.33E-20	3.89E-19
Bi-210	8.08E-18	7.43E-18	5.94E-18	2.63E-18	2.58E-16
Pb-210	4.65E-18	4.58E-18	3.49E-18	1.31E-18	4.51E-17
Pb-210+P	1.28E-17	1.21E-17	9.46E-18	3.95E-18	3.03E-16
Po-214	4.54E-19	4.46E-19	3.41E-19	1.31E-19	3.81E-18
Bi-214	8.65E-15	8.50E-15	6.51E-15	2.50E-15	7.25E-14
Pb-214	1.27E-15	1.25E-15	9.58E-16	3.67E-16	1.10E-14
Po-218	4.99E-20	4.91E-20	3.75E-20	1.44E-20	4.21E-19
Rn-222	2.10E-18	2.07E-18	1.58E-18	6.06E-19	1.78E-17
Ra-226	3.29E-17	3.23E-17	2.47E-17	9.46E-18	2.84E-16
Ra-226+P	9.97E-15	9.79E-15	7.5E-15	2.88E-15	8.41E-14
Th-230	1.64E-18	1.61E-18	1.23E-18	4.64E-19	1.49E-17
U-234	6.22E-19	6.11E-19	4.69E-19	1.71E-19	6.13E-18
Pa-234	1.04E-14	1.02E-14	7.8E-15	2.99E-15	8.73E-14
Th-234	3.27E-17	3.22E-17	2.46E-17	9.36E-18	2.95E-16
U-238	2.27E-19	2.23E-19	1.72E-19	5.91E-20	2.51E-18
U-238+P	1.04E-14	1.02E-14	7.83E-15	3.00E-15	8.76E-14

As with the Section 3.3 pathway conversion factors, the Native American PDCFs and PRCFs for Ra-226 included the contribution from its short-lived progeny, which are shown in both Table 3-19 and Table 3-20 as Ra-226+P. Table 3-20 also includes external dose and risk coefficients for Rn-222 and the two very short-lived polonium isotopes, Po-214 and Po-218. Because Rn-222

is a noble gas and does not remain within the body, and because the dose coefficients for Po-214 and Po-218 are so small relative to the Ra-226 dose coefficient, these three radionuclides do not significantly contribute to either the ingestion or inhalation exposure pathways. However, as the Table 3-20 external dose coefficients show, they may make a contribution to the external pathway dose and risk. Notice also, that while Pa-234 and Th-234 make very small contributions to the internal dose and risk, as compared to their parent U-238, their contribution (particularly Pa-234) is a significant contributor to the U-238 dose and risk for the external exposure pathway.

Table 3-21 presents the values for the other parameters used in the evaluation of Native American exposures due to the sweat lodge pathway. The source and rationale for selection of each of the other parameter values are discussed following Table 3-21.

Table 3-21: Other Parameters Used to Evaluate the Sweat Lodge Pathway

Parameter	Value	Units
Moisture content	0.026	kg/m ³
Number of sweats	365	sweats/yr ⁻¹
Sweat duration	1	hr/sweat
Rehydration water	1	L/sweat
Breathing rate	1.25	m ³ /hr
Decontamination factor	10	—

DOE 1997 (Table 5.7), Harris and Harper 2004 (Table 3), Rittmann 2004 (Table A17), and Harper et al. 2007 (Table B.2) all agree that the number of sweats and the sweat duration should be 365 sweats/yr and 1 hr/sweat, respectively.

The WSDOH 2003 (Section 3.2), Harris and Harper 2004 (Table 3), Harper et al. 2007 (Section 3.6), and Harper and Ranco 2009 (Section 8.3.1) all agree that 1 liter of water is needed to make up for water lost while inside the sweat lodge ($Ing_{Wat,NA,SL}$).

Although Harper and Ranco 2009 (Appendix 1) recommends a Native American breathing rate of 25 m³/day, DOE 1997 (Table 5.7), WSDOH 2003 (Table 3.2.2), Rittmann 2004 (Table A10), and Harper et al. 2007 (Table B.1) all recommend that 30 m³/day be used as the adult Native American breathing rate. Thus, for this analysis, a Native American breathing rate of 30 m³/day was assumed.

Many previous sweat lodge exposure analyses (e.g., DOE 1997, WSDOH 2003, ATSDR 2010) have based their values for the last two parameters, the sweat lodge air moisture content (M_{SL}) and the sweat lodge evaporation decontamination factor (DF_{SL}), on a methodology developed by Rodney S. Skeen, PhD, Confederated Tribes of the Umatilla Indian Reservation (CTUIR), Department of Science and Engineering, and presented in Harper et al. 2007 and elsewhere. Recently, the Skeen methodology has come under criticism. For example, in the *River Corridor Baseline Risk Assessment* (DOE 2010), the Hanford risk assessors expressed concern with using the Skeen methodology:

There is no physical basis provided in Harris and Harper (...) to correlate respirable aerosol concentrations with saturated water vapor, and exposure concentrations of nonvolatiles in sweat lodge air calculated in this manner are considered physically implausible. (page 3-71)

The Harris and Harper (...) equation for calculating air-phase EPCs [exposure point concentrations] for nonvolatile analytes (Equation 3-2) calculates the concentration of a nonvolatile COPC [contaminant of potential concern] in air as a function of the concentration of water vapor produced by the volatilization of water poured over hot rocks in a sweat lodge. Because nonvolatile contaminants have no vapor pressure, Equation 3-2 does not have a common physical basis with volatile chemicals. (page 6-77)

Furthermore, on page O-60, Rittmann (1999) said the following about the Skeen methodology as utilized by the Columbia River Comprehensive Impact Assessment (DOE 1997):

..., the sweat lodge temperature is 60° C (140° F) with a relative humidity of 100%, which means the air in the sauna is 20% water vapor. The sudden 20% reduction in oxygen concentration would certainly result in labored breathing, possibly fainting. The exposure to high temperature at saturated conditions for one hour would lead to skin burns over most of the body.

The Agency for Toxic Substances and Disease Registry (ATSDR) prepared a public health assessment (PHA) for the Midnite Mine site, and included an evaluation of sweat lodge exposures that utilized Skeen's methodology. Among the comments received on the ATSDR Midnite Mine PHA was the following (ATSDR 2010, page E-23):

Yet another flaw in the sweat lodge models relates to the assumption that nonvolatile chemicals in water brought into the sweat lodge will be released to the air. During use of a sweat lodge, the PHA assumes that water is poured over heated rocks to generate steam or water vapor via the evaporation process. Evaporation is defined as a process whereby atoms or molecules in a liquid state gain sufficient energy to enter the gaseous state. For evaporation to occur, the atoms or molecules of a chemical component in a liquid solution must be heated to a level that reaches the boiling point for that chemical. Although the heated rocks in the sweat lodge could be hot enough to evaporate the water, they would not be hot enough to vaporize the manganese and other metals present in the water. The boiling points for most of the metals are extremely high. For example, the boiling point for elemental manganese is 2,061° C (3,742° F). Chemical components with such high boiling points will remain in the solution (via processes of distillation and condensation) or will form a precipitate. Therefore, the assumption that the water vapor inside the sweat lodge contains metals at the same concentrations as in the water poured on the rocks is flawed.

WSDOH (2003, Section 5.0.2) had this to say regarding Skeen's methodology for calculating the sweat lodge airborne concentration:

The operating assumption is that 100% of the contaminants in the groundwater (used as the source of steam for the sweat lodge) will become airborne and remain available for inhalation. Uranium and plutonium compounds have a higher melting point than the temperature observed in a sweat lodge and must be entrained in the water transitioning to steam to be available for inhalation. Of those contaminant particles in the air, it is likely that the deposition rate will be higher than that of water vapor and would also serve to decrease the average air concentration. In addition, it is likely that a fraction of the contaminants will fail to become entrained in the water and become airborne, further reducing the air concentrations from those used in the calculation. The sweat lodge calculations are therefore considered a worst case estimate of the potential exposure to contaminants. Until data are available on the potential air concentration in a similar environment, the current model is considered the appropriate method for estimating exposure.

For this analysis, the Skeen methodology was set aside and the airborne radionuclide concentrations were calculated based on realistically conservative assumptions regarding the sweat lodge air moisture content (M_{SL}) and the sweat lodge evaporation decontamination factor (DF_{SL}).

Sweat Lodge Air Moisture Content (M_{SL})

The first of Skeen's assumptions that was challenged is that the air within the sweat lodge is at 100% humidity. While this is clearly a conservative assumption, it leads to conditions inside the sweat lodge that would make the sweat lodge uninhabitable. That is, at sweat lodge temperatures (i.e., between 60° C and 80° C), the humidity must be kept down to nearly zero in order to prevent scalding of the skin on contact with the air moisture. When the humidity approaches 100%, a much lower temperature of around 40° C (104° F) is necessary to prevent scalding. This analysis utilized a humidity level that, while conservative, is consistent with a habitable sweat lodge.

The heat index combines air temperature and relative humidity in an attempt to determine the human-perceived equivalent temperature, i.e., how hot it feels. When the heat index is above 80° F, the National Weather Service (NWS) will issue a caution, and the NWS considers a heat index above 130° F to be extremely dangerous, with the possibility of heatstroke highly likely. At the above sweat lodge temperature range, the assumption that the air is saturated (i.e., 100% humidity) would result in a heat index well above 500° F, which is unreasonable. Thus, the humidity within a sweat lodge must be considerably less than 100%.

For different temperatures, Table 3-22 shows what the moisture content of the air would be when the heat index is at 130° F. The maximum air moisture content (0.028 kg/m³) is achieved at the lowest temperature (100° F). Because the Sweat Lodge Ceremony pushes the individuals beyond their normal limits, Table 3-22 also shows what the air moisture content would be when the heat index is at 180° F, significantly higher than the extremely dangerous level. With a heat index of 180° F, the moisture content of the air is 0.026 kg/m³ or less in the sweat lodge temperature range (i.e., 145° to 180° F).

Table 3-22: Air Moisture Content with Heat Indices of 130° F and 180° F

Temp (° F)	Heat Index: 130° F		Heat Index: 180° F	
	RH	Moisture (kg/m ³)	RH	Moisture (kg/m ³)
100	60.4	0.028	92.3	0.042
110	36.0	0.022	64.1	0.039
120	20.1	0.016	44.1	0.035
130	11.1	0.011	30.2	0.031
140	6.65	0.0086	21.1	0.027
145	5.40	0.0079	17.8	0.026
150	4.50	0.0074	15.3	0.025
155	3.85	0.0071	13.2	0.024
160	3.41	0.0071	11.6	0.024
165	3.10	0.0072	10.3	0.024
170	2.87	0.0074	9.3	0.024
175	2.72	0.0078	8.4	0.024
180	2.62	0.0084	7.7	0.025

For this analysis, the moisture content of the air inside the sweat lodge (M_{SL}) was assumed to be 0.026 kg/m³, since that is the maximum over the 145° F to 180° F temperature range when the heat index is 180° F, and it is near the maximum over the 100° F to 189° F when the heat index is 130° F.

Sweat Lodge Evaporation Decontamination Factor (DF_{SL})

The second of Skeen's assumptions that was challenged is that the concentration of nonvolatiles in the sweat lodge airborne moisture is the same as the nonvolatile ground water concentration. Since evaporation is often used to remove impurities from water, this assumption is very conservative. For example, providers of distilled water first evaporate the water and then re-condense it, leaving behind virtually all of the impurities. Also, the NRC (1985, Section 2.19.1) recommends that, depending on its use, an evaporator can remove 99% to 99.9% of contamination from the re-condensed water, resulting in decontamination factors of 100 to 1,000. While pouring water onto hot stones in a sweat lodge is a far cry from a distiller or evaporator, it nonetheless results in the evaporation of the water.

From *Exposure Scenarios and Unit Dose Factors for the Hanford Immobilized Low-Activity Tank Waste Performance Assessment* (Rittmann 1999), page O-57:

Note that only a small fraction of the radioactivity in the evaporating water becomes airborne. In Airborne Release Fractions/Rates and Respirable Fractions for Nonreactor Nuclear Facilities, Volume 1 (DOE-HDBK-3010-94) data for the sudden depressurization of superheated aqueous solutions is presented in Table 3-5 for various initial pressures and volumes. With a source volume of 0.35 L at a pressure of 60 psig, the respirable release fraction is 0.006. A somewhat larger

value of 0.01 will be used to represent the resuspension from pouring water on hot rocks in the sweat lodge, and for the spray of a shower. (The only exception to this is tritium. Since it is assumed to be oxidized, 100% of the tritium becomes airborne.)

In the 1970s, the Oak Ridge National Laboratory performed a survey to evaluate the effectiveness of evaporation as a treatment method for reducing releases of radioactive effluents to the environment from nuclear power plants. The principal emphasis was placed upon data concerning the ratio of the feed to condensate concentrations, or decontamination factor (DF). For nonvolatile contaminants, Godbee (1973, page 2) found that:

An average system DF of 10^3 to 10^4 can be expected under routine operating conditions for nonvolatile radioactive contaminants treated in evaporators.

Godbee (1973) noted that the evaporation DF could be reduced by entrainment, which is liquid suspended in the vapor as fine droplets that are carried along with the rising vapor stream.

NUREG-1140 (NRC 1991), Section 2.3.1.2, recommends a release fraction be used when evaluating nuclear fuel cycle facility accidents. Regarding the release of nonvolatile compounds from non-flammable liquids (e.g., water), NUREG-1140 (page 77) states:

Nonvolatile compounds in nonflammable liquids are assigned a release fraction of 0.001. Several studies have measured releases in these circumstances. In general, release of these compounds can be expected to be small until the liquid is dried. After drying release fractions generally remain small because the material normally cakes on the substrate or binds into particles too large to be respirable.

It is recognized that none of the above examples exactly represents the pouring of water onto hot stones in a sweat lodge. However, taken together, they provide convincing evidence that only a small portion of nonvolatile contaminants are released during the evaporation of water. Although the above discussion suggests that a value of either 100 or 1,000 could be used, for this analysis, a sweat lodge evaporation decontamination factor (DF_{SL}) of 10 was assumed. By using this low value for the DF_{SL} , one acknowledges that a significant fraction of nonvolatile contaminants could become airborne, while still recognizing that, for water poured onto hot stones, the behavior of nonvolatile contaminants within the water is poorly understood.

3.4.5 Native American Pathway Dose and Risk Conversion Factors

Using the above described models and parameter values, the calculated Native American PDCFs and PRCFs are shown in Table 3-23.

Table 3-23: Calculated Native American Total Pathway Dose and Risk Conversion Factors

Nuclide	PDCF (mrem/yr / pCi/m ³)	PRCF (LCF/yr / pCi/m ³)
Pb-210+P	5.10E-03	6.63E-10
Ra-226+P	2.68E-02	4.86E-09
Th-230	1.94E-03	9.86E-11
U-234	4.14E-04	7.08E-11
U-238+P	3.70E-04	6.36E-11

Comparing the Native American PDCFs and PRCFs to the adult total PDCFs and PRCFs given in Table 3-12 and Table 3-13, respectively, shows that the Native American PDCFs and PRCFs are greater than the 90th percentile adult total PDCFs and PRCFs. As explained below in the discussion of the pathway contributions to the Native American PDCFs/PRCFs, this is due to the larger drinking water and vegetable consumption rates that were assumed for the Native American.

Table 3-24 presents the breakdown by exposure pathway of the Native American PDCFs, while Table 3-25 does the same for the Native American PRCFs. Because the Section 3.3 PDCFs and PRCFs only included ingestion pathways, the relative pathway contributions to the total PDCF are the same as to the total PRCF. However, since the Native American PDCFs/PRCFs include the inhalation and ingestion pathways, and because the dose-to-risk relationship differs between the inhalation and ingestion pathways, it was necessary to present the Native American pathway contributions on separate tables.

Table 3-24: Native American Pathway Contributions to the PDCF

Pathway – Adult		Pb-210+P	Ra-226+P	Th-230	U-234	U-238+P
Ingestion of Drinking Water		55.3%	33.0%	44.7%	48.5%	48.8%
Inadvertent Ingestion of Soil		0.1%	0.2%	0.2%	0.3%	0.3%
Ingestion of Vegetables	Leaf Deposition	18.1%	10.8%	14.6%	15.9%	16.0%
	Root Uptake	3.0%	32.4%	2.2%	3.5%	3.6%
Ingestion of Meat	Cattle Drinking	0.1%	0.1%	0.0%	0.1%	0.1%
	Leaf Deposition	0.4%	0.3%	0.0%	0.4%	0.4%
	Root Uptake	0.1%	0.3%	0.0%	0.1%	0.1%
	Soil Ingestion	0.0%	0.1%	0.0%	0.1%	0.1%
Ingestion of Milk	Cow Drinking	0.3%	0.7%	0.0%	0.4%	0.4%
	Leaf Deposition	2.4%	4.9%	0.0%	2.9%	2.9%
	Root Uptake	0.5%	4.2%	0.0%	0.6%	0.6%
	Soil Ingestion	0.6%	1.0%	0.1%	1.2%	1.2%
Sweat Lodge	Inhalation	0.5%	1.2%	23.1%	10.0%	9.6%
	Submersion	0.0%	0.0%	0.0%	0.0%	0.0%
	Drinking Water	18.4%	11.0%	14.9%	16.2%	16.3%

Table 3-24 shows that the drinking water pathway is the major contributor to the PDCF for four of the five radionuclides. For Ra-226+P, the vegetable consumption pathway (particularly the root uptake sub-pathway) is the major contributor to the PDCF. This is due to radium's large concentration soil uptake factor for vegetables (B_v), as indicated in Table 3-8. The sweat lodge contribution (particularly the rehydrate drinking water sub-pathway) to the PDCF is significant for all five radionuclides. For Th-230, U-234, and U-238, the sweat lodge inhalation sub-pathway is also a contributor. As with the Section 3.3 PDCFs, the inadvertent ingest of soil, meat, and milk pathways are small contributors to the Native American total PDCF.

Table 3-25: Native American Pathway Contributions to the PRCF

Pathway – Adult		Pb-210+P	Ra-226+P	Th-230	U-234	U-238+P
Ingestion of Drinking Water		53.6%	30.5%	44.0%	37.8%	38.6%
Inadvertent Ingestion of Soil		0.1%	0.2%	0.3%	0.2%	0.2%
Ingestion of Vegetables	Leaf Deposition	18.7%	10.8%	15.9%	13.7%	13.9%
	Root Uptake	3.1%	32.3%	2.4%	3.0%	3.1%
Ingestion of Meat	Cattle Drinking	0.1%	0.1%	0.0%	0.1%	0.1%
	Leaf Deposition	0.4%	0.3%	0.0%	0.3%	0.3%
	Root Uptake	0.1%	0.3%	0.0%	0.1%	0.1%
	Soil Ingestion	0.0%	0.1%	0.0%	0.1%	0.1%
Ingestion of Milk	Cow Drinking	0.4%	0.7%	0.0%	0.3%	0.3%
	Leaf Deposition	2.5%	4.8%	0.0%	2.5%	2.5%
	Root Uptake	0.6%	4.1%	0.0%	0.5%	0.5%
	Soil Ingestion	0.6%	1.0%	0.1%	1.0%	1.0%
Sweat Lodge	Inhalation	1.8%	4.9%	22.6%	27.8%	26.4%
	Submersion	0.0%	0.0%	0.0%	0.0%	0.0%
	Drinking Water	17.9%	10.2%	14.7%	12.6%	12.9%

Table 3-25 shows similar results for the pathway contributions to the Native American total PRCFs as the Table 3-24 PDCFs, except that the contribution from the sweat lodge inhalation sub-pathway has more than doubled. The reason for this is that on a per-Curie basis, the inhalation risk coefficients (Table 3-19) are a factor of 28 (Ra-226) to 612 (U-234) times larger than the ingestion risk coefficients (Table 3-2).

3.5 Exposure Pathways Not Analyzed in Detail

This section describes scoping calculations, which were performed for three potential exposure pathways: (1) radon in the home due to off-gas from well water, (2) exposure to the fetus while in the womb, and (3) infant exposure from the consumption of breast milk. Because these scoping calculations showed that they did not contribute significantly to the PDCFs, the three exposure pathways discussed in this section were not analyzed in detail.

3.5.1 External Exposure to Contaminated Ground

A screening calculation was performed to determine the impact from external exposure to soil relative to the soil ingestion pathway. It was assumed that an individual would spend 136.4 minutes per day outdoors at their residence (EPA 2011b, Table 16-22) (SNL 1999, Volume 3, Table 6.7 gives a slightly larger value of 158.5 min/day [40.2 24-hr days/year] as the mean time spent outdoors at a residence). As Table 3-26 shows, it was determined that relative to the soil ingestion pathway, the external exposure pathway can be a significant contributor to the dose, primarily due to the contributions from the daughter products (e.g., Bi-210, Bi-214, Pb-214, Th-234). However, based on Table 3-14, the external exposure pathway could contribute only about 1.3% to the Ra-226+P overall PDCFs/PRCFs, and much less for the other radionuclide.

Table 3-26: External Exposure to Contaminated Ground Screening Study Results

Nuclide	Soil Dose (Sv/yr)/(Bq/g)	
	External	Ingestion
Po-210	1.26E-09	2.21E-05
Bi-210	1.40E-07	2.39E-08
Pb-210	5.07E-08	1.27E-05
Pb-210+P	1.92E-07	3.48E-05
Bi-214	2.39E-04	2.05E-09
Pb-214	3.18E-05	2.54E-09
Ra-226	7.46E-07	5.11E-06
Ra-226+P	2.71E-04	4.00E-05
Th-230	2.74E-08	3.91E-06
U-234	8.80E-09	9.04E-07
Th-234	5.45E-07	6.21E-08
U-238	2.04E-09	8.13E-07
U-238+P	5.47E-07	8.75E-07

3.5.2 Exposure to Indoor Radon

If the well water contains radium-226, then it will also contain its decay product radon-222 (see Figure 3-2). Radon-222 is a noble gas, and once the water is in the home, the radon will escape and become airborne within the home. Individuals within the home will be exposed to radon and its short-lived daughter products (i.e., Po-218, Pb-214, Bi-214, and Po-214; see Figure 3-2) via two exposure pathways; inhalation and submersion. The amount of radon airborne in the home depends upon the amount of water brought into the home, how much of the radon escapes from the well water, and the home's air turnover rate. The following equation was used to calculate the exposure to radon that is released from well water brought into the home.

$$PDCF_{Radon} = \frac{U_{Wat} S_h f_{o-g}}{\lambda_h V_h} f_h [E_f B K DC_{Inh} + DC_{Sub}] \quad 3-14$$

where $PDCF_{Radon}$ is the PDCF due to radon in a home where well water is used (mrem/yr per pCi/m³ water), U_{Wat} is the per capita water usage rate (m³/day per person), S_h is the number of people living in the home (people), f_{o-g} is the radon off-gas fraction, λ_h is the home's air turnover rate (day⁻¹), V_h is the volume of the home (m³), f_h is the fraction of time spent in the home, E_f is the radon daughter product equilibrium fraction, B is the breathing rate (m³/day), DC_{Inh} is the radon daughter products dose coefficient for inhalation (mrem/pCi), K is a units conversion factor (day/year), and DC_{Sub} is the dose coefficient for radon submersion within the home (mrem/hr per pCi/m³). The value of each of the parameters used in equation 3-14 has been tabulated in Table 3-27.

Table 3-27: Data Used to Evaluate the PDCF for Home Radon Exposure

Parameter		Units	Value		Source
Per capita water usage rate	U_{Wat}	(m ³ /day per person)	0.26		EPA 2009
Number of people living in the home	S_h	(people)	2.58		USCB 2011
Radon off-gas fraction	f_{o-g}	None	0.90		NAS 1999a, page 91
Home's air turnover rate	λ_h	(day ⁻¹)	10.8	4.32	EPA 2011b, Table 19-1
Volume of the home	V_h	(m ³)	492	154	EPA 2011b, Table 19-1
Fraction f time spent in the home (residence)	f_h	None	0.66	0.99	EPA 2011b, Table 16-1
Breathing rate	B	(m ³ /day)	16.3	24.6	EPA 2011b, Table 5-1
Radon daughter product equilibrium fraction	E_f	None	0.4		NAS 1999b, Figure B-12
Radon daughter products dose coefficient for inhalation	DC_{Inh}	(mrem/pCi)	1.55E-04		FGR 13 CD Supplement, EPA 2002
Dose coefficient for radon submersion	DC_{Sub}	(mrem/yr per pCi/m ³)	2.07E-06		FGR 13 CD Supplement, EPA 2002

For the parameters whose values were obtained from the EFH (EPA 2011b), two values are presented in Table 3-27; the first value was used to calculate an estimate of the mean exposure, while the second value was used to calculate an upper estimate of the exposure. The radon off-gas fraction (f_{o-g}) was used to calculate how much radon escapes from the water into the air. The value for the off-gas fraction (90%) was taken from NAS 1999a, and is specifically for radon escaping in the shower, although it has been applied to all water for this scoping calculation. Other researchers have published a radon off-gas fraction closer to 70% (Hopke 2006).

The results of the radon exposure pathway PDCF scoping calculation are shown in Table 3-28. Comparing the radon PDCFs from Table 3-28 to the Ra-226+P PDCFs from Table 3-12 shows that the contributions from the radon exposure pathways are small (i.e., two to three orders of magnitude lower).

Table 3-28: PDCF for Home Radon Exposure

Exposure Pathway	Radon PDCF (mrem/yr per pCi/m ³)	
	Mean	Upper
Inhalation	3.10E-05	5.63E-04
Submersion	1.74E-10	2.09E-09
Total	3.10E-05	5.63E-04

3.5.3 Swimming Pool/Hot Tub Exposures

A screening calculation was performed to determine the impact from external exposure to water, such as by swimming or a hot tub. For this screening calculation it was assumed that an individual would spend 60 minutes per month in either a swimming pool or hot tub (EPA 2011b, Table 16-57, Overall, 50th Percentile). As Table 3-29 shows, it was determined that the external exposure pathways are not a significant contributor to the dose (relative to drinking water). Based on these results, the water immersion exposure pathways were not analyzed in detail in this analysis.

Table 3-29: Water Immersion Screening Calculation

Nuclide	Water Dose (Sv/yr)/(Bq/m ³)	
	Immersion	Drinking
Po-210	3.90E-17	6.54E-07
Bi-210	2.73E-15	7.08E-10
Pb-210	5.66E-15	3.76E-07
Pb-210+P	8.43E-15	1.03E-06
Bi-214	7.17E-12	6.05E-11
Pb-214	1.12E-12	7.51E-11
Ra-226	3.00E-14	1.51E-07
Ra-226+P	8.33E-12	1.18E-06
Th-230	1.70E-15	1.16E-07
U-234	7.56E-16	2.68E-08
Th-234	3.30E-14	1.84E-09
U-238	3.43E-16	2.41E-08
U-238+P	3.33E-14	2.59E-08

3.5.4 Exposures Due to Hydroponics and/or Aquaculture

Appendix V of the Background Information Document (BID) prepared by EPA for its 40 CFR 197 rulemaking (EPA 2001) addressed the impact of contaminated ground water on hydroponics farming (i.e., the science of growing plants without soil). After reviewing the literature on hydroponics, the BID concluded: *given that hydroponically-grown vegetables would not be subject to the buildup of radionuclides in soil, it is reasonable to conclude that they would have*

lower radionuclide concentrations than vegetables grown in soil. (EPA 2001, page 8-46) It is reasonable to make a similar conclusion for this analysis. Also, as shown in Table 3-13 through 3-16, with the exception of Ra-226, the root uptake component contributions to the total PDCFs/PRCFs are small (e.g., less than 4%). For these reasons, a detailed assessment of the hydroponics exposure pathway has not been included in this analysis.

Likewise, Appendix V of the Background Information Document (BID) prepared by EPA for its 40 CFR 197 rulemaking (EPA 2001) also addressed the impact of contaminated ground water on aquaculture (i.e., fish farming). After reviewing the literature on hydroponics, the BID found that: *In arid areas, fish farming is usually conducted in large tanks filled with ground water that is continually filtered and aerated. Food, in the form of commercial pelletized floating feed, is introduced into the tanks daily. The extensive literature on concentration factors for radionuclides in freshwater fish is not considered applicable to the unique conditions of aquaculture. Uptake is limited to direct sorption of radionuclides in the water.* (EPA 2001, page 8-46) For these reasons, a detailed assessment of the aquaculture exposure pathway has not been included in this analysis.

3.5.5 Embryo and Fetus Exposure

While in the womb, an embryo/fetus receives nourishment from its mother. If the mother ingests and/or inhales radioactivity during her pregnancy, then some of that radioactivity may be delivered to the fetus. This phenomenon has been studied by the ICRP, and their results and recommendations have been published in Publication 88 (ICRP 2001).

In Publication 88 new biokinetic and dosimetric models for calculating doses to the developing embryo and fetus are developed The models [which are developed] take account of transfer of radionuclides across the placenta, distribution and retention of radionuclides in fetal tissues, growth of the fetus, and photon irradiation from radionuclides in the placenta and maternal tissues. ... Intake scenarios comprising single or continuous maternal intakes are taken into account in the compilation of effective dose coefficients following ingestion or inhalation of the radionuclides considered. (ICRP 2001)

Table 3-30 gives the ICRP Publication 88 effective dose coefficients from conception to birth (in utero), as well as the effective dose coefficients from birth to age 70 years (post natal) due to exposures while in the womb.

Table 3-30: Dose Coefficients to the Offspring from Chronic Intake by the Mother

Nuclide	Time of Intake (weeks)	Dose Coefficient (Sv/Bq)	
		In Utero	Post Natal
Pb-210	-260	2.4E-08	5.1E-08
	-52	3.0E-08	7.0E-08
	0	1.1E-08	1.3E-07
Ra-226	-260	1.4E-09	5.0E-11
	-52	2.9E-09	8.3E-11
	0	2.9E-07	2.8E-08

Table 3-30: Dose Coefficients to the Offspring from Chronic Intake by the Mother

Nuclide	Time of Intake (weeks)	Dose Coefficient (Sv/Bq)	
		In Utero	Post Natal
Th-230	-260	1.9E-10	7.5E-10
	-52	2.2E-10	7.7E-10
	0	7.6E-10	7.8E-09
U-234	-260	7.6E-10	1.8E-10
	-52	9.9E-10	2.1E-10
	0	1.1E-08	4.1E-09
U-238	-260	6.8E-10	1.6E-10
	-52	8.8E-10	2.0E-10
	0	9.5E-09	3.8E-09

Source: ICRP 2001

The Table 3-30 dose coefficients are for chronic intake of radioactivity for three different time periods: (1) for 5 years (260 weeks) up to (but not after) conception, (2) for 1 year (52 weeks) up to (but not after) conception, and (3) during the pregnancy, starting from conception.

The first and third sets of dose coefficients were combined with the water consumption rate for non-pregnant and pregnant women (i.e., 1,243 and 1,318 mL/day, respectively) from EFH (EPA 2011b), Table 3-76. This model assumes that the woman drinks water from the contaminated well for 5 years prior to conception, and continues to drink from the well throughout her pregnancy. The results of this scoping calculation are shown in Table 3-31. Comparing the PDCFs from Table 3-31 to the PDCFs from Table 3-12 shows that the contribution to the total exposure from the chronic intake of radioactivity by the mother during pregnancy is small.

Table 3-31: PDCF to the Offspring from Chronic Intake by the Mother

Nuclide	PDCF (mrem / pCi/m ³)		
	In Utero	Post Natal	Total
Pb-210	2.14E-04	5.82E-04	7.96E-04
Ra-226	3.58E-04	3.39E-05	3.92E-04
Th-230	2.50E-06	1.56E-05	1.81E-05
U-234	1.95E-05	6.41E-06	2.59E-05
U-238	1.70E-05	5.88E-06	2.29E-05

3.5.6 Infant Consumption of Formula/Milk

Infants receive their nourishment from formula, breast milk, or cows' milk. Furthermore, formula is available in three forms; powder, liquid concentrate (which requires dilution), and premixed ready-to-feed. Currently, 74.6% of American infants have been breastfed at least once, with 35% of infants exclusively breastfed at 3 months, 44.3% receiving some breastfeeding at 6 months, and 23.8% receiving breastfeeding at 1 year (CDC 2011). Consumption of cows' milk is not recommended for infants under the age of 1 year; however, that recommendation is often ignored and cows' milk is introduced earlier. EFH (EPA 2011b), Table 3-72, shows that 5% of infants consumed cows' milk at 6 months, increasing to 25% at 9 months and to 79% at 12 months.

Except for premixed ready-to-feed formula, each of these means of feeding could result in exposure to an infant if the well water is contaminated. For powder or liquid concentrate formula, well water is mixed with the formula and fed directly to the infant. Section 3.1.1 presents the methodology used to calculate exposures due to water consumption, and this same methodology was used to calculate exposure from powder or liquid concentrate formula consumption. Table 3-5 and Figure 3-3 show the infant's water consumption distribution, which was obtained from EFH (EPA 2011b), Table 3-41. On Figure 3-3, the weight normalized infant's water consumption is significantly larger than the water consumption for the other age groups, reflecting the fact that water is used to prepare formula, which is the bulk of an infant's nourishment.

The methodology used to calculate exposures from the cows' milk pathway was described in Section 3.1.4. Table 3-10 and Figure 3-10 show the infant's cows' milk consumption distribution, which was obtained from EFH (EPA 2011b), Table 11-3. On Figure 3-10, the weight normalized infant's milk consumption is significantly smaller than the child's milk consumption; this reflects the fact that cows' milk is not recommended for infants under the age of 1 year.

Thus, the infant's exposures from consumption of formula and cows' milk have been included in the PDCF's that are presented in Section 3.3. However, the infant's exposure from breast milk consumption has not been addressed. The ICRP has studied this exposure pathway, and their results and recommendations have been documented in Publication 95 (ICRP 2004). In Publication 95, the ICRP adapted existing biokinetic models for the female adult to include transfer of radioactivity to milk. The fraction of the mother's radioactivity intake that reaches the breast milk was then combined with the infant's ingestion dose coefficient to arrive at a dose coefficient that relates the amount of radioactivity ingested by the mother to the dose received by the breastfeeding infant (i.e., Sv to the infant/Bq intake by the mother). Table 3-32 shows the fraction of mother's radioactivity intake that reaches the breast milk and the breastfeeding infant dose coefficient obtained from ICRP Publication 95, as well as the risk coefficient, which was calculated in the same manner as the dose coefficient.

Table 3-32: Dose and Risk Coefficients from Breast Milk Consumption

Nuclide	Fraction of Mother's Intake to Breast Milk*	Dose Coefficient (Sv/Bq)*	Risk Coefficient (LCF/Bq)
Pb-210	2.5E-02	2.2E-07	9.6E-09
Ra-226	5.9E-03	2.8E-08	2.5E-09
Th-230	2.4E-05	9.8E-11	3.0E-13
U-234	9.7E-04	3.6E-10	9.7E-12
U-238	9.7E-04	3.3E-10	1.3E-11

*ICRP 2004

Table 3-33 presents a comparison of the doses and risks received by infants consuming cows' milk, formula, and breast milk. For cows' milk and formula, it was assumed that the infant consumed 778 mL/day (EPA 2011b, Table 3-74), and for breast milk, it was assumed that the mother consumed 1,806 mL/day of water (EPA 2011b, Table 3-76). The radioactivity in the cows' milk was calculated using the methodology from Section 3.1.4 and the parameter values

from Section 3.2.6. In addition to consuming contaminated well water, the mother was assumed to consume contaminated vegetables, cows' milk, and meat, as described in Sections 3.1 and 3.2.

Table 3-33: PDCF/PRCF for Infant Milk Consumption

Infant Milk Ingestion – Dose (mrem/yr / pCi/m³)					
	Pb-210	Ra-226	Th-230	U-234	U-238
Cows' Milk	1.28E-02	1.76E-01	1.04E-04	3.52E-04	3.53E-04
Formula	3.61E-02	4.10E-02	4.34E-03	3.88E-04	3.93E-04
Breast Milk	6.59E-04	1.22E-04	2.80E-07	1.10E-06	1.01E-06
Infant Milk Ingestion – Risk (LCF/yr / pCi/m³)					
	Pb-210	Ra-226	Th230	U-234	U-238
Cows' Milk	1.43E-04	1.91E-03	3.20E-07	9.53E-06	1.28E-05
Formula	4.02E-04	4.44E-04	1.34E-05	1.05E-05	1.42E-05
Breast Milk	7.35E-06	1.32E-06	8.61E-10	2.99E-08	3.66E-08

As Table 3-33 shows, the infant's exposure due to consuming breast milk is small compared to the exposure due to either formula or cows' milk consumption. This is expected, since the mother's body only allows a fraction of the radioactivity entering her body to reach her breast milk (Table 3-32), where it can be consumed by the infant, whereas for formula consumption, all radioactivity in the well water is consumed by the infant.

4.0 DOSE AND RISK ASSESSMENT

4.1 Introduction

Chapter 3 described the methodology for calculating probabilistic pathway dose and risk conversion factors, while Chapter 2 described the ground water modeling for excursion and leakage scenarios. The ground water modeling was based on an initial source concentration of 1 mg/L for a generic species, and concentrations were calculated at down-gradient receptor wells located various distances from the source assuming no retardation. In this chapter, we evaluate expected doses and risks assuming source term strengths based on available measurements from the literature and include the effects of radionuclide-specific retardation factors.

4.2 Selection of Lixiviant Concentrations and K_{ds}

To be conservative, we have generally selected low-end K_{ds} and high-end lixiviant concentrations for calculating doses and risks.

4.2.1 Lixiviant Concentration

Table 4-1 summarizes reported ranges of concentrations of various species in ISL/ISR lixiviants (PNNL 2010).

Table 4-1: Representative Concentrations in Uranium Alkaline ISR Lixiviants

Constituent	Wyoming Site ^(a)	Texas Site ^(a)	Kingsville Dome Site, Texas ^(b)	Typical Chemistry ^(c)	Typical Lixiviant Chemistry Range ^(d)
Calcium	138	273	560	100–350	≤ 20–500
Magnesium	42	82	92	10–50	≤ 3–100
Sodium	365	1,007	800	500–1,600	≤ 400–6,000
Potassium	12	26.5	31	25–250	≤ 15–300
Carbonate	NR	NR	NR	0–500	≤ 0.5–2,500
Bicarbonate	NR	579	619	800–1,500	≤ 400–5,000
Chloride	140	1,009	919	250–1,800	≤ 200–5,000
Sulfate	229	1,181	1,660	100–1,200	≤ 400–5,000
Silica	24.6	NR	23.5	25–50	NR
pH (standard units)	6.7	6.71	6.82	7–9	≤ 6.5–10.5
Total dissolved solids	1,713	4,186	4,640	1,500–5,500	≤ 1,650–12,000
Alkalinity (as CaCO ₃)	620	NR	507	NR	NR
Arsenic	NR	NR	0.016	NR	NR
Iron	NR	NR	0.02	NR	NR
Manganese	NR	NR	1.7	NR	NR
Molybdenum	NR	NR	32	NR	NR
Radium-226 (pCi/L)	NR	NR	293	500	NR
Selenium	NR	NR	0.104	NR	NR
Uranium	18.2	28.6	29.0	50–250	≤ 0.008–424
Vanadium	NR	NR	<0.01	NR	≤ 0.006–56

All units are mg/L unless otherwise noted.

NR = Not reported

^(a) Deutsch et al. 1985

^(b) Schramke et al. 2009

^(c) Pelizza 2008

^(d) NRC 2009b

Additional information on lixiviant concentrations is included in Table 4-2: (CNWRA 2001). These are the maximum quoted concentrations based on a survey of licensing documents.

Table 4-2: Highest Observed Concentrations in Pregnant Lixiviants based on a Survey of Licensing Documents

Element/Isotope	Concentration
Ra-226	3,400 pCi/L
Lead	0.01 mg/L
Uranium	250 mg/L

Based on this information, lixiviant concentrations were established as follows.

Lead Concentration

The maximum amount of lead reported in lixiviants is 0.01 mg/L (Table 4-2).

Uranium Concentration

The maximum amount of uranium reported in lixiviants is 424 mg/L (Table 4-1). This value can be traced to NRC 1989, but that reference is silent on the source of the data, noting only that the “values represent the concentration ranges that could be found in barren lixiviant and pregnant lixiviant and would include the concentrations normally found in ‘injection fluids’” (NRC 1989, Table 3.4.01). Use of 424 mg/L as an upper bound on the uranium concentration thus lacks credibility. The values in Column 5 of Table 4-1 are from Pelizza 2008, but Pelizza also does not provide the source of the data. It likely came from NUREG-1508 (NRC 1997), which also lists the range for uranium from 50 to 250 mg/L. According to Table 2.1 of NUREG-1508, these data were obtained from HRI 1993 and are based on test data and operational licensing experience. This is presumably from the same source as cited in Table 4-2 above. CNWRA 2001 cites 60 mg/L as a typical concentration for pregnant lixiviant. Another source of information is spill incidents in 1999 at the Smith Ranch involving injection fluids with a natural uranium concentration of 2.7E-06 µCi/ml or 3.9 mg/L, and extraction fluids with a concentration of 5.3E-05 µCi/ml or 77 mg/L (NRC 2000). Additionally, NRC reported that since June 1997, uranium releases in spills at the Smith Ranch-Highland Uranium Project ranged from 0.7 to 152 mg/L, with about 70% of the releases below 10 mg/L (NRC 2007). Based on this information, we have selected a uranium concentration of 150 mg/L as a reasonable upper-end value for calculating doses and risks.

Radium Concentration

The highest observed Ra-226 concentration in lixiviants is 3,400 pCi/L (Table 4-2). Based on the specific activity of 1 Ci/g for Ra-226, this is equivalent to 3.4E-06 mg/L. This value is based on the Ra-226 concentration in production fluids at the Smith Ranch Facility in Converse County, Wyoming (NRC 2000). The Ra-226 concentration in injection fluids was similar (i.e., 3,300 pCi/L); radium is not removed when uranium is extracted from the pregnant lixiviant and is returned underground with the injection solutions.

Thorium Concentration

As noted by the NRC in its Standard Review Plan for ISLs (NRC 2003, Section 5.7.8.3):

.....many licensees have decided not to sample for Th-230; Th-230 is a daughter product from the decay of uranium-238, and studies have shown that it is mobilized by bicarbonate-laden leaching solutions. However, studies have also shown that after restoration, thorium in the ground-water will not remain in solution, because the chemistry of thorium causes it to precipitate and chemically react with the rock matrix (Hem, 1985). As a result of its low solubility in natural waters, thorium is found in only trace concentrations. Additionally, chemical tests for thorium are expensive, and are not commonly included in water analyses at in situ leach facilities. This example concerning Th-230 demonstrates an acceptable technical basis for excluding Th-230 from the list of sampled constituents.

In the absence of detailed geochemical modeling to support the immobility of thorium in ground water, we have selected a value of 640 pCi/L (3.05E-05 mg/L) for the Th-230 source term. This value was measured at the Irigaray Solution Mining Project in the post-leaching ground water prior to restoration (NRC 1978, Table 5.1).

4.2.2 Selection of K_d Values

Selection of K_d s was based on selecting low-end values to conservatively establish the time to reach peak dose at a down-gradient well. It should be noted that the K_d value affects the time at which the peak dose occurs, but not its magnitude in the absence of significant radioactive decay. Considerations in selecting the K_d values are described below.

Lead K_d

EPA 1999b provides a thorough survey of the adsorption behavior of lead in soil studies and identifies the factors that influence the behavior of lead. The pH of the aqueous phase had an important effect on lead sorption, which increases over the pH range of 4–11. Table 4-3 summarizes lead K_d values as a function of pH and aqueous lead concentrations from EPA 1999b. It is probable that in the ISL environment, lead will derive from the uranium series decay chain and will be present in low concentrations.

Table 4-3: Estimated Range of K_d Values for Lead as a Function of Soil pH, and Equilibrium Lead Concentrations

Equilibrium Lead Concentration (micro g/l)	K_d (ml/g)	Soil pH		
		4.0–6.3	6.4–8.7	8.8–11.0
0.1–0.9	Minimum	940	4,360	11,520
	Maximum	8,650	23,270	44,580
1.0–9.9	Minimum	420	1,950	5,160
	Maximum	4,000	10,760	20,620
10–99.9	Minimum	190	900	2,380
	Maximum	1,850	4,970	9,530
100–200	Minimum	150	710	1,880
	Maximum	860	2,300	4,410

Based on this information, we selected a minimum K_d for 10 $\mu\text{g/L}$ of lead in solution of 900 ml/g for pH 6.4–8.7. This pH range is consistent with observed values at ISL facilities (Davis and Curtis 2007, Table 3 and 4).

With a K_d of 900 ml/g for lead and conservative hydraulic data from existing ISL facilities (see Table 4-8 and Figure 4-1), it would take the isotopes of lead initially present in the ground water approximately 260,000 years to reach the nearest well located at a distance of 528 ft from the facility. Since the half-life of Pb-210 is 22.3 years, any Pb-210 contamination initially present in the lixiviant would completely decay away before it could arrive at the receptor well.

Furthermore, as described in Section 3.2.2, any in-growth of Pb-210 from the decay of Ra-226 has been accounted for in this analysis by adding the Pb-210 dose and risk factors (as well as the dose and risk factors for other short-lived Ra-226 progeny) to the Ra-226 dose and risk factors. Thus, the Ra-226 doses and risks presented in this report include the contribution from Pb-210 and the other Ra-226 short-lived progeny.

Uranium K_d

Aqueous uranium and its complexes sorb onto clays, organics, and iron oxides (EPA 1999b). Uranium sorption by soils generally reaches a maximum in the pH range from pH 5 to 8 (EPA 1999b). Higher ionic-strength solutions or the presence of carbonate ions tend to decrease uranium(VI) sorption. Uranium can also be attenuated in ground water through co-precipitation reactions with metal oxyhydroxides, such as iron hydroxide.

Table 4-4 provides a uranium K_d look-up table from EPA 2004. The general trend in uranium K_d values as a function of pH is that adsorption is low at pH values of 3 or less, increases rapidly from pH of 3 to 5, reaches a maximum between pH of 5 and 8, and then decreases with increasing pH greater than 8. The decrease in absorption at high pH is actually related to the presence of dissolved carbonate. At near- and above-neutral pH conditions, dissolved U(VI) forms strong anionic uranyl-carbonate complexes with dissolved carbonate, making it less likely to adsorb to the surface-charged soil minerals (EPA 2004).

Table 4-4: Estimated Range of K_d Values for Uranium based on pH

K_d (ml/g)	pH							
	3	4	5	6	7	8	9	10
Minimum	<1	0.4	25	100	63	0.4	<1	<1
Maximum	32	5,000	160,000	1,000,000	630,000	250,000	7,900	5

Source: EPA 1999b

As documented in EPA 1999b (Section J.40):

Under oxidizing conditions at pH values greater than 6, their derived K_d values were approximately 100 ml/g. At high concentrations of dissolved carbonate, and pH values greater than 6, the K_d values for uranium decrease considerably.

Based on these considerations, we have selected a value of 0.4 ml/g (the minimum value at pH 8 in Table 4-4).

Radium K_d

Radium, an alkaline earth element, is generally relatively immobile, but can be mobilized under some conditions. Radium-226 and radium-228 are present in uranium roll-front deposits, because of the decay of uranium-238 and thorium-232, respectively. Ground water radium concentrations commonly are elevated in the ore zone relative to the background levels present immediately up-gradient and down-gradient of the ore (Hoy 2006). In general, radium adsorption on mineral surfaces increases with increasing pH. For iron oxides, the increase in adsorption begins around pH of 6 to 8 and reaches a maximum of around 10 or less (EPA 2004). Radium can be attenuated by adsorption onto clays. Radium is also strongly adsorbed to mineral oxides, especially at near-neutral and alkaline pH conditions (EPA 2004).

Compared to most other radionuclides, very limited data are available on radium sorption, particularly K_d values. Moreover, EPA (2004) states that any data indicating high radium adsorption on geologic materials should be viewed carefully, as (Ba, Ra) SO_4 co-precipitation may have occurred during the measurements. However, from an attenuation standpoint, the amount of radium that is removed from ground water by adsorption versus precipitation is largely irrelevant. EPA (2004) presents ranges of K_d values by soil type, as shown in Table 4-5. As noted by EPA (2004), “radium is readily adsorbed to clays and mineral oxides present in soils, especially at near neutral and alkaline pH conditions.”

Table 4-5: Radium K_d Values by Soil Type

Soil Type	K_d Values (ml/g)		
	Geometric Mean	Number of Observations	Range
Sand	500	3	57 – 21,000
Silt	36,000	3	1,262 – 530,000
Clay	9,100	8	696 – 56,000
Organic	2,400	1	None Listed

Source: EPA 2004

As can be seen from Table 4-5, a minimum K_d value of 57 ml/g is cited for radium in sand. NRC recommends a value of 100 ml/g for alkaline (cementitious) environments (NRC 1998). This seems more relevant to alkaline ISL environments and has been selected for calculating retardation factors here.

Thorium K_d

NRC (1998) recommended a K_d value of 500 ml/g for thorium in a Type III environment, which is equivalent to highly weathered cement. EPA (1999b, Table 5-15) quotes a minimum value of 20 ml/g for Th concentrations of $<10^{-9}$ M (2.3E-07 g/L) and pH of 8 to 10. For the pH range of 5 to 8, EPA quotes a minimum value of 1,700 ml/g. For the analyses presented here, the intermediate value of 500 ml/g was selected.

4.2.3 Recommendations for K_d and Radionuclide Source Term

Recommended K_d values and source concentrations for radionuclides are summarized in Table 4-6. It is recognized that, if leakage is from an injection well as contrasted to an extraction well, the concentrations, particularly uranium, will be lower than cited in Table 4-6. If lixiviant concentrations at actual sites are different than those assumed in Table 4-6, the results can be scaled linearly from those used here.

Table 4-6: Summary of K_d Values and Lixiviant Concentrations Used in Dose and Risk Calculations

Radionuclide	K_d (ml/g)	Lixiviant Concentration (mg/L)
U nat	0.4	150
Th-230	500	3.05E-05
Ra-226	100	3.4E-06
Pb-210	900	0.01

Radionuclide-specific retardation factors may be calculated using the following equation:

$$R_i = 1 + \frac{\rho_b K_{d_i}}{p_t} \tag{4-1}$$

- R_i = Retardation factor of radionuclide i in the saturated zone —
- ρ_b = Saturated zone soil bulk density (g/cm³)
- K_{d_i} = Radionuclide i distribution coefficient in the saturated zone (cm³/g)
- p_t = Total porosity of the saturated zone (dimensionless) —

Radionuclide-specific retardation factors were calculated using equation 4-1, the above K_d s, a soil bulk density (ρ_b) of 2 g/cc, and a total porosity (p_t) of 0.3.

4.3 Dose and Risk Calculations

4.3.1 Limiting Doses and Risks

For illustrative purposes, limiting concentrations at the receptor well are derived for an assumed dose limit of 15 mrem/yr and a lifetime risk limit of 10^{-4} LCF¹², or assuming a 70-year life expectancy, an annual risk limit of 1.4×10^{-6} LCF/yr. The limiting radionuclide concentrations shown in Table 4-7 were derived using the adult, mean pathway dose and risk conversion factors (PDCFs and PRCFs) derived in Chapter 3. Based on the approach taken for the CAP88 computer program, the adult PDCFs and PRCFs were used to calculate the Table 4-7 limiting concentrations. The limiting concentrations for Ra-226 in Table 4-7 are shown both with and without progeny. Limits for one daughter product, Pb-210 with a 22.3-year half-life, are also shown separately.

Table 4-7: Radionuclide Well Limiting Concentrations

Nuclide	15 mrem/yr Dose Limit		10^{-4} LCF Lifetime Risk Limit	
	(pCi/L)	(mg/L)	(pCi/L)	(mg/L)
U-238+P	97	2.8E-01	63	1.8E-01
U-234	93	1.5E-05	65	1.0E-05
U-natural	95	1.4E-01	64	9.4E-02
Th-230	25	1.2E-06	47	2.2E-06
Ra-226	1.2	1.2E-09	0.6	6.3E-10
Ra-226 + P	2.4	3.1E-11	1.3	1.7E-11
Pb-210+P	97	2.8E-01	63	1.8E-01

U-238+P included progeny:Th-234

Ra-226+P included progeny:Pb-214, Bi-214, Pb-210, Bi-210, Po-210

Pb-210+P included progeny: Bi-210, Po-210

As Table 4-7 demonstrates, a lifetime risk limit of 10^{-4} LCF is slightly more restrictive than a dose limit of 15 mrem/yr for uranium, Ra-226, and Pb-210, while the dose limit is slightly more restrictive for Th-230. However, for all of the radionuclides considered, both dose and risk limiting concentrations are within a factor of two.

4.3.2 Doses and Risks from Excursion Scenarios

As described in Section 2.6.2, 63 excursion scenarios were analyzed in which some lixiviant leaked down-gradient from various injection/extraction pumping patterns. The ground water modeling studies described in Chapter 2 included broad ranges of selected hydraulic parameters to assist in evaluating the sensitivity of receptor well concentrations to parameter changes. While the selected ranges for individual parameters were based on literature reviews, some combinations of hydraulic parameters may not exist in actual licensed ISL facilities. For example, ground water velocity is defined as the product of hydraulic conductivity and hydraulic

¹² A lifetime cancer morbidity risk limit of 10^{-4} was specified in the National Contingency Plan (55 Federal Register 8665-8865, March 8, 1990). In this example the cancer morbidity risk limit is being applied to the risk of latent cancer fatalities (LCF). For the radionuclides analyzed in this study, the relationship between cancer morbidity and mortality is discussed in Section 3.2.2.

gradient divided by the effective porosity. In some of the modeling scenarios, both high conductivity and high gradient were included, which could result in unrealistically high velocities. To focus on doses and risks from those scenarios that are most representative of actual ISL conditions, we obtained data from several proposed and operating ISL facilities, as summarized in Table 4-8. From these data, we constructed the cumulative distribution for the product of hydraulic gradient times hydraulic conductivity function shown in Figure 4-1. It can be seen that all of the values fall below a limit of 0.13 (ft/day). Based on this limit, we developed doses and risks for those modeled excursion scenarios not exceeding this limit.

Table 4-8: ISL Site Hydraulic Data

Site / Identifier		Hydraulic Conductivity (ft/day)	Hydraulic Gradient	Reference
Crow Butte, NE		9.11	0.0004	Crow Butte 1995 (Table 2.7-6 and p.2-13)
Goliad County, TX		3.5	0.0009	DBS&A 2007 (Table 1 and Sec. 2.5)
Irigaray, WY	Major	1.55	0.033	NRC 1978 (p. 2-16)
	Minor	0.896	0.033	
Kingsville Dome, TX	PBL-1	24.48	0.005	Rice 2006 (Tables A-2, A-3, A-4)
	PBL-2	14.112	0.0009	
	PBL-3	20.16	0.005	
	PBL-5	12.672	0.0009	
Lost Creek, WY	Multi-well	1.8 to 4.4	0.003	Lost Creek 2007 (Tables 2.7-7 and 2.7-9)
	Single well	4.4 to 11.7	0.006	
Moore Ranch, Campbell County WY		5.36	0.004	NRC 2009a (Sec. 3.5.2.3)
Nichols Ranch, WY	A sand	0.5	0.0033	NRC 2009c (Sec. 3.5.2.3)
	F sand	0.6	0.005	
North Butte, WY	A sand	8.79	0.015	PRI 2006 (Table 10.1 and p. 10-13)
	B and C sand	8.43	0.0061	

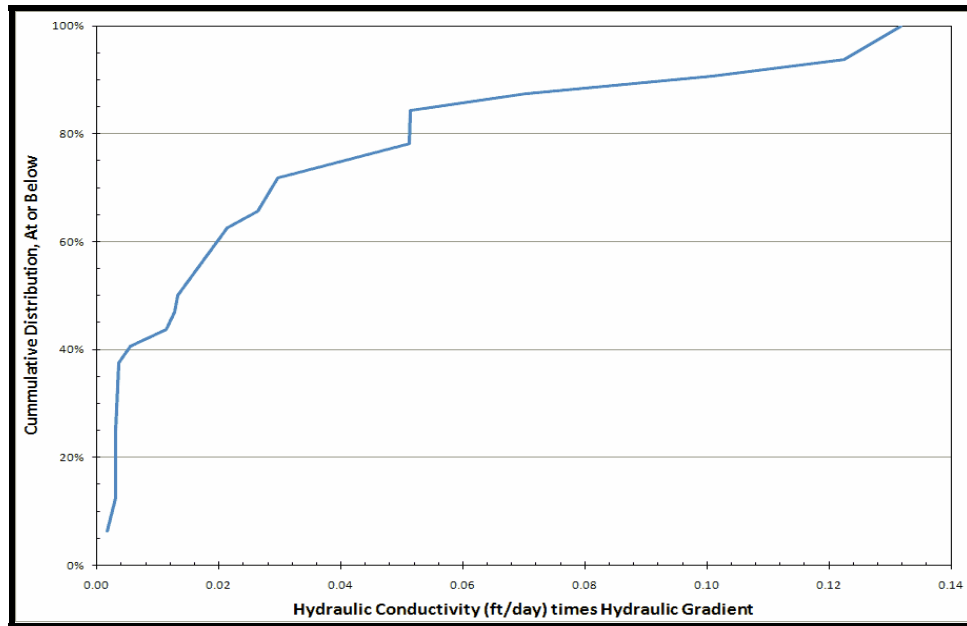


Figure 4-1: Cumulative Distribution of ISL Site Hydraulic Data

Thirty-seven (37) analyzed excursion scenarios met Figure 4-1 hydraulic data criteria and were included in the dose and risk analysis. Figure 4-2 shows the dose to an adult from uranium for scenario 6E at each of the four assumed down-gradient receptor well locations. From Figure 4-2, it is apparent that as the down-gradient distance to the well increases, two things occur; (1) the dose to the receptor decreases, and (2) the time after the release when the peak dose occurs increases. As an example, from Figure 4-2, the dose to an adult from a well at 528 ft is about 7,600 mrem/yr and occurs at about 20 years, whereas the dose to an adult from a well at 3,480 ft is about 610 mrem/yr and occurs at about 124 years. Unless otherwise specified, all of the remaining doses and risks discussed in this section are based on the assumption that the receptor well is located at a distance of 528 ft down-gradient.

Figure 4-2 also illustrates an important factor regarding wellfield restoration. If lixiviant has escaped from the wellfield during operations, it will not arrive at a well 528-ft away for at least 20 years, depending on the actual K_d . Thus, the peak uranium dose at the down-gradient well is likely to occur long after restoration of the wellfield has been completed, based on current practices.

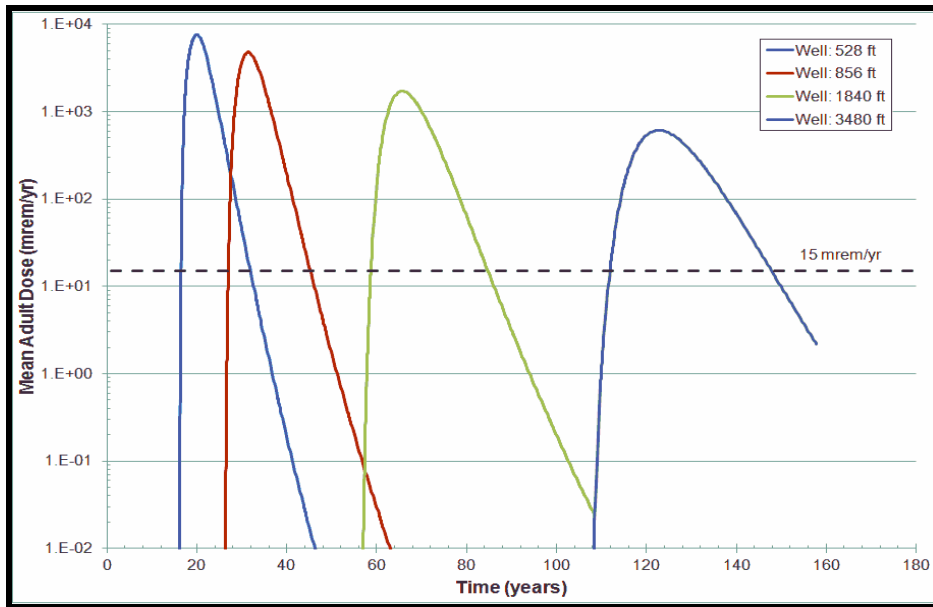


Figure 4-2: Excursion Scenario 6E Peak Dose Arrival Time, $K_d = 0.4$ ml/g

Figure 4-3 shows the adult mean doses at the time of maximum concentration that were calculated for each scenario and radionuclide. (Note that some of the 37 scenarios and radionuclide maximum doses were lower than the 0.01 mrem/yr cutoff and are not shown in Figure 4-3.) All of the doses shown in Figure 4-3 are for a receptor located at the nearest well, at a distance of 528 ft. In Figure 4-3 and all subsequent tables and figures in Chapter 4, radiological decay is not explicitly included; however, whether specifically noted or not, contribution of the progeny to the dose/risk is included as described in Section 3.2.2.

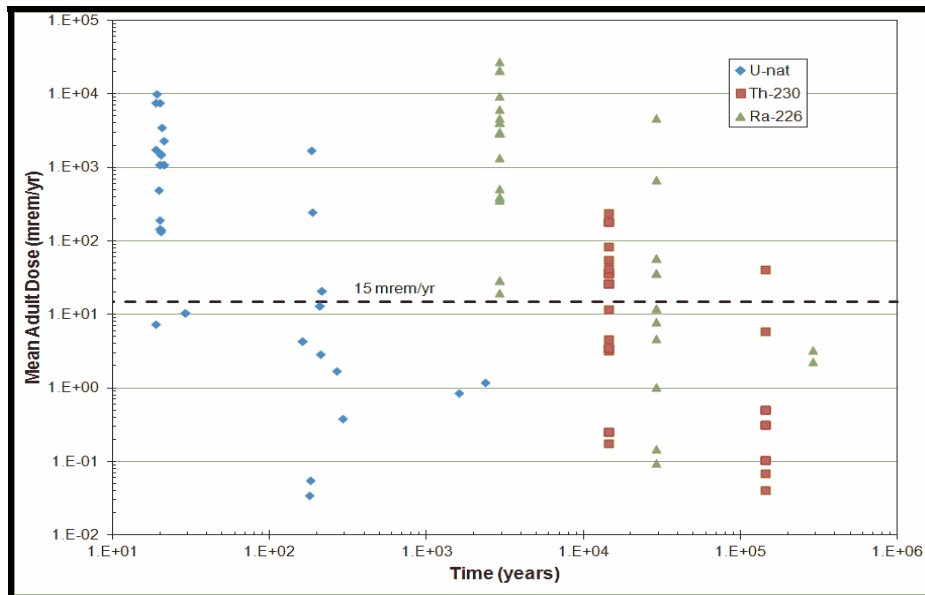


Figure 4-3: Excursion Scenario Dose Results versus Time

In Figure 4-3, the receptor doses due to uranium occur first, due to the assumed low value of the uranium K_d . Also, the uranium doses are received in two distinct groupings—the first around 30 years and the second around 120 years. This grouping tendency is due to the fact that the product of the hydraulic gradient and hydraulic conductivity for 36 of the 37 scenarios analyzed was either 0.01 or 0.1 ft/day (see Figure 4-4). This same pattern is shown in Figure 4-3 for the Th-230 and Ra-226 (+ progeny) doses. Because each radionuclide arrives at the receptor well at a different time, due to their different K_d values, it is not necessary to sum the exposure from different radionuclides. Table 4-9 shows the maximum calculated dose for each radionuclide from all 37 excursion scenarios that were analyzed. Clearly, uranium and Ra-226 (+ progeny) are the significant contributors to dose and risk.

Table 4-9: Excursion Scenario Maximum Doses and Risks – Mean Adult

Nuclide	Dose (mrem/yr)	Risk (LCF/yr)
U nat	1.0E+04	1.4E-03
Th-230	2.4E+02	1.2E-05
Ra-226+ P	2.8E+04	4.8E-03

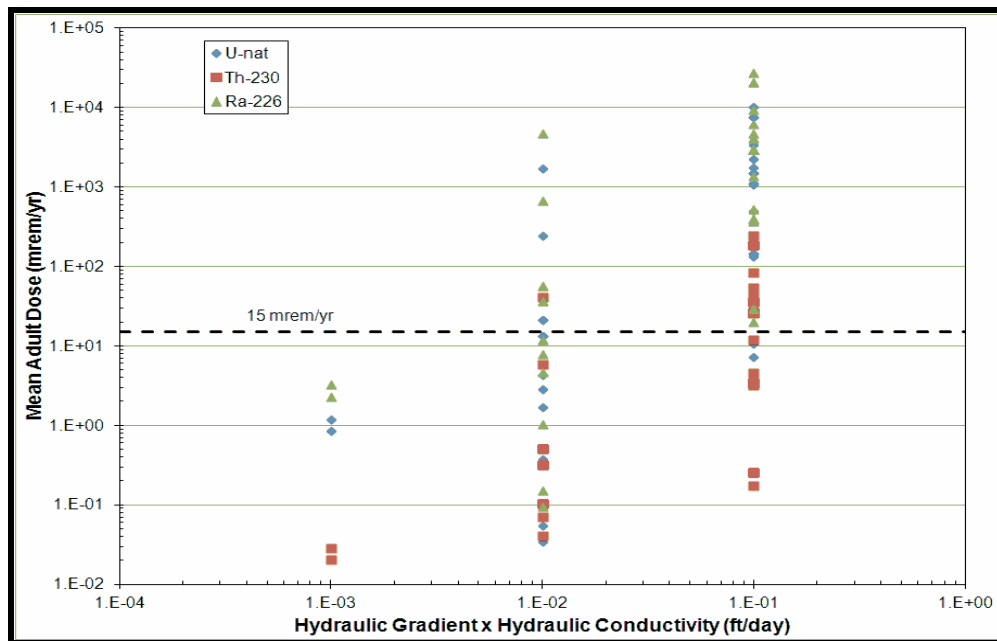


Figure 4-4: Excursion Scenario Dose Results versus Hydraulic Data

Figure 4-4 shows the same dose results as Figure 4-3, except as a function of their hydraulic data, instead of as a function of time. As indicated above, Figure 4-4 shows that 36 of the 37 excursion scenarios analyzed have the product of their hydraulic gradient and hydraulic conductivity equal to either 0.01 or 0.1 ft/day; in one scenario, the product was 0.001 ft/day. Figure 4-1 shows that a hydraulic data product of 0.1 ft/day or more occurs in only 10% of the actual ISL sites, whereas a hydraulic data product of 0.01 ft/day or less occurs in about 43% of the actual ISL sites. Thus, although very high doses were calculated for some of the excursion

scenarios, many of the scenarios with high doses are at hypothetical sites with hydraulic properties that occur very infrequently at actual ISL sites.

Figure 4-5 is similar to Figure 4-3, except that it shows the calculated risks. The above discussion of the dose results also applies to the risk results, and is not repeated.

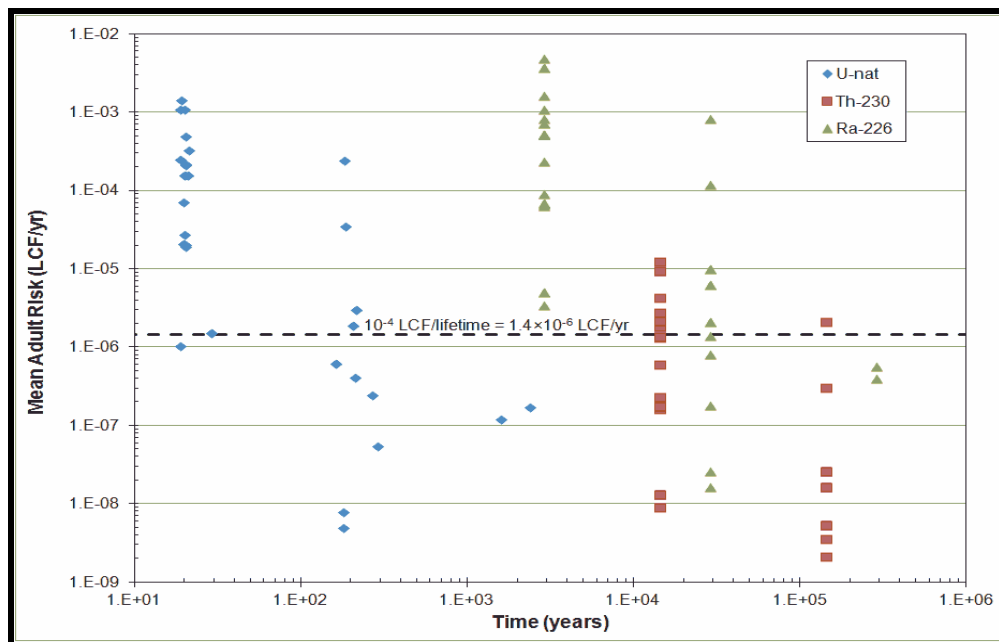


Figure 4-5: Excursion Scenario Risk Results versus Time

When viewing Figure 4-5, it should be remembered that a lifetime risk limit of 10^{-4} LCF corresponds to an annual risk of about 1.4×10^{-6} LCF/yr.

Figure 4-2 shows the annual doses that result at the various assumed well locations due to the passing of the uranium contamination plume. In developing Figure 4-2, it was assumed that the K_d for uranium was 0.4 ml/g, as described in Section 4.2.2. However, Section 4.2.2 also pointed out that there is a great deal of variability in the possible uranium K_d , with Table 4-4 showing that potentially the uranium K_d could be in the range of 100 to 1,000,000 ml/g.

Figure 4-6 shows the effect on the dose by arbitrarily increasing the uranium K_d by a order of magnitude from 0.4 to 4 ml/g. When comparing the Figure 4-6 doses to the Figure 4-2 doses, notice that the only thing that changes is the time when the plume arrives at each well location, but that the magnitude of the doses received remains unaffected by the choice of the uranium K_d . This effect is due to the very long half-life of uranium-238 (i.e., 4.47×10^9 years), which results in virtually no additional radiological decay during its longer travel time to the receptor wells. Because Th-230 and Ra-226 also have long half-lives (i.e., 75,380 and 1,600 years, respectively), the doses due to Th-230 and Ra-226 would likewise be unaffected by changes to their K_d values.

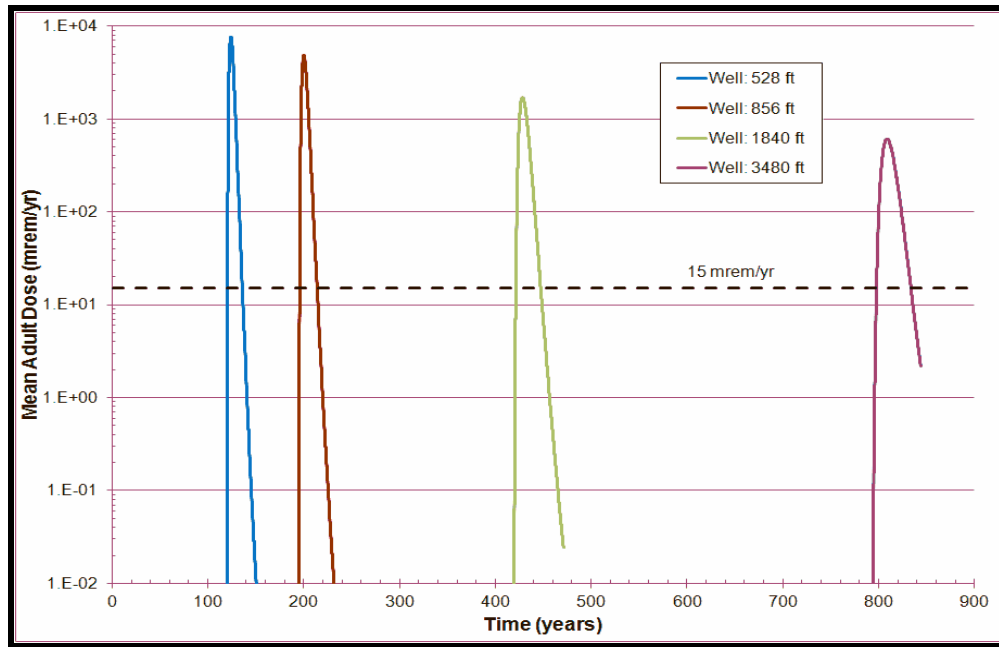


Figure 4-6: Excursion Scenario 6E Peak Dose Arrival Time, $K_d = 4.0$ ml/g

4.3.3 Doses and Risks from Surface Leak Scenarios

As described in Chapter 2, 24 scenarios were analyzed that postulated the spill of lixiviant onto the ground, with subsequent leakage into the ground water and transport to an offsite receptor well. As explained in Chapter 2, three types of surface leak scenarios were analyzed: (1) catastrophic spills ranging from 100,000 to 200,000 gallons, (2) a slow leak of 1 to 2 gpm for a period of 3 years, and (3) leaks varying from 1 to 45 gpm over a 28-day period. Figure 4-7 and Figure 4-8 show the calculated doses and risks for all of the 24 leak scenarios, respectively, and Table 4-10 shows the maximum and minimum dose and risks from Figure 4-7 and Figure 4-8. All of the doses and risks shown are for a receptor located at the nearest well at a distance of 328 ft. Notice on Figure 4-7 and Figure 4-8 that the first uranium doses are received earlier for some of the leak scenarios than for any of the excursion scenarios. This is due to the fact that for three leak scenarios, the product of their hydraulic gradient and hydraulic conductivity was equal to 1.0 ft/day. This higher hydraulic data product was felt to be reasonable for the leak scenarios, because it is believed that the leak could travel in regions near the ground surface that have both a high gradient and a high conductivity (UT 2010). Thus, for the surface leak scenarios, the uranium contamination plume could arrive at a receptor well very soon after the spill occurs (e.g., within 2 to 3 years).

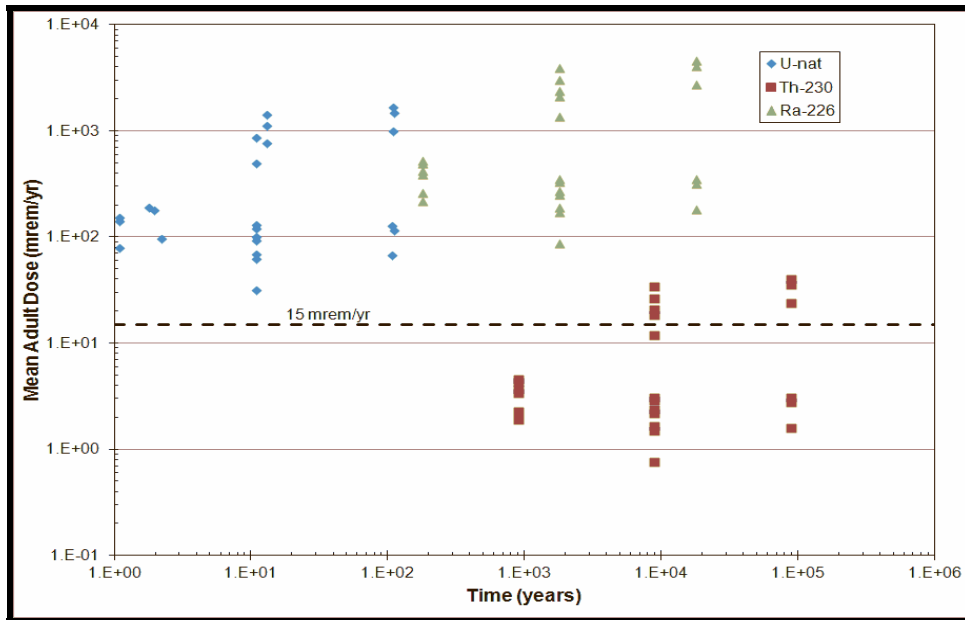


Figure 4-7: Surface Leak Scenario Risk Results versus Time

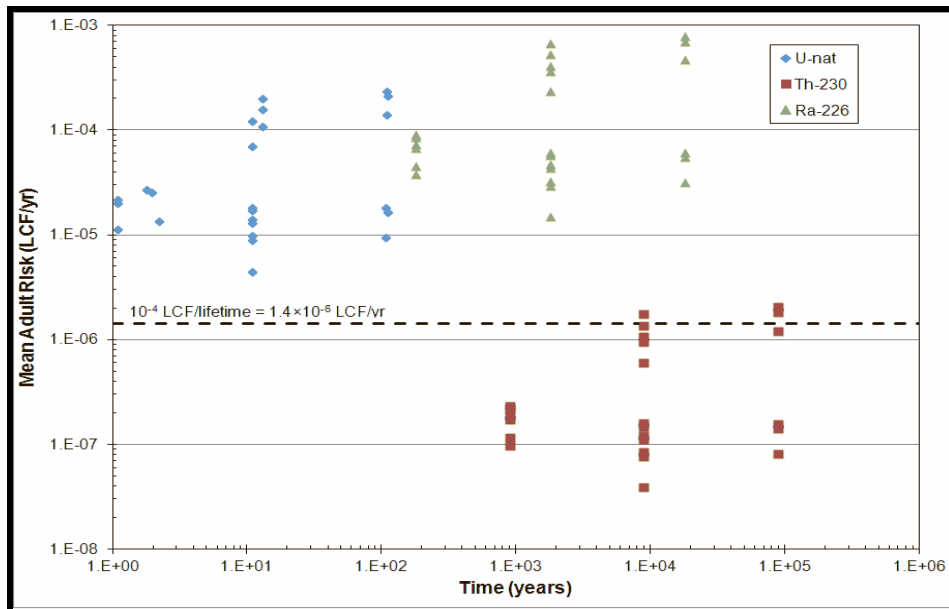


Figure 4-8: Surface Leak Scenario Risk Results versus Time

Table 4-10: Surface Leak Scenario Doses and Risks – Mean Adult

	Dose (mrem/yr)		Risk (LCF/yr)	
	Minimum	Maximum	Minimum	Maximum
U nat	3.2E+01	1.7E+03	4.5E-06	2.4E-04
Th-230	7.6E-01	4.0E+01	3.9E-08	2.0E-06
Ra-226 + P	8.7E+01	4.6E+03	1.5E-05	7.9E-04

Leak scenarios 19 through 24 assumed that leaks of different magnitudes occurred for 28 days. Figure 4-9 shows the doses due to uranium as a function of the various leak rates at each of the four assumed receptor well locations. As Figure 4-9 shows, there is almost a linear relationship between the amount of leaking lixiviant and the doses received at the receptor wells.

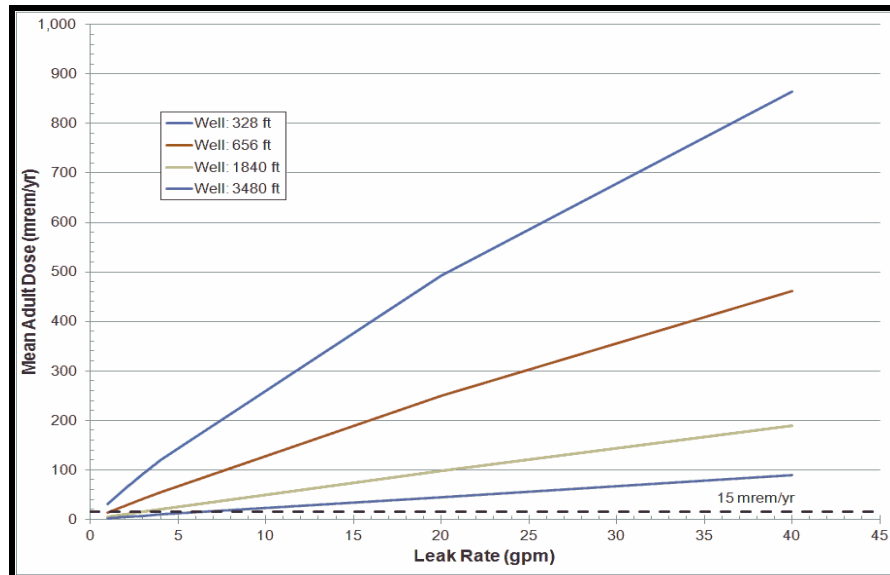


Figure 4-9: 28 Day Surface Leak Scenario Doses from Uranium

4.4 Risks to Non-standard Receptors

All of the doses and risks discussed in Section 4.3 were based on the receptor being an adult with mean usage rates, i.e., the adult mean PDCF and PRCFs from Tables 3-10 and 3-11, respectively. This was the approach taken in CAP88 to demonstrate compliance with 40 CFR Part 61, Subpart H. However, it is recognized that there may be individuals living near the ISL facility who are not adults, or who have usage rates that significantly deviate from the mean. To address those individuals, this section describes the results of calculations that have been performed for non-standard dose and risk receptors.

In Chapter 3, PDCF and PRCF were developed for a number of non-standard receptors, including:

- 90th Percentile Adult – an individual who has increased usage rates, such that his/her PDCF and PRCF are at the 90th percentile, as calculated from the usage rate distributions described in Chapter 3. Only 10% of adults would be expected to have larger PDCF and PRCF than this individual.
- Mean Teenager – an individual who is between the age of about 13 and 19 years old, with mean usage rates.
- Mean Child – an individual who is between the age of about 1 and 12 years old, with mean usage rates.
- Mean Infant – an individual who is less than 1-year old, with mean usage rates.

- Native American – an adult individual with exposure pathways and usage rates that are typical for a Native American (e.g., exposure during a Sweat Lodge Ceremony).

Refer to Section 3.4 for more information and discussion of the Native American exposure pathways and usage rates, and to Section 3.2 for more information regarding the other non-standard receptors. The Native American PDCFs and PRCFs are given in Table 3-20, while Tables 3-10 and 3-11 give the PDCFs and PRCFs for the other non-standard receptors, respectively.

Table 4-11 and Table 4-12 show the calculated doses and risks to the non-standard receptors for the excursion and leak scenarios, respectively. Notice that for the excursion scenarios, only the maximum dose and risks are presented in Table 4-11, while in Table 4-12, both the maximum and minimum doses and risks are presented. This was done because the minimum doses and risks for some of the excursion scenarios are negligibly small. For Table 4-11 and Table 4-12, it is apparent that the Mean Infant is the recipient of the largest calculated doses and risks.

Table 4-11: Excursion Scenario Non-standard Receptor Doses and Risks^a

Receptor	Nuclide	Maximum	
		Dose (mrem/yr)	Risk (LCF/yr)
90 th Percentile Adult	U nat	1.7E+04	2.5E-03
	Th-230	4.4E+02	2.2E-05
	Ra-226	4.7E+04	8.2E-03
Mean Teenager	U nat	9.6E+03	2.9E-03
	Th-230	1.5E+02	1.8E-05
	Ra-226	4.2E+04	8.2E-03
Mean Child	U nat	8.7E+03	5.1E-03
	Th-230	1.2E+02	1.9E-05
	Ra-226	5.6E+04	1.5E-02
Mean Infant	U nat	2.7E+04	8.5E-03
	Th-230	1.7E+03	5.3E-05
	Ra-226	1.5E+05	1.6E-02
Native American	U nat	2.5E+04	4.3E-03
	Th-230	7.8E+02	4.0E-05
	Ra-226	5.7E+04	1.0E-02

a – Doses for Ra-226 include progeny

Table 4-12: Leak Scenario Non-standard Receptor Doses and Risks^a

Receptor	Nuclide	Dose (mrem/yr)		Risk (LCF/yr)	
		Minimum	Maximum	Minimum	Maximum
90 th Percentile Adult	U nat	5.4E+01	2.9E+03	7.7E-06	4.1E-04
	Th-230	1.4E+00	7.2E+01	7.0E-08	3.7E-06
	Ra-226	1.5E+02	7.8E+03	2.6E-05	1.4E-03
Mean Teenager	U nat	3.0E+01	1.6E+03	9.1E-06	4.8E-04
	Th-230	4.5E-01	2.4E+01	5.7E-08	3.0E-06
	Ra-226	1.3E+02	7.0E+03	2.6E-05	1.3E-03
Mean Child	U nat	2.7E+01	1.4E+03	1.6E-05	8.4E-04
	Th-230	3.6E-01	1.9E+01	5.9E-08	3.1E-06
	Ra-226	1.7E+02	9.2E+03	4.8E-05	2.6E-03
Mean Infant	U nat	8.4E+01	4.4E+03	2.7E-05	1.4E-03

Table 4-12: Leak Scenario Non-standard Receptor Doses and Risks^a

Receptor	Nuclide	Dose (mrem/yr)		Risk (LCF/yr)	
		Minimum	Maximum	Minimum	Maximum
Native American	Th-230	5.4E+00	2.8E+02	1.6E-07	8.7E-06
	Ra-226	4.7E+02	2.5E+04	5.1E-05	2.7E-03
	U nat	7.8E+01	4.1E+03	1.3E-05	7.1E-04
Native American	Th-230	2.4E+00	1.3E+02	1.2E-07	6.5E-06
	Ra-226	1.8E+02	9.4E+03	3.2E-05	1.7E-03

a – Doses for Ra-226 include progeny

The doses and risks to the non-standard receptors in Table 4-11 and Table 4-12 can be compared to the dose and risks presented in Table 4-9 for the excursion scenarios and Table 4-10 for the leak scenarios. This comparison shows that the Mean Infant doses and risks are about a factor of three to eight times larger than the standard receptor doses and risks. The dose and risk ratios of the other non-standard receptors to the standard receptor are less than for the Mean Infant. For example, the Native American has a calculated maximum uranium risk that is three times greater than the standard receptor’s uranium risk for both excursion and leak scenarios. Also, the Native American’s maximum Ra-226 dose is two times greater than the standard receptor’s Ra-226 dose.

Finally, in Chapter 3, PDCFs and PRCFs were developed for a number of potential receptors who have not been included in this analysis, e.g., 90th Percentile Infant. If it is desired to include any of these individuals, that can be accomplished by simply multiplying the results shown in Table 4-11 and/or Table 4-12 by the ratio of the PDCFs or PRCFs, whichever is appropriate.

4.5 Non-Radiological Risks

In addition to radiological risks, the lixiviant used to leach the uranium from the ore will contain other potentially hazardous constituents. A screening calculation has been performed in order to obtain an indication as to how hazardous these other constituents in the lixiviant may be to an individual located at the nearest receptor well. The screening calculation consisted of comparing the well water concentration of the potentially hazardous constituents to the Safe Drinking Water Act concentration limits for that constituent.

Maximum lixiviant concentrations were obtained from NUREG/CR-6733 (CNWRA 2001, Table 4-7), with additional lixiviant concentrations from NUREG/CR-6970 for Highlands and Crow Butte (Davis and Curtis, 2007, Tables 3 and 5), as well as Smith Ranch Mine Unit B (MUB) (Power Resources 2004, Table 4), and Christensen MU2 and MU3 (COGEMA, 2008, MU2 Table 5.1 and MU3 Table 5.1). Table 4-13 shows all of the lixiviant concentrations at the end of mining that were collected.

Table 4-13 also provides the maximum concentration limit (MCL) for each of the potentially hazardous constituents. An MCL is the legal threshold limit on the amount of a substance that is allowed in public water systems under the Safe Drinking Water Act. When an MCL is unavailable, the Lifetime Health Advisory (HA) concentration is provided. The Lifetime HA is the concentration of a chemical in drinking water that is not expected to cause any adverse noncarcinogenic effects for a lifetime of exposure. Both the MCLs and the Lifetime HAs were

obtained from the 2011 Edition of the Drinking Water Standards and Health Advisories (EPA 2011a).

Table 4-13: Highest Contaminant Levels in Pregnant Lixiviant (mg/L)

Contaminant	NUREG/C R-6733	Crow Butte	Highland	Smith Ranch	Christensen MU2	Christensen MU3	Limit	Type
Ammonium	N.P.	0.37	0.1	0.52	0.52	1.14	30	Life-time
Arsenic	0.3	0.002	0.001	0.008	0.12	0.02	0.01	MCL
Barium	0.6	0.1	0.1	0.1	0.1	0.1	2	MCL
Boron	0.2	0.93	0.1	0.1	0.1	0.1	6	Life-time
Cadmium	0.01	0.006	0.01	0.01	0.01	0.01	0.005	MCL
Chloride	1800	204	4.7	232	122.9	155.4	4	MCL
Chromium	0.03	<0.03	0.05	0.1	0.05	0.05	0.1	MCL
Copper	0.04	0.017	0.01	0.01	0.01	0.01	1.3	MCL
Fluoride	1	0.69	0.2	0.1	0.1	0.1	4	MCL
Lead	0.01	0.031	0.05	0.1	0.05	0.05	0.015	MCL
Manganese	6	0.11	0.03	0.9	0.66	0.69	0.3	Life-time
Mercury	<0.0001	0.001	0.001	0	0.001	0.001	0.002	MCL
Molybdenum	62	0.069	0.1	0.1	0.1	0.1	0.04	Life-time
Nickel	0.09	0.034	0.05	0.07	0.12	0.05	0.1	Life-time
Nitrate	1	0.05	0	0.3	0.22	0.1	1	MCL
Nitrite	N.P.	0.01	0	0.1	0.12	0.1	10	MCL
Selenium	5	0.003	0.001	0.806	6.33	4.34	0.05	MCL
Uranium	250	0.092	0.05	22.3	11.75	15.58	0.03	MCL
Zinc	N.P.	0.036	0.01	0.11	0.05	0.01	2	Life-time

For each potentially hazardous constituent, Table 4-14 first shows the maximum lixiviant concentration (mg/L) from Table 4-13, and then shows the MCL (or Lifetime HA) divided by the maximum concentration. If the quotient is 1 or greater than that constituent is not at a hazardous concentration in the ore zone or at the nearest receptor well.

Finally, as stated previously (Section 4.3.2) there were 37 excursion scenarios that met the hydraulic data criteria and were included in the dose and risk analysis. Each potentially hazardous constituent concentration was compared to each analyzed scenario's dilution coefficient at the receptor well. For each constituent Table 4-14 shows the number of scenarios that have dilution coefficients which would reduce the concentration at the receptor well to below the MCL (or Lifetime HA). For example, there are 11 analyzed scenarios resulting in dilution coefficients that reduce the maximum molybdenum concentration at the receptor well to below the molybdenum Lifetime HA. The final column of Table 4-14 simply shows the percentage of scenarios that have constituent concentrations above the MCL (or Lifetime HA).

Table 4-14: Scenario Maximum Contaminant Levels Versus Limit

Contaminant	Maximum (mg/L)	Source	Limit Maximum	Scenarios Below Limit at Receptor Well	Scenarios Above Limit at Receptor Well
Nitrite	0.12	Christensen MU2	83.3	37	0.0%
Copper	0.04	NUREG/CR-6733	32.5	37	0.0%
Ammonium	1.14	Christensen MU3	26.3	37	0.0%

Table 4-14: Scenario Maximum Contaminant Levels Versus Limit

Contaminant	Maximum (mg/L)	Source	Limit Maximum	Scenarios Below Limit at Receptor Well	Scenarios Above Limit at Receptor Well
Zinc	0.11	Smith Ranch	18.2	37	0.0%
Boron	0.93	Crow Butte	6.45	37	0.0%
Fluoride	1	NUREG/CR-6733	4.00	37	0.0%
Barium	0.6	NUREG/CR-6733	3.33	37	0.0%
Mercury	0.001	Multiple Sources	2.00	37	0.0%
Chromium	0.1	Smith Ranch	1.00	37	0.0%
Nitrate	1	NUREG/CR-6733	1.00	37	0.0%
Nickel	0.12	Christensen MU2	0.83	37	0.0%
Cadmium	0.01	Multiple Sources	0.50	36	2.7%
Lead	0.1	Smith Ranch	0.15	33	10.8%
Manganese	6	NUREG/CR-6733	0.050	24	35.1%
Arsenic	0.3	NUREG/CR-6733	0.033	24	35.1%
Selenium	6.33	Christensen MU2	0.0079	17	54.1%
Chloride	1800	NUREG/CR-6733	0.0022	17	54.1%
Molybdenum	62	NUREG/CR-6733	0.00065	11	70.3%
Uranium	250	NUREG/CR-6733	0.00012	7	81.1%

From Table 4-14 it can be seen that there are about five (5) lixiviant constituents (in addition to uranium), which could have concentrations significantly above the MCL (or Lifetime HA). Also, there are three (3) lixiviant constituents (i.e., nickel, cadmium, and lead), which have receptor well concentration which are borderline hazardous. Finally, there are 10 lixiviant constituents which are unlikely to be at hazardous concentrations, even within the ore zone.

5.0 SUMMARY AND CONCLUSIONS

5.1 Ground Water Modeling Studies

Ground water modeling studies, described in Chapter 3, considered scenarios involving excursions of contaminants from an ore-bearing aquifer and surface spills or leakage from process components. Simulations of excursions within the ore zone aquifer evaluated the sensitivity of the relative concentrations at down-gradient receptor wells to selected parameters. Variables examined in these excursion simulations included:

- Well spacing (50, 150, and 250 ft)
- Hydraulic conductivity (1, 10, and 100 ft/day)
- Hydraulic gradient (0.001, 0.01, and 0.1 ft/ft)
- Pumping pattern (5-spot, multiple 5-spot, and 7-spot)
- Injection rates (7, 50, 150, and 500 gpm)
- Ore zone thickness (20 and 70 ft)

It is difficult to develop broad, general conclusions from these excursion simulations, because results of comparisons designed into the modeling runs are at times counter-intuitive. In spite of this difficulty, some conclusions are provided below. However, the reader is cautioned to read the full text in Chapter 3 to understand the limitations of these conclusions.

- As expected, steeper hydraulic gradients result in shorter travel times. Furthermore, since the pumping/injection wells are altering the regional hydraulic gradients, the arrival times are not linearly scaled.
- An increase in hydraulic conductivity causes the contaminant plume to become more dispersed and leads to lower relative peak concentrations.
- At higher regional gradients, wider well spacings provide better capture of the lixiviant. At lower regional hydraulic gradients, however, better capture can be maintained at smaller well spacings.
- The 7-spot well configuration results in lower relative peak concentrations for all of the runs, as compared to a 5-spot pattern.
- The effect of pumping/injection on hydraulic gradients is strongly affected by the transmissivity (i.e., hydraulic conductivity multiplied by thickness) of the geologic units. The lower transmissivity results in shorter times to peak arrivals at the low and high gradients, and a longer time at the medium gradient. These relationships are all related to how the regional and localized gradients created by the pumping/injection interact to form a capture zone. This also illustrates the complexity and need to understand the site-specific geology and flow system, since the effects of the interactions are not always intuitive.
- Comparison of a single 5-spot pattern with a multiple (25) 5-spot pattern shows that relative concentrations at down-gradient receptor wells are lower with the multiple 5-spot pattern. These results are explained by the larger capture zone that is created by the array of pumping/extraction wells.

As described in Chapter 3, 24 scenarios were analyzed, which postulated the spill of lixiviant onto the ground, with subsequent leakage into the ground water and transport to an offsite receptor well. The scenarios included (1) catastrophic spills ranging from 100,000 to 200,000 gallons, (2) a slow leak of 1 to 2 gpm for period of 3 years, and (3) leaks varying from 1 to 45 gpm over a 28-day period.

Transport from the mined aquifer to an overlying aquifer through an abandoned borehole that was not properly cemented was also evaluated. This excursion scenario can result in significant down-gradient leakage. This emphasizes the need to carefully cement and inspect abandoned boreholes to insure their integrity.

5.2 Pathway Dose and Risk Conversion Factors

In Chapter 2, probabilistic dose and risk pathway conversion factors were developed for the ingestion pathway for four age groups (infants, children, teens and adults) and five radionuclides of importance in the ISL process (Ra-226+P, Pb-210, Th-230, U-234, and U-238). The individual radionuclide-specific dose and risk conversion factors were based on FGR 13 and supporting documentation. Contributions of the various components of the ingestion pathway to dose and risk for adults are summarized in Table 5-1. Except for Ra-226, drinking water accounts for about three-quarters of the total ingestion dose/risk. With Ra-226, ingestion of vegetables is more significant than for the other radionuclides, accounting for about 35% of the total ingestion dose/risk.

Table 5-1: Typical Pathway Contributions to the Adult PDCF and PRCF

Pathway – Adult	Pb-210+P	Ra-226+P	Th-230	U-234	U-238+P
Ingestion of Drinking Water	78.3%	51.2%	82.8%	76.2%	76.2%
Inadvertent Ingestion of Soil	0.1%	0.2%	0.3%	0.3%	0.3%
Ingestion of Vegetables	15.7%	35.3%	16.4%	16.1%	16.1%
Ingestion of Meat	2.3%	2.9%	0.3%	2.4%	2.4%
Ingestion of Milk	3.5%	10.5%	0.2%	5.0%	5.0%

Table 5-2 summarizes the pathway contributions from uranium exposure for each age group. The shift from the dominance of the milk pathway to the drinking water pathway with increasing age from child to adult is apparent.

Table 5-2: Typical Pathway Contributions to the PDCF and PRCF for U-234 or U-238

Pathway – Adult	Adult	Teen	Child	Infant
Ingestion of Drinking Water	76.2%	68.1%	54.2%	81.2%
Inadvertent Ingestion of Soil	0.3%	0.5%	1.4%	1.6%
Ingestion of Vegetables	16.1%	17.2%	17.3%	10.2%
Ingestion of Meat	2.4%	3.4%	2.8%	0.0%
Ingestion of Milk	5.0%	10.9%	24.3%	6.9%

The pathway analysis for Native Americans was expanded from that of a standard receptor to address exposures associated with sweat lodge rituals. This included additional drinking water consumption, submersion in a cloud of contaminated vapor, and inhalation of contaminated

vapor. The deterministic dose conversion factor for a Native American for natural uranium (i.e., U-234+U-238) is 4.05E-04 mrem/yr per pCi/m³, as compared to the 90th percentile dose conversion factor for a standard adult receptor of 2.73E-04 mrem/yr per pCi/m³.

5.3 Dose/Risk Assessment for Modeled Scenarios

Doses and risks are calculated in Chapter 4 for some of the ground water flow and transport scenarios modeled in Chapter 3. All modeling results in Chapter 3 excluded effects of retardation and assumed a source term of 1 mg/L. In Chapter 4, source terms were selected based on operating experience at ISL facilities, and included effects of retardation at down-gradient wells. Distribution coefficients used to calculate the retardation factors were selected as minimum reasonable values to reduce the travel time from the source to the receptor. As described in Chapter 3, some combinations of hydrogeologic parameters, such as hydraulic conductivity and hydraulic gradient, may lie outside the range expected at operating ISL sites, but were included to examine the sensitivity of the modeling results to a range of parameters. In Chapter 4, doses and risks were calculated only for those excursion scenarios with combinations of hydraulic conductivity and hydraulic gradient that had been reported at operating ISL sites (i.e., gradient × conductivity < 0.13 ft/day). The product of hydraulic conductivity times hydraulic gradient was used as a surrogate for ground water velocity (i.e., hydraulic conductivity × gradient ÷ effective porosity). An empirical cumulative distribution function was developed from the site data and served to limit the range of parameters for which doses and risks for excursion scenarios were calculated.

Prior to calculating doses and risks for the selected modeling scenarios, scoping calculations were performed to illustrate the allowable radionuclide source term concentrations for representative dose and risk limits. Limiting concentrations were derived for an assumed dose limit of 15 mrem/yr and a lifetime risk limit of 10⁻⁴ latent cancer fatalities (LCF), or, assuming a 70-year life expectancy, an annual risk limit of 1.4 × 10⁻⁶ LCF/yr. The limiting radionuclide concentrations shown in Table 5-3 were calculated using the adult mean pathway dose and risk conversion factors (PDCFs and PRCFs) derived in Chapter 2. The distance from the source to the receptor well was 528 ft.

Table 5-3: Radionuclide Source Term Limiting Concentrations – Receptor Well at 528 ft

Nuclide	15 mrem/yr Dose Limit		10 ⁻⁴ LCF Lifetime Risk Limit	
	(pCi/L)	(mg/L)	(pCi/L)	(mg/L)
U-238	97	2.8E-01	63	1.8E-01
U-234	93	1.5E-05	65	1.0E-05
U-natural	95	1.4E-01	64	9.4E-02
Th-230	25	1.2E-06	47	2.2E-06
Ra-226	1.2	1.2E-09	0.6	6.3E-10
Ra-226+P	2.4	3.1E-11	1.3	1.7E-11
Pb-210	97	2.8E-01	63	1.8E-01

As Table 5-3 demonstrates, a lifetime risk limit of 10⁻⁴ LCF is slightly more restrictive than a dose limit of 15 mrem/yr for all the radionuclides except Th-230. However, for all of the radionuclides considered, dose- and risk-limiting concentrations are within a factor of two.

Of the 31 unique excursion simulations (37 total) within the ore-bearing aquifer that met the conductivity \times gradient cutoff of 0.13 ft/day, the dose from uranium was <15mrem/yr in 13 simulations. The highest estimated dose from uranium at a receptor well 528 ft down-gradient was 10,072 mrem/yr for Run 6i, while the lowest estimated dose was 1.69E-12 mrem/yr for Run 5g. Table 5-4 summarizes these excursion simulations. Doses from uranium (U-234 + U-238) are included in the last column for those simulations with a conductivity \times gradient product <0.13 ft/day. Runs where the uranium dose was less than 15 mrem/yr are highlighted in yellow.

Table 5-4: Summary of Excursion Runs

Run	Hydraulic Gradient	Hydraulic Conductivity (ft/day)	Well Spacing (ft)	Pumping Array	Pumping Rate (gpm)	Max. Relative Concentration at 528 ft	Ore Zone Thickness (ft)	U nat Dose ^a (mrem/yr)
1a	0.1	100	250	5-spot	153	6.94E-03	75	
1b	0.01	100	250	5-spot	153	6.54E-02	75	
1c	0.001	100	250	5-spot	153	9.32E-02	75	1.50E+03
1d	0.1	1	250	5-spot	153	2.14E-01	75	3.44E+03
1e	0.1	10	250	5-spot	153	6.55E-02	75	
1f	0.1	100	250	5-spot	153	6.94E-03	75	
1g	0.01	1	250	5-spot	153	1.80E-04	75	2.90E+00
1h	0.01	10	250	5-spot	153	9.27E-02	75	1.49E+03
1i	0.01	100	250	5-spot	153	6.54E-02	75	
2a	0.1	100	50	5-spot	153	9.62E-03	75	
2b	0.01	100	50	5-spot	153	2.35E-02	75	
2c	0.001	100	50	5-spot	153	8.75E-03	75	1.41E+02
2d	0.1	1	50	5-spot	153	1.18E-02	75	1.90E+02
2e	0.1	10	50	5-spot	153	2.35E-02	75	
2f	0.1	100	50	5-spot	153	9.62E-03	75	
2g	0.01	1	50	5-spot	153	3.39E-06	75	5.45E-02
2h	0.01	10	50	5-spot	153	8.22E-03	75	1.32E+02
2i	0.01	100	50	5-spot	153	2.35E-02	75	
3a	0.1	100	250	7-spot	153	2.78E-03	75	
3b	0.01	100	250	7-spot	153	3.53E-02	75	
3c	0.001	100	250	7-spot	153	6.79E-02	75	1.09E+03
3d	0.1	1	250	7-spot	153	1.41E-01	75	2.27E+03
3e	0.1	10	250	7-spot	153	3.53E-02	75	
3f	0.1	100	250	7-spot	153	2.78E-03	75	
3g	0.01	1	250	7-spot	153	4.46E-05	75	1.70E+00
3h	0.01	10	250	7-spot	153	6.75E-02	75	1.09E+03
3i	0.01	100	250	7-spot	153	3.53E-02	75	
4a	0.1	100	50	7-spot	153	1.25E-02	75	
4b	0.01	100	50	7-spot	153	4.03E-02	75	
4c	0.001	100	50	7-spot	153	9.01E-03	75	1.45E+02
4d	0.1	1	50	7-spot	153	3.07E-02	75	4.94E+02
4e	0.1	10	50	7-spot	153	4.03E-02	75	
4f	0.1	100	50	7-spot	153	1.25E-02	75	
4g	0.01	1	50	7-spot	153	2.14E-06	75	3.44E-02
4h	0.01	10	50	7-spot	153	8.94E-03	75	1.44E+02
4i	0.01	100	50	7-spot	153	4.03E-02	75	
5a	0.1	10	150	5-spot	51	3.76E-02	75	
5b	0.01	10	150	5-spot	51	6.79E-02	75	1.09E+03
5c	0.001	10	150	5-spot	51	8.24E-04	75	1.33E+01

Table 5-4: Summary of Excursion Runs

Run	Hydraulic Gradient	Hydraulic Conductivity (ft/day)	Well Spacing (ft)	Pumping Array	Pumping Rate (gpm)	Max. Relative Concentration at 528 ft	Ore Zone Thickness (ft)	U nat Dose ^a (mrem/yr)
5d	0.01	1	150	5-spot	7.15	1.53E-02	75	2.46E+02
5e	0.01	10	150	5-spot	51	6.79E-02	75	1.09E+03
5f	0.01	100	150	5-spot	510	1.01E-01	75	
5g	0.001	1	150	5-spot	7.15	1.05E-16	75	1.69E-12
5h	0.001	10	150	5-spot	51	8.24E-04	75	1.33E+01
5i	0.001	100	150	5-spot	510	1.08E-01	75	1.74E+03
6a	0.1	10	150	5-spot	51	3.31E-01	20	
6b	0.01	10	150	5-spot	51	4.75E-01	20	7.64E+03
6c	0.001	10	150	5-spot	51	1.30E-03	20	2.09E+01
6d	0.01	1	150	5-spot	7.15	1.06E-01	20	1.70E+03
6e	0.01	10	150	5-spot	51	4.75E-01	20	7.64E+03
6f	0.01	100	150	5-spot	510	6.45E-01	20	
6g	0.001	1	150	5-spot	7.15	3.07E-13	20	1.19E+00
6h	0.001	10	150	5-spot	51	1.30E-03	20	2.09E+01
6i	0.001	100	150	5-spot	510	6.26E-01	20	1.01E+04
7a	0.1	10	150	25 × 5-spot	51	3.12E-01	20	
7b	0.01	10	150	25 × 5-spot	51	6.61E-04	20	1.06E+01
7c	0.001	10	150	25 × 5-spot	51	2.70E-04	20	4.34E+00
7d	0.01	1	150	25 × 5-spot	7.15	8.11E-06	20	3.78E-01
7e	0.01	10	150	25 × 5-spot	51	6.61E-04	20	1.06E+01
7f	0.01	100	150	25 × 5-spot	510	1.10E-02	20	
7g	0.001	1	150	25 × 5-spot	7.15	5.25E-05	20	8.44E-01
7h	0.001	10	150	25 × 5-spot	51	2.70E-04	20	4.34E+00
7i	0.001	100	150	25 × 5-spot	510	4.50E-04	20	7.24E+00

a – Dose at receptor well 528 ft down-gradient for simulations where hydraulic conductivity × gradient < 0.13 ft/day

A breakdown of the unique simulations resulting in doses above and below 15 mrem/yr as a function of the conductivity × gradient product is presented in Table 5-5. It is clear that for most of the simulations with a dose of less than 15 mrem/yr, the product of hydraulic conductivity and gradient is 0.01 or less. However, in 10% of the cases, a conductivity × gradient product of 0.01 resulted in doses greater than 15 mrem/yr.

Table 5-5: Number of Simulations Resulting in Various Dose Levels as Function of Conductivity × Gradient Product

Conductivity (K) × Gradient (i)	Number of Simulations	
	Less Than 15 mrem/yr	Greater Than 15 mrem/yr
K × i = 0.1	2	16
K × I = 0.01	7	3
K × I = 0.001	3	0

To evaluate the effects of retardation on ground water transport, distribution coefficients were selected from the literature based on reasonable minimum values to reduce the travel time from the source wellfield to a down-gradient receptor well. Minimum peak travel times to a receptor well 528 ft down-gradient are about 20 years for uranium, about 3,000 years for radium and about 15,000 years for thorium. The significance is that, if any lixiviant escapes undetected from

the ring of monitor wells surrounding a wellfield, an appreciable amount of time will elapse before the radionuclide arrives at the receptor well. The elapsed time will exceed the monitoring times at any current ISL facilities.

Table 5-6 (which repeats Table 4-9) shows the maximum calculated dose for each radionuclide from all excursion scenarios that were analyzed for dose and risk as shown in Table 5-4. These values are mean adult exposures for a receptor well 528 ft down-gradient.

Table 5-6: Excursion Scenario Maximum Doses and Risks

Nuclide	Dose (mrem/yr)	Risk (LCF/yr)
U nat	1.0E+04	1.4E-03
Th-230	2.4E+02	1.2E-05
Ra-226+P	2.8E+04	4.8E-03

As described in Chapter 4 (Section 4.3.3), three surface leakage scenarios were evaluated: (1) catastrophic spills ranging from 100,000 to 200,000 gallons, (2) a slow leak of 1 to 2 gpm for period of 3 years, and (3) leaks varying from 1 to 40 gpm over a 28-day period. The highest doses were incurred for scenarios involving a slow leak over a 3-year period, while the lowest doses resulted from a 1-gpm surface leak over a 28-day period. In all cases, the mean annual doses to an adult from U nat were greater than 15 mrem. Results for all leakage scenarios are summarized in Table 5-7. These results emphasize the importance of detecting small leaks through adequate instrumentation and frequent inspections of process piping. Automatic shut-off controls should be used to minimize surface spills.

Table 5-7: Summary of Dose Rate for Leak Scenarios – Adult Male Exposed to U nat at Receptor Well 328 ft Down-gradient

Leak Scenario	Minimum Dose Rate (mrem/yr)	Maximum Dose Rate (mrem/yr)
Surface Spill (100,000–200,000 gal.)	6.7E+01 (Run L4)	1.5E+02 (Run L9)
Slow Leak (1–2 gpm) – 3 Years	9.5E+01 (Run L15)	1.7E+03 (Run L16)
Variable Leak (1–40 gpm) – 28 days	3.2E+01 (Run L19)	8.7E+02 (Run L24)

Doses and risks to non-standard receptors are compared to those for 90th percentile adults (relative dose/risk = 1.00) in Table 5-8. The basis for comparison is the excursion scenario, which occurs within the ore-bearing aquifer and where the receptor obtains water from a well 528 ft down-gradient. Doses and risks for the Mean Infant and Native American were greater than for the 90th percentile adult receptor for all radionuclides evaluated. Relative doses for the mean teenager and the mean child (except for Ra-226+P) were lower than for the 90th percentile adult. For example, doses and risks to Native Americans were greater by factors of about 1.2 to 1.8 than for the 90th percentile adult. Clearly, doses to several of the non-standard receptors do not fall within a reasonable upper limit for the standard receptor doses.

Table 5-8: Comparison of Excursion Scenario Non-standard Receptor Doses and Risks Relative to 90th Percentile Adult

Receptor	Nuclide	Maximum	
		Relative Dose	Relative Risk
90 th Percentile Adult	U nat	1.00	1.00
	Th-230	1.00	1.00
	Ra-226+P	1.00	1.00
Mean Teenager	U nat	0.55	1.18
	Th-230	0.33	0.81
	Ra-226+P	0.89	0.99
Mean Child	U nat	0.50	2.06
	Th-230	0.27	0.84
	Ra-226+P	1.17	1.88
Mean Infant	U nat	1.55	3.46
	Th-230	3.92	2.34
	Ra-226+P	3.17	1.97
Native American	U nat	1.44	1.74
	Th-230	1.78	1.76
	Ra-226+P	1.20	1.26

6.0 REFERENCES

- Abbott M.L., and A.S. Rood, 1993. "COMIDA: A Radionuclide Food Chain Model for Acute Fallout Deposition," Idaho National Engineering Laboratory, EGG-GEO-10367, Revision O. November 1993.
- ANL (Argonne National Laboratory) 2000. "Development of Probabilistic RESRAD 6.0 and RESRAD-BUILD 3.0 Computer Codes," prepared for U.S. Nuclear Regulatory Commission, NUREG/CR-6697, ANL/EAD/TM-98, November.
- ANL (Argonne National Laboratory) 2001. "User's Manual for RESRAD Version 6," Environmental Assessment Division, ANL/EAD-4, July.
- ATSDR (Agency for Toxic Substances and Disease Registry) 2010. "Public Health Assessment for Midnite Mine Site, Wellpinit, Stevens County, Washington, EPA Facility ID: WAD980978753, May 19.
- CBR (Crow Butte Resources, Inc.). 2007. "SUA-1535 License Renewal Application." Crawford, Nebraska: Crow Butte Resources, Inc. November 2007.
- CDC (Centers for Disease Control and Prevention) 2011. "Breastfeeding Report Card — United States, 2011." August 2011.
- Chowdhury, A.H., and R.E. Mace, 2007. Groundwater resource evaluation and availability model of the Gulf Coast aquifer in the Lower Rio Grande Valley of Texas: Texas Water Development Board, Report 368, 119 p.
- CNWRA (Center for Nuclear Waste Regulatory Analyses) 2001. "A Baseline Risk-Informed, Performance-Based Approach for In Situ Leach Uranium Extraction Licensees." NUREG-CR/6733. September 2001.
- COGEMA 2008. *Wellfield Restoration Report Christensen Ranch Project, Wyoming*. COGEMA Mining, Inc, and Petrotek Engineering Corp, NRC ADAMS Accession Number: ML081060131. March 5, 2008.
- Crow Butte 1995. Application for Renewal of USNRC Source Materials License SUA-1534. Crow Butte Resources, Inc. ML082140217.
- Davis, J.A. and G.P. Curtis, 2007. NUREG/CR-6870, "Consideration of Geochemical Issues in Groundwater Restoration at Uranium In-Situ Leaching Mining Facilities." Washington, DC: Nuclear Regulatory Commission. January 2007.
- DBS&A (Daniel B. Stephens and Associates, Inc.) 2007. "Evaluation of Potential Impacts Related to Proposed Uranium Mining in Goliad County, Texas." Prepared for Goliad County Groundwater Conservation District. June 25, 2007.

Deutsch W.J., W.J. Martin, L.E. Eary, and R.J. Serne, 1985. Methods of Minimizing Ground-Water Contamination from In Situ Leach Uranium Mining: Final Report. PNL-5319, U.S. Nuclear Regulatory Commission (Ed.), Washington, DC.

DOE (U.S. Department of Energy) 1997. "Screening Assessment and Requirements for a Comprehensive Assessment," DOE/RL-96-16, Revision 0, April.

DOE (U.S. Department of Energy) 2010. "River Corridor Baseline Risk Assessment," DOE/RL-2007-21, Volume II, "Human Health Risk Assessment," Part 1, Draft C, December.

Eckerman, K.F., R.W. Leggett, C.B. Nelson, J.S. Puskin, and A.C.B. Richardson, 1999. "Federal Guidance Report No. 13: Cancer Risk Coefficients for Environmental Exposure to Radionuclides," EPA-402-R-99-001, prepared for U.S. Environmental Protection Agency; Office of Radiation and Indoor Air, September.

EPA (U.S. Environmental Protection Agency) 1990. "National Contingency Plan," Federal Register, Volume 55, pages 8665–8865. March 8, 1990.

EPA (U.S. Environmental Protection Agency) 1991. "National Primary Drinking Water Regulation; Final Rule," Federal Register 56(20):3526-3597, January 30.

EIA (Energy Information Administration) 1995. DOE/EIA-0592, "Decommissioning of U.S. Uranium Production Facilities." Energy Information Administration, Office of Coal, Nuclear, Electric, and Alternate Fuels, Washington, DC. February 1995.

EPA (U.S. Environmental Protection Agency) 1999a. "Estimating Radiogenic Cancer Risks Addendum: Uncertainty Analysis," Office of Radiation and Indoor Air, EPA 402-R-99-003. May 1999.

EPA (U.S. Environmental Protection Agency) 1999b. "Understanding Variation in Partition Coefficient, K_d , Values: Volume II: Review of Geochemistry and Available K_d Values for Cadmium, Cesium, Chromium, Lead, Plutonium, Radon, Strontium, Thorium, Tritium (^3H) and Uranium," EPA 402-R-99-004B. Office of Radiation and Indoor Air, Office of Solid Waste and Emergency Response, EPA [and] Office of Environmental Restoration, U.S. Department of Energy, Washington, DC. August 1999.

EPA (U.S. Environmental Protection Agency) 2001. "Public Health and Environmental Radiation Protection Standards for Yucca Mountain, NV: Background Information Document for 40 CFR Part 197," EPA 402-R-01-004. June 2001.

EPA (U.S. Environmental Protection Agency) 2002. Report No. 13, Cancer Risk Coefficients for Environmental Exposure to Radionuclides: Updates and Supplements.

EPA 2004. "Understanding Variation in Partition Coefficient, K_d , Values: Volume III: Review of Geochemistry and Available K_d Values for Americium, Arsenic, Curium, Iodine, Neptunium, Radium and Technetium." EPA 402-R-99-004C. Office of Radiation and Indoor Air. July 2004.

- EPA 2005. "Guidance on Selecting Age Groups for Monitoring and Assessing Childhood Exposures to Environmental Contaminants," EPA/630/P-03/003F, November 2005.
- EPA (U.S. Environmental Protection Agency) 2008. "Radiation Protection Standards for Yucca Mountain," Federal Register, Volume 73, pages 61256- 61289. October 15, 2008.
- EPA (U.S. Environmental Protection Agency) 2009. "2009 Water Sense Single-Family New Home Specification, Supporting Statement," Version 1.0, December 9.
- EPA (U.S. Environmental Protection Agency) 2011a. "2011 Edition of the Drinking Water Standards and Health Advisories," Office of Water, EPA 820-R-11-002. January 2011.
- EPA (U.S. Environmental Protection Agency) 2011b. "Exposure Factors Handbook: 2011 Edition," National Center for Environmental Assessment, EPA/600/R-090/052F. September.
- Freeze, R.A. and J. Cherry, 1979. "Groundwater," Prentice-Hall, Englewood Cliffs, New Jersey.
- Gelhar, L.W., C. Welty, and K.R. Rehfeldt, 1992. "A critical review of data on field-scale dispersion in aquifers." *Water Resources Research* 28(7):1955-1974.
- Godbee, H.W., 1973. "Use of Evaporation for the Treatment of Liquids in the Nuclear Industry," ORNL-4790. Oak Ridge National Laboratory, Oak Ridge, Tennessee. September 1973.
- Harbaugh, A.W., E.R. Banta, M.C. Hill, and M.G. McDonald, 2000. "MODFLOW-2000, the U.S. Geological Survey Modular Ground-Water Model—User Guide to Modularization Concepts and the Ground-Water Flow Process." U.S. Geological Survey Open-File Report 00-92.
- Harper, B.L., A.K. Harding, T. Waterhous, and S.G. Harris, 2007. "Traditional Tribal Subsistence Exposure Scenario and Risk Assessment Guidance Manual," Oregon State University, Department of Public Health and Confederated Tribes of the Umatilla Indian Reservation, August.
- Harper, B., and D. Ranco, 2009. "Wabanaki Traditional Cultural Lifeways Exposure Scenario," Associated Environmental Scientists & Engineers (AESE) and Dartmouth College, prepared for the U.S. Environmental Protection Agency in collaboration with the Maine Tribes, July 9.
- Harris, S.G. and B.L. Harper, 2004. "Exposure Scenario for CTUIR Traditional Subsistence Lifeways," Department of Science & Engineering, Confederated Tribes of the Umatilla Indian Reservation, September 15.
- Hem, J.D., 1985. "Study and Interpretation of the Chemical Characteristics of Natural Water." USGS Water Supply Paper 2254. Third edition. Reston, Virginia: U.S. Geological Survey.
- Hopke, P.K., 2006. "Exposure and Risks from Showering with Radon-Rich Water." Presented at "Workshop on Radon Occurrence, Health Risks and Policy, With an Emphasis on Radon in Ground Water Drinking Supplies" (October 4).

Hoy, R.N., 2006. *Baseline Ground Water Quality Conditions at In Situ Uranium Wellfields in Wyoming*. Paper presented at the 2006 Billings Land Reclamation Symposium, June 4-8, 2006. Billings Montana. <http://www.asmr.us/Publications/Conference%20Proceedings/2006%20Billings/0246-Hoy-WY-1.pdf>

HRI 1993. "Church Rock Uranium Project Revised Environmental Report. March 16, 1993.

ICRP (International Commission on Radiological Protection), 1996. "Age-dependent Doses to the Members of the Public from Intake of Radionuclides Part 5, Compilation of Ingestion and Inhalation Coefficients," Publication 72, Annals of the ICRP Volume 26/1, September.

ICRP (International Commission on Radiological Protection), 2001. "Doses to the Embryo and Fetus from Intakes of Radionuclides by the Mother," Publication 88, Annals of the ICRP Volume 31/1-3, December.

ICRP (International Commission on Radiological Protection), 2004. "Doses to Infants from Ingestion of Radionuclides in Mothers' Milk," Publication 95, Annals of the ICRP Volume 34/-4, September.

ICRP (International Commission on Radiological Protection), 2006. "Assessing Dose of the Representative Person for the Purpose of the Radiation Protection of the Public," Publication 101, Annals of the ICRP Volume 36/3, September.

ISCORS (Interagency Steering Committee on Radiation Standards), 2002. "A Method for Estimating Radiation Risk from Total Effective Dose Equivalent (TEDE), Final Report," ISCORS Technical Report 2002-02.

Lalman, D., 2004. "Nutrient Requirements of Beef Cattle," E-974, Oklahoma State University, Oklahoma Cooperative Extension Service.

Looper, M.L., and D.N. Waldner, 2002. "Water for Dairy Cattle," New Mexico State University and Oklahoma State University, Guide D-107, February.

Lost Creek 2007. Lost Creek Project Technical Report, Application for U.S. NRC Source Material License," Docket 40-9068, Volume 2. ML081060505.

Mackin, P.C., D. Daruwalla, J. Winterle, M. Smith, and D.A. Pickett, 2001. "A Baseline Risk-Informed Performance-Based Approach for In-Situ Leach Uranium Extraction Licensees." NUREG/CR-6733, U.S. Nuclear Regulatory Commission, Washington, DC. September 2001.

Napier BA, Peloquin, Strenge DL, Ramsdell JV Jr., 1988. "GENII - the Hanford Environmental Radiation Dosimetry Software System. Volume 1: Conceptual Representation, Volume 2: Users' Manual, Volume 3: Code Maintenance Manual," PNL-6584, Pacific Northwest Laboratory, Richland, Washington.

NAS (National Academy of Sciences) 1995. "Technical Bases for Yucca Mountain Standards," National Research Council, Committee on Technical Bases for Yucca Mountain Standards, National Academy Press, Washington, DC. 1995.

NAS (National Academy of Sciences) 1999a, "Risk Assessment of Radon in Drinking Water," Commission on Life Sciences, Washington, DC.

NAS (National Academy of Sciences) 1999b, "Health Effects of Exposure to Radon, BEIR VI," Committee on Health Risks of Exposure to Radon, Washington, DC.

NAS (National Academy of Sciences) 2000. "Nutrient Requirements of Beef Cattle: Seventh Revised Edition: Update 2000," National Research Council.

NAS (National Academy of Sciences) 2001. "Nutrient Requirements of Dairy Cattle: Seventh Revised Edition," National Research Council.

NCRP (National Council on Radiation Protection and Measurements) 1999. "Recommended Screening Limits for Contaminated Surface Soil and Review of Factors Relevant to Site-Specific Studies," Report No. 129, January 29.

Nicot, J-P, B.R. Scanlon, C. Yang, and J.B. Gates, 2010. "Geological and Geographical Attributes of the South Texas Uranium Province." A report prepared for the Texas Commission on Environmental Quality. April 2010.

NRC (U.S. Nuclear Regulatory Commission) 1977. "Calculation of Annual Doses to Man from Routine Releases of Reactor Effluents for the Purpose of Evaluating Compliance With 10 CFR Part 50, Appendix I," Regulatory Guide 1.109, Revision 1, October.

NRC (U.S. Nuclear Regulatory Commission) 1978. "Environmental Statement Related to Operation of Wyoming Mineral Corporation Irigaray Solution Mining Project." NUREG-0399. Docket No. 40-8502. ML091120676.

NRC (U.S. Nuclear Regulatory Commission) 1985. "Calculation of Releases of Radioactive Materials in Gaseous and Liquid Effluents from Pressurized Water Reactors," NUREG-0017, Revision 1, April.

NRC (U.S. Nuclear Regulatory Commission) 1989. "Environmental Assessment by the Uranium Recovery Field Office in Consideration of an Application for a Source Material License for Ferret Exploration Company of Nebraska, Crow Butte Commercial In situ Leach Facility, Dawes County, Nebraska." Docket No, 40-8943. December 12, 1989. ML080740160.

NRC (U.S. Nuclear Regulatory Commission) 1991. "A Regulatory Analysis on Emergency Preparedness for Fuel Cycle and Other Radioactive Material Licensees," NUREG-1140, Reprinted August.

NRC (U.S. Nuclear Regulatory Commission) 1997. "Final Environmental Impact Statement to Construct and Operate the Crownpoint Uranium Solution Mining Project, Crownpoint, New

Mexico.” NUREG-1508. U.S. Nuclear Regulatory Commission, Washington, DC. February 1997.

NRC (U.S. Nuclear Regulatory Commission) 1998. “Effects on Radionuclide Concentrations by Cement/Ground-Water- Interactions in Support of Performance Assessment of Low-Level Radioactive Waste Disposal Facilities.” NUREG/CR-6377. Prepared by K.M. Krupa and R.J. Serne. Pacific Northwest National Laboratory, Richland, Washington.

NRC (U.S. Nuclear Regulatory Commission) 2000. “Inspection Report 40-8964/00-01- Smith Ranch.” U.S. Nuclear Regulatory Commission: Washington, DC. ML003683025.

NRC (U.S. Nuclear Regulatory Commission) 2003. “Standard Review Plan for In Situ Leach Uranium Extraction License Applications.” Final Report. NUREG-1569. Prepared by J. Lusher. Washington, DC. June 2003. ML032250177.

NRC (U.S. Nuclear Regulatory Commission) 2006. “Environmental Assessment for the Addition of the Reynolds Ranch Mining Area to Power Resources, Inc.’s Smith Ranch/Highlands Uranium Project Converse County, Wyoming.” Source Material License No. SUA-1548. Docket No. 40-8964. Nuclear Regulatory Commission, Washington, DC. 2006.

NRC (U.S. Nuclear Regulatory Commission) 2007. “Environmental Assessment Construction and Operation of In Situ Leach Satellite SR-2 Amendment No. 12 to Source Material License No. SUA-1548.” Power Resources, Inc., Smith Ranch-Highland Uranium Project (SR-HUP), Converse County Wyoming. ML071500581.

NRC (U.S. Nuclear Regulatory Commission) 2008. “Compliance with 10 CFR 40.42’s Timely Decommissioning Requirements.” Letter (July 7) from K.I. McConnell to S. Collings, Power Resources, Inc., Nuclear Regulatory Commission, Washington, DC. 2008.

NRC (U.S. Nuclear Regulatory Commission) 2009a. “Uranium Recovery Policy Regarding: (1) The Process for Scheduling Licensing Reviews of Applications for New Uranium Recovery Facilities and (2) The Restoration of Groundwater at Licensed Uranium In Situ Recovery Facilities.” Regulatory Information Summary 2009-05. ADAMS Accession No. ML083510622. NRC. April 29, 2009a.

NRC (U.S. Nuclear Regulatory Commission) 2009b. “Generic Environmental Impact Statement for In-Situ Leach Uranium Milling Facilities.” Chapters 1 through 4, Final Report. Nuclear Regulatory Commission, Washington, DC. May 2009b.

NRC (U.S. Nuclear Regulatory Commission) 2009c. “Environmental Impact Statement for the Nichols Ranch ISR Project in Campbell and Johnson Counties Wyoming.” NUREG-1910 Supplement 2. Draft Report for Comment. ML093340536.

Pawel D.J., R.W. Leggett, K.F. Eckerman, and C.B. Nelson, 2007. “Uncertainties in Cancer Risk Coefficients for Environmental Exposure to Radionuclides, An Uncertainty Analysis for Risk Coefficients Reported in Federal Guidance Report No. 13,” U.S. Environmental Protection Agency and Oak Ridge National Laboratory, ORNL/TM-2006/583, January.

- Pelizza, M.S., 2008. "In-Situ Recovery of Uranium." *Southwest Hydrology* 7:28–29.
- Peterson, H.T., Jr, 1983. "Terrestrial and Aquatic Food Chain Pathways," in Till JE, Meyer HR. *Radiological Assessment, A Textbook on Environmental Dose Analysis*, NUREG/CR-3332, U.S. Nuclear Regulatory Commission, Washington, DC.
- PNL (Pacific Northwest Laboratory) 1988. "GENII - The Hanford Environmental Radiation Dosimetry Software System, Volume 1: Conceptual Representation," PNL-6584, December.
- PNNL (Pacific Northwest National Laboratory) 2006. "Alternative Conceptual Models for Assessing Food-Chain Pathways in Biosphere Models," prepared for U.S. Nuclear Regulatory Commission, Office of Nuclear Regulatory Research, NUREG/CR-6910, PNNL-15872, June.
- PNNL (Pacific Northwest National Laboratory) 2010. "Evaluation of Soil Flushing for Application of Deep Vadose Zone in the Hanford Central Plateau." PNNL-19938. M.J. Truex et al., Pacific Northwest National Laboratory.
- Power Resources 2004. *Mine Unit B Ground Water Restoration Report, Smith Ranch – Highland Uranium Project*. NRC ADAMS Accession Number: ML091831100.
- PRI (Power Resources Inc.) 2006. "North Butte ISL Satellite Project, Campbell County, Wyoming." Volume 1. ML061740064.
- Rice, G., 2006. "Effects of URI's Kingsville Dome Mine on Groundwater Quality." Final Report, prepared for the Kleberg County URI Citizen Review Board.
- Rittmann, P.D., 1999. "Exposure Scenarios and Unit Factors for Hanford Tank Waste Performance Assessments," Fluor Government Group, HNF-SD-WM-TI-707, Revision 1, December.
- Rittmann, P.D., 2004. "Exposure Scenarios and Unit Factors for Hanford Tank Waste Performance Assessments," Fluor Government Group, HNF-SD-WM-TI-707, Revision 4, May.
- Rumbaugh, J.O., and D.B. Rumbaugh, 1998. "Groundwater Vistas." Version 5.16. Environmental Simulations.
- SC&A 2008. "Database Summary Analysis Report: Uranium Mills and In-Situ Leach Facilities." Contract EP-D-05-002, Work Assignment 4-17, Task 6. SC&A, Inc., Vienna, Virginia. September 2008.
- SC&A 2011a. "Considerations Related to Post-Closure Monitoring of Uranium In-Situ Leach/In-Situ Recovery (ISL/ISR) Sites." Contract Number EP-D-10-042, Work Assignment 2-06, Task 5. SC&A, Inc., Vienna, Virginia.
- SC&A 2011b. "Modeling of Heap Leach and In-Situ Leaching Operations." Contract Number EP-D-10-042, Work Assignment 1-11, Task 4. SC&A, Inc., Vienna, Virginia. March 26, 2011.

SC&A 2011c. "Modeling of Heap Leach and In-Situ Leaching Operations." Contract Number EP-D-10-042, Work Assignment 2-06, Task 2. SC&A, Inc., Vienna, Virginia. May 4, 2011.

Schramke, J.A., H. Demuth, and M.S. Pelizza, 2009. "Geochemistry of Uranium In-Situ Leach Aquifers After Restoration." Presented at U2009 Global Uranium Symposium, Keystone, Colorado, May 2009.

SNL (Sandia National Laboratory) 1999. "Residual Radioactive Contamination From Decommissioning, Parameter Analysis, Draft Report for Comment" prepared for U.S. Nuclear Regulatory Commission, NUREG/CR-5512, Vol. 3, SAND99-2148, October.

Terry, Robert 2011. Personnel communication, U.S. Environmental Protection Agency, Region 9, October.

Trinity (Trinity Engineering Associates, Inc.) 2007. "CAP88-PC Version 3.0 User Guide," prepared for the U.S. Environmental Protection Agency, December 9.

USCB (U.S. Census Bureau) 2011. "Profile of General Population and Housing Characteristics: 2010," DP-1.

USDA (U.S. Department of Agriculture) 2004. "2002 Census of Agriculture, Farm and Ranch Irrigation Survey (2003)," AC-02-SS-1, November.

USDA (U.S. Department of Agriculture) 2009. "2007 Census of Agriculture, Summary and State Data, Volume 1, Geographic Area Series, Part 51," AC-07-A-51, updated December.

USDA (U.S. Department of Agriculture) 2011. "2010 Vegetable Summary," National Agricultural Statistics Service, January.

UT (University of Texas) 2010. "Geological and Geographical Attributes of the South Texas Uranium Province." Jackson School of Geosciences, University of Texas at Austin.

Whicker, F.W. and T.B. Kirshner, 1987. "PATHWAY: A Dynamic Food-Chain Model to Predict Radionuclide Ingestion After Fallout Deposition." Health Physics, 52(6):717-737.

WSDOH (Washington State, Department of Health) 2003. "Radiological Risk Assessment, Low-Level Radioactive Waste Disposal Site, Richland, WA," Andrew H. Thatcher, October.

Yu C., A.J. Zielen, J.J. Cheng, D.J. LePoire, E. Gnanapragasam, S. Kamboj, J. Arnish, A. Wallo III, W.A. Williams, H. Peterson, 2002. "User's Manual for RESRAD Version 6," ANL/EAD-4, Argonne National Laboratory, Argonne, Illinois.

Zheng, C., and P. Patrick Wang, 1999. "MT3DMS: A modular three-dimensional multispecies transport model for simulation of advection, dispersion, and chemical reactions of contaminants in groundwater systems; documentation and user's guide," Contract Report SERDP-99-1, U.S. Army Engineer Research and Development Center, Vicksburg, Mississippi.